frontiers | Research Topics

Rising stars in Inflammation 2021

Edited by
Jolien Suurmond, Pedro Elias Marques, Luciana Padua Tavares and Andrea Baragetti

Published in
Frontiers in Immunology

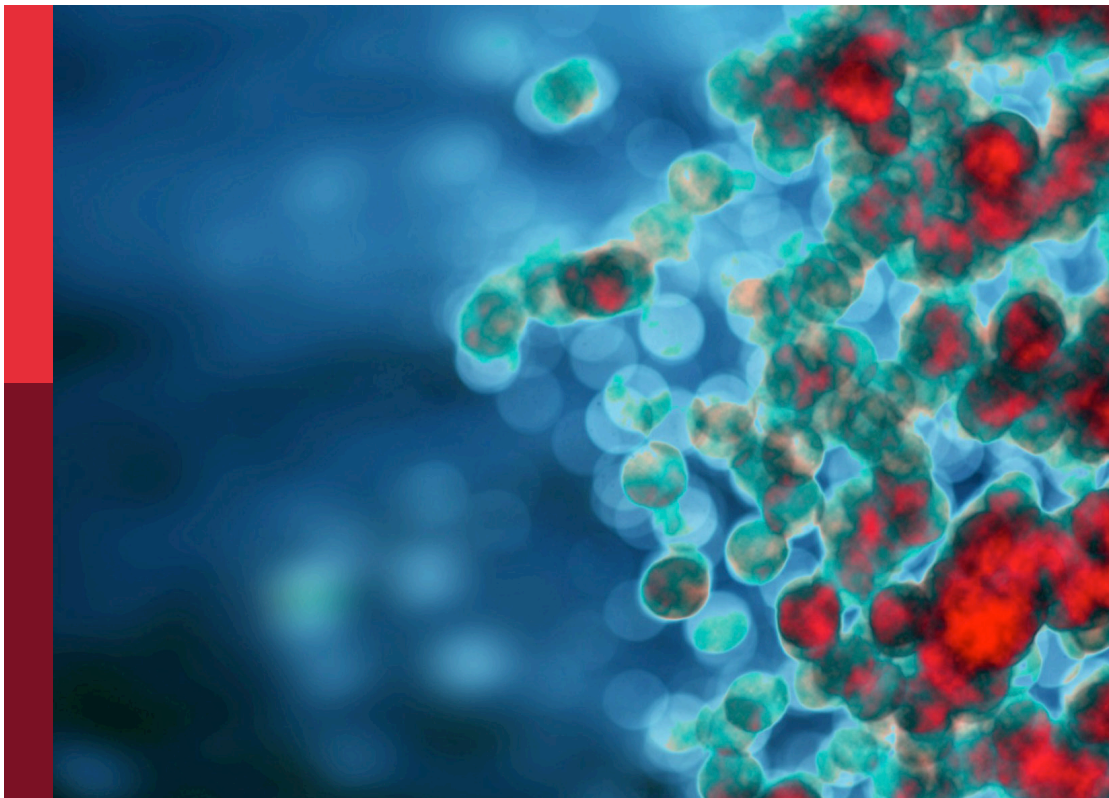

ISSN 1664-8714
ISBN 978-2-8325-2438-1
DOI 10.3389/978-2-8325-2438-1

About Frontiers

Frontiers is more than just an open access publisher of scholarly articles: it is a pioneering approach to the world of academia, radically improving the way scholarly research is managed. The grand vision of Frontiers is a world where all people have an equal opportunity to seek, share and generate knowledge. Frontiers provides immediate and permanent online open access to all its publications, but this alone is not enough to realize our grand goals.

Frontiers journal series

The Frontiers journal series is a multi-tier and interdisciplinary set of open-access, online journals, promising a paradigm shift from the current review, selection and dissemination processes in academic publishing. All Frontiers journals are driven by researchers for researchers; therefore, they constitute a service to the scholarly community. At the same time, the *Frontiers journal series* operates on a revolutionary invention, the tiered publishing system, initially addressing specific communities of scholars, and gradually climbing up to broader public understanding, thus serving the interests of the lay society, too.

Dedication to quality

Each Frontiers article is a landmark of the highest quality, thanks to genuinely collaborative interactions between authors and review editors, who include some of the world's best academicians. Research must be certified by peers before entering a stream of knowledge that may eventually reach the public - and shape society; therefore, Frontiers only applies the most rigorous and unbiased reviews. Frontiers revolutionizes research publishing by freely delivering the most outstanding research, evaluated with no bias from both the academic and social point of view. By applying the most advanced information technologies, Frontiers is catapulting scholarly publishing into a new generation.

What are Frontiers Research Topics?

Frontiers Research Topics are very popular trademarks of the *Frontiers journals series*: they are collections of at least ten articles, all centered on a particular subject. With their unique mix of varied contributions from Original Research to Review Articles, Frontiers Research Topics unify the most influential researchers, the latest key findings and historical advances in a hot research area.

Find out more on how to host your own Frontiers Research Topic or contribute to one as an author by contacting the Frontiers editorial office: frontiersin.org/about/contact

Rising stars in inflammation 2021

Topic editors

Jolien Suurmond — Leiden University Medical Center (LUMC), Netherlands
Pedro Elias Marques — KU Leuven, Belgium
Luciana Padua Tavares — Harvard Medical School, United States
Andrea Baragetti — University of Milan, Italy

Citation

Suurmond, J., Marques, P. E., Tavares, L. P., Baragetti, A., eds. (2023). *Rising stars in inflammation 2021*. Lausanne: Frontiers Media SA.
doi: 10.3389/978-2-8325-2438-1

Table of contents

frontiers | Frontiers in Immunology

TYPE Editorial
PUBLISHED 03 May 2023
DOI 10.3389/fimmu.2023.1193694

OPEN ACCESS

EDITED AND REVIEWED BY
Pietro Ghezzi,
University of Urbino Carlo Bo, Italy

*CORRESPONDENCE
A. Baragetti
andrea.baragetti@unimi.it

RECEIVED 25 March 2023
ACCEPTED 21 April 2023
PUBLISHED 03 May 2023

CITATION
Baragetti A, Suurmond J, Marques PE and Tavares LP (2023) Editorial: Rising stars in inflammation 2021.
Front. Immunol. 14:1193694.
doi: 10.3389/fimmu.2023.1193694

Editorial: Rising stars in inflammation 2021

A. Baragetti[1]*, J. Suurmond[2], P. E. Marques[3] and L. P. Tavares[4]

[1]Department of Pharmacological and Biomolecular Sciences "Rodolfo Paoletti", University of Milan, Milan, Italy, [2]Department of Rheumatology, Leiden University Medical Center (LUMC), Leiden, Netherlands, [3]Rega Institute for Medical Research, KU Leuven, Leuven, Belgium, [4]Pulmonary and Critical Care Medicine Division, Department of Medicine, Brigham and Women's Hospital and Harvard Medical School, Boston, MA, United States

KEYWORDS

inflammation, innate immunity, adaptive immunity, chronic pathologies, cellular reprogramming

Editorial on the Research Topic
Rising stars in inflammation 2021

Inflammation encompasses a wide range of cellular and molecular mechanisms that connect the pathophysiological aspects underlying most acute and chronic morbidities, such as cancers, cardiovascular, metabolic inflammatory diseases, autoimmune diseases, and neurodegeneration (1–5).

Discussing inflammation entails embracing a large spectrum of scientific backgrounds, interconnected by integrating different investigative approaches. Consequently, inflammation represents the perfect subject for scientific collaborations between early career researchers. On this shared foundation, they can explore rigorous, innovative, and cutting-edge strategies for advancing basic and translational science in the fields of biology, biotechnology, and biomedicine, among many others. Through this, they can aspire to become leaders in academia and science education.

To satisfy this sense of excitement, *Frontiers in Immunology* launched in 2021 the Research Topic "*Rising Stars in Inflammation 2021*", aimed at encouraging young scientists who have the potential to become future leaders in inflammation research to submit their works across the entire breadth of the field of inflammation and to showcase advancements in theory, experiment, and methodology with applications to compelling aspects of inflammation.

This Research Topic, moderated by four independent young editors, has been a successful experience, with 10 articles published by international research groups, including original articles and reviews.

This Research Topic includes a heterogeneous set of topics, spanning from "technical" research manuscripts, outlining methodologies to optimize the study of immune cells, to state-of-the-art reviews on topics of inflammation and research manuscripts with a basic science or translational perspective.

Among the technical research manuscripts, Blanter et al. carefully described the optimal methods for the isolation and functional characterization of neutrophils. Through a well-conducted methodology, the authors suggested the use of the magnetic-based separation of this immune cell subset for specific functional assays. Additionally, in

this Research Topic, Rumianek et al. presented an interesting transgenic reporter mouse to specifically target and label tissue-resident macrophages by using a tamoxifen-inducible Cre recombinase under the control of the human CD68 promoter (hCD68-CreERT2). The authors demonstrated that this tool guarantees the specific and long-term (6 weeks) targeting of tissue-resident macrophages with negligible labeling of other myeloid cells. This model provides an opportunity to gain more insights into the phenotype and function of different macrophage subsets in both healthy and diseased states.

Furthermore, this issue showcases different perspectives on the mechanisms by which both the innate and adaptive immune systems respond to pathogens and antigens and how immune cells "adapt" to chronic inflammatory and metabolic status in the long term. For instance, Lopes et al. described the role of Kupffer cells (KCs), the hepatic tissue-resident macrophage, in controlling systemic infection post-liver injury due to acetaminophen (APAP) overdose. More specifically, KCs, whose density in the liver decreases during the development of liver injury, rapidly repopulated the areas of necrosis to restore the liver firewall function. Hence, this study not only describes the impaired function of KCs in liver injury, but it also points to future therapeutic strategies directed to restoring liver function post-injury. On the other hand, Collier et al.'s study showed an interesting correlation of systemic inflammatory markers and innate immune cell activity in preschool children. Of interest, the authors found that a higher body mass index positively correlates with increased circulating levels of inflammatory markers and a pro-inflammatory potential by monocytes, suggesting that this imprinting can potentially indicate a higher risk for the development of non-communicable diseases later in life.

Wan et al. reviewed in detail the inflammatory immune-associated enhancer RNAs (eRNAs), providing a comprehensive overview about their molecular biology, outlining their involvement in inflammatory immune diseases and tumor inflammation, and discussing their therapeutic applications. In addition, Xiao et al. presented a comprehensive review about another target for inflammation control. The authors reviewed the non-classic role of transient receptor potential vanilloid 1 (TRPV1) channels in controlling T-cell-mediated inflammatory responses and diseases.

Aiding the complex understanding of inflammation as a whole, two reviews described the role of cellular organelles such as mitochondria and endosomes in immune cell activity. Cao et al. assessed the current knowledge on the role of mitochondria in shaping neutrophil response and phenotype, including regulating oxidative burden, migration, and the effector mechanisms of these short-living cells in tissues. Meanwhile, Gonzales and Canton reviewed the emerging evidence for the active cytosolic transfer of diverse macromolecular "danger" signals across endocytic organelle membranes in phagocytes. This process may have important implications for the cellular response to macromolecules such as double-stranded DNA, lipopolysaccharide, and peptidoglycan and mediating inflammatory responses.

An original research article by Nakandakari-Higa et al. describes their findings on a novel humanized mouse model designed to replicate and better comprehend SARS-Cov-2 infection. The authors elegantly developed a minimally edited tool to study the maturation of B cells and immune responses to SARS-Cov2 infection.

Finally, as in other fields of research, the experimental evidence needs to find clinical translation. The large epidemiological study of Hong et al., also published in this issue, recapitulated the abovementioned studies describing the mechanisms of inflammation. In this cross-sectional survey of more than 2600 subjects, the authors found significant correlations between markers of systemic inflammation, dyslipidemia, and lower antioxidant capacity.

In conclusion, we hope that the readers appreciate the varied research included in this Research Topic, "*Rising Stars in Inflammation*". The editorial team put substantial effort into screening and evaluating the high-quality manuscripts produced by young researchers and their groups. We hope that this issue will aid in the efforts to foster collaboration among and support to young researchers, as these are crucial elements in their progression towards more advanced stages in their scientific careers.

Author contributions

AB, JS, LPT and PEM contributed in writing and editing the original manuscript.

Funding

Author AB received the following funding: "Cibo, Microbiota, Salute" by "Vini di Batasiolo S.p.A" AL_RIC19ABARA_01; a research award (2021) from "the Peanut Institute"; Ministry of Health—Ricerca Corrente—IRCCS MultiMedica; PRIN 2017H5F943; ERANET ER- 2017-2364981; "PNRR M4C2-Investimento 1.4-CN00000041", European Union—NextGeneration EU. Author PEM received the following funding: the Research Foundation of Flanders (FWO-Vlaanderen; G058421N and G025923N) and a Marie Sklodowska-Curie Fellowship (MSCA-IF-2018-839632). The funder agencies for both these authors were not involved in the interpretation of data and the manuscripts reviewed in this Editorial, nor participated in any form in writing this article and in the decision to submit it for publication.

Conflict of interest

The authors declare that the research was conducted in the absence of any commercial or financial relationships that could be construed as a potential conflict of interest.

Publisher's note

References

1. Mason JC, Libby P. Cardiovascular disease in patients with chronic inflammation: mechanisms underlying premature cardiovascular events in rheumatologic conditions. *Eur Heart J* (2015) 36:482–9. doi: 10.1093/eurheartj/ehu403

2. Ransohoff RM. How neuroinflammation contributes to neurodegeneration. *Science* (2016) 353:777–83. doi: 10.1126/SCIENCE.AAG2590

3. Wyss-Coray T. Ageing, neurodegeneration and brain rejuvenation. *Nature* (2016) 539:180–6. doi: 10.1038/NATURE20411

4. Hotamisligil GS. Inflammation, metaflammation and immunometabolic disorders. *Nature* (2017) 542:177–85. doi: 10.1038/nature21363

5. Leiva O, Hobbs G, Ravid K, Libby P. Cardiovascular disease in myeloproliferative neoplasms: JACC: CardioOncology state-of-the-Art review. *JACC CardioOncol* (2022) 4:166–82. doi: 10.1016/J.JACCAO.2022.04.002

frontiers in Immunology

PERSPECTIVE
published: 08 February 2022
doi: 10.3389/fimmu.2021.830049

Innate Immune Activation and Circulating Inflammatory Markers in Preschool Children

Fiona Collier[1,2], Cerys Chau[3], Toby Mansell[3], Keshav Faye-Chauhan[1], Peter Vuillermin[1,2,3], Anne-Louise Ponsonby[1,4], Richard Saffery[3,4], Mimi L. K. Tang[3,5], Martin O'Hely[1,2,3], John Carlin[3,5], Lawrence E. K. Gray[2], Siroon Bekkering[3,6†], David Burgner[3,5,7†] and the Barwon Infant Study Investigator Group[‡]*

[1] School of Medicine, Deakin University, Geelong, VIC, Australia, [2] Child Health Research Unit, Barwon Health, Geelong, VIC, Australia, [3] Murdoch Children's Research Institute, Royal Children's Hospital, Parkville, VIC, Australia, [4] Department of Neuroepidemiology, The Florey Institute of Neuroscience and Mental Health, Parkville, VIC, Australia, [5] Department of Paediatrics, Melbourne University, Parkville, VIC, Australia, [6] Department of Internal Medicine and Radboud Institute for Molecular Life Science (RIMLS), Radboud University Medical Center, Nijmegen, Netherlands, [7] Department of Paediatrics, Monash University, Clayton, VIC, Australia

OPEN ACCESS

Edited by:
Andrea Baragetti, University of Milan, Italy

Reviewed by:
Fabrizia Bonacina, University of Milan, Italy
Elena Ciaglia, University of Salerno, Italy

***Correspondence:**
Fiona Collier
fmcol@deakin.edu.au

[†]*These authors share senior authorship*

[‡]*The Barwon Investigator Group: Sarath Ranganathan, Peter Sly, Leonard C Harrison, Terry Dwyer, Amy Loughman*

Specialty section:
This article was submitted to Inflammation, a section of the journal Frontiers in Immunology

Received: *06 December 2021*
Accepted: *28 December 2021*
Published: *08 February 2022*

Citation:
Collier F, Chau C, Mansell T, Faye-Chauhan K, Vuillermin P, Ponsonby A-L, Saffery R, Tang MLK, O'Hely M, Carlin J, Gray LEK, Bekkering S, Burgner D and the Barwon Infant Study Investigator Group (2022) Innate Immune Activation and Circulating Inflammatory Markers in Preschool Children. Front. Immunol. 12:830049. doi: 10.3389/fimmu.2021.830049

Early childhood is characterised by repeated infectious exposures that result in inflammatory responses by the innate immune system. In addition, this inflammatory response to infection is thought to contribute to the epidemiological evidence linking childhood infection and adult non-communicable diseases. Consequently, the relationship between innate immune responses and inflammation during early life may inform prevention of NCDs later in life. In adults, non-genetic host factors such as age, sex, and obesity, strongly impact cytokine production and circulating mediators, but data in children are lacking. Here, we assessed cytokine responses and inflammatory markers in a population of healthy preschool children (mean age 4.2 years). We studied associations between cytokines, plasma inflammatory markers and non-genetic host factors, such as sex, age, adiposity, season, and immune cell composition. Similar to adults, boys had a higher inflammatory response than girls, with IL-12p70 and IL-10 upregulated following TLR stimulation. Adiposity and winter season were associated with increased circulating inflammatory markers but not cytokine production. The inflammatory markers GlycA and hsCRP were positively associated with production of a number of cytokines and may therefore reflect innate immune function and inflammatory potential. This dataset will be informative for future prospective studies relating immune parameters to preclinical childhood NCD phenotypes.

Keywords: innate immune activation, cytokines, preschool children, human functional genomics, systemic inflammation

INTRODUCTION

Non-communicable diseases (NCDs) result in huge and increasing human and economic costs globally. Development of innovative and effective prevention of NCDs requires better understanding of modifiable pathogenic pathways across the life course (1). NCDs generally manifest in adulthood and disproportionately affect males (2, 3). The end-organ damage manifests

as a range of conditions and inflammation is the central pathogenic process (4). The trajectories that lead to chronic inflammation begin in early life (5). Understanding the variation and early determinants of inflammatory responses in healthy children may therefore highlight opportunities for NCD prevention.

Early childhood is characterised by repeated infectious exposures that result in inflammatory responses by the innate immune system (6, 7). The intensity of these responses in part determines the clinical severity of infection and varies markedly between individuals (8). This inflammatory response to infection is thought to contribute to the epidemiological evidence linking childhood infection and adult NCDs (9). Cytokines mediate these inflammatory responses, but to date, investigation of variation in cytokine production capacity in the general population has been limited to adults (10).

The toll-like receptor (TLR) pathway is central to innate immune responses to microbial stimuli (11) and a potential therapeutic target for inflammatory diseases (12). There are extensive data on TLR responses in older children and adults (13, 14), but few analogous data in preschool children, the age group with the highest incidence of infection (15). In particular, it is unclear whether variation in TLR responses with sex and environmental exposures reported in adults (16, 17) is also evident in early childhood. It is also unknown whether inflammatory markers, such as glycoprotein acetyls (GlycA), an NMR-derived marker of cumulative inflammation (18–20) and high sensitivity C-reactive protein (hsCRP) correlate with innate immune responses.

In the current study, we aimed to investigate innate immune responses to two key bacterial TLR ligands (lipopolysaccharide, LPS; and peptidoglycan, PGN) in a cohort of healthy preschool children, and relate these responses to GlycA and hsCRP. We also examined how host and environmental factors (sex, age, adiposity, granulocyte/monocyte proportions, or season) were related to cytokine production and circulating inflammatory markers.

METHODS

Study Cohort

Children in this study were participants of the Barwon Infant Study (BIS), which recruited pregnant mothers through antenatal clinics at two major hospitals in Geelong (Victoria, Australia) between 2010-2013 (20). The final inception cohort included 1,064 mothers with 1,074 infants (10 twin pairs). Children who visited the BIS for their preschool clinical review (age 3.9-5.6 years) were asked to complete a questionnaire, undergo a skin-prick allergy test (SPT) and provide a blood sample. The cohort used in this study was a selection of subjects that had both a TLR stimulation assay and relevant metadata. Ethics approval for BIS (Project number 10/24) was obtained through the Barwon Health Human Research Ethics Committee (HREC).

Data Collection

At the preschool clinical review, parents were asked to complete a survey including questions regarding their child's current wellbeing, health and any recent illness or temperature. Children also had their body weight [measured with bioelectrical impedance analysis (BIA) scale (Tanita, Kewdale, Australia, model BC-420MA)], height [measuring rod stadiometer (Seca, Hamburg, Germany, model no. 213)] and waist circumference (tape measure) recorded. BMI for each participant was calculated by dividing weight by height in metres squared (kg/m^2). Measurement of body fat were obtained using the BIA scale.

Blood Sampling and Innate Immune Assays

Blood samples were collected in preservative-free sodium heparinised tubes. To quantify cytokine responses of immune cells under conditions similar to those *in vivo*, and to maximise outputs from small paediatric blood volumes, we measured the production of monocyte-derived cytokines following stimulation of whole blood. Precisely two hours from blood collection, an aliquot of whole blood was diluted 1:2 with RPMI 1640 growth medium and transferred to plate strips that consist of 8 wells (the size of a 96 well plate) each containing 20µL of either RPMI (growth medium), the gram-negative bacterial membrane component, lipopolysaccharide (LPS, 100ng/mL final concentration) or gram-positive bacterial membrane component, peptidoglycan (PGN, 10ug/mL). These represent either unstimulated, TLR4, or TLR2-stimulated conditions respectively. 180µL of diluted blood was added to each well and cells were stimulated for 24 hours at 37°C in 5% CO_2. To reduce evaporation, additional plate strips containing only water were incubated alongside the experimental strips. Following the 24-hour incubation, the strips were centrifuged to pellet the blood cells, and the supernatant collected in two 50µL aliquots to be stored at -80°C until cytokine analysis.

Flow Cytometry

Following phlebotomy, a separate aliquot of 100µL whole blood underwent flow cytometry (Becton Dickinson (BD) FACSCanto^{TM}) to identify proportions of target cell populations including monocytes and granulocytes, expressed as the percentage of total white blood cells (WBC). WBC were stained with (i) anti-human CD4-FITC, anti-human CD3-PE and anti-human CD45-PerCP; or (ii) anti-human CD14-FITC, anti-human CD16-PE and anti-human HLA-DR-PECy5, before red cell lysis and formalin fixation. Monocytes and granulocytes were discriminated based on side scatter (SSC) and CD45 expression (21). The proportion of activated nonclassical monocytes ($CD14^+$/$CD16^{++}$, as % of total monocytes) was also determined by gating to the HLA-DR^+ monocytes. All antibodies were sourced from BD Biosciences (San Jose, California, US).

Cytokine Quantification

Cytokines were quantified using the Bio-Rad Bio-Plex Pro^{TM} cytokine assay kit and detection software, with small modifications to manufacturer instructions. Standards were prepared in a dilution series using the standard kit-provided diluent. Frozen samples were thawed and added to plates that contained 8 standards in duplicate (including blank), and inter-

plate controls. Manual steps in the assay included addition of magnetic beads, detection antibodies and streptavidin-phycoerythrin dye, with washing and incubation in between each step. Plates were analysed using the xPONENT MAGPIX ® instrument (Bio-Rad ®). Standard curves were produced based on the standard dilutions and optimised for a recovery rate of 70-130%. Final measures in pg/mL for IL-1β, IL-6, TNFα, IL-12p70 (pro-inflammatory), IL-1RA and IL-10 (anti-inflammatory) were derived by the Bio-Plex Manager™ Software using the standard curves. Cytokine concentrations above the standard curve's upper limit of quantification (ULOQ) were excluded whereas cytokine concentrations below the lower level of quantification (LLOQ) were replaced with a value equal to 50% of LLOQ.

GlycA and hsCRP Quantification

Markers of inflammation (GlycA and hsCRP) were measured in plasma samples from the bloods collected in sodium heparin tubes. High-throughput proton NMR metabolomics (Nightingale Health, Helsinki, Finland) quantified GlycA (mmol/L) (22), and hsCRP (ug/ml) was determined using ELISA Human C-Reactive Protein/CRP assay (R&D systems, DY1707). Both measures were log-transformed (base 10), and CRP measurements equal to zero (n=47) were assigned a value equal to 50% of the lowest measure (0.001ug/ml).

Statistical Analysis

Cytokine measures were log transformed (base 10). BMI z-score standardised for age and sex (based on WHO Child Growth Charts (age <5 years) and the WHO Reference 2007 (age >=5 years) was calculated using the *zanthro* function from the *dm0004_1* user-developed Stata package (23). Spearman correlations were used to quantify the magnitude and direction of association between the cytokines with the coefficient (r_s) given for each pair of cytokines. Univariable linear regression was used to investigate the associations between exposures, including sex, age, adiposity and innate immune cell proportions, and cytokine levels (log transformed) in the three conditions (unstimulated, and following stimulation with LPS and PGN), as well as the inflammatory markers. The p-values are presented unadjusted for multiple comparisons. Directed acyclic graphs (http://www.dagitty.net) were constructed to determine the minimal sufficient adjustment set for estimating the total effect of the inflammatory markers (GlycA or hsCRP) on the stimulated cytokine levels (**Supplementary Figure 4**). Sensitivity analyses were performed by excluding children with hsCRP above 5ug/ml, which may be indicative of an active infection (24, 25). All statistical analysis and graphics were completed using *Stata Statistical Software: Release 15* (College Station, TX: StataCorp LLC).

RESULTS

Baseline Host and Environmental Characteristics

Complete baseline characteristics of the cohort are described elsewhere (20). We have presented the most important baseline characteristics for this study in **Supplementary Table 1** according to sex. 285 participants were included in this study, with 52% male. The mean age for both sexes was 4.2 years. Bloods were collected across all seasons of the year. Mean weight and fat mass was 17.9kg (range 12.6-34.4kg) and 19.7% (range 10.2-29.0%), respectively. Thirty-three children (14.2%) were classified as overweight (BMI z-score >1SD), and 5 children (1.9%) as obese (BMI z-score >2SD) and boys had slightly higher height, weight, BMI and fat mass. Monocyte proportions, but not granulocytes, were modestly higher in boys (mean 7.1± SD 2.1% compared to 6.5 ± 1.9% in girls) whereas the proportion of activated nonclassical monocytes in boys was lower (median 5.4 (IQR 3.4-8.1)% compared to 6.5 (4.2-10.2)%). hsCRP levels were overall lower in males, however 9 (6.1%) boys and 3 (2.1%) girls had hsCRP levels above 5ug/ml possibly indicative of active infection.

Circulating Inflammatory Markers (GlycA and hsCRP) Associate With Host- and Environmental Factors

Following log transformation of the inflammatory markers, levels of GlycA were only moderately correlated with hsCRP (r=0.41, **Supplementary Figure 1**). Levels of hsCRP were lower in boys (**Supplementary Table 1**, **Table 1**), and GlycA and hsCRP were both positively associated with BMI z-score (**Table 1**). In addition, levels of both inflammatory markers were higher in winter (**Supplementary Figure 2**, **Table 1**), and were associated with the proportion of granulocytes (**Table 1**), indicating overall increased inflammatory status.

TLR-Stimulation and Monocyte Derived Cytokines

To quantify cytokine responses of immune cells under conditions similar to those *in vivo*, and to maximise outputs from small paediatric blood volumes, we measured the production of monocyte-derived cytokines after stimulation of whole blood, rather than purified cell populations. Cells were stimulated for 24 hours using either gram-negative or gram-positive bacterial ligands.

Cytokine Correlations

Pro-inflammatory and anti-inflammatory monocyte-derived cytokines (IL-1β, IL-6, TNFα, IL-12p70, IL-1RA, IL-10) were measured following stimulation of TLR4 (LPS) and TLR2 (PGN) in whole blood (**Supplementary Table 2**). Unstimulated cytokine levels moderately predicted the TLR-stimulated levels (except for IL-1β in response to LPS) (**Supplementary Figure 3**). Overall, intra-individual cytokine production in unstimulated and following stimulation by each TLR ligand were modestly to strongly correlated (r_s range 0.23-0.84) (**Supplementary Figure 4**).

Associations of Cytokines With Host and Environmental Factors

Both pro- and anti-inflammatory cytokine production following TLR stimulation was higher in boys, particularly for IL-12p70 and IL-10 after LPS stimulation, and IL-6, IL-1RA, IL-12p70 and IL-10 following PGN stimulation (**Figure 1**, **Table 2**). Following adjustment for sex, IL-1β was correlated with age in the

TABLE 1 | Associations between inflammatory factors and sex, child age, adiposity (BMI and %fat mass), seasons and innate immune cell proportions.

		Adjusted for	GlycA Log10 (mmol/L)	95% CI	p-value	hsCRP Log10(ug/ml)	95%CI	p-value
Sex (compared to female)			-0,01	(-0.02, 0.01)	0,285	-0,33		
Log10 (Age, yr)		Sex	0,03	(-0.21, 0.26)	0,820	-0,30		
BMI z-score			0,01	(0.00, 0.02)	**0,010**	0,16		
Log10 (%Fat Mass)		Sex, Age	0,19	(-0.01, 0.39)	0,061	4,52		
Season (compared to Winter)	Summer		-0,03	(-0.05, -0.02)	**<0.0001**	-0,34		
	Autumn		-0,02	(-0.03, 0.00)	**0,035**	-0,63		
	Spring		0,02	(-0.04, 0.00)	**0,017**	-0,38		
Innate Immune Populations	Granulocytes (% of WB)		0,14	(0.08, 0.21)	**<0.0001**	3,85		
	Log10(Monocytes, % of WB)	Sex, Age	-0,03	(-0.08, 0.02)	0,684	0,24		
	Log10 (activated nonclassical Monocytes, % of total monocytes)		0,00	(-0.02, 0.02)	0,730	0,65		

*Linear regression analysis, *denotes adjusted for sex. Beta coefficients (units=Log10(mmol/L GlycA or ug/ml hsCRP) per variable) with 95% confidence interval (CI) and p value. The strength of association is denoted by either shades of blue (negative) or red (positive).*

unstimulated and LPS stimulated group (**Table 2**). There was no evidence that adiposity was associated with cytokine responses (**Table 2**). Season of blood collection was also not associated with cytokine production (data not shown).

TNFα levels were positively associated with the percentage of monocytes in the stimulated conditions (adjusted for sex, **Supplementary Table 3**). IL-12p70 was associated with the proportion of monocytes in unstimulated blood and following PGN stimulation (**Supplementary Table 3**). IL-1RA was associated with the proportion of granulocytes in unstimulated and TLR-stimulated blood (**Supplementary Table 3**) and there was weaker evidence that IL-6 was associated with granulocyte proportion in unstimulated blood (**Supplementary Table 3**).

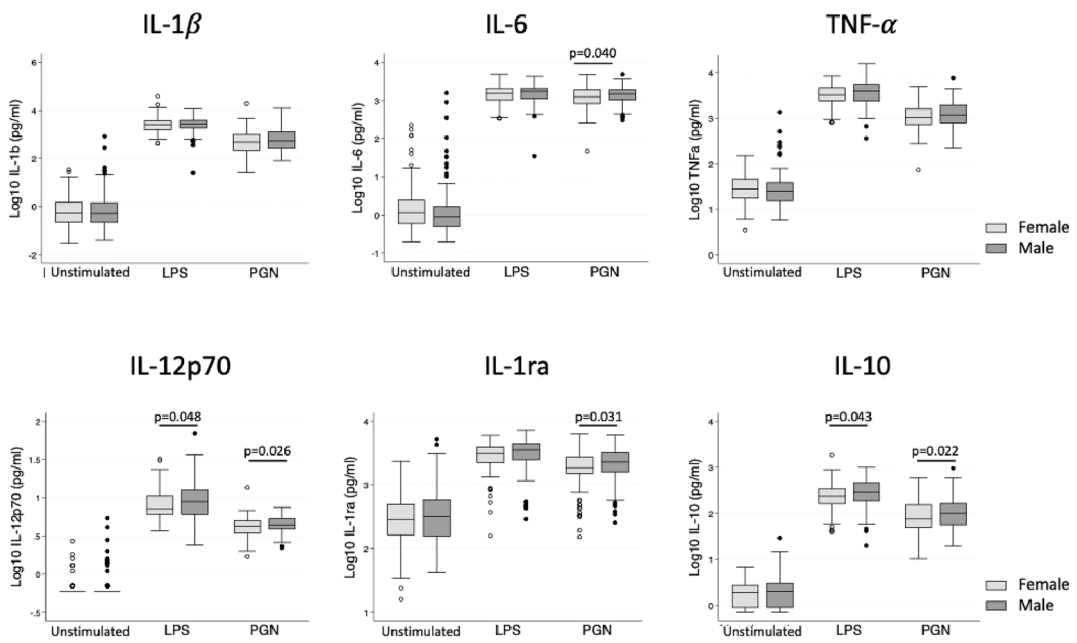

FIGURE 1 | Cytokine levels following *in vitro* stimulation with TLR ligands in female and male children. Box plot graphs (with median and upper and lower quartiles) of cytokine levels (Log_{10}(pg/ml)) from whole blood following 24 hour stimulation with medium (unstimulated), LPS (TLR4 stimulation) and PGN (TLR2 stimulation), n=285 (149 males, 136 females). Male children had modestly higher production of IL-12p70 and IL-10 upon both LPS and PGN stimulation and additionally higher IL-6 and IL-1RA upon PGN stimulation (unadjusted linear regression at each treatment).

TABLE 2 | Association between sex, child age, and adiposity, and log transformed cytokine levels under unstimulated and stimulated conditions.

	Stimulation Conditions	Sex Compared to Female	Log_{10}(Age, yr) Adjusted for Sex	BMI z-score	Log_{10}(% Fat Mass) Adjusted for Age and Sex
IL-1β	Unstimulated	-0.00 (-0.16, 0.15)	**0.30 (0.02, 0.57)**	0.07 (-0.01, 0.16)	0.01 (-0.01, 0.04)
	LPS	0.00 (-0.08, 0.08)	**-0.18 (-0.33, -0.04)**	-0.03 (-0.07, 0.02)	-0.01 (-0.02, 0.01)
	PGN	0.07 (-0.03, 0.18)	-0.06 (-0.25, 0.13)	-0.00 (-0.03, 0.01)	-0.00 (-0.02, 0.01)
IL-6	Unstimulated	-0.07 (-0.22, 0.08)	0.18 (-0.09, 0.44)	0.01 (-0.07, 0.09)	0.00 (-0.02, 0.03)
	LPS	0.02 (-0.03, 0.08)	-0.04 (-0.15, 0.06)	0.01 (-0.02, 0.04)	0.01 (-0.00, 0.02)
	PGN	**0.06 (0.00, 0.12)**	-0.07 (-0.17, 0.04)	0.02 (-0.02, 0.05)	0.00 (-0.01, 0.01)
TNFα	Unstimulated	-0.01 (-0.09, 0.07)	0.09 (-0.05, 0.23)	0.01 (-0.04, 0.05)	0.00 (-0.01, 0.02)
	LPS	0.05 (-0.01, 0.11)	0.00 (-0.11, 0.11)	-0.01 (-0.04, 0.02)	0.00 (-0.01, 0.01)
	PGN	0.06 (-0.01, 0.12)	0.00 (-0.12, 0.12)	-0.02 (-0.05, 0.02)	-0.01 (-0.02, 0.01)
IL-12p70	Unstimulated	0.02 (-0.01, 0.05)	0.04 (-0.01, 0.09)	0.00 (-0.01, 0.02)	0.00 (-0.00, 0.01)
	LPS	**0.05 (0.00, 0.10)**	-0.02 (0.12, 0.07)	-0.01 (-0.04, 0.02)	0.00 (-0.01, 0.01)
	PGN	**0.03 (0.00, 0.06)**	-0.00 (-0.05, 0.05)	-0.01 (-0.02, 0.01)	-0.00 (-0.01, 0.00)
IL-1RA	Unstimulated	0.04 (-0.05, 0.14)	0.13 (-0.02, 0.30)	0.03 (-0.01, 0.08)	0.00 (-0.01, 0.02)
	LPS	0.05 (-0.01, 0.10)	-0.04 (-0.14, 0.07)	0.02 (-0.01, 0.05)	0.01 (-0.00, 0.02)
	PGN	**0.07 (0.01, 0.13)**	-0.01 (-0.12, 0.10)	0.01 (-0.02, 0.04)	-0.00 (-0.01, 0.01)
IL-10	Unstimulated	0.02 (-0.05, 0.08)	0.04 (-0.08, 0.16)	0.02 (-0.02, 0.06)	-0.00 (-0.01, 0.01)
	LPS	**0.07 (0.00, 0.14)**	0.04 (-0.08, 0.16)	0.02 (-0.02, 0.05)	0.00 (-0.01, 0.01)
	PGN	**0.09 (0.01, 0.17)**	-0.13 (-0.27, 0.00)	-0.01 (-0.05, 0.03)	0.00 (-0.01, 0.01)

Linear regression analysis. Beta coefficients (units=Log_{10}(pg/ml of cytokine) per variable) with 95% confidence interval (CI). Those in bold indicate a p value <0.05

Relationships Between Circulating Inflammatory Markers and TLR-Stimulated Monocyte-Derived Cytokines

We next investigated associations between circulating inflammatory markers GlycA and CRP and cytokine levels in regression models adjusted for age and sex. There was evidence that both unstimulated and TLR-stimulated cytokine levels were positively associated with GlycA and hsCRP. GlycA was positively associated with the pro-inflammatory cytokines IL-1β and IL-6 in the unstimulated and PGN stimulated group (**Figure 2A**), and with the anti-inflammatory cytokines IL-1RA and IL-10 positively associated with GlycA in the LPS and PGN stimulated groups (**Figure 2A**). High sensitivity CRP was associated with IL-1β and IL-6 in unstimulated blood, with IL-6 following LPS and PGN stimulation (**Figure 2B**), and with IL-1RA and IL-10 following LPS and PGN stimulation (**Figure 2B**).

Sensitivity analyses were performed by excluding children with hsCRP > 5ug/ml, levels possibly indicative of recent or active infection. The associations observed between the circulating inflammatory markers and cytokines in

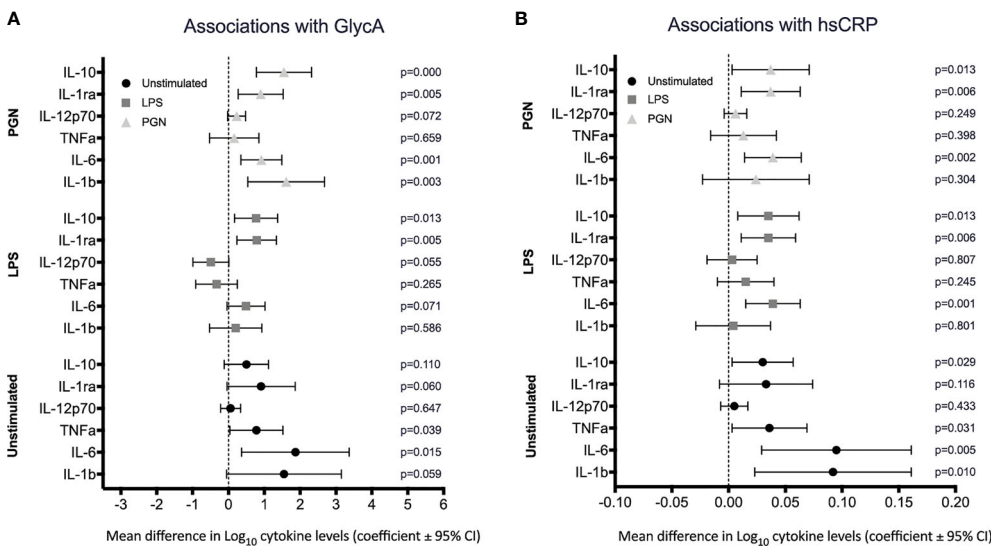

FIGURE 2 | Association between circulating inflammatory markers GlycA and hsCRP and cytokine levels. Cytokines were quantified following stimulation of whole blood in either media (unstimulated) or TLR ligands, LPS and PGN. The estimated mean differences in cytokine levels (Log_{10}(pg/ml)) were calculated per 10-fold difference in **(A)** GlycA, Log_{10}(mmol/L) and **(B)** hsCRP, Log_{10}(μg/ml). Linear regression analyses of cytokine level on inflammatory marker adjusted for sex, age and innate immune cell populations (as determined a priori).

unstimulated and stimulated conditions persisted but were modestly attenuated (**Supplementary Figures 4A, B**).

DISCUSSION

Here we present the largest study to date investigating the relationships between cytokine responses following TLR stimulation in young children and circulating inflammatory markers. The findings provide novel insights into innate immune activity in healthy preschool children and will inform future studies into early onset of inflammatory diseases in this and other cohorts. Knowledge on healthy innate immune responses provides opportunities for comparison in other cohorts with children or young adults at risk for or with NCDs. Furthermore, the children in our cohort are being followed longitudinally, and further innate immune and CVD related measures are to be performed at 8-10 years of age. In this study, levels of cytokines, both unstimulated and TLR-stimulated, were broadly correlated with each other, and with sex, age and innate immune cell populations, but not with BMI or adiposity measures. Circulating inflammatory markers were associated with cytokine production following TLR stimulation, independent of recent infection.

Infections, which are common in early childhood (15), are associated with increased risk of later NCDs (3, 26, 27). In early childhood, the innate immune responses are central to the defence against infection and are characterised by inflammatory responses (7). Variation in these immune responses in adults is extensively reported (10, 28), but data regarding innate immune capacity and inflammation in preschool children are scarce. In our cohort, prototypical monocyte derived inflammatory cytokines (IL-1β, IL-6 and TNFα) were strongly intercorrelated, particularly in the unstimulated and TLR2-stimulated groups, suggesting co-regulation of cytokine production. This is in keeping with a smaller study of young children (n=57, age 5-96 months), which reported correlations between TNFα and IL-6 in whole blood following LPS stimulation (29). We also found moderate to strong correlations between the anti-inflammatory cytokines, IL-1RA and IL-10, following TLR stimulation, which is consistent with the complex co-regulation of cytokine responses and mechanisms for resolution of inflammation (30, 31).

As NCD prevalence is higher in males, we investigated sex differences in cytokine production in children. In adults, sex differences in cytokine responses are marked (29, 32–34), although this may partly reflect increased monocyte proportions (16). In our preschool cohort, only minor sex differences were evident for some cytokines following TLR stimulation; IL-12p70, IL-10, IL-6 and IL-1RA were modestly increased in boys, who also had higher monocyte proportions. Adjusting for the monocyte proportion attenuated the relationship of male sex and IL-6 and IL-1RA, but not for IL-12p70 and IL-10 (data not shown). In addition, in sex-adjusted models, we found no association between BMI z-score or adiposity and cytokine levels, in contrast to reports from adults (35). This may reflect the relatively small number of children in this study with high BMI z-scores, or the relationship between BMI and innate immune responses may become evident later in life. This is also true for other potential confounders of NCDs, that have not been tested here. Although the adiposity measures were not correlated with innate immune cytokine levels, we noted that both GlycA and hsCRP were positively associated with BMI z-score, in line with similar findings in adults and children (36). Both inflammatory markers were also positively associated with the proportion of granulocytes in these children, consistent with our previous findings from this cohort at 12 months (22) and reflective of generalised inflammatory status. Lastly, we found a correlation between levels of GlycA and CRP and season, which is in line with findings in adults (10).

The association between inflammatory status and cytokine levels in unstimulated and TLR-stimulated blood, which was independent of recent infection, has not previously been reported. As expected, the pro-inflammatory cytokines, IL-1β and IL-6 were most strongly associated with GlycA and hsCRP, particularly in the unstimulated group. This association was not evident following TLR-4 stimulation, and interestingly the fold-change for these cytokines (stimulated/unstimulated) tended to decrease (data not shown); possibly reflecting the association between GlycA and hsCRP with anti-inflammatory cytokines following TLR2 and TLR4 stimulation.

This study has a number of strengths, including the relatively large sample size of young children with data on GlycA and hsCRP levels, as well as detailed cohort meta-data and immune measures. This allowed assessment of potential relationships and adjustment for important confounding variables, including the granulocyte and monocyte proportions, and sensitivity analysis for possible recent infection, which is common in this age group. All experiments were performed on fresh blood within 2 hours of collection, minimising process variation. We also acknowledge some limitations, including the cross-sectional design and the potential for type I errors, given the exploratory nature of the study and the multiple cytokines measured. In addition, it would have been valuable to have complete white blood cell counts, to expand our adjusted assays to lymphocyte counts in addition to monocytes and granulocytes. Although consideration was made for children with hsCRP levels above 5ug/ml, we did not have clinical or microbiological data on recent infections. Finally, future studies in later age groups should also adjust for other metabolic risk factors than BMI, such as lipid profile, glycemia, medication use or auto-immune diseases, which are not clearly apparent at the age of the children in our current study.

In summary, in healthy preschool children, levels of pro- and anti-inflammatory cytokines were correlated before and after TLR2 and TLR4 stimulation of whole blood samples. The inflammatory markers hsCRP and GlycA were positively correlated with innate immune cell activity. The findings support the concept that TLR activation contributes to the development of inflammatory NCD (12). Longitudinal studies from early life, with repeated, standardised measures of innate immune activation and circulating inflammatory markers may

inform prediction of later NCD risk and highlight modifiable exposures and opportunities for early prevention.

DATA AVAILABILITY STATEMENT

The data generated for this study are part of the Barwon Infant Study and are available upon reasonable request. Requests to access the datasets should be directed to https://www.barwoninfantstudy.org.au/.

ETHICS STATEMENT

The studies involving human participants were reviewed and approved by Barwon Health Human Research Ethics Committee (HREC), project number 10/24. Written informed consent to participate in this study was provided by the participants' legal guardian/next of kin.

AUTHOR CONTRIBUTIONS

FC, CC, TM, and KF-C performed acquisition, analysis and interpretation of data. SB and DB contributed to the conceptualization and design of the study. FC, SB, and DB drafted the manuscript. All authors contributed to manuscript revision, read, and approved the submitted version.

FUNDING

The initial establishment work and infrastructure for the BIS was supported by the Murdoch Children's Research Institute and Barwon Health. Deakin University is now a partner organization and has provided funding and infrastructure. Funding for this study was provided by the National Health and Medical Research Council of Australia, NHMRC (1030701). SB is supported by the Dutch Scientific Organisation (452173113) and the Dutch Heart Foundation (2018T028). DB is supported by a NHMRC Investigator Grant (1175744). Research at the Murdoch Children's Research Institute is supported by the Victorian Government's Operational Infrastructure Program. The funding bodies did not play any role in the study.

ACKNOWLEDGMENTS

We would like to acknowledge the participation and commitment of the families in the Barwon Infant Study (BIS).

SUPPLEMENTARY MATERIAL

The Supplementary Material for this article can be found online at: https://www.frontiersin.org/articles/10.3389/fimmu.2021.830049/full#supplementary-material

REFERENCES

1. Daniels ME, Donilon TE, Bollyky TJ. The Emerging Global Health Crisis: Noncommunicable Diseases in Low- and Middle-Income Countries. *SSRN Electron J* (2016) 115:1–135. doi: 10.2139/ssrn.2685111
2. Lindblom R, Ververis K, Tortorella SM, Karagiannis TC. The Early Life Origin Theory in the Development of Cardiovascular Disease and Type 2 Diabetes. *Mol Biol Rep* (2015) 42:791–7. doi: 10.1007/s11033-014-3766-5
3. Coates MM, Kintu A, Gupta N, Wroe EB, Adler AJ, Kwan GF, et al. Burden of Non-Communicable Diseases From Infectious Causes in 2017: A Modelling Study. *Lancet Glob Heal* (2020) 8:e1489–98. doi: 10.1016/S2214-109X(20)30358-2
4. Camps J, García-Heredia A. Introduction: Oxidation and Inflammation, a Molecular Link Between Non-Communicable Diseases. *Adv Exp Med Biol* (2014) 824:1–4. doi: 10.1007/978-3-319-07320-0_1
5. Furman D, Campisi J, Verdin E, Carrera-Bastos P, Targ S, Franceschi C, et al. Chronic Inflammation in the Etiology of Disease Across the Life Span. *Nat Med* (2019) 25:1822–32. doi: 10.1038/s41591-019-0675-0
6. Coates BM, Staricha KL, Wiese KM, Ridge KM. Influenza a Virus Infection, Innate Immunity, and Childhood. *JAMA Pediatr* (2015) 169:956–63. doi: 10.1001/jamapediatrics.2015.1387
7. Simon AK, Hollander GA, McMichael A. Evolution of the Immune System in Humans From Infancy to Old Age. *Proc R Soc B Biol Sci* (2015) 282:20143085. doi: 10.1098/rspb.2014.3085
8. Öner D, Drysdale SB, McPherson C, Lin GL, Janet S, Broad J, et al. Biomarkers for Disease Severity in Children Infected With Respiratory Syncytial Virus: A Systematic Literature Review. *J Infect Dis* (2020) 222:S648–57. doi: 10.1093/INFDIS/JIAA208
9. Burgner D, Liu R, Wake M, Uiterwaal CSP. Do Childhood Infections Contribute to Adult Cardiometabolic Diseases? *Pediatr Infect Dis J* (2015) 34:1253–5. doi: 10.1097/INF.0000000000000882
10. ter Horst R, Jaeger M, Smeekens SP, Oosting M, Swertz MA, Li Y, et al. Host and Environmental Factors Influencing Individual Human Cytokine Responses. *Cell* (2016) 167:1111–24.e13. doi: 10.1016/j.cell.2016.10.018
11. Kawasaki T, Kawai T. Toll-Like Receptor Signaling Pathways. *Front Immunol* (2014) 5:461. doi: 10.3389/fimmu.2014.00461
12. Wong SK, Chin K-Y, Ima-Nirwana S. Toll-Like Receptor as a Molecular Link Between Metabolic Syndrome and Inflammation: A Review. *Curr Drug Targets* (2019) 20:1264–80. doi: 10.2174/1389450120666190405172524
13. Shaw AC, Panda A, Joshi SR, Qian F, Allore HG, Montgomery RR. Dysregulation of Human Toll-Like Receptor Function in Aging. *Ageing Res Rev* (2011) 10:346–53. doi: 10.1016/j.arr.2010.10.007
14. Ziakas PD, Prodromou ML, El Khoury J, Zintzaras E, Mylonakis E. The Role of TLR4 896 a>G and 1196 C>T in Susceptibility to Infections: A Review and Meta-Analysis of Genetic Association Studies. *PloS One* (2013) 8:e81047. doi: 10.1371/journal.pone.0081047
15. Miller JE, Goldacre R, Moore HC, Zeltzer J, Knight M, Morris C, et al. Mode of Birth and Risk of Infection-Related Hospitalisation in Childhood: A Population Cohort Study of 7.17 Million Births From 4 High-Income Countries. *PloS Med* (2020) 17 :e1003429. doi: 10.1371/journal.pmed.1003429
16. Beenakker KGM, Westendorp RGJ, De Craen AJM, Chen S, Raz Y, Ballieux BEPB, et al. Men Have a Stronger Monocyte-Derived Cytokine Production Response Upon Stimulation With the Gram-Negative Stimulus Lipopolysaccharide Than Women: A Pooled Analysis Including 15 Study Populations. *J Innate Immun* (2020) 12:142–53. doi: 10.1159/000499840
17. Lefevre N, Noyon B, Biarent D, Corazza F, Duchateau J, Casimir G. SEX DIFFERENCES in INFLAMMATORY RESPONSE and ACID'base BALANCE in PREPUBERTAL CHILDREN With SEVERE SEPSIS. *Shock* (2017) 47:422–8. doi: 10.1097/SHK.0000000000000773
18. Fuertes-Martín R, Correig X, Vallvé JC, Amigó N. Human Serum/Plasma Glycoprotein Analysis By1h-NMR, an Emerging Method of Inflammatory Assessment. *J Clin Med* (2020) 9:354. doi: 10.3390/jcm9020354
19. Kettunen J, Ritchie SC, Anufrieva O, Lyytikäinen LP, Hernesniemi J, Karhunen PJ, et al. Biomarker Glycoprotein Acetyls Is Associated With the Risk of a Wide Spectrum of Incident Diseases and Stratifies Mortality Risk in

Angiography Patients. *Circ Genomic Precis Med* (2018) 11:e002234. doi: 10.1161/CIRCGEN.118.002234
20. Vuillermin P, Saffery R, Allen KJ, Carlin JB, Tang MLK, Ranganathan S, et al. Cohort Profile: The Barwon Infant Study. *Int J Epidemiol* (2015) 44:1148–60. doi: 10.1093/ije/dyv026
21. Collier FM, Tang MLK, Martino D, Saffery R, Carlin JB, Jachno K, et al. The Ontogeny of Naive and Regulatory CD4+ T-Cell Subsets During the First Postnatal Year: A Cohort Study. *Clin Transl Immunol* (2015) 4:e34. doi: 10.1038/cti.2015.2
22. Collier F, Ellul S, Juonala M, Ponsonby AL, Vuillermin P, Saffery R, et al. Glycoprotein Acetyls (GlycA) at 12 Months Are Associated With High-Sensitivity C-Reactive Protein and Early Life Inflammatory Immune Measures. *Pediatr Res* (2019) 85:584–5. doi: 10.1038/s41390-019-0307-x
23. Lycett K, Juonala M, Magnussen CG, Norrish D, Mensah FK, Liu R, et al. Body Mass Index From Early to Late Childhood and Cardiometabolic Measurements at 11 to 12 Years. *Pediatrics* (2020) 146:e20193666. doi: 10.1542/peds.2019-3666
24. Lemiengre MB, Verbakel JY, Colman R, Van Roy K, De Burghgraeve T, Buntinx F, et al. Point-Of-Care CRP Matters: Normal CRP Levels Reduce Immediate Antibiotic Prescribing for Acutely Ill Children in Primary Care: A Cluster Randomized Controlled Trial. *Scand J Prim Health Care* (2018) 36:423–36. doi: 10.1080/02813432.2018.1529900
25. Verbakel JY, Lemiengre MB, De Burghgraeve T, De Sutter A, Aertgeerts B, Shinkins B, et al. Should All Acutely Ill Children in Primary Care be Tested With Point-of-Care CRP: A Cluster Randomised Trial. *BMC Med* (2016) 14:131. doi: 10.1186/s12916-016-0679-2
26. Burgner DP, Cooper MN, Moore HC, Stanley FJ, Thompson PL, De Klerk NH, et al. Childhood Hospitalisation With Infection and Cardiovascular Disease in Early-Mid Adulthood: A Longitudinal Population-Based Study. *PloS One* (2015) 10:e0125342. doi: 10.1371/journal.pone.0125342
27. Burgner DP, Sabin MA, Magnussen CG, Cheung M, Kähönen M, Lehtimäki T, et al. Infection-Related Hospitalization in Childhood and Adult Metabolic Outcomes. *Pediatrics* (2015) 136:e554–62. doi: 10.1542/peds.2015-0825
28. Lefèvre N, Corazza F, Duchateau J, Desir J, Casimir G. Sex Differences in Inflammatory Cytokines and CD99 Expression Following *In Vitro* Lipopolysaccharide Stimulation. *Shock* (2012) 38:37–42. doi: 10.1097/SHK.0b013e3182571e46
29. Casimir GJ, Heldenbergh F, Hanssens L, Mulier S, Heinrichs C, Lefevre N, et al. Gender Differences and Inflammation: An *In Vitro* Model of Blood Cells Stimulation in Prepubescent Children. *J Inflamm* (2010) 7:28. doi: 10.1186/1476-9255-7-28
30. Schmitz ML, Weber A, Roxlau T, Gaestel M, Kracht M. Signal Integration, Crosstalk Mechanisms and Networks in the Function of Inflammatory Cytokines. *Biochim Biophys Acta - Mol Cell Res* (2011) 1813:2165–75. doi: 10.1016/j.bbamcr.2011.06.019
31. Wolf AM, Wolf D, Rumpold H, Enrich B, Tilg H. Adiponectin Induces the Anti-Inflammatory Cytokines IL-10 and IL-1RA in Human Leukocytes. *Biochem Biophys Res Commun* (2004) 323:630–5. doi: 10.1016/j.bbrc.2004.08.145
32. Von Aulock S, Deininger S, Draing C, Gueinzius K, Dehus O, Hermann C. Gender Difference in Cytokine Secretion on Immune Stimulation With LPS and LTA. *J Interf Cytokine Res* (2006) 26:887–92. doi: 10.1089/jir.2006.26.887
33. Temple S EL, Pham K, Glendenning P, Phillips M, Waterer GW. Endotoxin Induced TNF and IL-10 mRNA Production Is Higher in Male Than Female Donors: Correlation With Elevated Expression of TLR4. *Cell Immunol* (2008) 251:69–71. doi: 10.1016/j.cellimm.2008.04.013
34. Wirtz PH, Von Känel R, Rohleder N, Fischer JE. Monocyte Proinflammatory Cytokine Release Is Higher and Glucocorticoid Sensitivity Is Lower in Middle Aged Men Than in Women Independent of Cardiovascular Risk Factors. *Heart* (2004) 90:853–8. doi: 10.1136/hrt.2002.003426
35. Scholtes VPW, Versteeg D, De Vries JPPM, Hoefer IE, Schoneveld AH, Stella PR, et al. Toll-Like Receptor 2 and 4 Stimulation Elicits an Enhanced Inflammatory Response in Human Obese Patients With Atherosclerosis. *Clin Sci* (2011) 121:205–14. doi: 10.1042/CS20100601
36. Bartlett DB, Slentz CA, Connelly MA, Piner LW, Willis LH, Bateman LA, et al. Association of the Composite Inflammatory Biomarker Glyca, With Exercise-Induced Changes in Body Habitus in Men and Women With Prediabetes. *Oxid Med Cell Longev* (2017) 2017:3608287. doi: 10.1155/2017/5608287

Conflict of Interest: The authors declare that the research was conducted in the absence of any commercial or financial relationships that could be construed as a potential conflict of interest.

frontiers in Immunology

ORIGINAL RESEARCH
published: 10 February 2022
doi: 10.3389/fimmu.2022.820058

Method Matters: Effect of Purification Technology on Neutrophil Phenotype and Function

*Marfa Blanter†, Seppe Cambier†, Mirre De Bondt†, Lotte Vanbrabant, Noëmie Pörtner, Sara Abouelasrar Salama, Mieke Metzemaekers, Pedro Elias Marques, Sofie Struyf, Paul Proost and Mieke Gouwy**

Laboratory of Molecular Immunology, Department of Microbiology, Immunology and Transplantation, Rega Institute, KU Leuven, Leuven, Belgium

OPEN ACCESS

Edited by:
Krishna Rajarathnam, University of Texas Medical Branch at Galveston, United States

Reviewed by:
Silvano Sozzani, Sapienza University of Rome, Italy
Shuvasree Sengupta, University of Michigan, United States

***Correspondence:**
Mieke Gouwy
mieke.gouwy@kuleuven.be

†These authors have contributed equally to this work and share first authorship

Specialty section:
This article was submitted to Inflammation, a section of the journal Frontiers in Immunology

Received: *22 November 2021*
Accepted: *19 January 2022*
Published: *10 February 2022*

Citation:
Blanter M, Cambier S, De Bondt M, Vanbrabant L, Pörtner N, Abouelasrar Salama S, Metzemaekers M, Marques PE, Struyf S, Proost P and Gouwy M (2022) Method Matters: Effect of Purification Technology on Neutrophil Phenotype and Function. Front. Immunol. 13:820058. doi: 10.3389/fimmu.2022.820058

Neutrophils are the most abundant leukocytes in human blood and the first cells responding to infection and injury. Due to their limited *ex vivo* lifespan and the impossibility to cryopreserve or expand them *in vitro*, neutrophils need to be purified from fresh blood for immediate use in experiments. Importantly, neutrophil purification methods may artificially modify the phenotype and functional characteristics of the isolated cells. The aim of this study was to expose the effects of 'classical' density-gradient purification *versus* the more expensive but faster immunomagnetic isolation on neutrophil phenotype and functionality. We found that in the absence of inflammatory stimuli, density-gradient-derived neutrophils showed increased polarization responses as well as enhanced release of reactive oxygen species (ROS), neutrophil extracellular traps (NETs) and granular proteins compared to cells derived from immunomagnetic isolation, which yields mostly quiescent neutrophils. Upon exposure to pro-inflammatory mediators, immunomagnetic isolation-derived neutrophils were significantly more responsive in polarization, ROS production, phagocytosis, NETosis and degranulation assays, in comparison to density-gradient-derived cells. We found no difference in chemotactic response in Multiscreen and under-agarose migration assays, but Boyden assays showed reduced chemotaxis of immunomagnetic isolation-derived neutrophils. Finally, we confirmed that density-gradient purification induces artificial activation of neutrophils, evidenced by *e.g.* higher expression of CD66b, formyl peptide receptor 1 (FPR1) and CD35, and the appearance of a separate neutrophil population expressing surface molecules atypical for neutrophils (*e.g.* CXCR3, MHC-II and CD14). Based on these results, we recommend using immunomagnetic separation of neutrophils for studying neutrophil polarization, phagocytosis, ROS production, degranulation and NETosis, whereas for Boyden chemotaxis assays, the density-gradient purification is more suitable.

Keywords: neutrophil activation, immunomagnetic separation, density-gradient centrifugation, migration, degranulation, phagocytosis, NETosis, respiratory burst

1 INTRODUCTION

Neutrophilic granulocytes, or neutrophils, constitute the majority (50-70%) of circulating human leukocytes (1). These innate immune cells have a broad variety of effector functions and are the first responding cells during inflammation and infection. Under physiological conditions, neutrophils circulate in a resting state to patrol the body for pathogens, being indispensable for the initiation, modulation and resolution of inflammation. The presence of an inflammatory or infectious trigger induces priming and activation of neutrophils. This process is tightly regulated, as activated neutrophils release toxic content, which can be detrimental to healthy tissue. Upon appropriate stimulation, neutrophils initiate the process of rolling and adhesion to the vessel wall, followed by transmigration into the inflamed tissue where they exert their effector functions (2, 3). These functions include phagocytosis, production of reactive oxygen species (ROS), release of pre-synthesized proteins (*e.g.* defensins) and enzymes (*e.g.* myeloperoxidase [MPO], neutrophil elastase [NE] and matrix metalloproteinases [MMPs]), release of neutrophil extracellular traps (NETs) and the production of cytokines (*e.g.* interleukin-1β [IL-1β], tumor necrosis factor-α [TNF-α]) and chemokines (4). After eliminating the potentially harmful agent, neutrophils either undergo apoptosis and clearance by local macrophages or return to the bone marrow (5, 6). Circulating blood neutrophils that are not recruited to tissue are believed to have a limited lifespan of only 7-10 hours, whereas neutrophils in inflamed tissues may live up to 7 days (7).

To study neutrophils *ex vivo*, the cells should ideally resemble the circulating, quiescent population found in human blood. However, as neutrophils are terminally differentiated cells, they cannot be expanded *in vitro* nor successfully cryopreserved, making them challenging to use in experiments (8). Therefore, the most valid approach for studying human neutrophils in their most physiological state is the use of freshly isolated cells from peripheral blood samples. Following blood collection, neutrophils should be purified as soon as possible (within 1 hour after collection) to prevent artificial activation and apoptosis (9). To date, several methods have been established to isolate neutrophils from whole blood samples. However, the isolation procedure may significantly influence the quantity and quality of the purified cells. The oldest established method by Boyum et al. (10) relies on density-gradient purification, in which blood is pipetted on top of a polysaccharide solution (*e.g.* Pancoll, Ficoll) and subsequently centrifuged. This leads to the formation of a gradient, with peripheral blood mononuclear cells (PBMCs) resting on top of the polysaccharide layer while the granulocytes sediment together with the erythrocytes. After removing the PBMC layer, the cells are subjected to a dextran treatment (sedimenting the majority of erythrocytes) and subsequently exposed to a hypotonic shock (for lysis of residual erythrocytes) (10). Over time, new methods have been developed such as fluorescence-activated cell sorting (FACS). With this technique, cells are selected based on their size, morphology and protein expression, which allows the separation of different cell types from a mixture. However, this method is time-consuming and expensive, and not ideal for neutrophils due to the activation induced by cross-linking of surface receptors with antibodies (11). The most recently established technique is immunomagnetic selection using magnetic beads coupled to antibodies against non-neutrophil lineage markers. This technique is less time-consuming (approximately 1 hour of purification compared to *circa* 3 hours needed for density-gradient purification) but is more expensive compared to the standard density-gradient purification. Moreover, comparing studies that use different neutrophil isolation methods may be challenging, as research suggests that cells isolated with different methods may have a distinct activation state (12, 13). Nowadays, this is especially important since a variety of isolation methods are being used by different research groups.

The aim of this study was to dismantle and compare the effects of density-gradient or immunomagnetic purification methods on neutrophil phenotype and function. We found that neutrophils purified by immunomagnetic beads generally possess a lower activation state and respond more potently to activating stimuli in a variety of functional assays, compared to density-gradient-derived neutrophils. This shows that the purification method is a significant confounding factor. Our findings underline the importance of choosing the correct methodology for the unbiased study of neutrophils *in vitro*.

2 MATERIALS AND METHODS

2.1 Reagents

Recombinant human CXCL8(6-77), TNF-α, interferon-γ (IFN-γ), IL-1β and granulocyte-macrophage colony-stimulating factor (GM-CSF) were purchased from Peprotech (Rocky Hill, NJ, USA). The bacterial tripeptide N-formyl-methionyl-leucyl-phenylalanine (fMLF), peptidoglycan from *Staphylococcus aureus* (PGN), phorbol 12-myristate 13-acetate (PMA), lipopolysaccharide (LPS) from *Klebsiella pneumoniae* and LPS from *Escherichia coli* were purchased from Sigma-Aldrich (St. Louis, MO, USA). CpG oligodeoxynucleotides were purchased from InvivoGen (San Diego, CA, USA).

2.2 Neutrophil Purification

Venous blood from healthy human volunteers was collected in EDTA-coated vacutainer tubes (BD Biosciences, Franklin Lakes, NJ, USA) and processed within 15 minutes after withdrawal.

2.2.1 Density-Gradient Purification

Whole blood was diluted 1:2 in sterile Dulbecco′s Phosphate Buffered Saline (DPBS) without Ca^{2+} and Mg^{2+} and slowly pipetted on top of Pancoll (1.077 g/ml) (PAN-Biotech, Aidenbach, Germany) in a 2:3 volume ratio. The blood was spun down for 30 minutes at 400g without braking. Following centrifugation, the three top layers (*i.e.* diluted plasma, PBMCs and Pancoll) were carefully discarded, leaving a red pellet with erythrocytes and granulocytes. The pellet was then mixed with

equal volumes of DPBS and 6% (*w/v*) dextran in DPBS, followed by incubation for 30 minutes at 37°C. Next, the supernatant containing neutrophils was transferred to a clean tube, and the cells were washed twice with DPBS (centrifugations were performed for 10 minutes at 177g). Subsequently, the cell pellet was suspended in 5 ml DPBS, and 25 ml sterile ultrapure water was added. After 30 seconds, 10 ml 3.6% (*w/v*) NaCl was added and mixed by inversion. The cells were spun down and washed with DPBS, whereupon a small aliquot was diluted in Turk's solution (Sigma-Aldrich) and used to determine the cell concentration using a Bürker chamber. The average yield (± SD) was 1.72×10^6 (± 0.66×10^6) neutrophils/ml blood. The average purity (± SD) of the neutrophils (defined as live $CD16^+CD66b^+$ cells) was 95.2 (± 1.6) %.

2.2.2 Immunomagnetic Isolation

Immunomagnetic isolation was performed using the EasySep Direct Human Neutrophil Isolation kit (StemCell Technologies, Vancouver, BC, Canada) according to the manufacturer's instructions. Briefly, whole blood was transferred to 15 ml tubes (5 ml/tube) and supplemented with Isolation Cocktail (50 µl/ml of blood) and Rapidspheres (50 µl/ml of blood). After thorough mixing, the blood was incubated for 5 minutes at room temperature (RT). Subsequently, the mixture was diluted in DPBS without Ca^{2+} and Mg^{2+} (final volume of 12 ml/tube), and the tubes were transferred to an EasyEights magnet (StemCell Technologies). After incubation for 10 minutes at RT, the supernatant (containing plasma, neutrophils and a small percentage of contaminating cells) was carefully collected, transferred to a clean tube, supplemented with Rapidspheres (same volume as in the first step), mixed and incubated for 5 minutes at RT. The tube was placed back in the magnet and incubated for 5 minutes at RT. The neutrophils were carefully transferred to a clean tube and incubated for another 5 minutes in the magnet. Finally, the neutrophils were collected, spun down (8 minutes at 177g) and suspended in DPBS. A small aliquot of the cells was mixed with Turk's solution and used to determine the cell concentration using a Bürker chamber. The average yield (± SD) was 1.75×10^6 (± 0.51×10^6) neutrophils/ml blood. The average purity (± SD) of the neutrophils (defined as live $CD16^+CD66b^+$ cells) was 97.3 (± 1.3) %.

2.3 Actin Polymerization Assay

The degree of actin polymerization in purified neutrophils was measured as previously described (14). Briefly, neutrophils were stimulated in suspension with CXCL8 (1-30 ng/ml) or fMLF (10^{-9}-10^{-7} M) for 30 seconds in an uncoated U-bottom 96-well plate (1.5×10^6 cells/ml [70 µl/well] in pre-warmed [37°C] RPMI-1640 + 1 mg/ml human serum albumin [HSA; Belgian Red Cross]). After stimulation, cells were placed on ice, fixed and permeabilized using the BD Cytofix/Cytoperm kit (BD Biosciences). Subsequently, the cells were resuspended in BD Perm/Wash buffer (BD Biosciences) containing Alexa Fluor 555-Phalloidin (2 U/ml; Invitrogen, Waltham, MA, USA), a dye which selectively stains filamentous (F)-actin. The cells were incubated for 20 minutes at 4°C, whereupon they were washed twice with BD Perm/Wash buffer and resuspended in flow cytometry buffer (PBS + 2% [*v/v*] fetal calf serum [FCS; Sigma-Aldrich] + 2 mM EDTA). The cellular F-actin content was quantified by flow cytometry using a BD LSRFortessa™ X-20 (BD Biosciences) equipped with DIVA software (BD Biosciences). FlowJo software (BD Biosciences, v.10.8.1) was used for downstream analysis.

2.4 Shape Change Assay

Shape change assays were performed to determine the responsiveness of suspended neutrophils to chemoattractants. Serial dilutions of CXCL8 (3-30 ng/ml) or fMLF (10^{-9}-10^{-7} M) in shape change buffer (HBSS without Ca^{2+} and Mg^{2+}, supplemented with 10 mM HEPES) were added to a flat-bottom 96-well plate (50 µl/well). Shape change buffer without chemoattractants served as negative control. Neutrophils (50 µl/well) were added to the plate at a concentration of 0.6×10^6 cells/ml in prewarmed (37°C) shape change buffer. Following a stimulation period of 3 minutes, neutrophils were fixed with 100 µl of ice-cold 4% (*w/v*) formaldehyde in shape change buffer. One hundred cells per condition were counted microscopically and categorized as either activated (blebbed and elongated cells) or resting/not activated (round). The assessment was performed by two independent researchers, of whom at least one was blinded to the experimental conditions.

2.5 *In Vitro* Cell Migration Assays

The chemotactic response of purified neutrophils towards CXCL8 (3-150 ng/ml) or fMLF (10^{-9}-10^{-6} M) was measured in three different *in vitro* chemotaxis assay systems, namely the Boyden chamber assay, the Multiscreen assay and the under-agarose assay. For the classical 48-well Boyden chamber technique, chemoattractants and neutrophils (1×10^6 cells/ml) were suspended in Boyden chamber buffer (HBSS buffer enriched with 1 mg/ml HSA). Chemoattractants were added to the lower compartment of the Boyden chamber (30 µl/well) and were covered with a 5 µm pore size polyvinylpyrrolidone (PVP)-free polycarbonate membrane (GE Water & Process Technologies, Feasterville-Trevose, PA, USA). Buffer without chemoattractant was used as negative control. Neutrophils were added to the upper part of the chamber (50 µl/well) and migration was allowed during 45 minutes at 37°C. Subsequently, cells on the membranes were fixed and stained (Hemacolor Solution I–III, Merck, Kenilworth, NJ, USA). Migrated neutrophils were microscopically counted at the lower side of the membrane in 30 separate fields for each test condition. The directional migration of the neutrophils towards a chemoattractant is expressed as the chemotactic index (CI), which was calculated by dividing the total number of neutrophils migrated towards chemoattractant by the total number of cells migrated towards buffer.

The Multiscreen plate (Millipore Corporation, Billerica, MA, USA) is a disposable device with a 96-well filter plate (5 µm pore-size) and a 96-well receiver plate (15). Neutrophil cell migration through the 96-well filter plate occurs in response to a chemotactic gradient. The cell suspension (100 µl/well in the 96-well filter plate at a concentration of 2.5 x 10^6 cells/ml) and chemoattractant

dilutions (150 µl/well in the 96-well receiver plate) were prepared in HBSS buffer supplemented with 0.1% (*w/v*) bovine serum albumin (BSA; endotoxin free, Sigma-Aldrich). The plate was incubated for 1 hour at 37°C, whereupon the 96-well filter plate was removed and the neutrophils in the receiver plate were quantified using the luminescence ATP detection assay system (PerkinElmer, Waltham, MA, USA). The chemotactic index was calculated by dividing the luminescence value of the chemoattractant condition by the luminescence value of the buffer condition.

The under-agarose assay uses the migration distance of neutrophils under an agarose gel as a parameter to measure the chemotactic effect of substances (16). Agarose gels were prepared in 53 mm Ø plastic tissue culture dishes one day before the assay. To prepare the gels, equal volumes of prewarmed (48°C) solution A and solution B were mixed. Solution A contained 20% (*v/v*) FCS and 20% (*v/v*) 10x concentrated Eagle's minimum essential medium with Earle's salts (EMEM; Invitrogen) in pure water. Solution B consisted of 1.8% (*w/v*) agarose (Indubiose A37; Biosepra Inc., Marlborough, MA, USA) in pure water. This mixture was warmed up in a microwave until complete dissolving of the agarose. The solution was then cooled down to 48°C before mixing it with solution A. Immediately after mixing, 6 ml of solution A/B was poured per tissue culture dish; this was left for 30 minutes to cool down to RT before transfer to 4°C. The gels were left to settle overnight at 4°C. The day that the agarose assay was performed, six series (per dish) of three wells (3 mm Ø and 3 mm inter-space) were cut in the gel in a straight line using a template and a stainless steel punch with inside bevel. The agarose cores were removed with the same steel punch connected to a vacuum system. The gels were allowed to equilibrate at 37°C in a 5% CO_2 incubator until sample dilutions and cells were prepared. Neutrophil suspension (3×10^7 cells/ml) and chemokine dilutions were prepared in HBSS buffer supplemented with 1 mg/ml HSA. The center well of each series of three wells was loaded with human neutrophils (3×10^5 cells in 10 µl), whereas the inner and outer wells were loaded with a buffer control and varying concentrations of chemoattractant, respectively. The agarose gels with the cells were incubated for 2 hours at 37°C/5% CO_2, allowing sufficient time for the neutrophils to migrate towards the chemotactic gradient of the chemoattractant (distance X) or the buffer control (random migration distance Y). The migration distance (X-Y) was estimated and expressed as the percentage of maximal possible migration (3 mm).

2.6 Phagocytosis Assay

The capacity of purified neutrophils to phagocytose *S. aureus*-coated beads was evaluated microscopically. Black clear-bottom 96-well plates (Greiner Bio-One, Vilvoorde, Belgium) were coated with poly-L-lysine (0.1 mg/ml in sterile water; Sigma-Aldrich) for 1 hour at RT. Afterwards, the plate was washed twice with sterile distilled water and air-dried. Purified neutrophils were suspended in Live Cell Imaging solution (Invitrogen) supplemented with HEPES (20 mM) and calcein acetoxymethyl ester (Calcein AM; 1 µM; Invitrogen) to monitor viability. Subsequently, cells were added to the plate (0.05×10^6 cells/well) and incubated for 30 minutes at 37°C. Afterwards, inducers (fMLF [10^{-7} M], LPS from *K. pneumoniae* [100 ng/ml] or CXCL8 (50 ng/ml) and pHrodo *S. aureus*-coated beads (62.5 µg/ml; Invitrogen) were carefully added on top of the cells. Phagocytic uptake of the beads was quantified and continuously monitored for 4 hours using the Incucyte S3 live cell imaging system v.2020A (Sartorius, Göttingen, Germany).

2.7 ROS Production Assay

A chemiluminescence-based assay was used to determine ROS production by neutrophils. Cells were suspended in RPMI-1640 medium without phenol red at a final concentration of 1.5×10^6 cells/ml and were pre-incubated at 37°C in the presence or absence of the priming agent TNF-α (50 ng/ml). Following 10 minutes of incubation, cells were added to a white, clear-bottom, 96-well microtiter plate (PerkinElmer) and stimulated with PMA (150 ng/ml), ultrapure LPS from *E. coli* (10 µg/ml), PGN from *S. aureus* (10 µg/ml), CpG oligodeoxynucleotides (3 µM), TNF-α (50 ng/ml) or IL-1β (500 ng/ml) in the presence of 5 mM luminol (Sigma-Aldrich). Kinetic measurements of luminol oxidation were performed during 1.5 hours at 37°C using a Clariostar Monochromator Microplate Reader (BMG Labtech, Orthenberg, Germany). The results were subtracted by values obtained with PMA stimulation in the absence of luminol.

2.8 NETosis Assay

To assess the capacity of neutrophils to release DNA in response to stimuli, a NETosis assay was performed as described by Cockx et al. (17). In short, neutrophils were suspended at a concentration of 0.5×10^6 cells/ml in RPMI-1640 medium without phenol red containing 50 nM SYTOX Green (Invitrogen). The cells were transferred to flat-bottom 96-well plates coated with poly-L-lysine (0.1 mg/ml in sterile water) and incubated for 30 minutes at 37°C to allow adherence. Subsequently, one of the following compounds was added: PMA (150 ng/ml), PGN (0.1-10 µg/ml), TNF-α (30 ng/ml), IL-1β (100 ng/ml) or IFN-γ (100 ng/ml). Additionally, for IL-1β and IFN-γ stimulation, a priming agent (TNF-α [30 ng/ml]) was included. In that case, the cells were first pre-incubated for 10 minutes at 37°C with the priming agent before adding the stimulus. After addition of the stimuli, the cells were incubated for 5 hours at 37°C and continuously monitored by the Incucyte S3 live cell imaging system. The relative area of the DNA released by neutrophils was determined using the Incucyte S3 software as described (17).

To confirm that the neutrophils released DNA due to NETosis, an additional immunofluorescence staining was performed. To this end, a 12-well tissue culture plate was filled with 18 mm Ø sterile glass coverslips. The coverslips were coated with poly-L-lysine (0.1 mg/ml in sterile water) for 1 hour at RT, washed twice with PBS and air-dried. Neutrophils were suspended in RPMI-1640 without phenol red at a concentration of 0.6×10^6 cells/ml, and 900 µl was added per well. The plate was incubated for 30 minutes at 37°C to allow adherence of the cells. After 30 minutes, 100 µl of PMA (final concentration 150 ng/ml)

or RPMI-1640 medium was carefully added on top of the cells. The plate was incubated for 3 hours at 37°C, whereupon the medium was removed and the cells were fixed with 4% (*w/v*) paraformaldehyde (AlfaAesar, Ward Hill, MA, USA) in HBSS buffer containing Ca^{2+} and Mg^{2+} for 15 minutes at RT. After fixation, the cells were washed twice with HBSS buffer and blocked with blocking agent (PBS + 2% [*w/v*] BSA + 10% [*v/v*] FCS) for 30 minutes at RT. The cells were then treated with 500 µl polyclonal rabbit anti-human MPO antibody (diluted 1:1000 in blocking agent; Agilent Technologies, Santa Clara, CA, USA; cat nr #A0398) and incubated overnight at 4°C in the dark. Following incubation, the cells were washed twice with HBSS buffer and incubated for 1 hour at RT with 500 µl HBSS buffer containing Hoechst (10 µg/ml; Molecular Probes, Eugene, OR, USA), Alexa Fluor 594-conjugated wheat germ agglutinin (10 µg/ml; Invitrogen) and Alexa Fluor 488-conjugated chicken-anti-rabbit antibody (dil 1:1000, Invitrogen, cat nr #A21441). Subsequently, the cells were washed three times with HBSS buffer, and the coverslips were fixed on glass microscope slides using ProLong Diamond (Invitrogen). The cells were imaged using a Zeiss fluorescence microscope with a 63x magnification objective.

2.9 Neutrophil Degranulation and CXCL8 Production Assays

Neutrophils were induced with a variety of stimuli to assess their capacity to release granular proteins and to produce cytokines. Neutrophils were suspended at a concentration of 1×10^6 cells/ml in RPMI-1640 medium containing 10% (*v/v*) FCS, GM-CSF (5 ng/ml) and one of the following compounds: PGN (1 µg/ml), LPS from *E. coli* (5 µg/ml), IL-1β (10 ng/ml), TNF-α (10 ng/ml) or IFN-γ (10 ng/ml). After 2 and 24 hours, the cells were collected and spun down (5 min, 16000g). The supernatants were stored at -20°C until further analysis.

Release of NE and MPO after 2 hours of stimulation was determined by commercially available DuoSet ELISAs (R&D, Minneapolis, MN, USA; resp. cat nr DY9167 and DY3174), according to the manufacturer's instructions. The concentration of CXCL8 in the supernatant after 24 hours of stimulation was measured by a sandwich ELISA developed in-house (18).

2.10 Phenotypical Analysis of Neutrophils

2×10^5 purified neutrophils were incubated with 1:20 diluted FcR block (Miltenyi Biotec, Bergisch Gladbach, Germany) and 1:1000 diluted Zombie Aqua 516 (Biolegend, San Diego, CA, USA) or 1:20000 diluted Fixable Viability Stain 620 (BD Biosciences) in PBS for 15 minutes at RT. Subsequently, cells were washed twice with flow cytometry buffer (PBS + 2% [*v/v*] FCS + 2 mM EDTA) and stained with fluorescently labeled antibodies. Antibodies used in this study were titrated in-house and are listed in **Supplementary Table 1**. Following incubation for 25 minutes at 4°C, cells were washed twice with flow cytometry buffer and fixed with BD Cytofix (BD Biosciences). Samples were run on a BD LSRFortessa™ X-20 equipped with DIVA software. FlowJo software was used for downstream analysis. Neutrophils were gated as $CD16^+CD66b^+$ cells within the population of live, single cells (**Supplementary Figure 1**).

2.11 Statistics

No normal distribution of data was detected as evaluated by Shapiro-Wilk tests. Wilcoxon matched-pairs signed rank tests were used to determine statistical differences between neutrophils purified with immunomagnetic or density-gradient separation. Statistical tests for comparison were two-sided, and $p < 0.05$ was considered significant. Data are shown as box-and-whiskers plots with the central line in the box representing the median, while the box spands the interquartile range, with the whiskers indicating the full distribution of the data. Alternatively, results from each individual donor are connected by lines. All outliers were included in the data and all data points are shown. Statistical analysis and visualization of the data was performed using GraphPad Prism 9.3.1.

2.12 Study Approval

The study was approved by the Ethics Committee of the University Hospital Leuven, and all participants signed an informed consent form according to the ethical guidelines of the Declaration of Helsinki (study number: S58418).

3 RESULTS

3.1 Neutrophils Purified by Immunomagnetic Isolation Are More Responsive to Chemoattractants in Polarization Assays but Not in Migration Assays

To compare the chemoattractant sensitivity of neutrophils purified through density-gradient centrifugation *versus* immunomagnetic separation, we performed two different polarization assays: actin polymerization and shape change assays. The former quantifies the cellular content of polymerized (F-)actin while the latter detects visible morphological changes in neutrophils as a measure of activation. Baseline F-actin contents did not significantly differ between neutrophils purified by density-gradient centrifugation or immunomagnetic isolation (**Figure 1A**). Stimulation by CXCL8 or fMLF increased the levels of F-actin in neutrophils purified by both methods, but this increase was significantly greater in immunomagnetically purified cells (**Figures 1B, C**). Compared to density-gradient-derived cells, neutrophils isolated through immunomagnetic separation showed less pronounced morphological signs of activation at baseline, but were significantly more responsive to CXCL8 (10-30 ng/ml) and fMLF (10^{-9}–10^{-7} M) in shape change assays (**Figures 1D–F**).

Next, we compared the migratory properties of isolated neutrophils in three different *in vitro* chemotaxis assays: the 96-well Multiscreen assay, the under-agarose assay and the 48-well Boyden assay (**Figures 1G–O**). The Multiscreen and the Boyden assay are both based on vertical migration of neutrophils through a membrane. The substantial difference between these approaches is that the Boyden assay only allows to microscopically count cells adhered to the lower side of the membrane. The Multiscreen technique, on the other hand, uses chemiluminescence to quantify all cells that have passed the membrane to the lower compartment in response to chemoattractants. The under-agarose

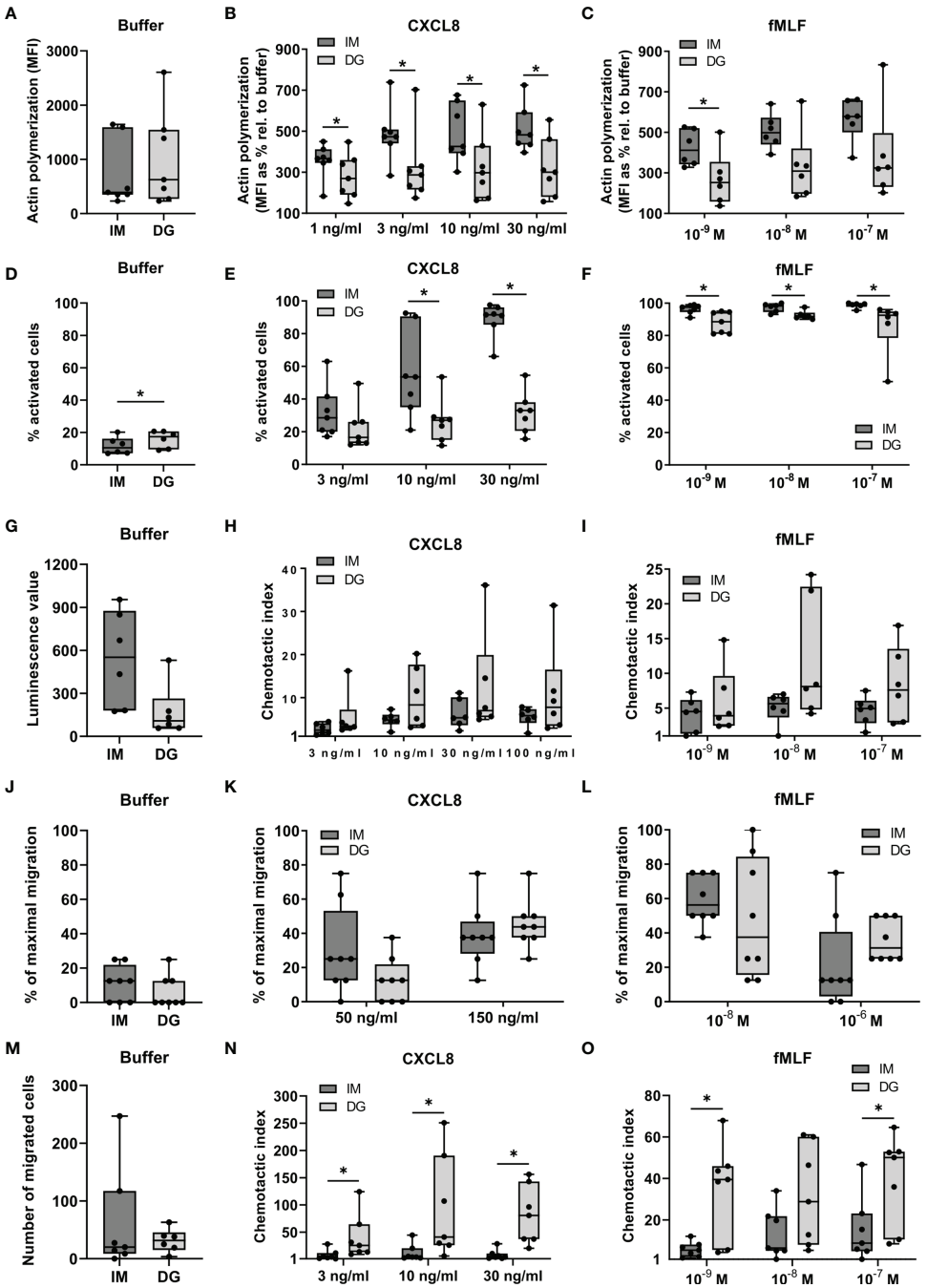

FIGURE 1 | Neutrophils purified by immunomagnetic isolation are more responsive to chemoattractants in polarization assays but not in migration assays. Peripheral blood neutrophils were isolated by immunomagnetic (IM) or density-gradient (DG) purification. **(A–C)** A flow cytometric assay was used to quantify the content of polymerized (F-) actin in the cells. Neutrophils in suspension were stimulated with CXCL8, fMLF or buffer (pre-warmed RPMI-1640 medium supplemented with 1 mg/ml HSA) for 30 seconds. Fixed and permeabilized cells were stained with Alexa Fluor 555 Phalloidin, which selectively binds to polymerized actin. **(A)** Results from unstimulated neutrophils (only buffer) are represented as median fluorescence intensities (MFI). **(B, C)** Results from chemoattractant-stimulated neutrophils are represented as the MFIs relative to buffer control (in %). **(D–F)** Shape change assays were used to assess the morphological changes occurring in neutrophils in response to chemoattractants. Neutrophils in suspension were **(D)** left untreated or stimulated with **(E)** CXCL8 or **(F)** fMLF for a period of 3 minutes. Results are represented as the % activated neutrophils. **(G–O)** The **(G, J, M)** spontaneous and **(H–I, K–L, N–O)** chemoattractant-induced migratory response of neutrophils was evaluated in three different *in vitro* chemotaxis assays, namely: **(G–I)** the Multiscreen chemotaxis assay, **(J–L)** the under-agarose assay and **(M–O)** the 48-well Boyden chamber chemotaxis assay. Results are represented as **(G)** the luminescence value, **(J–L)** % of maximal migration, **(M)** number of migrated cells or **(H, I, N, O)** chemotactic indices (CI). Data are shown as box-and-whisker plots (box: median with interquartile range, whiskers: full data distribution), with each dot representing an individual healthy donor (n = 6-8). Results were statistically analyzed by Wilcoxon matched-pairs signed rank test (*$p < 0.05$ for statistical differences between neutrophils purified with immunomagnetic or density-gradient separation).

assay examines horizontal migration of the neutrophils along a chemoattractant gradient, the extent of which is estimated through microscopical examination.

The spontaneous migratory responses in all three assays were not significantly different between neutrophils derived from immunomagnetic and density-gradient separation (**Figures 1G, J, M**). The migratory response towards CXCL8 or fMLF was not significantly different between neutrophils purified by immunomagnetic and density-gradient separation in the 96-well Multiscreen and the under-agarose assay (**Figures 1H, I, K, L**). However, neutrophils purified by immunomagnetic beads showed a significantly reduced potency to migrate towards CXCL8 and fMLF in the Boyden chamber chemotaxis assay (**Figures 1N, O**).

3.2 Neutrophils Purified by Immunomagnetic Isolation Show Increased Phagocytosis of Bacteria-Coated Beads

Purified neutrophils were stimulated with the chemokine CXCL8 or bacterial products (LPS, fMLF), and the phagocytosis of *S. aureus*-coated beads was monitored for 4 hours (**Figures 2A, B**). Spontaneous uptake of beads, displayed as buffer condition, was significantly higher in neutrophils purified with immunomagnetic separation compared to density-gradient-derived cells. Furthermore, after stimulation with fMLF, LPS or CXCL8, the increased phagocytosis of beads by cells purified by immunomagnetic selection is maintained (**Figures 2A, B**).

3.3 Neutrophils Purified by Immunomagnetic Isolation Release More ROS Following Priming With TNF-α

To evaluate ROS generation by purified neutrophils, a chemiluminescence-based assay was employed. Density-gradient-derived neutrophils showed enhanced basal ROS production compared to cells isolated by immunomagnetic separation (**Figure 3A**). Upon PMA stimulation, neutrophils from both purifications readily produced ROS, but the production was significantly higher by cells derived from immunomagnetic purification (**Figure 3B**). Priming with TNF-α caused a 5-10 fold increase in ROS production compared to the buffer condition independently of the purification method (**Figure 3C**). Next, we examined the capacity of TNF-α-primed neutrophils to produce

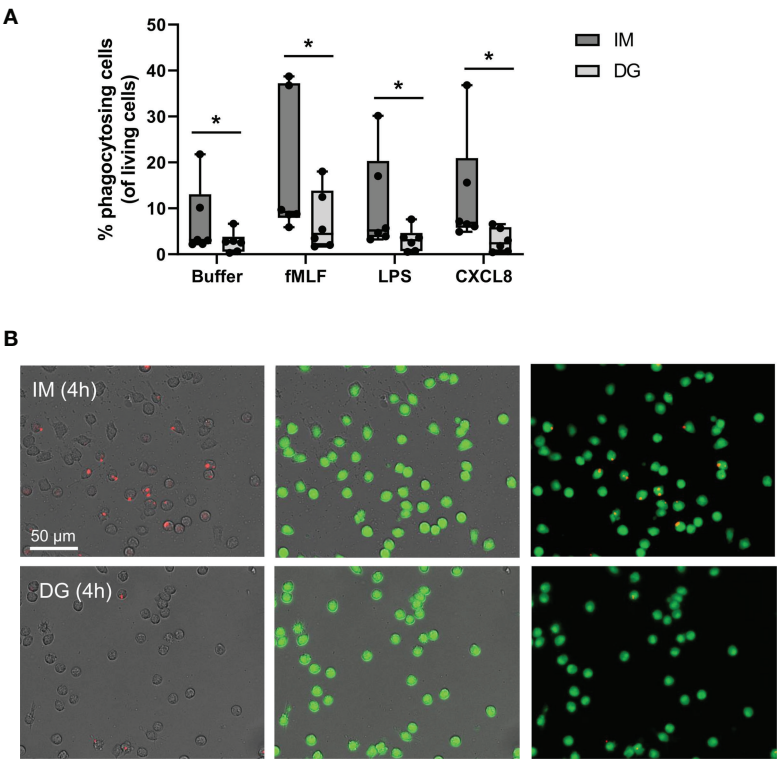

FIGURE 2 | Neutrophils purified by immunomagnetic isolation show increased phagocytosis of bacteria-coated beads. Peripheral blood neutrophils were isolated by immunomagnetic (IM) or density-gradient (DG) purification. The capacity of neutrophils to actively engulf extracellular particles was quantified using *S. aureus*-coated beads and imaged using the Incucyte S3 live cell imaging system. **(A)** Neutrophils were additionally stimulated with buffer, fMLF (10^{-7} M), LPS (100 ng/ml) or CXCL8 (50 ng/ml). **(B)** Representative image of phagocytosed beads (red) and purified, living neutrophils (green) after 4 hours of stimulation with fMLF. Results are represented as the percentage phagocytosing neutrophils normalized to the amount of living cells. Data are shown as box-and-whisker plots (box: median with interquartile range, whiskers: full data distribution), with each dot representing an individual healthy donor (n = 6) and were statistically analyzed by Wilcoxon matched-pairs signed rank test (*$p < 0.05$ for statistical differences between neutrophils purified with immunomagnetic or density gradient separation).

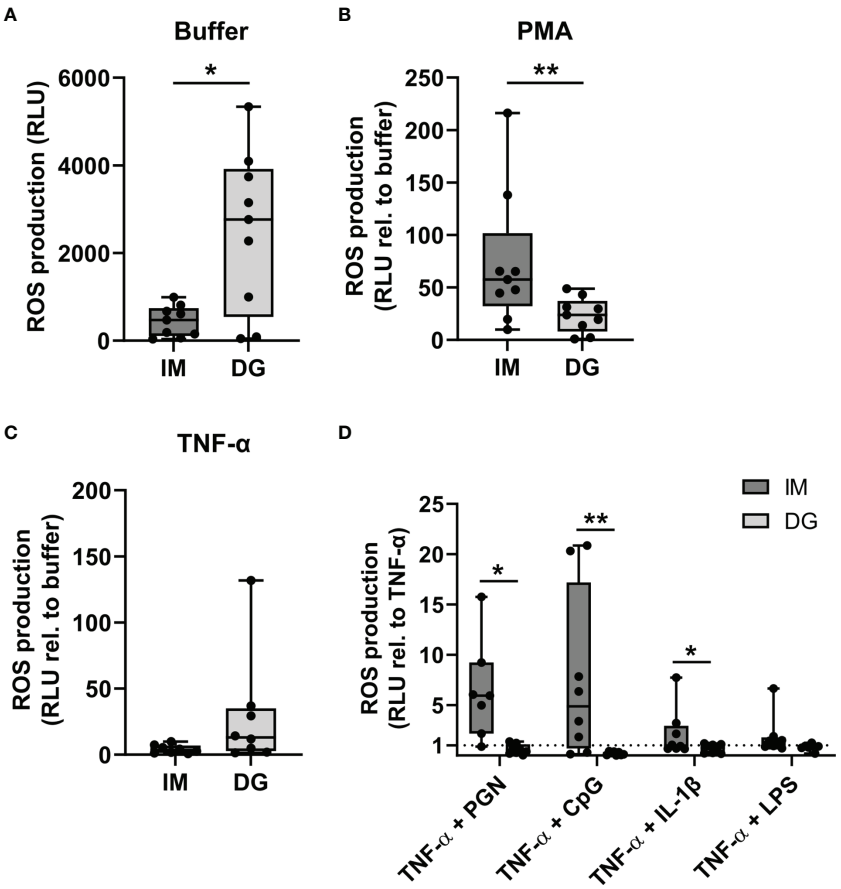

FIGURE 3 | Neutrophils purified by immunomagnetic isolation release more ROS following priming with TNF-α. Peripheral blood neutrophils were isolated by immunomagnetic (IM) or density-gradient (DG) purification. ROS production was assessed by kinetic measurements of luminol oxidation during 1.5 hours after stimulation with **(A)** buffer, **(B)** 150 ng/ml PMA or **(C)** 50 ng/ml TNF-α. Results are represented as relative light units (RLU) for unstimulated neutrophils (only buffer) or as the fold change in RLU relative to the corresponding buffer values for the stimulated neutrophils. **(D)** Neutrophils were pretreated (primed) with 50 ng/ml TNF-α during 10 minutes at 37°C, followed by stimulation with 10 μg/ml PGN, 3 μM CpG, 500 ng/ml IL-1β, or 10 μg/ml LPS. Kinetic measurements of luminol oxidation were performed during 1.5 hours. Results are represented as the fold change in RLU relative to stimulation with TNF-α alone. Data are shown as box-and-whisker plots (box: median with interquartile range, whiskers: full data distribution), with each dot representing an individual healthy donor (n = 8-9). Results were statistically analyzed by Wilcoxon matched-pairs signed rank test (*$p < 0.05$; **$p < 0.01$ for statistical differences between neutrophils purified with immunomagnetic or density-gradient separation).

ROS in response to subsequent stimulation with cytokines (IL-1β) or pathogen-associated molecular patterns (CpG, LPS, and PGN). Immunomagnetic isolation-derived neutrophils primed with TNF-α produced substantially higher ROS levels upon stimulation with PGN or CpG in most of the donors (**Figure 3D**). Only a moderate increase in ROS production was seen upon IL-1β or LPS stimulation of immunomagnetic isolation-derived neutrophils primed with TNF-α. In stark contrast to neutrophils isolated by immunomagnetic purification, TNF-α-primed density-gradient-derived neutrophils failed to enhance ROS production upon subsequent stimulation with IL-1β, CpG, LPS, or PGN (**Figure 3D**).

3.4 Neutrophils Purified by Immunomagnetic Isolation Release Stimulus-Induced NETs More Readily

To compare the capacity of purified neutrophils to release NETs, neutrophils were exposed to cytokines (TNF-α, IL-1β, IFN-γ) or bacterial components (PGN) for a period of 5 hours, during which the release of DNA was monitored. By staining extracellular DNA, NETs could efficiently be detected, as confirmed by immunofluorescent co-staining of DNA and MPO (**Supplementary Figure 2**). PMA, a direct activator of protein kinase C (PKC) was used as a positive control. Upon buffer stimulation, significantly less free DNA was released by immunomagnetic beads-purified neutrophils as compared to density-gradient-derived neutrophils (**Figure 4A**). Upon stimulation with PMA, neutrophils purified with either method underwent NETosis, although the amount of extracellular DNA was significantly higher in immunomagnetic beads-purified neutrophils as compared to density-gradient-derived neutrophils (**Figure 4B**). PGN (10 μg/ml), IL-1β and IFN-γ (the latter two in combination with TNF-α priming) induced NET formation in immunomagnetic bead-purified neutrophils but not in density-gradient-derived neutrophils (**Figure 4B**). Lower concentrations of PGN (0.1-1 μg/ml) or TNF-α, IFN-γ and IL-1β alone did not result in

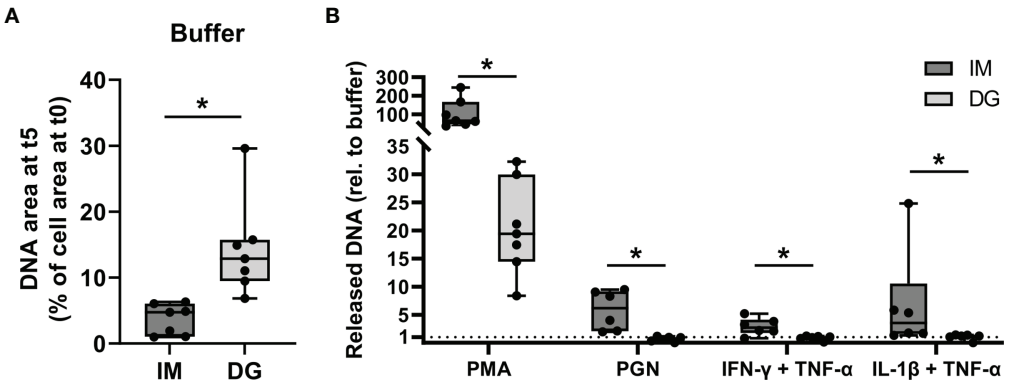

FIGURE 4 | Neutrophils purified by immunomagnetic isolation release stimulus-induced NETs more readily. Peripheral blood neutrophils were isolated by immunomagnetic (IM) or density-gradient (DG) purification. The cells were unprimed (buffer, PMA, PGN conditions) or primed with TNF-α (30 ng/ml) for 10 minutes (IFN-γ, IL-1β conditions). Subsequently, the neutrophils were exposed for 5 hours to **(A)** buffer or **(B)** PMA (150 ng/ml), PGN (10 µg/ml), IFN-γ (100 ng/ml) or IL-1β (100 ng/ml) and the release of NETs was monitored using the Incucyte S3 live cell imaging system. **(A, B)** The area of the released DNA after 5 hours was measured and corrected for the amount of DNA present at the start of the exposure. Data for the stimuli are presented as fold change relative to the corresponding buffer values. Data are shown as box-and-whisker plots (box: median with interquartile range, whiskers: full data distribution), with each dot representing an individual healthy donor (n = 7). Results were statistically analyzed by Wilcoxon matched-pairs signed rank test (*$p < 0.05$ for statistical differences between neutrophils purified with immunomagnetic or density-gradient separation).

NET formation by neutrophils isolated with either method (data not shown).

3.5 Neutrophils Purified by Immunomagnetic Isolation Show Less Spontaneous But More Stimulus-Provoked Degranulation

Neutrophils were stimulated with cytokines (TNF-α, IL-1β, IFN-γ) or Toll-like receptor (TLR) ligands (LPS, PGN) for 2 hours, whereupon the levels of NE and MPO were measured in the supernatant (**Figures 5A, B**). NE and MPO are stored in azurophilic granules and are released through degranulation (19). Compared to cells purified with immunomagnetic beads, density-gradient-derived neutrophils spontaneously released significantly higher amounts of NE and MPO. In contrast, when stimulated with pro-inflammatory stimuli, immunomagnetic beads-purified neutrophils released significantly more MPO (in response to PGN, LPS and TNF-α) and NE (in response to TNF-α). IL-1β and IFN-γ did not evoke any degranulation responses in neutrophils isolated with either method in our setup (data not shown).

3.6 Neutrophils Produce CXCL8 in Response to Cytokines and TLR Ligands Irrespective of the Purification Method

Neutrophils were stimulated with cytokines (TNF-α, IL-1β, IFN-γ) or TLR ligands (LPS, PGN) for 24 hours, whereupon the levels of CXCL8 in the supernatant were measured. CXCL8 is normally not contained in neutrophil granules but must be synthesized *de novo* in order to be released (20). Unstimulated neutrophils purified with immunomagnetic or density-gradient methods produced virtually no CXCL8. In contrast, stimulation with LPS, PGN or TNF-α evoked substantial CXCL8 production. The levels of CXCL8 tended to be higher in neutrophils purified with immunomagnetic beads (**Figure 5C**). IL-1β and IFN-γ did not trigger the production of CXCL8 in our setup (data not shown).

3.7 Neutrophils Acquire an Activated Phenotype and Partially Express Atypical Markers After Density-Gradient Purification

Purified peripheral blood neutrophils (defined as live $CD16^+CD66b^+$ cells) were phenotypically characterized using multicolor flow cytometry, with a focus on the expression of adhesion molecules, activation/maturation markers and chemoattractant receptors. As expected, >90% of neutrophils from healthy donors were mature cells ($CD10^+$) (**Supplementary Figure 3A**). However, purification method-dependent changes in neutrophil phenotype were observed. Density-gradient purification, but not immunomagnetic isolation, induced a partial shift towards reduced size (lower forward scatter [FSC]) and granularity (lower side scatter [SSC]) (**Figures 6A, B**). In addition, neutrophils derived from density-gradient purification expressed a distinct expression pattern of multiple markers related to activation (**Figures 6C–J**). The most prominent characteristics of density-gradient-derived neutrophils include increased expression of CD66b (a granulocyte-specific surface molecule), decreased levels of CD16 (a low-affinity Fcγ receptor) and partial downregulation of CD62L (L-selectin) (**Figures 6C–E**). This expression pattern points to activation of neutrophils, as reported in literature (19). No significant differences were found in the expression of the integrin chain CD11b between neutrophils isolated by immunomagnetic and density-gradient purification (**Supplementary Figure 3B**). A remarkable difference between neutrophils derived from immunomagnetic and density-gradient isolation was the altered expression of chemoattractant receptors. Density-gradient purification (but not immunomagnetic isolation purification) yielded a large proportion of cells that completely

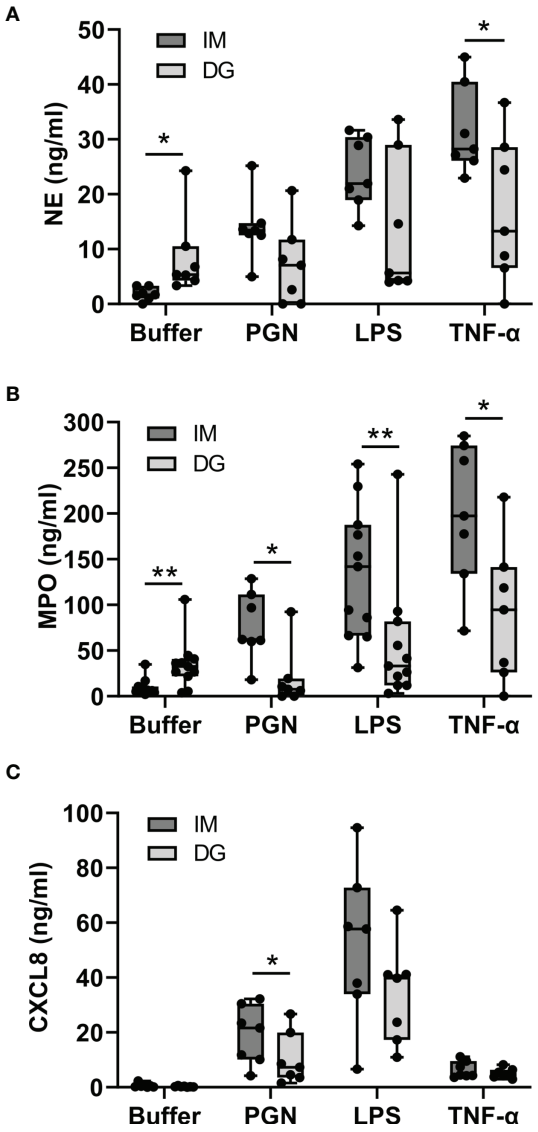

FIGURE 5 | Neutrophils purified by immunomagnetic isolation show less spontaneous but more stimulus-provoked degranulation, whereas CXCL8 is produced irrespective of the purification method. Peripheral blood neutrophils were isolated by immunomagnetic (IM) or density-gradient (DG) purification and stimulated for **(A, B)** 2 hours or **(C)** 24 hours with buffer, PGN (1 µg/ml), LPS (5 µg/ml) or TNF-α (10 ng/ml). Subsequently, the concentration of **(A)** neutrophil elastase (NE), **(B)** myeloperoxidase (MPO) and **(C)** CXCL8 in the cell culture supernatant was determined by ELISA. Data are shown as box-and-whisker plots (box: median with interquartile range, whiskers: full data distribution), with each dot representing an individual healthy donor (n = 7-11). Statistical differences were determined by Wilcoxon matched-pairs signed rank test (*$p < 0.05$; **$p < 0.01$ for statistical differences between neutrophils purified with immunomagnetic or density gradient separation).

lacked the chemokine receptor CXCR2 (**Figure 6F**). This was in contrast to chemokine receptor CXCR1, which was present on all cells derived from both purification methods (**Supplementary Figure 3C**). Both CXCR1 and CXCR2 surface expression levels per cell seemed to be slightly lower on density-gradient-derived cells, but these data did not reach significance (**Supplementary Figures 3D, E**). Furthermore, density-gradient-derived neutrophils were characterized by decreased leukotriene B4 receptor (BLTR1), increased formyl peptide receptor 1 (FPR1) and a trend towards lower expression of complement receptor C5aR, as compared to immunomagnetic isolation-derived cells (**Figures 6G–H** and **Supplementary Figure 3F**). Other markers that were more abundantly expressed on density-gradient-derived cells than on those purified by immunomagnetic isolation included complement receptor 1 (CD35) and the Fcγ receptor CD32 (**Figures 6I, J**). No significant differences were found in the expression of Sialyl-Lewis X (CD15), the tetraspanin CD63 and the Fcγ receptor CD64 (**Supplementary Figures 3G–I**). Finally, we measured the expression levels of several TLRs on neutrophils. Compared to cells purified by immunomagnetic isolation, density-gradient-derived neutrophils expressed lower levels of TLR2, but similar levels of TLR4, TLR6 and TLR9 (**Figure 6K** and **Supplementary Figures 3J–L**).

Remarkably, density-gradient-derived neutrophils expressed several markers that are generally absent on neutrophils purified with the immunomagnetic method (**Figure 7**). We detected significant upregulation of CD11c (an integrin chain), chemokine receptors CXCR3 and CXCR4, FPR2, CD14 (a co-receptor for TLR4), and the antigen-presenting molecules HLA-DR and HLA-DQ (**Figures 7A–G**). It is worth mentioning that these atypical markers were mainly present on the smaller and less granular neutrophil population (20-45% of all neutrophils) that was only detected in cells purified by density-gradient centrifugation (**Figure 7H** and **Supplementary Figures 4**, **5**). Moreover, compared to cells isolated using immunomagnetic beads, density-gradient-derived neutrophils contained a significantly higher proportion of cells that were positive for Annexin V but negative for the live/dead marker FVS620 (**Figure 7I**). These cells also represented a part of the small neutrophil population expressing neutrophil atypical markers (**Figure 7J** and **Supplementary Figure 4I**).

Next, we wanted to exclude the possibility that the observed phenotypic differences between neutrophils purified by the two different methods merely resulted from removal of cells with atypical markers during the immunomagnetic isolation. For example, CD14 is a marker which is commonly found on monocytes. Therefore, it could be possible that the immunomagnetic bead cocktail contains antibodies against CD14, removing not only the contaminating monocyte population but also CD14-expressing neutrophils – if present. To test this hypothesis, we performed a second, immunomagnetic, purification step on neutrophils isolated by density-gradient centrifugation. Following the additional purification step, we still observed the presence of the low-FSC/SSC neutrophil population expressing atypical surface markers (**Figures 7K, L**). Hence, we can conclude that the atypical marker expression is likely induced by the density-gradient purification method rather than being masked by the immunomagnetic bead isolation.

4 DISCUSSION

Neutrophils, representing an indispensable part of the mammalian immune system, can eliminate pathogens through

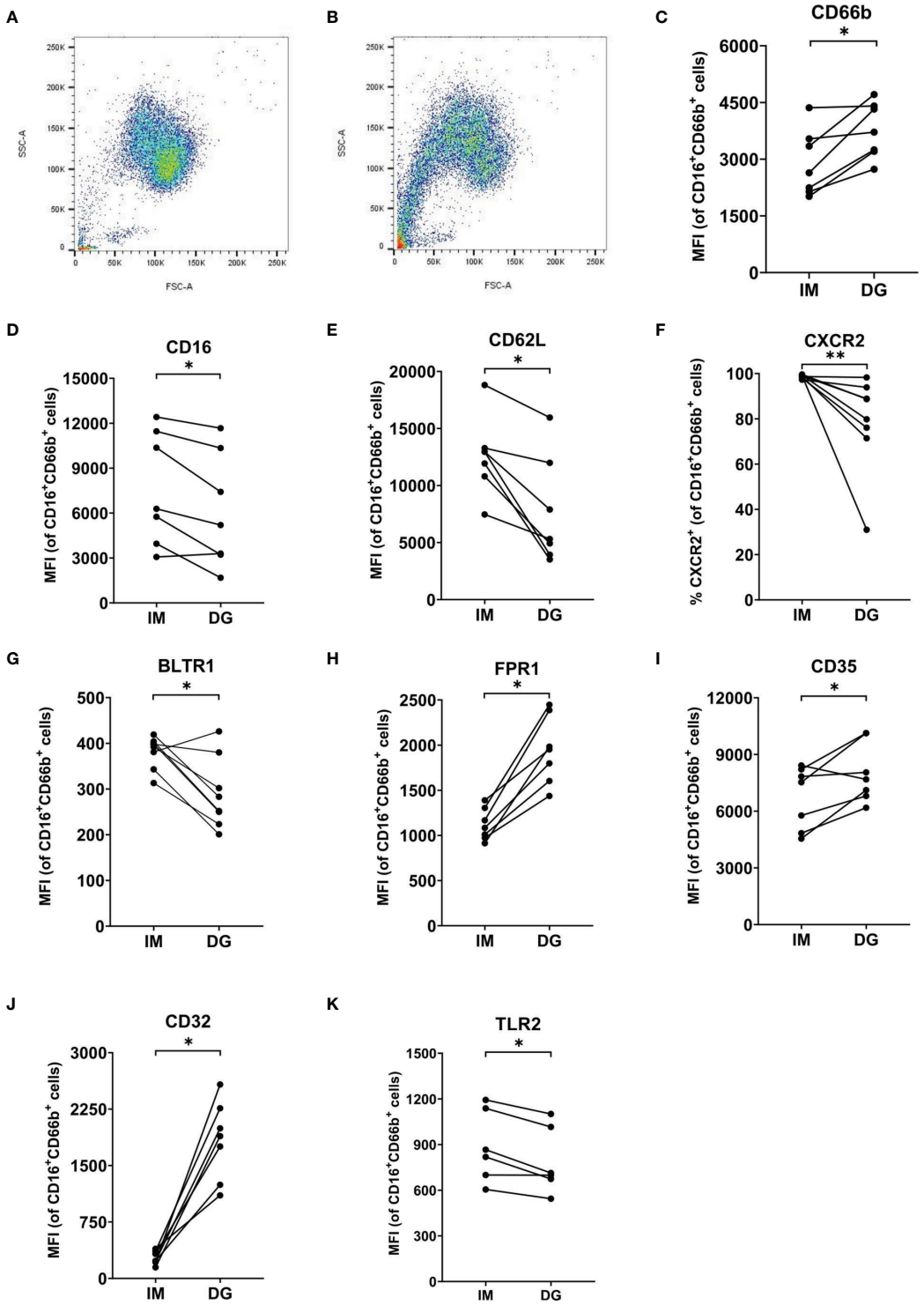

FIGURE 6 | Neutrophils purified by density-gradient centrifugation display an activated phenotype. Flow cytometry was used to evaluate the **(A, B)** size (FSC), granularity (SSC) and surface expression of **(C)** CD66b, **(D)** CD16, **(E)** CD62L, **(F)** CXCR2, **(G)** BLTR1, **(H)** FPR1, **(I)** CD35, **(J)** CD32 and **(K)** TLR2 on neutrophils (gated as $CD16^+CD66b^+$ cells) isolated by immunomagnetic (IM) or density-gradient purification (DG) from peripheral blood of healthy donors. Results are represented as percentage of neutrophils positive for the marker or median fluorescence intensity (MFI). Results from each individual donor (n = 6-8) are connected by lines and were statistically analyzed by Wilcoxon matched-pairs signed rank test (*$p < 0.05$; **$p < 0.01$ for statistical differences between neutrophils purified with immunomagnetic or density-gradient separation).

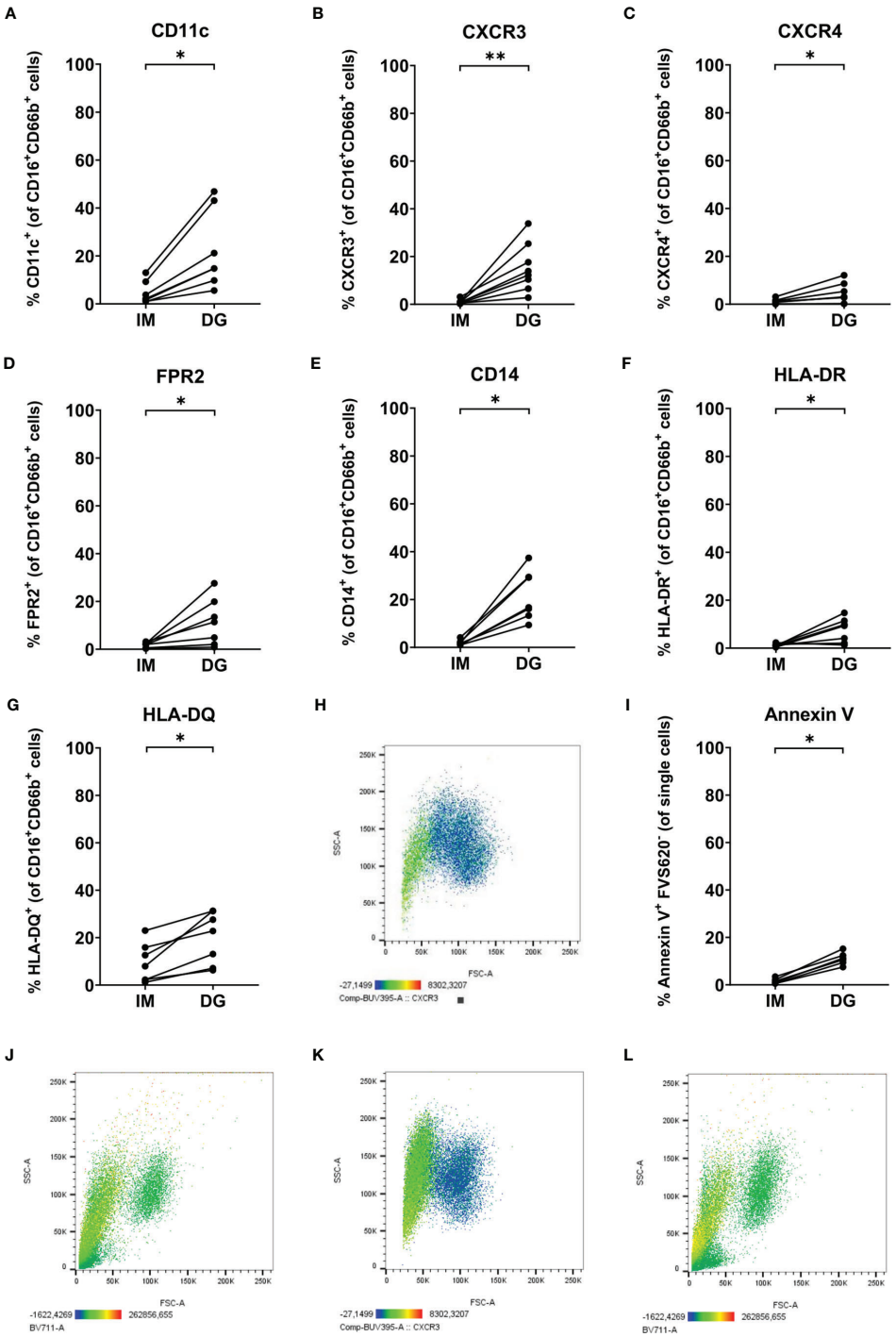

FIGURE 7 | Neutrophils purified by density-gradient centrifugation partially express markers atypical for neutrophils. Flow cytometry was used to evaluate the surface expression of **(A)** CD11c, **(B)** CXCR3, **(C)** CXCR4, **(D)** FPR2, **(E)** CD14, **(F)** HLA-DR and **(G)** HLA-DQ on neutrophils (gated as $CD16^+CD66b^+$ cells) isolated by immunomagnetic (IM) or density-gradient purification (DG) from peripheral blood of healthy donors. **(H)** CXCR3 (BUV395) staining (indicated by color code below the plot) on FSC/SSC plot of neutrophils purified by density-gradient centrifugation. **(I)** Annexin V and FVS620 staining on neutrophils isolated by IM or DG purification from peripheral blood of healthy donors. **(J)** Annexin V (BV711) staining (indicated by color code below the plot) on FSC/SSC plot of neutrophils purified by density-gradient centrifugation. **(K, L)** CXCR3 (BUV395) and Annexin V (BV711) staining (indicated by color code below the plot) on FSC/SSC plot of neutrophils purified by immunomagnetic purification immediately after a density-gradient purification. Results are represented as percentage of neutrophils positive for the marker. Results from each individual donor (n = 6-8) are connected by lines and were statistically analyzed by Wilcoxon matched-pairs signed rank test (*$p < 0.05$; **$p < 0.01$ for statistical differences between neutrophils purified with immunomagnetic or density-gradient separation).

phagocytosis, production of ROS, release of NETs, and secretion of antibacterial peptides and enzymes (2). The short life span of neutrophils and their high sensitivity to external stimuli pose a challenge to those aiming to study these cells *in vitro* (8). However, an extensive comparison of the functionality of neutrophils purified by different techniques has so far not been performed.

In this study, we compared the functional characteristics of neutrophils purified by two routinely used purification methods: (I) density-gradient centrifugation followed by dextran sedimentation and hypotonic lysis of erythrocytes; and (II) immunomagnetic isolation based on negative selection. We found that immunomagnetic isolation-derived unstimulated neutrophils exhibited reduced baseline polarization and spontaneously released less ROS, NETs and granular proteins as compared to unstimulated density-gradient-derived cells. When stimulated with pro-inflammatory mediators, immunomagnetic beads-isolated neutrophils polarized more readily and released more ROS, NETs and granular proteins than stimulated density-gradient-derived cells. In addition, immunomagnetically purified neutrophils showed enhanced phagocytosis of *S. aureus*-coated beads. No major differences in CXCL8 production were found between neutrophils isolated by the two methods. A summary of the results can be found in **Table 1**. Overall, neutrophils separated using immunomagnetic beads seemed to be less activated at baseline but more responsive to activating stimuli than density-gradient-derived neutrophils. This was further supported by the observation that density-gradient-derived neutrophils displayed higher levels of activation markers (*e.g.* CD66b, FPR1, CD35, CD11c) on their surface. Together, these results suggest that neutrophils purified by immunomagnetic separation most closely resemble the quiescent cells found in the bloodstream and are therefore more representative of naïve blood neutrophils.

Having found density-gradient-derived neutrophils to be artificially activated, we further explored the expression of typical and atypical surface markers on neutrophils. Density-gradient-derived neutrophils expressed lower levels of BLTR1, CD62L, CXCR2, CD16 and TLR2 and higher levels of CXCR4, FPR1, CD11c, CD66b, CD32 and CD35. The lower expression levels of CXCR2 and TLR2 on density gradient-derived neutrophils could partially explain the reduced response to CXCL8 and PGN in the different functional assays. However, this is not the case for FPR1, which was more highly expressed on density-gradient-derived cells, despite most functional responses to fMLF being decreased as compared to immunomagnetically purified neutrophils. Nevertheless, increased receptor expression does not necessarily exclude reduced responsiveness. Indeed, enhanced levels of CCR1 and/or CCR5 were shown to be present on monocytes from hemolytic uremic syndrome (HUS) or chronic obstructive pulmonary disease (COPD) patients, even though HUS or COPD monocytes did not respond as well as monocytes from healthy individuals in functional assays (21, 22).

In addition, we found that a significant proportion of neutrophils (up to 45% of all neutrophils, as defined by expression of both CD16 and CD66b), present among density-gradient-derived cells but not immunomagnetically purified cells, expressed a range of atypical receptors, including CXCR3, FPR2, CD14 and MHC class II molecules. Using a two-step purification procedure, we showed that the expression of these markers was specifically induced by density-gradient purification, and not masked by immunomagnetic bead purification. The atypical markers in question are involved in many different diseases (23–26). Thus, if their expression on healthy peripheral blood neutrophils is induced by the density-gradient isolation method, this should be kept in mind to avoid bias when studying patient samples. Cells expressing these atypical markers were typically smaller in size and less granular compared to the rest of the neutrophil population. To assess whether this atypical marker expression could be explained by neutrophil apoptosis, we performed an additional staining with annexin V and found a small percentage (5-15%) of density-gradient-derived neutrophils to be annexin V-positive. We believe that this small population of neutrophils comprises aging ($CXCR4^+$) neutrophils which are slowly going into apoptosis (27). Of note, we did not include a positive control for the annexin V staining and therefore have no indication of the signal intensity we measured. For mast cells, it is known that a high degree of degranulation can also lead to the appearance of phosphatidylserine on the outer cell membrane and as such annexin V binding (28). Whether a similar phenomenon occurs in neutrophils is as of yet unknown; therefore our findings should be interpreted with care.

Despite significant differences in stimulus-induced polarization, we found no difference in Multiscreen and under-agarose migration

TABLE 1 | Summary of the results.

Neutrophil function	Spontaneous	In response to stimulus
Cell polarization	IM < DG	IM > DG
Migration	IM ≈ DG	IM ≈ DG
Phagocytosis	/	IM > DG
ROS production	IM < DG	IM > DG
NETosis	IM < DG	IM > DG
Degranulation	IM < DG	IM > DG
Cytokine production	IM ≈ DG	IM ≈ DG

Neutrophils purified by immunomagnetic isolation (IM) and density-gradient centrifugation (DG) were subjected to several functional tests. The baseline activation in the test (spontaneous) and stimulus-induced activation (in response to stimulus) were compared. IM < DG means the response was lower in IM-derived cells than in DG-derived cells; IM > DG means the response was higher in IM-derived cells than in DG-derived cells; / means the response was not assessed; IM ≈ DG means the response was comparable in IM-derived and DG-derived neutrophils.

of neutrophils isolated by the two different purification methods. These findings point to other mechanisms that may compensate for the lack of polarization in density-gradient-derived neutrophils in the process of migration. Surprisingly, not all three chemotaxis assays showed the same results. While immunomagnetically and density-gradient-derived neutrophils migrated equally well in the Multiscreen and under-agarose assay, relatively little chemotaxis by immunomagnetically purified neutrophils was observed in the Boyden chamber assay. This observation could not be attributed to lower levels of the chemokine receptors CXCR1 or CXCR2, both receptors for CXCL8. The increased chemotactic migration of density-gradient-derived neutrophils towards fMLF could potentially be explained by the increased expression of FPR1 on the membrane compared to immunomagnetically purified neutrophils, but this is not reflected in the actin polymerization and shape change assays. However, it should be noted that very few neutrophils purified with immunomagnetic beads were visible on the Boyden microchamber membrane after staining. Therefore, it is possible that these neutrophils did migrate but did not remain attached to the membrane due to different expression levels of adhesion molecules. This hypothesis is supported by the observation that density-gradient-derived neutrophils expressed higher levels of the integrin CD11c, and by the fact that activated neutrophils tend to express integrins in an open conformation, facilitating adhesion (29).

The profound differences in functionality and receptor expression of neutrophils purified by immunomagnetic and density-gradient methods are important, as literature reports describe neutrophils in the circulation to be largely quiescent (7). Therefore, neutrophils purified by immunomagnetic beads may be a more accurate representation of peripheral blood neutrophils *in vivo*. However, the exact mechanism causing the activation of neutrophils purified by density-gradient centrifugation remains as of yet unclear. An obvious difference between both purification methods is the time required for the purification: *circa* 1 hour for immunomagnetic separation *versus circa* 3 hours in the case of the density-gradient method. However, time alone cannot be responsible for the difference in activation, as immunomagnetically purified neutrophils left at room temperature for 2 hours after the purification did not show upregulation of activation markers to a similar extent as was seen in density-gradient-derived neutrophils (data not shown).

Other factors implicated in density-gradient purification only are Pancoll, dextran, repeated centrifugation steps and hypotonic lysis of erythrocytes. Previous research showed that dextran sedimentation may cause neutrophil activation if it is performed prior to density-gradient centrifugation, since monocytes from blood can become activated and release TNF-α, which in turn stimulates the neutrophils (30). Whether contaminating eosinophils or basophils (which are isolated by the density-gradient purification method together with the neutrophils) exhibit a similar neutrophil-activating effect, remains yet to be investigated. Another important difference between both purification methods is that immunomagnetic bead separation does not lead to the loss of low-density neutrophils (LDNs), which normally end up in the PBMC layer and are removed during density-gradient separation of neutrophils. Immune suppression (in particular suppression of T cells) is one of the functions ascribed to LDNs (31). We should also mention that the percentage of LDNs in healthy individuals is typically less than 3% (32) and is therefore unlikely to affect neutrophil function to the extent of our findings. Another study found that free MPO can activate neutrophils by binding to the CD11b/CD18 integrin (33). MPO is stored in the azurophilic granules and is released through degranulation upon stimulation of the neutrophil (34). Repeated centrifugation steps of neutrophils during density-gradient isolation may lead to physical disruption of some cells and artificial release of MPO. This process could initiate a positive feedback loop, activating other neutrophils and triggering premature ROS release and NETosis. This theory could explain the spontaneously increased release of NETs, ROS and granular proteins of unstimulated density-gradient-derived neutrophils and the low response of stimulated density-gradient-derived neutrophils in most functional assays, compared to immunomagnetic beads-derived neutrophils. We anticipate that the initial MPO could have been released by the less granular cell population present among density-gradient-derived neutrophils. In addition to the mechanical stress due to repeated centrifugation, release of damage-associated molecular patterns by lysed red blood cells may stimulate neutrophils during density-gradient purification (35, 36).

In conclusion, we have compared the effects of immunomagnetic and density-gradient purification on neutrophil phenotype and functionality. The two purification methods had similar yield and purity of neutrophils. We found that peripheral blood neutrophils isolated by immunomagnetic purification were generally less activated as compared to those isolated by density-gradient purification, and responded more readily to activating stimuli in functional assays. Based on our results, we recommend using the faster immunomagnetic separation with negative selection to test neutrophil polarization, phagocytosis, ROS production, degranulation response and NETosis. For Boyden chamber migration assays, we recommend using density-gradient centrifugation. For Multiscreen chemotaxis, under-agarose and cytokine production assays both neutrophil purification methods are suitable. Our study highlights the importance of choosing the correct methodology for the unbiased study of neutrophils *in vitro*.

DATA AVAILABILITY STATEMENT

The original contributions presented in the study are included in the article/**Supplementary Material**. Further inquiries can be directed to the corresponding author.

ETHICS STATEMENT

The studies involving human participants were reviewed and approved by Ethics Committee of the University Hospital Leuven.

The patients/participants provided their written informed consent to participate in this study.

AUTHOR CONTRIBUTIONS

Experiment design: PM, SS, PP, and MG. Execution of experiments and data analysis: MB, SC, MDB, LV, NP, SAS, MM, and MG. Manuscript writing: MB, SC, MDB, SAS, MM, and MG. Writing – review & editing: all authors. All authors approved the submitted version.

FUNDING

This research was supported by a C1 grant of KU Leuven (C16/17/010) and a research project of FWO-Vlaanderen (G080818N). MB, SC, and MDB are supported by PhD fellowships and SAS by a postdoctoral fellowship of FWO-Vlaanderen. MM is supported by a L'Oréal/UNESCO/FWO PhD fellowship For Women in Science. The funder was not involved in the study design, collection, analysis, interpretation of data, the writing of this article or the decision to submit it for publication.

ACKNOWLEDGMENTS

We particularly thank Stefanie Sente, Francesca Van Maercke and Helga Ceunen for providing invaluable assistance in collecting blood samples. Furthermore, we want to thank all healthy volunteers who donated blood samples.

SUPPLEMENTARY MATERIAL

The Supplementary Material for this article can be found online at: https://www.frontiersin.org/articles/10.3389/fimmu.2022.820058/full#supplementary-material

REFERENCES

1. Rosales C. Neutrophil: A Cell With Many Roles in Inflammation or Several Cell Types? *Front Physiol* (2018) 9:113. doi: 10.3389/fphys.2018.00113
2. Burn GL, Foti A, Marsman G, Patel DF, Zychlinsky A. The Neutrophil. *Immunity* (2021) 54(7):1377–91. doi: 10.1016/j.immuni.2021.06.006
3. Vandendriessche S, Cambier S, Proost P, Marques PE. Complement Receptors and Their Role in Leukocyte Recruitment and Phagocytosis. *Front Cell Dev Biol* (2021) 9:624025. doi: 10.3389/fcell.2021.624025
4. Liew PX, Kubes P. The Neutrophil's Role During Health and Disease. *Physiol Rev* (2019) 99(2):1223–48. doi: 10.1152/physrev.00012.2018
5. Ley K, Hoffman HM, Kubes P, Cassatella MA, Zychlinsky A, Hedrick CC, et al. Neutrophils: New Insights and Open Questions. *Sci Immunol* (2018) 3 (30):eaat4579. doi: 10.1126/sciimmunol.aat4579
6. Martin C, Burdon PC, Bridger G, Gutierrez-Ramos JC, Williams TJ, Rankin SM. Chemokines Acting *via* CXCR2 and CXCR4 Control the Release of Neutrophils From the Bone Marrow and Their Return Following Senescence. *Immunity* (2003) 19(4):583–93. doi: 10.1016/S1074-7613(03)00263-2
7. Summers C, Rankin SM, Condliffe AM, Singh N, Peters AM, Chilvers ER. Neutrophil Kinetics in Health and Disease. *Trends Immunol* (2010) 31 (8):318–24. doi: 10.1016/j.it.2010.05.006
8. Blanter M, Gouwy M, Struyf S. Studying Neutrophil Function *In Vitro*: Cell Models and Environmental Factors. *J Inflamm Res* (2021) 14:141–62. doi: 10.2147/JIR.S284941
9. Krabbe J, Beilmann V, Alamzad-Krabbe H, Böll S, Seifert A, Ruske N, et al. Blood Collection Technique, Anticoagulants and Storing Temperature Have Minor Effects on the Isolation of Polymorphonuclear Neutrophils. *Sci Rep* (2020) 10(1):14646. doi: 10.1038/s41598-020-71500-1
10. Böyum A. Isolation of Mononuclear Cells and Granulocytes From Human Blood. Isolation of Mononuclear Cells by One Centrifugation, and of Granulocytes by Combining Centrifugation and Sedimentation at 1 G. *Scand J Clin Lab Invest Suppl* (1968) 97:77–89.
11. Zhang L, Parry GC, Levin EG. Inhibition of Tumor Cell Migration by LD22-4, an N-Terminal Fragment of 24-kDa FGF2, Is Mediated by Neuropilin 1. *Cancer Res* (2013) 73(11):3316–25. doi: 10.1158/0008-5472.CAN-12-3015
12. Watson F, Robinson JJ, Edwards SW. Neutrophil Function in Whole Blood and After Purification: Changes in Receptor Expression, Oxidase Activity and Responsiveness to Cytokines. *Biosci Rep* (1992) 12(2):123–33. doi: 10.1007/BF02351217
13. Son K, Mukherjee M, McIntyre BAS, Eguez JC, Radford K, LaVigne N, et al. Improved Recovery of Functionally Active Eosinophils and Neutrophils Using Novel Immunomagnetic Technology. *J Immunol Methods* (2017) 449:44–55. doi: 10.1016/j.jim.2017.06.005
14. Abouelasrar Salama S, De Bondt M, De Buck M, Berghmans N, Proost P, Oliveira VLS, et al. Serum Amyloid A1 (SAA1) Revisited: Restricted Leukocyte-Activating Properties of Homogeneous Saa1. *Front Immunol* (2020) 11:843. doi: 10.3389/fimmu.2020.00843
15. Gouwy M, Struyf S, Noppen S, Schutyser E, Springael JY, Parmentier M, et al. Synergy Between Coproduced CC and CXC Chemokines in Monocyte Chemotaxis Through Receptor-Mediated Events. *Mol Pharmacol* (2008) 74 (2):485–95. doi: 10.1124/mol.108.045146
16. Nelson RD, Quie PG, Simmons RL. Chemotaxis Under Agarose: A New and Simple Method for Measuring Chemotaxis and Spontaneous Migration of Human Polymorphonuclear Leukocytes and Monocytes. *J Immunol* (1975) 115(6):1650–6.
17. Cockx M, Blanter M, Gouwy M, Ruytinx P, Abouelasrar Salama S, Knoops S, et al. The Antimicrobial Activity of Peripheral Blood Neutrophils Is Altered in Patients With Primary Ciliary Dyskinesia. *Int J Mol Sci* (2021) 22(12):6172. doi: 10.3390/ijms22126172
18. Proost P, Struyf S, Loos T, Gouwy M, Schutyser E, Conings R, et al. Coexpression and Interaction of CXCL10 and CD26 in Mesenchymal Cells by Synergising Inflammatory Cytokines: CXCL8 and CXCL10 Are Discriminative Markers for Autoimmune Arthropathies. *Arthritis Res Ther* (2006) 8(4):R107. doi: 10.1186/ar1997
19. Sengeløv H, Follin P, Kjeldsen L, Lollike K, Dahlgren C, Borregaard N. Mobilization of Granules and Secretory Vesicles During *In Vivo* Exudation of Human Neutrophils. *J Immunol* (1995) 154(8):4157–65.
20. Wertheim WA, Kunkel SL, Standiford TJ, Burdick MD, Becker FS, Wilke CA, et al. Regulation of Neutrophil-Derived IL-8: The Role of Prostaglandin E2, Dexamethasone, and IL-4. *J Immunol* (1993) 151(4):2166–75.
21. Ramos MV, Ruggieri M, Panek AC, Mejias MP, Fernandez-Brando RJ, Abrey-Recalde MJ, et al. Association of Haemolytic Uraemic Syndrome With Dysregulation of Chemokine Receptor Expression in Circulating Monocytes. *Clin Sci (Lond)* (2015) 129(3):235–44. doi: 10.1042/CS20150016
22. Ravi AK, Plumb J, Gaskell R, Mason S, Broome CS, Booth G, et al. COPD Monocytes Demonstrate Impaired Migratory Ability. *Respir Res* (2017) 18 (1):90. doi: 10.1186/s12931-017-0569-y
23. Hartl D, Krauss-Etschmann S, Koller B, Hordijk PL, Kuijpers TW, Hoffmann F, et al. Infiltrated Neutrophils Acquire Novel Chemokine Receptor Expression and Chemokine Responsiveness in Chronic Inflammatory Lung Diseases. *J Immunol* (2008) 181(11):8053–67. doi: 10.4049/jimmunol.181.11.8053
24. De Bondt M, Hellings N, Opdenakker G, Struyf S. Neutrophils: Underestimated Players in the Pathogenesis of Multiple Sclerosis (MS). *Int J Mol Sci* (2020) 21(12):4558. doi: 10.3390/ijms21124558
25. Sundqvist M, Christenson K, Gabl M, Holdfeldt A, Jennbacken K, Møller TC, et al. *Staphylococcus aureus*-Derived Psmα Peptides Activate Neutrophil FPR2 But Lack the Ability to Mediate β-Arrestin Recruitment and

Chemotaxis. *J Immunol* (2019) 203(12):3349–60. doi: 10.4049/jimmunol.1900871
26. Cohen G. Effect of High-Density Lipoprotein From Healthy Subjects and Chronic Kidney Disease Patients on the CD14 Expression on Polymorphonuclear Leukocytes. *Int J Mol Sci* (2021) 22(6):2830. doi: 10.3390/ijms22062830
27. Metzemaekers M, Gouwy M, Proost P. Neutrophil Chemoattractant Receptors in Health and Disease: Double-Edged Swords. *Cell Mol Immunol* (2020) 17(5):433–50. doi: 10.1038/s41423-020-0412-0
28. Demo SD, Masuda E, Rossi AB, Throndset BT, Gerard AL, Chan EH, et al. Quantitative Measurement of Mast Cell Degranulation Using a Novel Flow Cytometric Annexin-V Binding Assay. *Cytometry* (1999) 36(4):340–8. doi: 10.1002/(SICI)1097-0320(19990801)36:4<340::AID-CYTO9>3.0.CO;2-C
29. Langereis JD. Neutrophil Integrin Affinity Regulation in Adhesion, Migration, and Bacterial Clearance. *Cell Adh Migr* (2013) 7(6):476–81. doi: 10.4161/cam.27293
30. Quach A, Ferrante A. The Application of Dextran Sedimentation as an Initial Step in Neutrophil Purification Promotes Their Stimulation, Due to the Presence of Monocytes. *J Immunol Res* (2017) 2017:1254792. doi: 10.1155/2017/1254792
31. Tsai CY, Hsieh SC, Liu CW, Lu CS, Wu CH, Liao HT, et al. Cross-Talk Among Polymorphonuclear Neutrophils, Immune, and Non-Immune Cells *via* Released Cytokines, Granule Proteins, Microvesicles, and Neutrophil Extracellular Trap Formation: A Novel Concept of Biology and Pathobiology for Neutrophils. *Int J Mol Sci* (2021) 22(6):3119. doi: 10.3390/ijms22063119
32. Blanco-Camarillo C, Alemán OR, Rosales C. Low-Density Neutrophils in Healthy Individuals Display a Mature Primed Phenotype. *Front Immunol* (2021) 12:672520. doi: 10.3389/fimmu.2021.672520
33. Lau D, Mollnau H, Eiserich JP, Freeman BA, Daiber A, Gehling UM, et al. Myeloperoxidase Mediates Neutrophil Activation by Association With CD11b/CD18 Integrins. *Proc Natl Acad Sci USA* (2005) 102(2):431–6. doi: 10.1073/pnas.0405193102
34. Yin C, Heit B. Armed for Destruction: Formation, Function and Trafficking of Neutrophil Granules. *Cell Tissue Res* (2018) 371(3):455–71. doi: 10.1007/s00441-017-2731-8
35. Mendonça R, Silveira AA, Conran N. Red Cell DAMPs and Inflammation. *Inflammation Res* (2016) 65(9):665–78. doi: 10.1007/s00011-016-0955-9
36. Bozza MT, Jeney V. Pro-Inflammatory Actions of Heme and Other Hemoglobin-Derived DAMPs. *Front Immunol* (2020) 11:1323. doi: 10.3389/fimmu.2020.01323

Conflict of Interest: The authors declare that the research was conducted in the absence of any commercial or financial relationships that could be construed as a potential conflict of interest.

Publisher's Note: All claims expressed in this article are solely those of the authors and do not necessarily represent those of their affiliated organizations, or those of the publisher, the editors and the reviewers. Any product that may be evaluated in this article, or claim that may be made by its manufacturer, is not guaranteed or endorsed by the publisher.

frontiers | Frontiers in Immunology

REVIEW
published: 19 April 2022
doi: 10.3389/fimmu.2022.849451

Inflammatory Immune-Associated eRNA: Mechanisms, Functions and Therapeutic Prospects

Lilin Wan[1,2†], Wenchao Li[2†], Yuan Meng[3†], Yue Hou[4], Ming Chen[2,3*] and Bin Xu[2,3*]*

[1] Medical School, Southeast University, Nanjing, China, [2] Department of Urology, Affiliated Zhongda Hospital of Southeast University, Nanjing, China, [3] Department of Urology, Nanjing Lishui District People's Hospital, Zhongda Hospital, Southeast University, Nanjing, China, [4] Key Laboratory of Biomedical Information Engineering of Ministry of Education, Biomedical Informatics and Genomics Center, School of Life Science and Technology, Xi'an Jiaotong University, Xi'an, China

OPEN ACCESS

Edited by:
Andrea Baragetti, University of Milan, Italy

Reviewed by:
Masaki Miyazaki, Kyoto University, Japan
Changchang Cao, Institute of Biophysics (CAS), China

***Correspondence:**
Bin Xu
njxbseu@seu.edu.cn
Yue Hou
houyue@xjtu.edu.cn
Ming Chen
mingchenseu@126.com

[†]These authors have contributed equally to this work

Specialty section:
This article was submitted to Inflammation, a section of the journal Frontiers in Immunology

Received: *06 January 2022*
Accepted: *21 March 2022*
Published: *19 April 2022*

Citation:
Wan L, Li W, Meng Y, Hou Y, Chen M and Xu B (2022) Inflammatory Immune-Associated eRNA: Mechanisms, Functions and Therapeutic Prospects. Front. Immunol. 13:849451. doi: 10.3389/fimmu.2022.849451

The rapid development of multiple high-throughput sequencing technologies has made it possible to explore the critical roles and mechanisms of functional enhancers and enhancer RNAs (eRNAs). The inflammatory immune response, as a fundamental pathological process in infectious diseases, cancers and immune disorders, coordinates the balance between the internal and external environment of the organism. It has been shown that both active enhancers and intranuclear eRNAs are preferentially expressed over inflammation-related genes in response to inflammatory stimuli, suggesting that enhancer transcription events and their products influence the expression and function of inflammatory genes. Therefore, in this review, we summarize and discuss the relevant inflammatory roles and regulatory mechanisms of eRNAs in inflammatory immune cells, non-inflammatory immune cells, inflammatory immune diseases and tumors, and explore the potential therapeutic effects of enhancer inhibitors affecting eRNA production for diseases with inflammatory immune responses.

Keywords: eRNA, immune inflammatory, enhancer transcription events, cancers, therapeutic prospects

HIGHLIGHTS

This review summarized the relevant roles of eRNAs in inflammatory immune functions, mechanisms and therapies, and explored the research directions and target therapy prospects for inflammatory immune-related eRNAs.

INTRODUCTION

The rapid development of high-throughput sequencing technologies has made it possible to identify potential functional regulatory elements. To date, studies have identified numerous regulatory elements, such as enhancers, promoters and silencers (1).

Enhancers, which are distal regulatory DNA sequences, are approximately 500–2000 bp in length and function independently of orientation (2, 3). Since the discovery of the first enhancer

SV40 by Banerji J et al. in 1981 (4), the specific function and mechanism of enhancers have been extensively explored. Numerous studies have revealed that pioneer transcription factors enhance nucleosome DNA to generate open chromatin (5), which promotes the recruitment of lineage-determining transcription factors (LDTFs) to maintain the activated state of enhancers (6). Subsequently, collaborative transcription factors (cTFs) and co-cofactors (CoFs), such as histone methyltransferases, are recruited, which promote histone 3 lysine 4 monomethylation (H3K4me1) and dimethylation (H3K4me2) (6–10). Following this, histone acetyltransferases (HAT) [e.g. CBP/p300 to promote H3K27 acetylation (ac)] (10, 11), general transcription factors (GTFs) (12) and RNA polymerase II (RNAPII) (3, 13) are further recruited to initiate enhancer-associated bidirectional transcription. Additionally, DNA demethylase (DME) is recruited during the initial phase of enhancer activation to regulate dynamic DNA methylation and p300 binding (14, 15) (**Figure 1A**). Consistent with previous studies, the above study suggests that enhancers positively regulate spatiotemporal gene expression (4, 16, 17).

Super enhancers (SEs) were first found in mouse embryonic stem cells and tumour cell lines (18, 19). Compared to typical enhancers, SEs consist of large enhancer clusters with longer genomic regions, higher cell-specific transcription factor (TF) levels (e.g. Oct4, Sox2, Nanog, Eseeb and Klf4) (18, 20–22), CoFs (e.g. BRD4, Mediator and CDK9) (21), higher H3K4me1 expressions and H3K27ac modifications (23, 24). These characteristics allow SEs to highly express super enhancer derived super RNAs (seRNAs) (**Figure 1B**). Therefore, SEs have been speculated to be the key determinants of cell identity and fate (18, 23), and thereby lead to increased disease susceptibility when mutated (20, 23).

eRNA, as the enhancers transcription product, belongs to the class of non-coding RNA (ncRNA). Based on differences in function and size, ncRNAs are classified as long non coding RNA (lncRNA), promoter associated RNA (paRNA), enhancer RNA (eRNA), small RNA (sRNA), PIWI interacting RNA (piRNA), small nucleolar RNA (snoRNA), Small nuclear RNA (snRNA), ribosomal RNA (rRNA), micro RNA (miRNA) etc (25–28). Similarly, they are generated in different parts of the

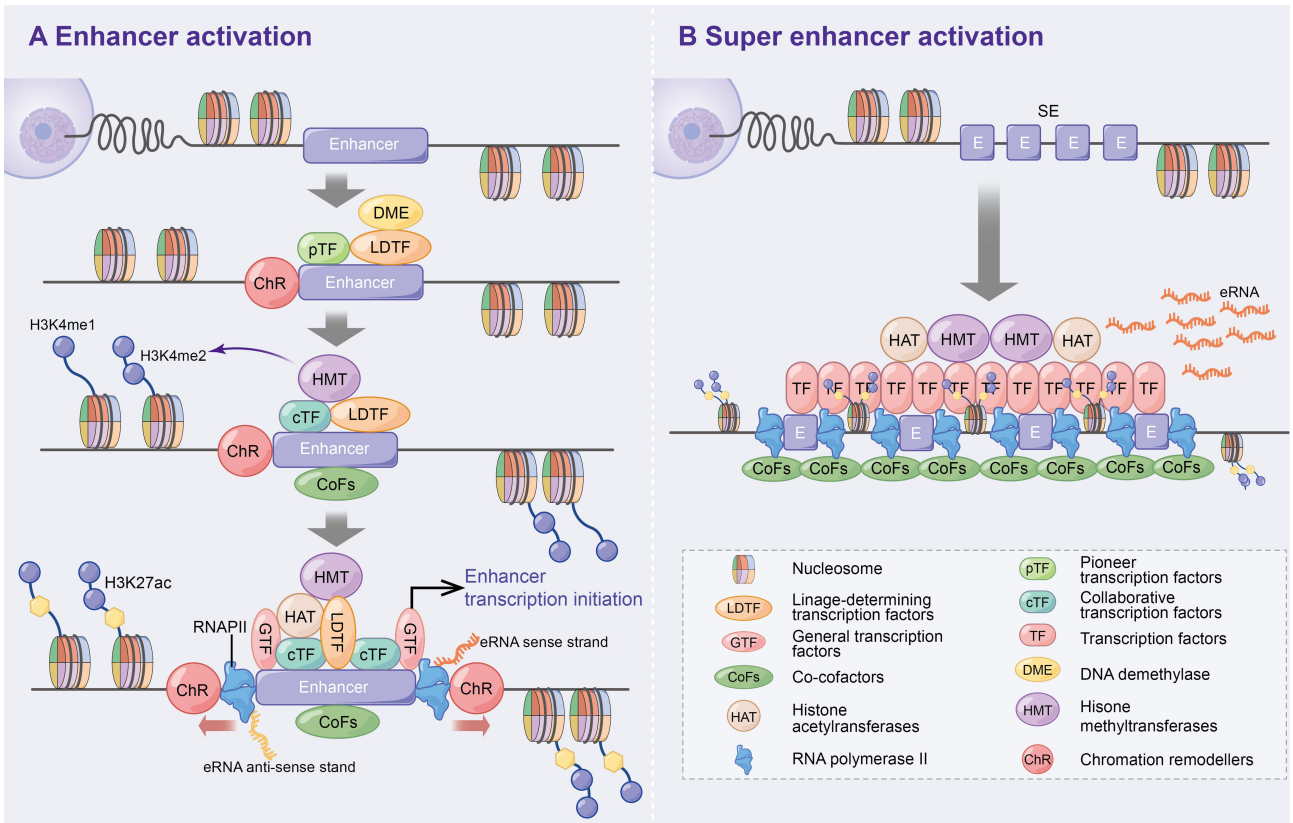

FIGURE 1 | Activation mechanism of enhancers and super enhancer. **(A)** Enhancer activation. Multifactorial stimulation causes pTFs binding to nucleosomes leading to ChR and further recruitment of LDTFs, cTFs and CoFs that assist enhancer activation and histone methylation. On this basis, HAT, GTFs and RNAPII are recruited and ultimately contribute to enhancer transcription bi-directionally. In addition, DME are recruited to regulate DNA methylation and p300 status at the initial stage of enhancer activation. **(B)** Super enhancers are large clusters of enhancers with high levels of cell-specific transcription factors and cofactors that can ultimately express higher levels of eRNAs.

genome and can be obtained by unidirectional or bidirectional transcription, with variable stability and longevity (26–28). The section will briefly describe the differences and commonalities between eRNA and lncRNA. eRNAs are similar in length to lncRNAs, about 0.1-9 Kb, but are divided into two classes of ncRNAs by their associated histone profiles (29). In the 2010 study, Orom UA et al. (30) found that lncRNAs can regulate the expression of neighboring genes. Subsequently, this type of lncRNA was revealed to be an enhancer of some protein-coding genes, but its chromatin characteristics differ from typical enhancers and it is usually polyadenylated and does not have the characteristics of bidirectional transcription of eRNA. Further studies suggest that such lncRNAs carry intermediary complexes to neighboring genes *via* chromatin loops to influence their expression (30, 31). However, most eRNA transcripts are 5' cap-shaped, unspliced, unpolyadenylated and have a short half-life, but are also dynamically regulated with signaling and correlate with increased expression of neighboring genes (32).

To date, numerous reviews have summarized the mechanisms and potential functions of enhancers, SEs and their transcription products (eRNAs) in tumours (33–36). Moreover, the expansion of the study dimension revealed that enhancers, SEs and their eRNAs were immediately altered in response to inflammatory stimuli, leading to abnormal inflammatory gene expression. This observation strongly suggests their involvement in biological processes, such as inflammation, immunity and neurodegeneration (24, 37–39). Yoshiki et al. (21) have summarized the potential role of SEs in inflammatory gene transcription.

However, to the best of our knowledge, the potential mechanisms and roles of eRNAs in inflammatory immune diseases are yet to be reviewed. This study aims to summarize the potential roles of eRNAs in inflammatory immune cells, non-inflammatory immune cells, inflammatory immune diseases and tumour inflammatory alterations, and thereby elucidate the relevance of eRNAs in inflammatory immunity (**Figure 2**). Additionally, the potential role of eRNAs as novel therapeutic targets and prognostic biomarkers for diseases with inflammatory immune alterations are explored.

RESULTS

Mechanism of Enhancer Transcription and eRNA in Regulating Target Genes

Effect of Enhancer Transcription on Their Products and Target Genes

The mechanism of enhancer activation has been discussed in the Introduction (**Figure 1A**); therefore, the regulation of downstream target genes by enhancer transcription (including initiation, elongation, termination and degradation) will be discussed in this section.

GTFs (e.g. TBP) and the serine 5-phosphorylated form of RNAPII (Ser5p was engaged in RNA capping mechanism) have been detected in the enhancer region in the transcription of lncRNAs or mRNAs (40). Moreover, global nuclear run-on sequencing (GRO-seq) and cap analysis gene expression (CAGE) results further suggest that eRNAs are capped (5′ end 7-methylguanosine (m7G) cap facilitates cap-binding complex (CBC) recruitment), with significant similarities in DNA sequences, core promoter elements and nucleosome spacing at enhancer and promoter transcription start sites (TSSs) (41–43), and promote bidirectional transcription (29, 32, 42, 44), thus indicating that the rules of transcription initiation apply to enhancers and promoters. Similar to promoters, the direction of enhancer transcription is also determined by the ratio of the relative density of polyA cleavage sites (PASs) and the U1 splice motif downstream of the TSSs, which affects the production of eRNAs initiated by RNAPII elongation (41, 42, 44–46) (**Figure 3A**).

The elongation, termination and RNA processing stages highlight transcriptional differences between enhancers and promoters. Ser2p, a form of RNAPII that is involved in elongation, is characterized by low enrichment, which results in low H3K36me3 levels and affects enhancer transcription elongation (40, 47, 48). The enhancer transcription elongation phase was found to be partially impacted by the overlapping mechanisms of the coding genes, including positive transcription elongation factor-b complex (pTEFb) and bromodomain-containing protein 4 (BRD4, which is recruited by H3K27ac) (10–12). Additionally, eRNAs undergoing transcription bind to the mediator complex and affect transcription elongation (18, 31, 49) (**Figure 3A**).

Numerous studies have found that PAS-mediated early termination regulates eRNA stability, and RNA exosomes degrade eRNAs. A study by Lai et al. confirmed that the integrator, which interacts with the RNAPII carboxy-terminal domain (RNAPII CTD), is an important regulator of eRNA termination (50) that functions after the nascent eRNAs have the PAS (AAUAAA) (42, 44, 50, 51). Integrator subunit deletion decreases eRNA levels and increases enhancer transcription activity, indicating the disruption of eRNA termination (50). Additionally, WD repeat-containing protein 82 (WDR82) acts as an adaptor protein that targets SET1 H3K4 methyltransferase, affecting enhancer transcription termination (52). Interestingly, Tyrosine 1-phosphorylated form of RNAPII (Tyr1p) was highly enriched in the active enhancer and PROMPT (upstream transcripts of the promoter) regions, whereas it was slightly enriched in the gene promoter region (53, 54). Moreover, Yeast Tyr1p was shown to be associated with eRNA termination (55, 56). In addition, under the mediation of the trimeric nuclear exosome targeting (NEXT) complex, wherein RBM7 directly binds to eRNAs, exosome component 10 (EXOSC10/RRP6) and EXOSC3 (RP40) were reported to be responsible for the final degradation of eRNAs (57). The recruitment of NEXT may also be facilitated by the CBC (57, 58) (**Figure 3A**).

The chromatin loop, including enhancer-promoter loop or E-P loop, as the optimal mediator of target gene expression, was found to play an important role in enhancer transcription and eRNA production *via* enhancer-promoter proximity facilitation (59–61) (**Figure 3B**). Since β-globin loci discovery, enhancer-promoter-mediated chromatin loops have been detected at multiple enhancer locus control regions (LCRs) interacting with target genes through chromosome conformation capture (3C) (62, 63).

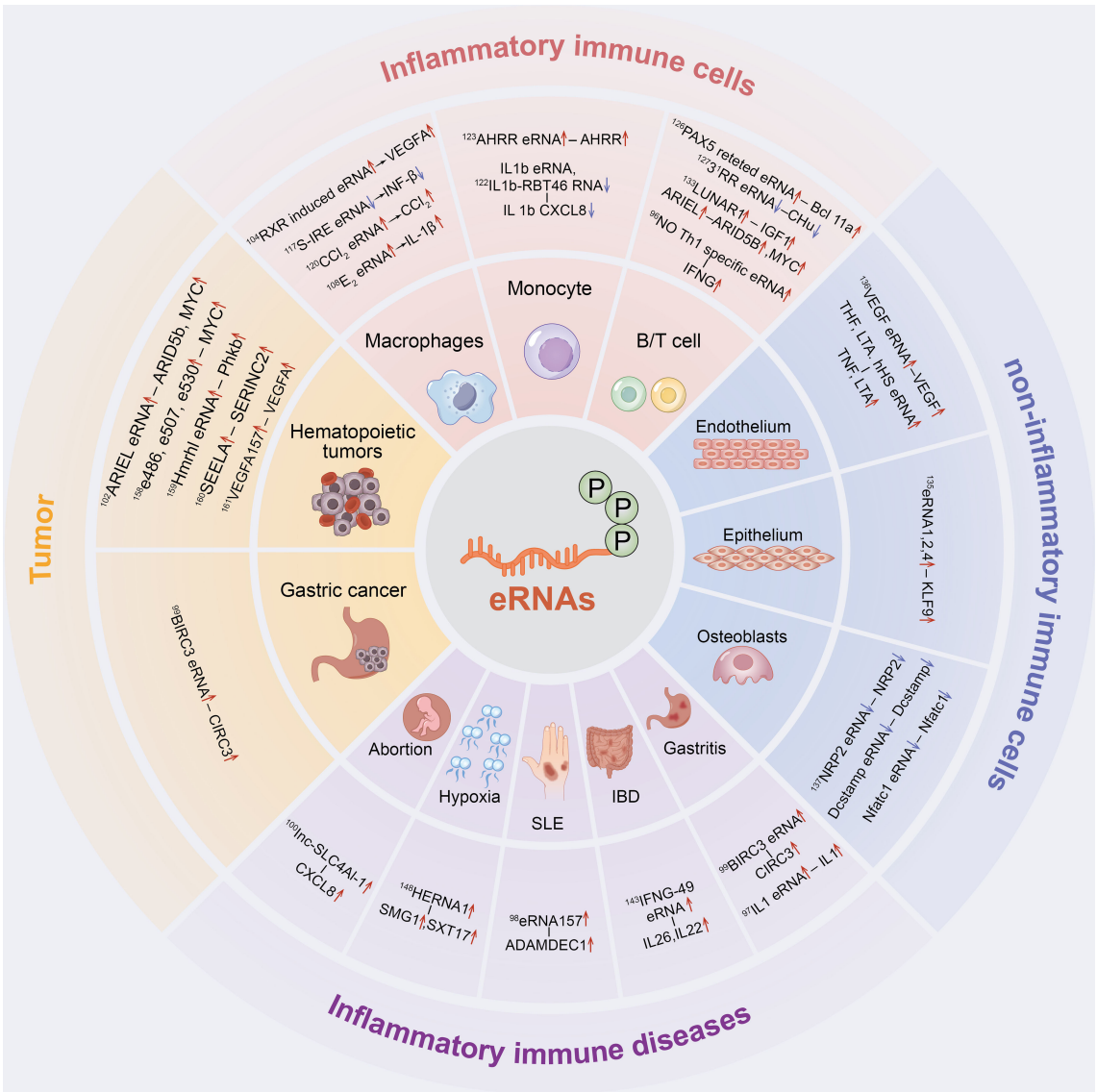

FIGURE 2 | The inflammatory immune role of eRNAs in cells and diseases. eRNAs have a significant contribution in inflammatory immune cells, non-inflammatory immune cells, inflammatory immune diseases and tumor inflammatory alterations.

LDTFs [e.g. NF-E2 (64)] were found to directly anchor E-P loop regions to recruit cTFs, CoFs or histone-modifying enzymes, which affects E-P loop formation and enhancer activation (64–68). H3K4me1 improves interchromatin interactions between enhancers and promoters by promoting chromatin recruitment to the cohesin complex (69), whereas H3K27ac affects enhancer-promoter activity by destabilising nucleosomes or recruiting H3K27ac-binding proteins (70). CCCTC-binding factor (CTCF), a highly conserved zinc finger protein, is co-localized with cohesin and has an independent cohesion binding site (71, 72). The cohesin-CTCF complex creates repressor regions (blocking chromatin repressor region diffusions and blocking enhancer activity) and active regions (promoting enhancer to promoter proximity) to regulate chromatin homeostasis, which contributes to the formation and stabilization of long-term chromatin interactions, thus, affecting E-P loop formation and transcription progression (73–78). Using molecular dynamics models, Dusan et al. (79) demonstrated that transcription-induced superhelix in the interphase chromosome topologically associated domain (TAD) formation is the driving force for chromatin loop extrusion, which stimulated enhancer-promoter contacts and activates mRNA transcription in a given TAD.

Effect of eRNA on Target Genes

eRNAs, a transcription product of enhancers, affect enhancer activity, E-P loop formation and downstream target gene transcription. Numerous studies have found that eRNA has several mechanisms as follows (**Figure 3C**): 1) eRNA positively

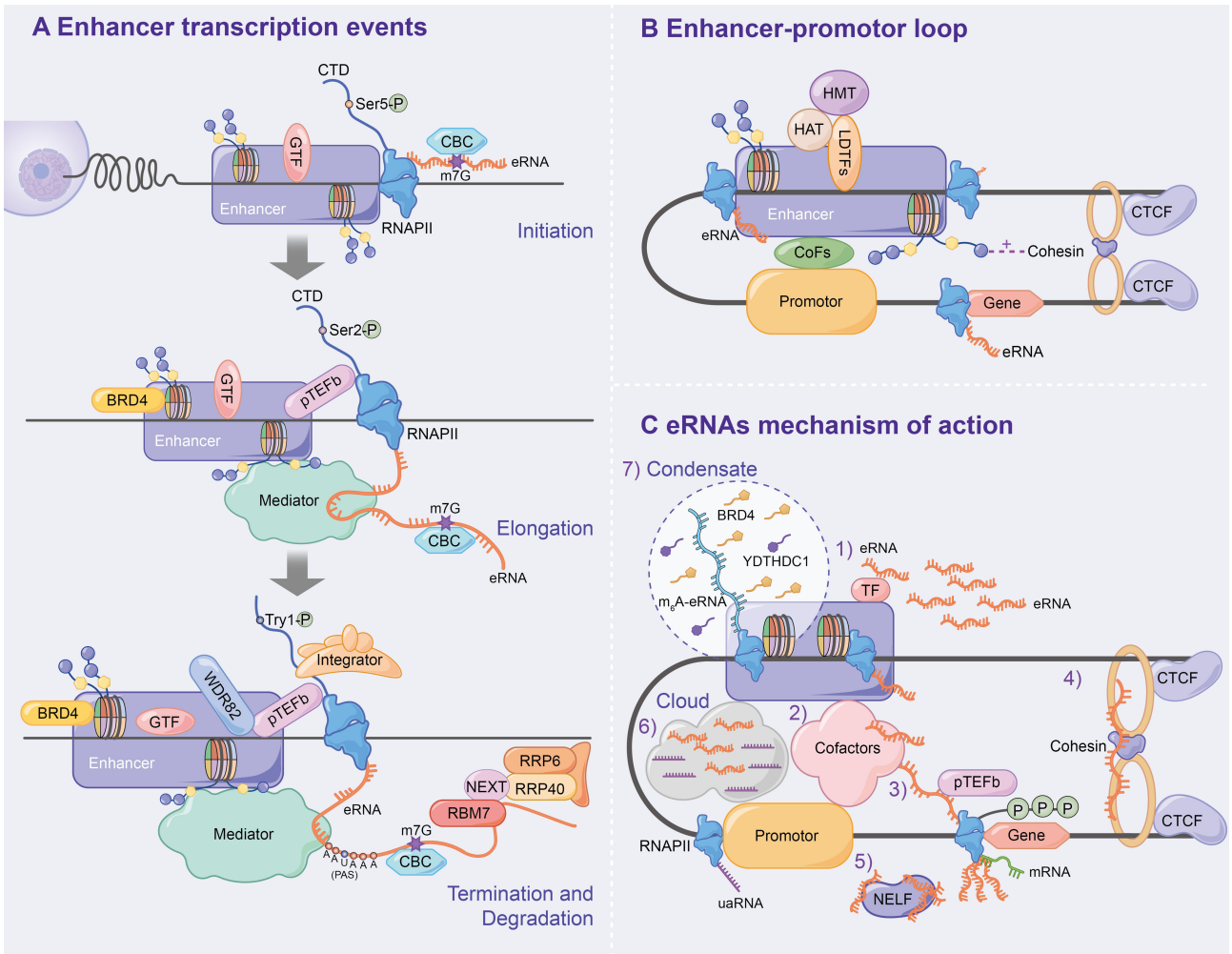

FIGURE 3 | Mechanism of enhancer transcription and eRNAs to regulate target genes. **(A)** Following enhancer activation, GTFs and serine 5-phosphorylated form of RNAPII (Ser5p) are recruited, which leads CBC to binding to eRNA *via* m7G, ultimately initiating enhancer transcription. During the enhancer elongation, Ser2p is hypoenriched. pTEFb, BRD4 and the eRNAs being transcribed all affect transcription elongation. Subsequently, the nascent eRNAs interacts with RNAPII CTD to terminate transcription. In addition, the integrator, WDR82 and Tyr1p assist in correct enhancer transcription termination. Finally, the NEXT complex mediates the degradation of eRNAs. **(B)** Chromatin loops are generated under the influence of LDTFs, histone methylation or acetylation, cohesin-CTCF complex and interphase chromosome topologically associated domain, and ultimately activate target gene transcription. **(C)** Specific mechanisms have been demonstrated for eRNAs to affect enhancer activity, E-P loop formation, and transcription of downstream target genes.

regulates enhancer transcription and stabilizes gene expression by binding to TFs (e.g. YY1) (12); 2) eRNA promotes active enhancer acetylation by recruiting Cofactors (e.g. CBP/300) (80) and interacts with various other Cofactors Complexes [e.g. RAD21 and heterogeneous nuclear ribonucleoprotein U (hnRNPU)] to stabilize the E-P loop and regulate target gene expression (81–83); 3) eRNAs directly induce E-P loop formation and histone modification by linking p300 (as Cofactors) and RNAP II (whose RNAP II are present on the enhancer and promoter, respectively) (84); 4) eRNA stabilizes the E-P loop structure by absorbing cohesin and subsequently regulating gene expression (85); 5) eRNA binds to the paused RNAPII by competing with mRNA, which allows the negative elongation factor (NELF) complex to separate from RNAPII and bind to eRNA, leading to RNAPII phosphorylation and the positive transcription elongation factor b (P-TEFb) recruitment and allowing RNAPII to enter the transcription elongation phase and produce mRNAs (86); 6) Cai et al. proposed for the first time that enhancers and promoters form a local molecular cloud during transcription, which consists of eRNA and uaRNA (eRNA promoter transcription analogues), bringing enhancers and promoters closer to facilitate E-P loop formation (87); 7) The recent studies have confirmed the prevalence of m6A modification in nascent eRNA, which recruits the nuclear m6A reader YTHDC1 to form a liquid-like condensate in a manner dependent on its C terminus intrinsically disordered region and arginine residues. Subsequently, the m6A-eRNA/YTHDC1 condensate co-mixes with and facilitates the formation of

BRD4 coactivator condensate, ultimately activating the gene (88); 8) Aguilo et al. (89) demonstrated that NOP2/Sun RNA methyltransferase (NSUN7) can deposit 5-cytosine methylation on eRNA, which affects eRNA stability and regulates enhancer transcription; 9) eRNA regulates gene expression by modulating E-P interactions and higher chromatin structure topology (9).

Potential Regulatory Mechanisms of eRNA in Inflammatory Immunity

Acute and chronic inflammation is the adaptive response to the internal environment and external stimuli, and the underlying pathological events leading to atherosclerosis, cancer, infectious diseases and immune disorders. The production of active enhancers and eRNA production in the nucleus precedes inflammatory gene expression in response to lipopolysaccharide (LPS) stimuli (90–92). Comprehensive studies of eRNA inflammatory immune-related mechanisms have revealed that the binding of LDTF (e.g. PU.1/T-bet/AP-1 and C/EBP) to the enhancer regions under inflammatory mediator stimulation promotes nucleosome remodeling to create nucleosome-free regions and H3K4me1/2 modification and recruits RNAPII (13, 80, 93–96). Subsequently, inflammation-associated signal-dependent TF NFκB-p65/p50 binds to the enhancer region and leads to histone H3K27ac modification and eRNA transcriptional production (10, 13, 93, 97–100). The generated eRNAs assist the tight junctions of the mediator complexes (p300-BRD and pTEFb-MLL) using enhancer-promoter interactions to stabilize the E-P loop (13, 97, 99, 101, 102). Conversely, eRNAs coordinate cohesin-CTCF loop formation to promote chromosome cyclisation (13, 79, 103, 104). Therefore, eRNA regulates enhancers and downstream target gene transcription through the aforementioned methods, and the mRNA produced is translocated outside the nucleus and generates associated inflammatory factors (such as INF-β, IL-1β, TNF and CXCL8), which affect inflammatory immune cell response and related pathological responses.

In the following sections, we will summarize in detail the role of eRNAs in inflammatory immune cells, non-inflammatory immune cells, inflammatory immune diseases and tumors as well as their related mechanisms (**Figure 2**).

eRNA in Inflammatory Immune Cells

LPS, a major component of the outer wall of the gram-negative bacterial cell wall, activate mononuclear macrophages, lymphocyte, endothelial cells and epithelial cells through cellular signaling systems. Various cytokines and inflammatory mediators are synthesized and released in this process, which induces an inflammatory immune response (105–107). Nasun et al. (91) were the first to use toll-like receptor 4 signaling in macrophages as a model to clarify that SE-associated eRNA transcription is dynamically induced in most key genes driving innate immunity and inflammation using GRO-seq. Subsequently, CAGE data further verified that enhancer transcription preceded the target gene activation in monocytes under LPS stimulation (41, 90). Recently, Ma et al. (92) used simultaneous high-throughput ATAC and RNA expression with sequencing (SHARE-seq) to identify domains of regulatory chromatin (DORCs) that significantly overlap with SEs, which showed both chromatin accessibility and enhancer lineage-priming precede gene expression. This suggests that altered chromatin accessibility could be a pre-condition for cell lineage formation. Therefore, current studies have shown that both enhancer transcription and eRNA precede the transcriptional induction of inflammatory genes in the LPS response (90–92) and eRNA links enhancer activity to inflammatory gene expression through CBP-mediated H3K27 acetylation (80). Conversely, the plasticity of mature immune cells attracts us to explore the potential function of eRNAs in inflammatory immune cells (108, 109) (**Table 1**).

eRNA in Macrophages

Macrophages, the key cells that maintain the tissue's internal environment and regulate the inflammatory immune response, perform tissue-specific functions and defend against infections (91, 120). Numerous studies have suggested the presence of PU.1 TFs in the active enhancer region of macrophages, which identify chromatin DNA recognition motifs and C/EBP, thereby creating nucleosome-free regions and undergoing histone tail H3K4me1/2 modifications (10, 13, 29, 54, 93, 95, 110–113, 121). Subsequently, similar signal-dependent TFs, p65 and NFκB, bind to the enhancer region under LPS stimulation, resulting in histone H3K27ac modifications and eRNA transcriptional generation (10, 93).

After activation of the RXR signaling pathway, the RXR-induced eRNAs were detected on Vegfa and Tgm2 enhancers, with studies showing that the eRNAs maintained macrophage angiogenic activity *via* enhancer interactions (104). In 2018, a study by Bence et al. revealed that macrophages under multiple IL-4 stimulations showed increased IL-4-sensitive (Arg1 and Hbegf) and RSG/IL-4-sensitive (Tgm2) eRNA expressions, leading to active STAT6 recruitment, which induced macrophage phenotypic changes by affecting the nuclear receptor PPAR (122). Meanwhile, Zsolt et al. (111) revealed that eRNA expression levels in IL4-STAT6-mediated responses correlated with the enrichment of RNAPII-Ser5p and RNAPII-Ser2p and levels of the inhibitory and activating factor STAT6 locus H3K27ac, which reduced macrophage responsiveness to LPS and suppressed inflammatory responses, including inflammatory vesicle activation, IL-1b production and pyroptosis. Further studies have clarified that Kdm6a, a demethylase, not only promotes macrophage IL-6 expression through promoter H3K27me3 demethylation but also interacts with MLL4 to increase IFN-β-specific eRNA S-IRE1, thereby promoting IFN-β transcription in macrophages (114). Ha et al. (115) suggested that the PU.1-mediated E2 eRNA (E_2 is a potential regulatory element of approximately 10 kbp that is located upstream of the TSS) in macrophages is essential for IL-1β mRNA transcription, which might influence the macrophage-assisted regulation of disease states, such as endotoxic shock, sepsis and infection. Additionally, Oishi et al. (116) found that RevErb expression regulated by Bmal1 was repressed in $Arntl^{-/-}$ macrophages, with further studies revealing that RevErbs repressed eRNA transcription by recruiting the NCoR- histone deacetylase3 (HDAC) repressor complex and increasing enhancer H3K27 acetylation, thereby regulating enhancer

TABLE 1 | List of eRNAs involved in inflammatory immune cells.

Cell type	Affected cell	Enhancer or SE	eRNA	Regulated gene	Mechanism	Function	Reference
Macrophages	Macrophages	Vegfa and Tgm2	RXR-induced eRNA	Angiogenic genes (Vegfa)	Stabilization of RXR-induced E-P loop	Induce angiogenesis	(110)
	Macrophages	IFN-β-specific enhancer	S-IRE1 eRNA	IFN-β and IFNB1	Interaction of Kdm6a with MLL4	Promote production of inflammatory factors	(111)
	Macrophages	Enhancer2	E2 eRNA	IL-1β	Mediated by PU.1 and NF-kB	Promote production of inflammatory factors	(112)
	Macrophages	Ccl2 enhancer	Ccl2 eRNA	Ccl2 (MCP-1)	(GPS2 and SMRT)-eRNA-CCL2 regulatory axis	Promote inflammation and insulin resistance	(113)
Monocyte	Primary monocytes	Enhancer	IL1b eRNA	IL1b	Mediation of the pro-inflammatory transcription factor NF-kB	Promotes the release of pro-inflammatory factors	(114)
			IL1b-RBT46 eRNA	CXCL8			
	CD14+ monocyte	AHRR enhancer	AHRR eRNA	AHRR	Affection of pol II recruitment in transcription	Influence cell type-specific AHRR	(115)
	THP-1 monocytes	hHS-8 enhancer	TNF eRNA, LTA eRNA, hHS eRNA	TNF, LTA	No	Influence monocyte inflammatory immunity	(116)
B lymphocytes	B cell	No	LNCGme00432, 00344, 00345	Bcl11a	No	Cause malignant development of B cells	(117)
	B cell	3′RR SE Eμ enhancer	3′RR eRNA	CHμ	Regulation of SHM and conventional CSR	Affect the B-cell maturation process	(118)
T lymphocytes	T-ALL cells	No	LUNAR1	IGF1R	Mediation of notch signaling pathway	Maintain the malignant progression of T-ALL	(119)
	T-ALL cells	ARID5B enhancer	ARIEL	ARID5B MYC	Regulation of the TAL1-induced transcriptional program	Accelerate T-cell malignant progression	(97)
	T cells	T-bet SE	eRNA	IFNG	Mediation of NF-kB	Regulation of Th cell differentiation	(91)
	CD4+ T cell	hHS-8 enhancer	TNF eRNA. LTA eRNA, hHS eRNA	TNF LTA	No	Affect T-cell pathological changes	(116)

epigenetic state to control macrophage inflammatory response (43, 116). Huang et al. (123) used inflammatory macrophage activation models to demonstrate that the inflammation activation-associated corepressor (GPS2 and SMRT)-eRNA-CCL2 regulatory axis, in addition to finding that LNA-targeted Ccl2 enhancer E-transcribed eRNA in white adipose tissue macrophages of obese (ob/ob) mice, can partially reverse meta inflammation and insulin resistance.

Therefore, macrophages activate intranuclear enhancer transcription and eRNA production in response to inflammatory stimuli, which regulates inflammatory factors and chemokine release and affects macrophage polarisation. However, the specific mechanisms of inflammatory genotypic and phenotypic changes by eRNA remain unclear and require further experimental exploration.

eRNA in Monocytes

Circulating monocytes, innate immune response cells, prevent infection by rapidly removing invading pathogens. Heward (117) and IIott (118) reported in the same year that monocytes are differentially expressed with large amounts of eRNAs in response to LPS stimulation. Heward James et al. (117) identified the expression of six eRNAs induced by human monocyte THP1 cells after the LPS activation of the intrinsic immune response, including MARCKS-eRNA, ACSL1-eRNA, AZIN1-eRNA, TNFSF8-eRNA. SLC30A4-eRNA and SOCS3-eRNA. Moreover, the intracellular signaling pathways, such as NFκB and mitogen-activated protein kinase (MAPK), were demonstrated to regulate extracellular kinase 1/2 and p38, which could promote inflammation-associated eRNA expression (117). IIott Nicholas et al. (118) identified 76 differentially expressed eRNAs in primary human monocytes stimulated by LPS and found that the knockdown of the pro-inflammatory TFs, NFκB-mediated IL1b eRNA and IL1b-RBT46 eRNA, attenuated LPS-induced mRNA transcription and pro-inflammatory mediator release, including IL1b and CXCL8. Using reduced representation bisulfite sequencing (RRBS) technology, smoking-associated differentially methylated regions (SM-DMR) was found to up-regulate AHRR mRNA by activating the AHRR enhancer that expressed AHRR eRNA (124). Additionally, smoking-altered methylation and intragenic AHRR enhancer-produced eRNA were found to be necessary prerequisites for monocyte type-specific AHRR transcription (124). Moreover in THP-1 monocytes, hHS-8 was shown to target dCas9-KRAB at the IRF1 binding site to impair IFN-gamma expression on LPS-induced TNF genes and eRNA, thereby affecting monocyte inflammatory immune action (125). Current studies suggest that eRNAs regulate the direction of monocyte function; however, their functional mechanism remains unknown.

eRNA in Lymphocyte

As important cellular components of inflammatory immune response, lymphocytes are the main performers of the lymphatic system immune function. They are mainly responsible for fighting external infections and monitoring cellular mutations in the body, and are categorized into B lymphocytes, T lymphocytes and natural killer cells.

eRNA in B Lymphocytes

Studies have reported that eRNA transcription during B lymphocyte growth and development is closely associated with large-scale changes in DNA cytosine modifications (126). Moreover, Brazao et al. (127) identified 73 PAX5-dependent eRNAs near protein-coding genes in B-ALL cells, such as LNCGme00432, LNCGme0034 and LNCGme00345, that were the downstream genes of B-cell lymphoma 11a (Bcl11a), whose dysfunction may lead to the malignant development of B cells. Furthermore, Saintamand et al. (128) reported that LPS-induced stimulation *in vitro*, whereas 3RR eRNA deletion reduced transcription and disrupted downstream CH basal transcription, which affected the resting and active states of B cells.

Many eRNA studies have been conducted in the classical B lymphocyte line (GM12878); however, only a few studies have explored the direct effects of enhancer transcription and eRNAs on B lymphocytes. Kim et al. (119) confirmed that enhancers dynamically modulate the transcriptional activities of eRNAs and pre-mRNAs in B-lymphoblasts. Furthermore, the knockdown of TNFSF10-related eRNAs leads to selective regulation in interferon-induced apoptosis, indicating that eRNAs are necessary for target gene induction and can be potential target genes *via* transcriptional reprogramming (119). Katla et al. (129) identified quantitative trait loci associated with eRNA expression and direction-dependent enrichment at enhancer regions in human lymphoblastoid cell lines using capped-nascent-RNA sequencing. These loci were correlated with gene expression, defined central TF binding regions and flanking eRNA initiation cores, which are important indicators of non-coding regulatory variants. Therefore, B lymphocytes have important functionality in enhancer transcription and eRNAs, which affect the growth, differentiation and malignant progression of B lymphocytes; however, further extensive studies are required.

eRNA in T Lymphocytes

The exploration of acute T lymphocytic leukaemia leads to unrevealing the relationship between eRNAs and T lymphocytes, confirming the presence of a large number of eRNAs in T-ALL cells (130, 131). Ets1 is a sequence-specific transcription factor that plays an important role during hematopoiesis, and is essential for the transition of CD4–/CD8– double negative (DN) to CD4+/CD8+ double positive (DP) thymocytes. During early T cell differentiation, eRNA shows a DN to DP transition pattern and the Ets1 pattern in DP transition, similar to the RNAPII pattern, suggesting that eRNAs act as active regulatory elements that regulate Ets1 on nucleosome occupancy and enhancer activity to influence T cell differentiation (132). Trimarch et al. (133) identified the first functional eRNA (LUNAR1) in T-ALL cells in 2014, which enhances IGF1R mRNA expression and maintains the IGF1 signaling pathway *via* Notch signaling, thereby maintaining T-Acute lymphoblastic leukaemia (ALL) malignant progression. Subsequently, Tan et al. (102) identified the second functional eRNA (XLOC_005968) in T-ALL cells, namely ARIEL, which recruits intermediary proteins to the ARID5B enhancer, promotes enhancer-promoter interaction and activates ARID5B expression, and thereby positively regulating TAL1-induced transcription and MYC oncogene expression, to accelerate T cells malignant progression.

Recently, some studies have explored the effect of eRNAs on the generation and differentiation of T cells. Hertweck et al. (96) revealed that eRNAs transcribed by T-bet SE were mostly Th1-specific in T cells. In Th1 cells, eRNAs of IFNG upstream SEs were transcribed, while the downstream enhancer exhibited lower levels of P-TEFb occupancy and eRNA production, which affects Th cell differentiation. Luke et al. (125) found that activated CD4+ T cell increased hHS-8, TNF and LTA promoter H3K27 acetylation and nuclease sensitivity while synergistically inducing TNF, LTA and hHS-8 eRNA transcription to regulate TNF mRNA and LTA mRNA, affecting T cell pathology.

eRNA in Natural Killer Cells

To date, no studies have explored the effects of eRNAs on natural killer (NK) cells generation, development and differentiation. Only one study has shown that the H3K27me3 histone demethylase UTX controls specific gene expression programs during development of natural killer T cells through demethylase activity-dependent manner (134). We believe that enhancer transcription events and eRNAs have a potentially important role in NK cells as potential therapeutic targets and prognostic biomarkers in inflammatory immune diseases and tumors.

Inflammatory Function of eRNA in Non-Inflammatory Immune Cells

The inflammatory immune functions of eRNAs are not limited to inflammatory immune cells. The recent studies showed that non-immune inflammatory cells have inflammatory changes and altered cellular states under eRNA regulation (135–138). Isidore et al. (136) found that VEGFA-eRNA5 and VEGFC-eRNA3 in endothelial cells affect angiogenesis and lymphangiogenesis by regulating endogenous transcription and VEGFA and VEGFC expression. Additionally, eRNAs were found to be well correlated with VEGF expression across cell types and in response to hypoxic stimuli using GRO-Seq. Zhou et al. (138), in the same year, revealed that lncRNA-MAP3K affects inflammatory factor (e.g. ICAM-1, E-selectin and MCP-1) expression, reduces monocyte-endothelial cell adhesion and decreases TNF-α, IL-1β and COX2 expression in macrophages through the p38 MAPK signaling pathway and MAP3K4 cis-modulation, which ultimately regulates vascular inflammation. Despite that the overlapping features of lncRNA-MAP3K with 1D-eRNA, strong evidence supporting lncRNA-MAP3K4 as an eRNA that is transcribed from the MAP3K4 enhancer region is lacking (138). Conversely, glucocorticoids have been shown to induce KLF9 expression in lung epithelial cells, with the identification of three common glucocorticoid receptor binding sites that influenced KLF9 mRNA and protein expression levels by generating eRNAs, which ultimately affected glucocorticoid-induced anti-inflammatory effects (135). Additionally, Yukako et al. (137) showed that Nrp2-eRNA, Dcstamp-eRNA and Nfatc1-eRNAs could regulate the corresponding promoters to control gene expression, thereby positively regulating osteoclast differentiation to maintain bone resorption function.

These studies, therefore, indicate the potential inflammatory role of eRNAs in non-inflammatory immune cells. However, further studies are required to explore their specific mechanisms and functions.

eRNA in Inflammatory Immune Diseases

NFκB is an important gene regulator involved in innate and adaptive immune responses as well as survival and proliferation of certain cell types (139), and eRNAs have been shown to be involved in the regulation of inflammatory transcriptional networks (10, 118, 140). Studies have shown that NFκB contributes to the synthesis of inflammatory gene-associated enhanced eRNAs, which further enhances transcription by looping enhancers and promoters or by recruiting RNA polymerase II to the promoter, creating a transcription-mediated multilevel cascade regulating transcription (10, 13, 81, 91). Therefore, this paper further summarizes the potential functions and mechanisms of eRNAs in various inflammatory immune-related diseases (**Table 2**).

eRNA in Gastritis

The chronic inflammation and apoptosis resistance associated with Helicobacter pylori infection contributes to gastric disease development, including gastritis and gastric cancer (142). Chen et al. (97) were the first to report that H. pylori stimulated the recruitment of RelA and Brd4 to inflammatory gene-related enhancers and promoters. Following this, IL1A and IL1B eRNA expressions were up-regulated to affect NFκB-dependent inflammatory gene expressions (e.g. IL1); however, JQ1 was found to attenuate the H. pylori-induced eRNA and mRNA synthesis of NFκB-dependent inflammatory gene subpopulations by inhibiting Brd4-related functions, which suppresses inflammatory immune cell proliferation in H. pylori-infected mice (97). Subsequently, Brd4 was shown to de-activate cIAP2 expression by activating BIRC3 eRNA synthesis in H. pylori infection, which in turn inhibited caspase-3 activation, and ultimately inhibiting cell apoptosis. Therefore, the novel role of BIRC3 eRNA in H. pylori-mediated apoptosis resistance was speculated (99).

eRNA in Inflammatory Bowel Disease

Inflammatory bowel disease (IBD), a chronic inflammatory intestinal immune disease, has an unknown molecular pathology. Studies have reported significant differences in eRNA expression levels among multiple chemokine gene-related enhancer regions (including CXCL1-3, CXCL5-6 and CXCL8), which are all up-regulated in IBD, Crohn's disease (CD), ulcerative colitis (UC) and controls using CAGE and qPCR (143). Baillie et al. (90) used the human monocyte-derived macrophage as a model to explore the genetic aetiology of IBD. They found that transient eRNA transcripts at multiple loci precede promoter-associated transcripts under LPS induction, which affects the adaptation of monocytes to the gastrointestinal mucosal environment, thus leading to IBD. Additionally, Aune et al. (141) revealed a significant association between eRNA genomic location and disease-specific genetic polymorphisms in IBD. It also suggested that

TABLE 2 | List of eRNAs involved in inflammatory immune diseases.

Disease	Affected cell	Enhancer or SE	eRNA	Regulated gene	Mechanism	Function	Reference
Gastritis	Gastric adenocarcinoma cells	IL1 enhancer	IL1 eRNA	IL1	Mediation of NF-kB	Influence inflammatory gene expression	(92)
	Gastric epithelial cells	BIRC3 enhancer	BIRC3 eRNA	BIRC3 cIAP2	Induction of caspase-3 activation	Improve apoptosis resistance in gastric epithelial cells	(94)
Inflammatory bowel disease	CD14+ cells	IFNG	IFNG-R-49	IL22 IL26	No	Regulate inflammatory factors	(138)
Systemic Lupus Erythematosus	Monocyte	Enhancer 2	eRNA157	ADAMDEC1	Mediation of MAP kinase and p300-NFκB	Regulate of SLE-related inflammatory gene expression	(93)
Autoimmune uveitis	CD4+ T cells	SEs	Ifng eRNA	Th1 gene	Recruition of media and P-TEFb	Promote cell-specific gene expression	(91)
Recurrent pregnancy loss	Trophoblast cells	No	lnc-SLC4A1-1	CXCL8	Recruition of NFκB and CXCL8	Exacerbate inflammatory response	(95)
Hypoxia	Cardiomyocytes	No	HERNA1	SMG1 SYT17	Mediation of phosphatidylinositol 3-kinase-related kinases	Regulate of hypoxic progression and metabolism	(141)

the transcription site of the IFNG-R-49 eRNA was more than 100 kb away from the IL26 and IL22 genes, which are consistent with the biological functions exhibited by the eRNA.

eRNA in Rheumatoid Arthritis

Rheumatoid arthritis (RA) is a systemic autoimmune disease characterized by chronic synovial inflammation. Various studies have identified the basic leucine zipper transcription factor 2 (BACH2) protein to be a key transcription factor of Treg cells for immune homeostasis. It regulates the expression of various cytokines, including INF-γ and cytokine receptors, whose mutations are associated with RA development and progression (144). BACH2 proteins have been reported to negatively regulate eRNA expression; however, eRNA types and potential mechanisms remain unclear (144). Many disease-associated variants in non-coding regions act by affecting gene transcription and are known as eQTL (145). Studies found that eQTLs were involved in eRNA transcriptional regulation and produced cell type-specific effects, such as STAT6 eQTL up-regulation in patients with RA upregulated inflammatory cytokine production (145–147). Unfortunately, there are no studies that specifically identify which eRNAs influence the occurrence and progression of RA by which mechanisms.

eRNA in Other Inflammatory Immune Diseases

Many studies have shown that eRNAs plays a critical role in various inflammatory diseases. The close correlation between ADAMDEC1 and ADAM28 in systemic lupus erythematosus (SLE) regulates the disease inflammatory process. Shi et al. (98) found that monocyte ADAMDEC1 over-expression in patients with SLE was induced by the stimulation of pro-inflammatory cytokines, moreover, under LPS stimulation, the binding of the p300-NFκB complex to enhancer 2 generates eRNA157 that promotes p300 activation, leading to an increase in H3K27ac at the enhancer and promoter region, thus, affecting the regulation of ADAMDEC1 mRNA and SLE-related inflammatory gene expression. Hertweck et al. (96) found that in a mouse model of autoimmune uveitis, T-bet allows mediator and P-TEFb recruitment in the form of SE by extending the SE-generating Ifng eRNA. Therefore, Th1 expression is activated, which triggers IFN-gamma-mediated CD4+ T cells to promote immunoretinol-like binding proteins in the retina. Additionally, flavanols and JQ1 can inhibit SE and its products to down-regulate related gene expression (such as Ifng, Tnf, Fasl, Il18r1 and Ctla4), and ultimately decrease the severity of the disease. Furthermore, Huang et al. (100) first found that lnc-SLC4A1-1 was retained in the nucleus as an eRNA and facilitated TF NF-κB binding to CXCL8 promoter region, leading to an increase in H3K27ac in the CXCL8 promoter and subsequently elevated CXCL8 expression. CXCL8 activation is exacerbated by the induction of TNF-α and IL-1β inflammatory response in trophoblast cells, resulting in unexplained recurrent pregnancy loss. It was also found that hypoxia-inducible enhanced RNA 1 (HERNA1) is produced by direct hypoxia-inducible factor 1α binding to the hypoxia response element of histone h3-lysine27. Synaptotagmin XVII, membrane transport proteins, Ca2+ sensing protein and SMG1 are also encoded by phosphatidylinositol 3-kinase-related kinase, thereby regulating immune disease progression, metabolism and contraction (148). Spurlock et al. (149) found that whole blood eRNA expression data effectively classified and differentiated patients with multiple sclerosis from those with other inflammatory and non-inflammatory neurological diseases.

Inflammatory Function of eRNA in Cancers

Cancer is currently a significant cause of death worldwide and it is a heterogeneous disease controlled by genetic and epigenetic alterations and transcriptional dysregulation (150). Numerous studies have been conducted to show that the abnormal expression levels of eRNAs, as an excellent marker of active enhancers and genes, are associated with dysregulation of enhancer transcription and gene expression in tumors (34, 151–153). Santanu Adhikary (33), Joo-Hyung Lee (34) and Zhao Zhang et al. (154) have each summarized in detail the potential functions, regulatory mechanisms and clinical therapeutic implications of eRNAs in cancer. Nevertheless, this study will focus on the potential functions and mechanisms of eRNAs in tumorigenesis development on its immune microenvironment and related inflammation (**Table 3**).

eRNA in Haematologic Malignancies

The relevant functions and mechanisms of eRNAs in inflammatory immune cells have been previously summarized, along with the exploration of the potential functions and mechanisms of eRNAs in immune hematopoietic system-related tumors. Almamun et al. (155) were the first to report that the aberrant methylation of enhancer regions was associated with the altered expression of neighboring genes involved in cell cycle processes, lymphocyte activation and apoptosis in pre-B ALL. Further studies have suggested an overall downregulation of eRNA transcripts in patients with pre-B ALL, which may affect the downregulation of target genes (such as ICOSLG, IRF4 and MSA1) in B-cell migration, proliferation and apoptosis (156). Further, Teppo et al. (157) used eRNA quantification to elucidate the aberrant transcriptional activity downstream of fusion TFs and demonstrated that the ETV6-RUNX1 axis regulates cell adhesion and transmembrane signaling pathways, which ultimately disrupts normal B lymphangiogenesis. Tan et al. (102) were the first to demonstrate the involvement of lncRNA in the regulation of TAL1-induced T-ALL oncogenic regulatory program. They also showed that XLOC_005968, the ARIEL eRNA, is oncogenic and positively regulated by ARID5B and MYC oncogene expression in T-ALL cells by recruiting mediator complexes and promoting ARID5B enhancer-promoter interactions (102). Additionally, Kaposi's sarcoma-associated herpesvirus (KSHV), a human tumorigenic γ-2 herpesvirus, is the pathogen responsible for Kaposi's sarcoma and primary effusion lymphoma. It is proposed that KSHV reactivation decreases MYC gene expression by downregulating MYC eRNA expression and enhancer activity, and shRNA-mediated and vIRF4-mediated cIRF4 suppression, which promotes lytic replication (158).

In leukaemia, a novel Hmrhl eRNA was shown to be highly upregulated in chronic granulocytic leukaemia (CML) cells and

TABLE 3 | List of eRNAs involved in inflammatory effects in tumors.

Cancer	Affected cell	Enhancer or SE	eRNA	Regulated gene	Mechanism	Function	Reference
Pre-B ALL	Pre-B ALL cell GREAT	No	eRNA	ICOSLG, IRF4, MSA1	Down-regulate migration, proliferation and apoptosis gene	Promotes malignant progression	(151)
Pre-B ALL	Pre-B ALL cell	CD19+/CD20+ spectrum SE	eRNA	ETV6-RUNX1	Interference with B-cell signaling and adhesion signaling	Disrupt normal B lymphopoiesis	(152)
T ALL	Leukemia cell	ARID5B enhancer	ARIEL eRNA	ARID5B MYC	Recruition of intermediary complexes and Stable E-P rings	Involve in T-cell leukemia formation	(97)
KSHV-infected primary effusion lymphoma	TREx BCBL1 cell	MYC SE	MYC eRNA (e486, e507, e530)	MYC	Alteration of host epigenome status	Promote viral lysis and replication	(153)
Chronic granulocytic leukemi	Leukemia cell	Hmrhl enhancer	Hmrhl eRNA	phkb	No	Regulate positively phkb genes	(154)
MLL rearranged leukemia	MLL leukemia cells	Enhancer	SEELA eRNA	SERINC2	Promotion of histone recognition	Regulate tumor metabolism	(155)
Chronic myeloid leukemia	Leukemia cell	VEGFA157 enhancer	VEGFA157 eRNA	VEGFA	Selective splicing of target genes	Promote CML pathology	(156)
Gastric cancer	Gastric epithelium	BIRC3 enhancer	BIRC3 eRNA	BIRC3 cIAP2	Inhibition of caspase-3 activation	Enhance apoptosis resistance in gastric epithelial cells	(92, 94)
Colorectal cancer	CRC cell	Carcinogenic SE	eRNA	IL-20RA	Elevated expression of cell proliferation and immune evasion genes	Modulate carcinogenic and immune pathways	(157)

positively regulate its host gene phkb expression (159). Additionally, Fang et al. (160) found that eRNAs such as SEELA are widely activated in mixed-lineage leukaemia and demonstrated that SEELA directly binds to amino acid K31 of histone 4 and mediates the cis-activated transcription of the neighboring oncogene serine incorporate 2, which regulates oncogene transcription and tumour metabolism (sphingolipid synthesis) to influence leukaemia progression. The demethylation of vascular endothelial growth factor A (VEGFA) enhancer in CML promotes the overexpression of cancer signature genes. A study by Dahan showed that VEGFA+157 eRNA regulates its selective splicing, which affects CML cell proliferation by increasing RNAPII elongation *via* CCNT2 (161).

eRNA in Other Cancers

To date, eRNA inflammatory immune-related functions are only marginally studied in solid tumors. H. pylori infection is a major cause of gastric cancer, and its pathogenicity is associated with chronic inflammation induction and apoptosis resistance. The inflammatory immune role of eRNA in tumors was first reported by Chen et al. (99), demonstrating that H. pylori stimulate bromodomain-containing factor Brd4 recruitment to the BIRC3 enhancer, which promotes BIRC3 eRNA synthesis and cIAP2 expression, which inhibits caspase-3 activation and enhances apoptosis resistance in gastric epithelial cells. Additionally, some studies have suggested the presence of oncogenic SEs in colorectal cancer and confirmed their involvement in regulating oncogenic and immune pathways in colorectal cancer by modulating IL-20RA expression, affecting cell proliferation and immune evasion-related gene ecpression (162). Pancreatitis accelerates Kras mutation-driven tumorigenesis in mice, which is mostly found in pancreatic ductal adenocarcinoma (163). Li et al. (163) reported that under inflammatory stimulation, KrasG12D mutation targets a transient enhancer network driving proto-oncogene transcription and provides a sustained Kras-dependent oncogenic program to drive tumour tissue-specific progression. However, they did not explore the specific mechanism and types of enhancers and eRNAs.

The rapidly rising development of bioinformatic technologies provides novel means and directions to study the role of eRNA in inflammatory immunity in tumors. Various bioinformatics analyses have initially suggested that eRNA expression levels are significantly correlated with malignancy prognosis and can affect the tumour immune microenvironment (164–170). Furthermore, Xiao et al. (164) found that LINC02257 eRNA was significantly associated with cancer survival and immunotherapy-related indicators (e.g. tumour microenvironment, tumour mutational load and microsatellite instability). A study by Wang et al. (165) identified WAKMAR2 eRNA as a key candidate biomarker in invasive breast cancer, which may influence the tumour microenvironment by regulating the relevant immune-related genes, such as RAC2, IL27RA, IGLV1-51, IGHD, IGHA1 and FABP7. AC003092.1 eRNA and glioblastoma multiforme (GBM) overall survival were significantly correlated, and AC003092.1 eRNA was shown to be associated with the immunosuppressive microenvironment of GBM using single gene set enrichment

analysis and CIBERSORTx system analysis (166). Using similar bioinformatic techniques, several studies have suggested that functional FOXO6-eRNA can regulate FOXO6 expression to influence EGFR and SOX2 expression and function in lung cancer progression (167); furthermore, the aberrant expression of LINC00987/A2M axis was closely associated with immune cell infiltration in lung adenocarcinoma (168). AC007255.1 in esophageal cancer was reported to be closely associated with tumour immune response and neutrophil activation (169). Additionally, AP001056.1 was shown to be enriched in the biological function analysis of head and neck squamous cell carcinoma, mainly in immune system processes (170). However, bioinformatic analyses can only tentatively suggest the potential role of relevant eRNAs in tumors. Therefore, further basic research and clinical trials are required to validate these results.

Clinical Perspectives of Enhancer Inhibitors Affecting eRNA Production

Many eRNAs are significantly differentially expressed in tumour tissues compared with paracancerous tissues (151, 154), which is consistent with the results of enhancer overactivation in cancer (171–174). Therefore, eRNAs can be considered as potential targets to overcome enhancer activation in cancer therapy. eRNAs have high specificity across tissues and tumours (41, 151, 154), with the antisense oligomer-based targeting of specific eRNAs effectively inhibiting target genes and tumour growth without theoretically affecting other unrelated tissues (49, 82, 102, 154, 175, 176). Therefore, eRNAs can be used as effective and highly precise therapeutic targets in cancer therapy. Regrettably, no relevant eRNA-targeted drugs are currently on the market or in clinical trials. In this section, we will therefore concentrate mainly on enhancer inhibitors affecting eRNA production to elucidate their potential therapeutic effects on inflammatory immune diseases and even cancer. The eRNA-related agents in cancer have been previously reviewed, including bromodomain and extra-terminal (BET) inhibitors, cyclin-dependent kinases (CDKs), HAT inhibitors and HDAC inhibitors (33, 34, 177). Since inhibitors that fully target eRNAs in inflammatory immune-related diseases have been rarely studied, the combined inhibitors of eRNAs and active enhancers, which produce eRNAs, have been summarized along with their therapeutic potential in inflammatory immune diseases in **Figure 4**.

ET Inhibitors in eRNA

Estradiol cypionate (ET) inhibitors, such as JQ1 and I-BET762, can recognize acetylated histones by interfering with the BET family proteins BRD2, BRD3, BRD4 and BRDT (178). Thus, targeting this protein class can promote LPS-induced inflammatory gene expression in macrophages and significantly improve survival, as observed in an *in vivo* sepsis model (178, 179). JQ1 primarily targets BRD4 to inhibit TNF-α or IL-1β-induced inflammatory cytokines expression and reduces enhancer-mediated inflammatory responses and diseases (180–183) (**Figure 4**). H. pylori stimulates NFκB-dependent BRD4 to enhance inflammatory gene-related eRNA synthesis, similarly, JQ1 inhibits BRD4 to reduce eRNA synthesis and inhibits RNAPII recruitment that is induced by BRD4 interaction with RelA. Additionally, JQ1 has been reported to inhibit inflammatory gene expression and inflammatory

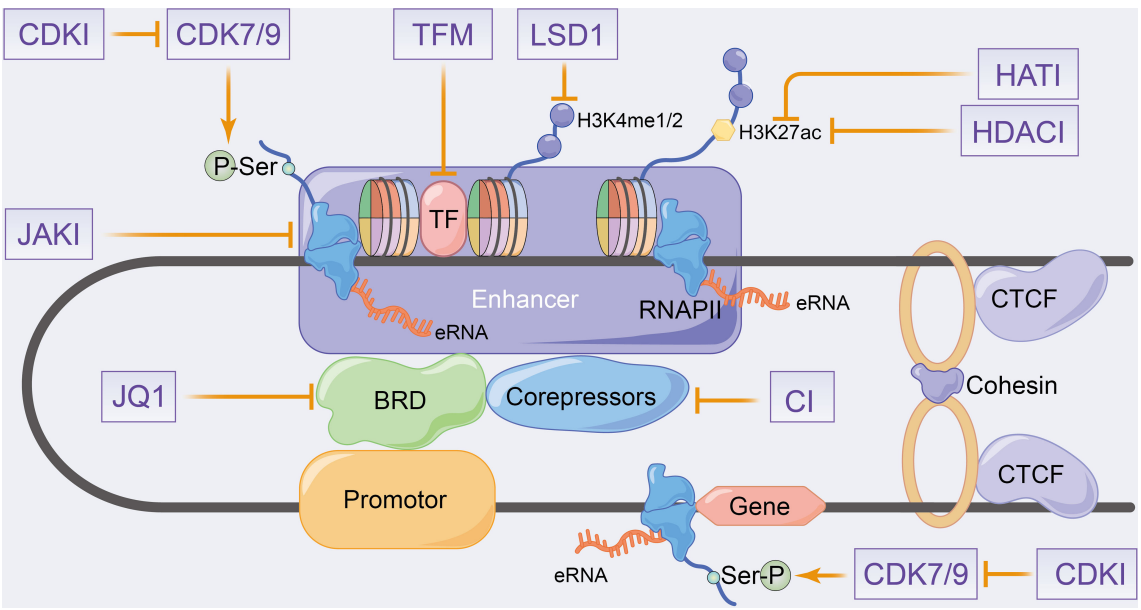

FIGURE 4 | Schematic representation of putative therapeutic targets to enhancer transcription events and eRNA landscapes. CDKI, cyclin-dependent kinase inhibitors; HATI, histone acetyltransferase inhibitors; HDACI, histone deacetylase inhibitors; LSD1, lysine-specific demethylase 1; JAKI, janus kinase inhibitors; TFM, transcription factors inhibitors; CI, co-repressors inhibitors.

immune cell proliferation in H. pylori-infected mice (97). Arnulf et al. (96) demonstrated that the treatment of Th1 cells with JQ1 and xanthinol resulted in the inhibition of P-TEFb, which produced a significant reduction in eRNA levels, including Ifng eRNA. This also promoted reduction in SE-related Th1 gene expression (e.g. Ifng, Tnf, Fasl, IL18 and Ctla4), which caused disease remission in autoimmune uveitis mice. Angela et al. (158) reported that the associated MYC eRNAs (including e486, e507 and e530) was significantly decreased after the JQ1 treatment of KSHV-infected primary effusion lymphomas, which inhibited MYC expression and KSHV cleavage gene expression induction. Additionally, a decrease in MYC mRNA was found on the knockdown of the corresponding eRNA (158). JQ1 was demonstrated to decrease the transcriptionally activated eRNAs of SEs, causing the down-regulation of IL-20RA expression and inhibition of growth, metastasis and immune escape in colorectal cancer (162). Therefore, JQ1 regulates enhancer transcription and eRNA synthesis by affecting the mediator complex, which regulates the downstream target genes to modulate the disease process.

CDK Inhibitors in eRNA

CDK7 is a component of the transcription initiation factor IIH (TFIIH) in the GTF complex that regulates enhancer and target gene transcription by phosphorylating Ser5 and Ser7 on RNAPII (184). Additionally, CDK7 activates and phosphorylates the P-TEFb catalytic subunit of CDK9, which phosphorylates Ser2 in the RNAPII CTD to control transcriptional elongation and termination (184) (**Figure 4**). Currently, transcriptional CDKs are considered potent targets for cancer therapy (185–189), and recently, some studies have also evaluated the role of CDK inhibitors in inflammatory-immune diseases (190–192). The therapeutic role of CDK7 in haematologic malignancies has been widely reported that demonstrate the deletion of oncogenic transcription factors, such as RUNX1, by small-molecule CDK inhibitors in acute T-lymphoblastic leukaemia (189). Moreover, SY-1365, a highly selective CDK7 inhibitor, is currently used in clinical trials in patients with ovarian and breast cancer (187). These studies have confirmed that CDK7 inhibitors reduce enhancer-associated oncogene expression by modulating eRNA expression levels. CDK inhibitors such as THZ1, NVP-2 and THZ531 that inhibit CDK7, CDK9, CDK12 and CDK13, respectively, have been shown to downregulate SE-related oncogene expression and promote DNA damage response gene loss in chordoma and acute T-lymphoblastic leukaemia cells, respectively (185, 186, 188). Furthermore, the blocking of CDK7 has been reported to regulate the onset and intensity of immune-inflammatory responses by activating the tumour immune response and regulating granulocyte apoptosis and cytokine secretion (193, 194). Recently, transcriptional CDKs have been speculated to play an important role in pro-inflammatory gene expression (190), with Wei et al. to be the first to demonstrate in the cytokine release syndrome (CRS) that the CDK7 covalent inhibitor THZ1 downregulates inflammatory gene transcription in macrophages after preferential target inhibition associated with SEs, such as STAT1 and IL1, decreases cytokine release, alleviates the hyperinflammatory state and rescues lethal CRS mice (191).

Other Inhibitors in eRNA

Furthermore, enhancer transcription analyses and eRNA generation processes revealed that TF modulators, HAT inhibitors and HDAC inhibitors influence eRNA and mRNA production by modulating enhancer epigenetic characteristics (177) (**Figure 4**). HATs, such as p300-CBP, enable histone tail acetylation modifications (195), whereas polycomb repressive complex (PRC) mediates histone methylation. The drugs targeting PRC inhibit leukaemia-associated enhancer transcription, control pro-apoptotic B cell lymphoma-2 like 11 and mediate apoptosis in breast cancer cells (196, 197). HDACs mediate histone deacetylation, with numerous studies demonstrating the effect of HDAC inhibitors on enhancer landscape in various cancer types (197–199). Lysine-specific demethylase 1 (LSD1) was identified as a selective mediator of H3K4 demethylation, with LSD1 inhibitors affecting the progression of acute myeloid leukaemia by disrupting the enhancer with the SNAG structural domain transcriptional repressor GFI1 (200). Additionally, LSD1 inhibitors have been shown to affect enhancer activity in various tumors, such as androgen receptor function in prostate cancer (201, 202) and ERα activity in breast cancer (203). However, relevant studies exploring the potential therapeutic efficacy of HAT inhibitors and HDAC inhibitors in inflammatory immunity as along with their mechanisms and function on eRNA are lacking.

Notably, a study by Huang et al. demonstrated that corepressor recruitment (GPS2 and SMRT) is a genome-wide signature of inflammatory immune enhancers, which antagonizes eRNA transcription and CBP-mediated H3K27 acetylation. This reverses subinflammation and insulin resistance by providing targeted eRNA therapeutics for immunometabolic diseases (123). A Janus kinase inhibitor (tofacitinib) has been shown to block cytokine signaling in T cells, thereby affecting RA risk gene expressions and SE structure, which ultimately targets autoimmune diseases (144). Therefore, targeted small molecule drugs that affect enhancer transcription and eRNAs can be considered as potential therapeutic targets for inflammatory immune-related diseases and tumors. Although enhancer inhibitors have great potential in diseases with inflammation immune alterations, further clinical trials are needed to validate. In addition, small molecule inhibitors specifically targeting eRNA still have great potential for exploration and development.

DISCUSSION

Rapid advances in sequencing and microscope technologies suggest the potential contribution of enhancer transcription and eRNAs in inflammatory immune-altered diseases. eRNAs have been considered to have induced a breakthrough in the field of targeted therapy, spurring various studies centered on transcriptional precision and complexity. The activation modes of enhancers and SEs and regulatory mechanisms of enhancer

transcription and eRNAs on target genes have been extensively analysed in this review. However, owing to the limited understanding of enhancer transcription and eRNA biology, multiple questions remain to be addressed: 1) What are the basic features of enhancer-promoter communication, interdependence and base coexistence sequence? 2) How does enhancer transcription regulate eRNA and mRNA expression? 3) How does eRNA activate paired-promoter gene transcription? 4) How do specific structures (e.g. molecular clouds and condensates) formed by eRNA regulate the enhancer and promoter gene and affect related diseases? 5) How does the eRNA epigenetic modification affect the enhancer and promoter gene transcription?

Although studies on enhancer transcription and eRNAs are limited to the fields of cancer development and differentiation, recent studies demonstrate that both enhancer transcription activation and eRNA expression are preferentially expressed over inflammatory immune-related genes under LPS induction. This suggests a potential regulatory mechanism between eRNAs and inflammatory immune genes, which alters inflammatory immune responses in diseases. This review summarizes that eRNA expression levels in inflammatory and non-inflammatory immune cells are significantly correlated with inflammatory gene expression in response to inflammatory stimuli, leading to a rapid transition from a quiescent to an inflammatory transcriptional program, thus affecting the development and differentiation of associated immune and non-immune cells. Notably, the inflammation-associated NFκB signaling pathway contributes to inflammation-associated eRNA synthesis and positively regulates enhancer transcription to form a multi-cascade regulatory transcription that affects various inflammatory immune diseases, such as gastritis, SLE and inflammatory bowel disease. Currently, the inflammatory immunomodulatory role of eRNAs in tumors is limited to hematopoietic malignancies, while studies in substantive tumors are scarce. Consequently, the enhancer transcription processes and eRNAs have been speculated to not only affect the development and differentiation of inflammatory immune cells (monocyte-macrophage and lymphocytes predominantly) but also lead to the alteration in inflammatory-immune responses in various diseases, including tumors. However, the specific mechanisms or signaling pathways by which eRNAs affect cells and diseases remain unclear. However, bioinformatic analyses have made it possible to identify and screen functional eRNAs associated with inflammatory immunity and utilize them as a basis for extensive functional, mechanistic and therapeutic exploration.

Significant advances have been made in the treatment of inflammatory immune diseases and tumors using small-molecule drugs targeting enhancer transcription processes, which provide novel therapeutic directions and tools for diseases with inflammatory immune alterations and their drug resistance. However, further studies are required as the regulation of downstream target genes by eRNAs and the instability and dynamics of eRNA have been scarcely explored. Currently, no relevant studies have explored briefly the efficacy of small-molecule drugs that directly target eRNA on lesioned cells or diseases. However, some RNA-based inhibitors such as locked nucleic acid antisense oligonucleotides (LNA ASOs) have been to identified to have significant efficacy in targeting lncRNAs for silencing, which predicts that LNA ASO may be a potential targeting inhibitor in the eRNA field. Nevertheless, eRNA-associated protein chaperones can be identified using genomics and proteomics, and structure analyses can help in designing small-molecule regulators that specifically target eRNA protein chaperones. Additionally, further studies considering altered eRNA epigenetic modifications (e.g. 5-cytosine methylation, n6-adenosine methylation) and eRNA interactions in higher-order chromatin organization as potential eRNA targets are required. Therefore, this review aims to highlight the usefulness of eRNA as an effective potential therapeutic target and prognostic biomarker for inflammatory immune diseases and tumors with inflammatory immune alterations. However, further studies are required to confirm the functions and regulatory mechanisms of eRNAs in inflammatory-immune alterations and explore the potential therapeutic effects of relevant eRNA small molecule inhibitors in diseases with inflammatory-immune alterations.

AUTHOR CONTRIBUTIONS

Overview concept: LW and BX. Literature data collection: LW and YH. Literature analysis: LW, YH, MC, and BX. Funding acquisition: YM, MC, and BX. Software and Visualization: LW. Writing-original draft: LW. Writing-review and editing: LW, WL, YH, MC, and BX.

FUNDING

National Natural Science Foundation of China (No. 81872089, 81370849, 81672551); Six talent peaks project in Jiangsu Province; Jiangsu Provincial Medical Innovation Team (CXTDA2017025); The National Key Research and Development Program of China (SQ2017YFSF090096); Innovative Team of Jiangsu Provincial (2017ZXKJQWO7).

REFERENCES

1. Heintzman ND, Ren B. Finding Distal Regulatory Elements in the Human Genome. *Curr Opin Genet Dev* (2009) 19, 541–9. doi: 10.1016/j.gde.2009.09.006
2. Tippens ND, Vihervaara A, Lis JT. Enhancer Transcription: What, Where, When, and Why? *Genes Dev* (2018) 32:1–3. doi: 10.1101/gad.311605.118
3. Li W, Notani D, Rosenfeld MG. Enhancers as Non-Coding RNA Transcription Units: Recent Insights and Future Perspectives. *Nat Rev Genet* (2016) 17:207–23. doi: 10.1038/nrg.2016.4
4. Banerji J, Rusconi S, Schaffner W. Expression of a Beta-Globin Gene Is Enhanced by Remote SV40 DNA Sequences. *Cell* (1981) 27:299–308. doi: 10.1016/0092-8674(81)90413-x
5. Zaret KS, Carroll JS. Pioneer Transcription Factors: Establishing Competence for Gene Expression. *Genes Dev* (2011) 25:2227–41. doi: 10.1101/gad.176826.111

6. Spitz F, Furlong EE. Transcription Factors: From Enhancer Binding to Developmental Control. *Nat Rev Genet* (2012) 13:613–26. doi: 10.1038/nrg3207
7. Junion G, Spivakov M, Girardot C, Braun M, Gustafson E, Birney EH, et al. A Transcription Factor Collective Defines Cardiac Cell Fate and Reflects Lineage History. *Cell* (2012) 148:473–86. doi: 10.1016/j.cell.2012.01.030
8. Liu Z, Merkurjev D, Yang F, Li W, Oh S, Friedman M, et al. Enhancer Activation Requires Trans-Recruitment of a Mega Transcription Factor Complex. *Cell* (2014) 159:358–73. doi: 10.1016/j.cell.2014.08.027
9. Rothschild G, Basu U. Lingering Questions About Enhancer RNA and Enhancer Transcription-Coupled Genomic Instability. *Trends Genet* (2017) 33:143–54. doi: 10.1016/j.tig.2016.12.002
10. Kaikkonen MU, Spann NJ, Heinz S, Romanoski CE, Allison KA, Stender JD, et al. Remodeling of the Enhancer Landscape During Macrophage Activation Is Coupled to Enhancer Transcription. *Mol Cell* (2013) 51:310–25. doi: 10.1016/j.molcel.2013.07.010
11. Kanno T, Kanno Y, LeRoy G, Campos E, Sun H, Brooks SR, et al. BRD4 Assists Elongation of Both Coding and Enhancer RNAs by Interacting With Acetylated Histones. *Nat Struct Mol Biol* (2014) 21:1047–57. doi: 10.1038/nsmb.2912
12. Sigova AA, Abraham JB, Ji X, Molinie B, Hannett NM, Guo YE, et al. Transcription Factor Trapping by RNA in Gene Regulatory Elements. *Science* (2015) 350:978–81. doi: 10.1126/science.aad3346
13. Lam MT, Li W, Rosenfeld MG, Glass CK. Enhancer RNAs and Regulated Transcriptional Programs. *Trends Biochem Sci* (2014) 39:170–82. doi: 10.1016/j.tibs.2014.02.007
14. Shen L, Wu H, Diep D, Yamaguchi S, D'Alessio AC, Fung H, et al. Genome-Wide Analysis Reveals TET- and TDG-Dependent 5-Methylcytosine Oxidation Dynamics. *Cell* (2013) 153:692–706. doi: 10.1016/j.cell.2013.04.002
15. Song CX, Szulwach KE, Dai Q, Fu Y, Mao SQ, Lin L, et al. Genome-Wide Profiling of 5-Formylcytosine Reveals Its Roles in Epigenetic Priming. *Cell* (2013) 153:678–91. doi: 10.1016/j.cell.2013.04.001
16. Lomvardas S, Barnea G, Pisapia DJ, Mendelsohn M, Kirkland J, Axel R. Interchromosomal Interactions and Olfactory Receptor Choice. *Cell* (2006) 126:403–13. doi: 10.1016/j.cell.2006.06.035
17. Geyer PK, Green MM, Corces VG. Tissue-Specific Transcriptional Enhancers may Act in Trans on the Gene Located in the Homologous Chromosome: The Molecular Basis of Transvection in Drosophila. *EMBO J* (1990) 9:2247–56. doi: 10.1002/j.1460-2075.1990.tb07395.x
18. Whyte WA, Orlando DA, Hnisz D, Abraham BJ, Lin CY, Kagey MH, et al. Master Transcription Factors and Mediator Establish Super-Enhancers at Key Cell Identity Genes. *Cell* (2013) 153:307–19. doi: 10.1016/j.cell.2013.03.035
19. Loven J, Hoke HA, Lin CY, Lau A, Orlando DA, Vakoc CR, et al. Selective Inhibition of Tumor Oncogenes by Disruption of Super-Enhancers. *Cell* (2013) 153:320–34. doi: 10.1016/j.cell.2013.03.036
20. Parker SC, Stitzel ML, Taylor DL, Orozco JM, Erdos MR, Akiyama JA, et al. Chromatin Stretch Enhancer States Drive Cell-Specific Gene Regulation and Harbor Human Disease Risk Variants. *Proc Natl Acad Sci USA* (2013) 110:17921–6. doi: 10.1073/pnas.1317023110
21. Higashijima Y, Kanki Y. Potential Roles of Super Enhancers in Inflammatory Gene Transcription. *FEBS J* (2021). doi: 10.1111/febs.16089
22. Siersbaek R, Rabiee A, Nielsen R, Sidoli S, Traynor S, Loft A, et al. Transcription Factor Cooperativity in Early Adipogenic Hotspots and Super-Enhancers. *Cell Rep* (2014) 7:1443–55. doi: 10.1016/j.celrep.2014.04.042
23. Hnisz D, Abraham BJ, Lee TI, Lau A, Saint-André V, Sigova AA, et al. Super-Enhancers in the Control of Cell Identity and Disease. *Cell* (2013) 155:934–47. doi: 10.1016/j.cell.2013.09.053
24. Pott S, Lieb JD. What Are Super-Enhancers? *Nat Genet* (2015) 47:8–12. doi: 10.1038/ng.3167
25. Laham-Karam N, Laitinen P, Turunen TA, Yla-Herttuala S. Activating the Chromatin by Noncoding RNAs. *Antioxid Redox Sign* (2018) 29:813–31. doi: 10.1089/ars.2017.7248
26. Janowski BA, Younger ST, Hardy DB, Ram R, Huffman KE, Corey DR. Activating Gene Expression in Mammalian Cells With Promoter-Targeted Duplex RNAs. *Nat Chem Biol* (2007) 3:166–73. doi: 10.1038/nchembio860
27. Rinn JL, Chang HY. Genome Regulation by Long Noncoding RNAs. *Annu Rev Biochem* (2012) 81:145–66. doi: 10.1146/annurev-biochem-051410-092902
28. Sas-Chen A, Srivastava S, Yarden Y. The Short and the Long: Non-Coding RNAs and Growth Factors in Cancer Progression. *Biochem Soc Trans* (2017) 45:51–64. doi: 10.1042/BST20160131
29. De Santa F, Barozzi I, Mietton F, Ghisletti S, Polletti S, Tusi BK, et al. A Large Fraction of Extragenic RNA Pol II Transcription Sites Overlap Enhancers. *PloS Biol* (2010) 8:e1000384. doi: 10.1371/journal.pbio.1000384
30. Orom UA, Derrien T, Beringer M, Gumireddy K, Gumireddy A, Bussotti G, et al. Long Noncoding RNAs With Enhancer-Like Function in Human Cells. *Cell* (2010) 143:46–58. doi: 10.1016/j.cell.2010.09.001
31. Lai F, Orom UA, Cesaroni M, Beringer M, Taatjes DJ, Blobel GA, et al. Activating RNAs Associate With Mediator to Enhance Chromatin Architecture and Transcription. *Nature* (2013) 494:497–501. doi: 10.1038/nature11884
32. Kim TK, Hemberg M, Gray JM, Costa AM, Bear DM, Wu J, et al. Widespread Transcription at Neuronal Activity-Regulated Enhancers. *Nature* (2010) 465:182–7. doi: 10.1038/nature09033
33. Adhikary S, Roy S, Chacon J, Gadad SS, Das C. Implications of Enhancer Transcription and eRNAs in Cancer. *Cancer Res* (2021) 81:4174–82. doi: 10.1158/0008-5472.CAN-20-4010
34. Lee JH, Xiong F, Li W. Enhancer RNAs in Cancer: Regulation, Mechanisms and Therapeutic Potential. *RNA Biol* (2020) 17:1550–9. doi: 10.1080/15476286.2020.1712895
35. Thandapani P. Super-Enhancers in Cancer. *Pharmacol Ther* (2019) 199:129–38. doi: 10.1016/j.pharmthera.2019.02.014
36. Sengupta S, George RE. Super-Enhancer-Driven Transcriptional Dependencies in Cancer. *Trends Cancer* (2017) 3:269–81. doi: 10.1016/j.trecan.2017.03.006
37. Higashijima Y, Matsui Y, Shimamura T, Nakaki R, Nagai N, Tsutsumi S, et al. Coordinated Demethylation of H3K9 and H3K27 Is Required for Rapid Inflammatory Responses of Endothelial Cells. *EMBO J* (2020) 39:e103949. doi: 10.15252/embj.2019103949
38. Fanucchi S, Fok ET, Dalla E, Shibayama Y, Börner K, Chang EY, et al. Immune Genes Are Primed for Robust Transcription by Proximal Long Noncoding RNAs Located in Nuclear Compartments. *Nat Genet* (2019) 51:138–50. doi: 10.1038/s41588-018-0298-2
39. Fanucchi S, Shibayama Y, Burd S, Weinberg MS, Mhlanga MM. Chromosomal Contact Permits Transcription Between Coregulated Genes. *Cell* (2013) 155:606–20. doi: 10.1016/j.cell.2013.09.051
40. Koch F, Fenouil R, Gut M, Cauchy P, Albert TK, Zacarias-Cabeza J, et al. Transcription Initiation Platforms and GTF Recruitment at Tissue-Specific Enhancers and Promoters. *Nat Struct Mol Biol* (2011) 18:956–63. doi: 10.1038/nsmb.2085
41. Andersson R, Gebhard C, Escalada IM, Hoof I, Bornholdt J, Boyd M, et al. An Atlas of Active Enhancers Across Human Cell Types and Tissues. *Nature* (2014) 507:455–61. doi: 10.1038/nature12787
42. Core LJ, Martins AL, Danko CG, Waters CT, Siepel A, Lis JT, et al. Analysis of Nascent RNA Identifies a Unified Architecture of Initiation Regions at Mammalian Promoters and Enhancers. *Nat Genet* (2014) 46:1311–20. doi: 10.1038/ng.3142
43. Lam MT, Cho H, Lesch HP, Gosselin D, Heinz S, Heinz YT, et al. Rev-Erbs Repress Macrophage Gene Expression by Inhibiting Enhancer-Directed Transcription. *Nature* (2013) 498:511–5. doi: 10.1038/nature12209
44. Andersson R, Andersen PR, Valen E, Core LJ, Bornholdt J, Boyd M, et al. Nuclear Stability and Transcriptional Directionality Separate Functionally Distinct RNA Species. *Nat Commun* (2014) 5:5336. doi: 10.1038/ncomms6336
45. Ntini E, Järvelin AI, Bornholdt J, Chen Y, Boyd M, Jørgensen M, et al. Polyadenylation Site-Induced Decay of Upstream Transcripts Enforces Promoter Directionality. *Nat Struct Mol Biol* (2013) 20:923–8. doi: 10.1038/nsmb.2640
46. Almada AE, Wu X, Kriz AJ, Burge CB, Sharp PA. Promoter Directionality Is Controlled by U1 snRNP and Polyadenylation Signals. *Nature* (2013) 499:360–3. doi: 10.1038/nature12349
47. Keogh MC, Kurdistani SK, Morris SA, Ahn SH, Podolny V, Collins SR, et al. Cotranscriptional Set2 Methylation of Histone H3 Lysine 36 Recruits a

Repressive Rpd3 Complex. *Cell* (2005) 123:593–605. doi: 10.1016/j.cell.2005.10.025
48. Bonn S, Zinzen RP, Girardot C, Gustafson EH, Gonzalez AP, Delhomme N, et al. Tissue-Specific Analysis of Chromatin State Identifies Temporal Signatures of Enhancer Activity During Embryonic Development. *Nat Genet* (2012) 44:148–56. doi: 10.1038/ng.1064
49. Hsieh CL, Fei T, Chen Y, Li T, Gao Y, Wang X, et al. Enhancer RNAs Participate in Androgen Receptor-Driven Looping That Selectively Enhances Gene Activation. *Proc Natl Acad Sci USA* (2014) 111:7319–24. doi: 10.1073/pnas.1324151111
50. Lai F, Gardini A, Zhang A, Shiekhattar R. Integrator Mediates the Biogenesis of Enhancer RNAs. *Nature* (2015) 525:399–403. doi: 10.1038/nature14906
51. Baillat D, Hakimi MA, Näär AM, Shilatifard A, Cooch N, Shiekhattar R, et al. Integrator, a Multiprotein Mediator of Small Nuclear RNA Processing, Associates With the C-Terminal Repeat of RNA Polymerase II. *Cell* (2005) 123:265–76. doi: 10.1016/j.cell.2005.08.019
52. Austenaa LM, Barozzi I, Simonatto M, Masella S, Chiara GD, Ghisletti S, et al. Transcription of Mammalian Cis-Regulatory Elements Is Restrained by Actively Enforced Early Termination. *Mol Cell* (2015) 60:460–74. doi: 10.1016/j.molcel.2015.09.018
53. Hsin JP, Li W, Hoque M, Tian B, Manley JL. RNAP II CTD Tyrosine 1 Performs Diverse Functions in Vertebrate Cells. *Elife* (2014) 3:e02112. doi: 10.7554/eLife.02112
54. Descostes N, Heidemann M, Spinelli L, Schüller R, Maqbool MA, Fenouil R, et al. Tyrosine Phosphorylation of RNA Polymerase II CTD Is Associated With Antisense Promoter Transcription and Active Enhancers in Mammalian Cells. *Elife* (2014) 3:e02105. doi: 10.7554/eLife.02105
55. Bentley DL. Coupling mRNA Processing With Transcription in Time and Space. *Nat Rev Genet* (2014) 15:163–75. doi: 10.1038/nrg3662
56. Mayer A, Heidemann M, Lidschreiber M, Schreieck A, Sun M, Hintermair C, et al. CTD Tyrosine Phosphorylation Impairs Termination Factor Recruitment to RNA Polymerase II. *Science* (2012) 336:1723–5. doi: 10.1126/science.1219651
57. Lubas M, Andersen PR, Schein A, Dziembowski A, Kudla G, Jensen TH, et al. The Human Nuclear Exosome Targeting Complex Is Loaded Onto Newly Synthesized RNA to Direct Early Ribonucleolysis. *Cell Rep* (2015) 10:178–92. doi: 10.1016/j.celrep.2014.12.026
58. Muller-McNicoll M, Neugebauer KM. Good Cap/Bad Cap: How the Cap-Binding Complex Determines RNA Fate. *Nat Struct Mol Biol* (2014) 21:9–12. doi: 10.1038/nsmb.2751
59. Blackwood EM, Kadonaga JT. Going the Distance: A Current View of Enhancer Action. *Science* (1998) 281:60–3. doi: 10.1126/science.281.5373.60
60. Bulger M, Groudine M. Looping Versus Linking: Toward a Model for Long-Distance Gene Activation. *Genes Dev* (1999) 13:2465–77. doi: 10.1101/gad.13.19.2465
61. de Laat W, Klous P, Kooren J, Noordermeer D, Palstra RJ, Simonis M, et al. Three-Dimensional Organization of Gene Expression in Erythroid Cells. *Curr Top Dev Biol* (2008) 82:117–39. doi: 10.1016/S0070-2153(07)00005-1
62. Carter D, Chakalova L, Osborne CS, Dai YF, Fraser P. Long-Range Chromatin Regulatory Interactions *In Vivo*. *Nat Genet* (2002) 32:623–6. doi: 10.1038/ng1051
63. Tolhuis B, Palstra RJ, Splinter E, Grosveld F, de Laat W. Looping and Interaction Between Hypersensitive Sites in the Active Beta-Globin Locus. *Mol Cell* (2002) 10:1453–65. doi: 10.1016/s1097-2765(02)00781-5
64. Kooren J, Palstra RJ, Klous P, Splinter E, Lindern MV, Grosveld F, et al. Beta-Globin Active Chromatin Hub Formation in Differentiating Erythroid Cells and in P45 NF-E2 Knock-Out Mice. *J Biol Chem* (2007) 282:16544–52. doi: 10.1074/jbc.M701159200
65. Kim SI, Bultman SJ, Kiefer CM, Dean A, Bresnick EH. BRG1 Requirement for Long-Range Interaction of a Locus Control Region With a Downstream Promoter. *Proc Natl Acad Sci USA* (2009) 106:2259–64. doi: 10.1073/pnas.0806420106
66. Kellner WA, Ramos E, Van Bortle K, Takenaka N, Corces VG. Genome-Wide Phosphoacetylation of Histone H3 at Drosophila Enhancers and Promoters. *Genome Res* (2012) 22:1081–8. doi: 10.1101/gr.136929.111
67. Vakoc CR, Letting DL, Gheldof N, Sawado T, Bender MA, Groudine M, et al. Proximity Among Distant Regulatory Elements at the Beta-Globin Locus Requires GATA-1 and FOG-1. *Mol Cell* (2005) 17:453–62. doi: 10.1016/j.molcel.2004.12.028
68. Drissen R, Palstra RJ, Gillemans N, Splinter E, Grosveld F, Philipsen S, et al. The Active Spatial Organization of the Beta-Globin Locus Requires the Transcription Factor EKLF. *Genes Dev* (2004) 18:2485–90. doi: 10.1101/gad.317004
69. Yan J, Chen SA, Local A, Liu T, Qiu Y, Dorighi KM, et al. Histone H3 Lysine 4 Monomethylation Modulates Long-Range Chromatin Interactions at Enhancers. *Cell Res* (2018) 28:204–20. doi: 10.1038/cr.2018.1
70. Catarino RR, Stark A. Assessing Sufficiency and Necessity of Enhancer Activities for Gene Expression and the Mechanisms of Transcription Activation. *Genes Dev* (2018) 32:202–23. doi: 10.1101/gad.310367.117
71. Wendt KS, Yoshida K, Itoh T, Bando M, Koch B, Schirghuber E, et al. Cohesin Mediates Transcriptional Insulation by CCCTC-Binding Factor. *Nature* (2008) 451:796–801. doi: 10.1038/nature06634
72. Parelho V, Hadjur S, Spivakov M, Leleu M, Sauer S, Gregson HC, et al. Cohesins Functionally Associate With CTCF on Mammalian Chromosome Arms. *Cell* (2008) 132:422–33. doi: 10.1016/j.cell.2008.01.011
73. Splinter E, Heath H, Kooren J, Palstra RJ, Klous P, Grosveld F, et al. CTCF Mediates Long-Range Chromatin Looping and Local Histone Modification in the Beta-Globin Locus. *Genes Dev* (2006) 20:2349–54. doi: 10.1101/gad.399506
74. Handoko L, Xu H, Li G, Ngan CY, Chew E, Schnapp M, et al. CTCF-Mediated Functional Chromatin Interactome in Pluripotent Cells. *Nat Genet* (2011) 43:630–8. doi: 10.1038/ng.857
75. Botta M, Haider S, Leung IX, Lio P, Mozziconacci J. Intra- and Inter-Chromosomal Interactions Correlate With CTCF Binding Genome Wide. *Mol Syst Biol* (2010) 6:426. doi: 10.1038/msb.2010.79
76. Dixon JR, Selvaraj S, Yue F, Kim A, Li Y, Shen Y, et al. Topological Domains in Mammalian Genomes Identified by Analysis of Chromatin Interactions. *Nature* (2012) 485:376–80. doi: 10.1038/nature11082
77. Mishiro T, Ishihara K, Hino S, Tsutsumi S, Aburatani H, Shirahige K, et al. Architectural Roles of Multiple Chromatin Insulators at the Human Apolipoprotein Gene Cluster. *EMBO J* (2009) 28:1234–45. doi: 10.1038/emboj.2009.81
78. Faure AJ, Schmidt D, Watt S, Schwalie PC, Wilson MD, Xu H, et al. Cohesin Regulates Tissue-Specific Expression by Stabilizing Highly Occupied Cis-Regulatory Modules. *Genome Res* (2012) 22:2163–75. doi: 10.1101/gr.136507.111
79. Racko D, Benedetti F, Dorier J, Stasiak A. Transcription-Induced Supercoiling as the Driving Force of Chromatin Loop Extrusion During Formation of TADs in Interphase Chromosomes. *Nucleic Acids Res* (2018) 46:1648–60. doi: 10.1093/nar/gkx1123
80. Bose DA, Donahue G, Reinberg D, Shiekhattar R, Bonasio R, Berger SL. RNA Binding to CBP Stimulates Histone Acetylation and Transcription. *Cell* (2017) 168:135–49.e122. doi: 10.1016/j.cell.2016.12.020
81. Li W, Notani D, Ma Q, Tanasa B, Nunez E, Chen AY, et al. Functional Roles of Enhancer RNAs for Oestrogen-Dependent Transcriptional Activation. *Nature* (2013) 498:516–20. doi: 10.1038/nature12210
82. Jiao W, Chen Y, Song H, Li D, Mei H, Yang F, et al. HPSE Enhancer RNA Promotes Cancer Progression Through Driving Chromatin Looping and Regulating hnRNPU/P300/EGR1/HPSE Axis. *Oncogene* (2018) 37:2728–45. doi: 10.1038/s41388-018-0128-0
83. Pezone A, Zuchegna C, Tramontano A, Romano A, Russo G, Rosa M, et al. RNA Stabilizes Transcription-Dependent Chromatin Loops Induced By Nuclear Hormones. *Sci Rep* (2019) 9:3925. doi: 10.1038/s41598-019-40123-6
84. Yang Y, Su Z, Song X, Liang B, Zeng F, Chang X, et al. Enhancer RNA-Driven Looping Enhances the Transcription of the Long Noncoding RNA DHRS4-AS1, a Controller of the DHRS4 Gene Cluster. *Sci Rep* (2016) 6:20961. doi: 10.1038/srep20961
85. Tsai PF, Orso SD, Rodriguez J, Vivanco KO, Ko KD, Jiang K, et al. A Muscle-Specific Enhancer RNA Mediates Cohesin Recruitment and Regulates Transcription In Trans. *Mol Cell* (2018) 71:129–41.e128. doi: 10.1016/j.molcel.2018.06.008
86. Schaukowitch K, Joo JY, Liu X, Watts JK, Martinez C, Kim TK, et al. Enhancer RNA Facilitates NELF Release From Immediate Early Genes. *Mol Cell* (2014) 56:29–42. doi: 10.1016/j.molcel.2014.08.023

87. Cai Z, Cao C, Ji L, Ye R, Wang D, Xia C, et al. RIC-Seq for Global *In Situ* Profiling of RNA-RNA Spatial Interactions. *Nature* (2020) 582:432–7. doi: 10.1038/s41586-020-2249-1
88. Lee JH, Wang R, Xiong F, Krakowiak J, Liao Z, Nguyen PT, et al. Enhancer RNA M6a Methylation Facilitates Transcriptional Condensate Formation and Gene Activation. *Mol Cell* (2021) 81:3368–85.e3369. doi: 10.1016/j.molcel.2021.07.024
89. Aguilo F, Li S, Balasubramaniyan N, Sancho A, Benko S, Zhang F, et al. Deposition of 5-Methylcytosine on Enhancer RNAs Enables the Coactivator Function of PGC-1alpha. *Cell Rep* (2016) 14:479–92. doi: 10.1016/j.celrep.2015.12.043
90. Baillie JK, Arner E, Daub C, Hoon MD, Itoh M, Kawaji H, et al. Analysis of the Human Monocyte-Derived Macrophage Transcriptome and Response to Lipopolysaccharide Provides New Insights Into Genetic Aetiology of Inflammatory Bowel Disease. *PloS Genet* (2017) 13:e1006641. doi: 10.1371/journal.pgen.1006641
91. Hah N, Benner C, Chong LW, Yu RT, Downes M, Evans RM, et al. Inflammation-Sensitive Super Enhancers Form Domains of Coordinately Regulated Enhancer RNAs. *Proc Natl Acad Sci USA* (2015) 112:E297–302. doi: 10.1073/pnas.1424028112
92. Ma S, Zhang B, LaFave LM, Earl AS, Chiang Z, Hu Y, et al. Chromatin Potential Identified by Shared Single-Cell Profiling of RNA and Chromatin. *Cell* (2020) 183:1103–16.e1120. doi: 10.1016/j.cell.2020.09.056
93. Heinz S, Romanoski CE, Benner C, Allison KA, Kaikkonen MU, Orozco LD, et al. Effect of Natural Genetic Variation on Enhancer Selection and Function. *Nature* (2013) 503:487–92. doi: 10.1038/nature12615
94. Ghisletti S, Barozzi I, Mietton F, Polletti S, Santa FD, Venturini E, et al. Identification and Characterization of Enhancers Controlling the Inflammatory Gene Expression Program in Macrophages. *Immunity* (2010) 32:317–28. doi: 10.1016/j.immuni.2010.02.008
95. Heinz S, Benner C, Spann N, Bertolino E, Lin YC, Laslo P, et al. Simple Combinations of Lineage-Determining Transcription Factors Prime Cis-Regulatory Elements Required for Macrophage and B Cell Identities. *Mol Cell* (2010) 38:576–89. doi: 10.1016/j.molcel.2010.05.004
96. Hertweck A, Evans CM, Eskandarpour M, Lau JCH, Oleinika K, Jackson I, et al. T-Bet Activates Th1 Genes Through Mediator and the Super Elongation Complex. *Cell Rep* (2016) 15:2756–70. doi: 10.1016/j.celrep.2016.05.054
97. Chen J, Wang Z, Hu X, Chen R, Romero-Gallo J, Peek RM Jr, et al. BET Inhibition Attenuates Helicobacter Pylori-Induced Inflammatory Response by Suppressing Inflammatory Gene Transcription and Enhancer Activation. *J Immunol* (2016) 196:4132–42. doi: 10.4049/jimmunol.1502261
98. Shi L, Li S, Maurer K, Zhang Z, Petri M, Sullivan K. Enhancer RNA and NFkappaB-Dependent P300 Regulation of ADAMDEC1. *Mol Immunol* (2018) 103:312–21. doi: 10.1016/j.molimm.2018.09.019
99. Chen Y, Sheppard D, Dong X, Hu X, Chen M, Chen R, et al. H. Pylori Infection Confers Resistance to Apoptosis *via* Brd4-Dependent BIRC3 eRNA Synthesis. *Cell Death Dis* (2020) 11:667. doi: 10.1038/s41419-020-02894-z
100. Huang Z, Du G, Huang X, Han L, Han X, Xu B, et al. The Enhancer RNA lnc-SLC4A1-1 Epigenetically Regulates Unexplained Recurrent Pregnancy Loss (URPL) by Activating CXCL8 and Nfkb Pathway. *EBioMedicine* (2018) 38:162–70. doi: 10.1016/j.ebiom.2018.11.015
101. van Arensbergen J, van Steensel B, Bussemaker HJ. In Search of the Determinants of Enhancer-Promoter Interaction Specificity. *Trends Cell Biol* (2014) 24:695–702. doi: 10.1016/j.tcb.2014.07.004
102. Tan SH, Leong WZ, Ngoc PCT, Tan TK, Bertulfo FC, Lim MB, et al. The Enhancer RNA ARIEL Activates the Oncogenic Transcriptional Program in T-Cell Acute Lymphoblastic Leukemia. *Blood* (2019) 134:239–51. doi: 10.1182/blood.2018874503
103. Zhang X, Pang P, Jiang M, Cao Q, Li H, Xu Y, et al. eRNAs and Superenhancer lncRNAs Are Functional in Human Prostate Cancer. *Dis Markers* (2020) 2020:8847986. doi: 10.1155/2020/8847986
104. Daniel B, Nagy G, Hah N, Horvath A, Czimmerer Z, Poliska S, et al. The Active Enhancer Network Operated by Liganded RXR Supports Angiogenic Activity in Macrophages. *Genes Dev* (2014) 28:1562–77. doi: 10.1101/gad.242685.114
105. Bierhaus A, Chen J, Liliensiek B, Nawroth PP. LPS and Cytokine-Activated Endothelium. *Semin Thromb Hemost* (2000) 26:571–87. doi: 10.1055/s-2000-13214
106. Orecchioni M, Ghosheh Y, Pramod AB, Ley K. Macrophage Polarization: Different Gene Signatures in M1(LPS+) vs. Classically and M2(LPS-) vs. Alternatively Activated Macrophages. *Front Immunol* (2019) 10:1084. doi: 10.3389/fimmu.2019.01084
107. Rathinam VAK, Zhao Y, Shao F. Innate Immunity to Intracellular LPS. *Nat Immunol* (2019) 20:527–33. doi: 10.1038/s41590-019-0368-3
108. Cobaleda C, Busslinger M. Developmental Plasticity of Lymphocytes. *Curr Opin Immunol* (2008) 20:139–48. doi: 10.1016/j.coi.2008.03.017
109. Kondilis-Mangum HD, Wade PA. Epigenetics and the Adaptive Immune Response. *Mol Aspects Med* (2013) 34:813–25. doi: 10.1016/j.mam.2012.06.008
110. Creyghton MP, Cheng AW, Welstead GG, Kooistra T, Carey BW, Steine EJ, et al. Histone H3K27ac Separates Active From Poised Enhancers and Predicts Developmental State. *Proc Natl Acad Sci USA* (2010) 107:21931–6. doi: 10.1073/pnas.1016071107
111. Czimmerer Z, Daniel B, Horvath A, Rückerl D, Nagy G, Kiss M, et al. The Transcription Factor STAT6 Mediates Direct Repression of Inflammatory Enhancers and Limits Activation of Alternatively Polarized Macrophages. *Immunity* (2018) 48:75–90.e76. doi: 10.1016/j.immuni.2017.12.010
112. Hsu E, Zemke NR, Berk AJ. Promoter-Specific Changes in Initiation, Elongation, and Homeostasis of Histone H3 Acetylation During CBP/p300 Inhibition. *Elife* (2021) 10:e63512. doi: 10.7554/eLife.63512
113. Narita T, Ito S, Higashijima Y, Chu WK, Neumann K, Walter J, et al. Enhancers Are Activated by P300/CBP Activity-Dependent PIC Assembly, RNAPII Recruitment, and Pause Release. *Mol Cell* (2021) 81:2166–82.e2166. doi: 10.1016/j.molcel.2021.03.008
114. Li X, Zhang Q, Shi Q, Liu Y, Zhao K, Shen Q, et al. Demethylase Kdm6a Epigenetically Promotes IL-6 and IFN-Beta Production in Macrophages. *J Autoimmun* (2017) 80:85–94. doi: 10.1016/j.jaut.2017.02.007
115. Ha SD, Cho W, DeKoter RP, Kim SO. The Transcription Factor PU.1 Mediates Enhancer-Promoter Looping That Is Required for IL-1beta eRNA and mRNA Transcription in Mouse Melanoma and Macrophage Cell Lines. *J Biol Chem* (2019) 294:17487–500. doi: 10.1074/jbc.RA119.010149
116. Oishi Y, Hayashi S, Isagawa T, Oshima M, Iwama A, Shimba S, et al. Bmal1 Regulates Inflammatory Responses in Macrophages by Modulating Enhancer RNA Transcription. *Sci Rep* (2017) 7:7086. doi: 10.1038/s41598-017-07100-3
117. Heward JA, Roux BT, Lindsay MA. Divergent Signalling Pathways Regulate Lipopolysaccharide-Induced eRNA Expression in Human Monocytic THP1 Cells. *FEBS Lett* (2015) 589:396–406. doi: 10.1016/j.febslet.2014.12.026
118. NE II, Heward JA, Roux B, Tsitsiou E, Fenwick PS, Lenzi L, et al. Long Non-Coding RNAs and Enhancer RNAs Regulate the Lipopolysaccharide-Induced Inflammatory Response in Human Monocytes. *Nat Commun* (2014) 5:3979. doi: 10.1038/ncomms4979
119. Kim YJ, Xie P, Cao L, Zhang MQ, Kim TH. Global Transcriptional Activity Dynamics Reveal Functional Enhancer RNAs. *Genome Res* (2018) 28:1799–811. doi: 10.1101/gr.233486.117
120. Ginhoux F, Guilliams M. Tissue-Resident Macrophage Ontogeny and Homeostasis. *Immunity* (2016) 44:439–49. doi: 10.1016/j.immuni.2016.02.024
121. Link VM, Gosselin D, Glass CK. Mechanisms Underlying the Selection and Function of Macrophage-Specific Enhancers. *Cold Spring Harb Symp Quant Biol* (2015) 80:213–21. doi: 10.1101/sqb.2015.80.027367
122. Daniel B, Nagy G, Czimmerer Z, Horvath A, Hammers DW, Monroy IC, et al. The Nuclear Receptor PPARgamma Controls Progressive Macrophage Polarization as a Ligand-Insensitive Epigenomic Ratchet of Transcriptional Memory. *Immunity* (2018) 49:615–26.e616. doi: 10.1016/j.immuni.2018.09.005
123. Huang Z, Liang N, Goñi S, Damdimopoulos A, Wang C, Ballaire R, et al. The Corepressors GPS2 and SMRT Control Enhancer and Silencer Remodeling *via* eRNA Transcription During Inflammatory Activation of Macrophages. *Mol Cell* (2021) 81:953–68.e959. doi: 10.1016/j.molcel.2020.12.040
124. Wan M, Bennett BD, Pittman GS, Campbell MR, Reynolds LM, Porter DK, et al. Identification of Smoking-Associated Differentially Methylated Regions Using Reduced Representation Bisulfite Sequencing and Cell Type-Specific Enhancer Activation and Gene Expression. *Environ Health Perspect* (2018) 126:047015. doi: 10.1289/EHP2395
125. Jasenosky LD, Nambu A, Tsytsykova AV, Ranjbar S, Haridas V, Kruidenier L, et al. Identification of a Distal Locus Enhancer Element That Controls Cell

Type-Specific TNF and LTA Gene Expression in Human T Cells. *J Immunol* (2020) 205:2479–88. doi: 10.4049/jimmunol.1901311
126. Benner C, Isoda T, Murre C. New Roles for DNA Cytosine Modification, eRNA, Anchors, and Superanchors in Developing B Cell Progenitors. *Proc Natl Acad Sci USA* (2015) 112:12776–81. doi: 10.1073/pnas.1512995112
127. Brazao TF, Johnson JS, Müller J, Heger A, Ponting CP, Tybulewicz VLJ, et al. Long Noncoding RNAs in B-Cell Development and Activation. *Blood* (2016) 128:e10–19. doi: 10.1182/blood-2015-11-680843
128. Saintamand A, Vincent-Fabert C, Marquet M, Ghazzaui N, Magnone V, Pinaud E, et al. Emu and 3'rr IgH Enhancers Show Hierarchic Unilateral Dependence in Mature B-Cells. *Sci Rep* (2017) 7:442. doi: 10.1038/s41598-017-00575-0
129. Kristjansdottir K, Dziubek A, Kang HM, Kwak H. Population-Scale Study of eRNA Transcription Reveals Bipartite Functional Enhancer Architecture. *Nat Commun* (2020) 11:5963. doi: 10.1038/s41467-020-19829-z
130. Ngoc PCT, Tan SH, Tan TK, Chan MM, Li Z, Yeoh AEJ, et al. Identification of Novel lncRNAs Regulated by the TAL1 Complex in T-Cell Acute Lymphoblastic Leukemia. *Leukemia* (2018) 32:2138–51. doi: 10.1038/s41375-018-0110-4
131. Wallaert A, Durinck K, Loocke WV, Walle IV, Matthijssens F, Volders PJ, et al. Long Noncoding RNA Signatures Define Oncogenic Subtypes in T-Cell Acute Lymphoblastic Leukemia. *Leukemia* (2016) 30:1927–30. doi: 10.1038/leu.2016.82
132. Cauchy P, Maqbool MA, Cabeza JZ, Vanhille L, Koch F, Fenouil R, et al. Dynamic Recruitment of Ets1 to Both Nucleosome-Occupied and -Depleted Enhancer Regions Mediates a Transcriptional Program Switch During Early T-Cell Differentiation. *Nucleic Acids Res* (2016) 44:3567–85. doi: 10.1093/nar/gkv1475
133. Trimarchi T, Bilal E, Ntziachristos P, Fabbri G, Favera RD, Tsirigos A, et al. Genome-Wide Mapping and Characterization of Notch-Regulated Long Noncoding RNAs in Acute Leukemia. *Cell* (2014) 158:593–606. doi: 10.1016/j.cell.2014.05.049
134. Beyaz S, Kim JH, Pinello L, Xifaras ME, Hu Y, Huang J, et al. The Histone Demethylase UTX Regulates the Lineage-Specific Epigenetic Program of Invariant Natural Killer T Cells. *Nat Immunol* (2017) 18:184–95. doi: 10.1038/ni.3644
135. Mostafa MM, Bansa A, Michi AN, Sasse SK, Proud D, Gerber AN, et al. Genomic Determinants Implicated in the Glucocorticoid-Mediated Induction of KLF9 in Pulmonary Epithelial Cells. *J Biol Chem* (2021) 296:100065. doi: 10.1074/jbc.RA120.015755
136. Mushimiyimana I, Bosch VT, Niskanen H, Downes NL, Moreau PR, Hartigan K, et al. Genomic Landscapes of Noncoding RNAs Regulating VEGFA and VEGFC Expression in Endothelial Cells. *Mol Cell Biol* (2021) 41:e0059420. doi: 10.1128/MCB.00594-20
137. Sakaguchi Y, Nishikawa K, Seno S, Matsuda H, Takayanagi H, Ishii M, et al. Roles of Enhancer RNAs in RANKL-Induced Osteoclast Differentiation Identified by Genome-Wide Cap-Analysis of Gene Expression Using CRISPR/Cas9. *Sci Rep* (2018) 8:7504. doi: 10.1038/s41598-018-25748-3
138. Zhou H, Simion V, Pierce JB, Haemmig S, Chen AF, Feinberg MW, et al. LncRNA-MAP3K4 Regulates Vascular Inflammation Through the P38 MAPK Signaling Pathway and Cis-Modulation of MAP3K4. *FASEB J* (2021) 35:e21133. doi: 10.1096/fj.202001654RR
139. Chen LF, Greene WC. Shaping the Nuclear Action of NF-Kappab. *Nat Rev Mol Cell Biol* (2004) 5:392–401. doi: 10.1038/nrm1368
140. Lee TI, Young RA. Transcriptional Regulation and Its Misregulation in Disease. *Cell* (2013) 152:1237–51. doi: 10.1016/j.cell.2013.02.014
141. Aune TM, Crooke PS 3rd, Patrick AE, Tossberg JT, Olsen NJ, Spurlock CF 3rd, et al. Expression of Long Non-Coding RNAs in Autoimmunity and Linkage to Enhancer Function and Autoimmune Disease Risk Genetic Variants. *J Autoimmun* (2017) 81:99–109. doi: 10.1016/j.jaut.2017.03.014
142. Israel DA, Peek RM. Pathogenesis of Helicobacter Pylori-Induced Gastric Inflammation. *Aliment Pharmacol Ther* (2001) 15:1271–90. doi: 10.1046/j.1365-2036.2001.01052.x
143. Boyd M, Thodberg M, Vitezic M, Bornholdt J, Seerup KV, Chen Y, et al. Characterization of the Enhancer and Promoter Landscape of Inflammatory Bowel Disease From Human Colon Biopsies. *Nat Commun* (2018) 9:1661. doi: 10.1038/s41467-018-03766-z
144. Vahedi G, Kanno Y, Furumoto Y, Jiang K, Parker SCJ, Erdos MR, et al. Super-Enhancers Delineate Disease-Associated Regulatory Nodes in T Cells. *Nature* (2015) 520:558–62. doi: 10.1038/nature14154
145. Suzuki A, Terao C, Yamamoto K. Linking of Genetic Risk Variants to Disease-Specific Gene Expression *via* Multi-Omics Studies in Rheumatoid Arthritis. *Semin Arthritis Rheum* (2019) 49:S49–53. doi: 10.1016/j.semarthrit.2019.09.007
146. Okada Y, Wu D, Trynka G, Raj T, Terao C, Ikari K, et al. Genetics of Rheumatoid Arthritis Contributes to Biology and Drug Discovery. *Nature* (2014) 506:376–81. doi: 10.1038/nature12873
147. Okada Y, Eyre S, Suzuki A, Kochi Y, Yamamoto K. Genetics of Rheumatoid Arthritis: 2018 Status. *Ann Rheum Dis* (2019) 78:446–53. doi: 10.1136/annrheumdis-2018-213678
148. Mirtschink P, Bischof C, Pham MC, Sharma R, Khadayate S, Rossi G, et al. Inhibition of the Hypoxia-Inducible Factor 1alpha-Induced Cardiospecific HERNA1 Enhance-Templated RNA Protects From Heart Disease. *Circulation* (2019) 139:2778–92. doi: 10.1161/CIRCULATIONAHA.118.036769
149. Spurlock CF, Tossberg JT, Shaginurova G, Sriram S, Wingstrom J, Crooke PS, et al. A Molecular-Based Approach Using Long, Non-Coding RNA and Enhancer-Associated lncRNA Gene Expression Signatures to Classify Multiple Sclerosis Using Peripheral Whole Blood. *Mult Scler J* (2017) 23:94–4. doi: 10.1093/jmcb/mjz047
150. Suzuki A, Makinoshima H, Wakaguri H, Esumi H, Sugano S, Kohno T, et al. Aberrant Transcriptional Regulations in Cancers: Genome, Transcriptome and Epigenome Analysis of Lung Adenocarcinoma Cell Lines. *Nucleic Acids Res* (2014) 42:13557–72. doi: 10.1093/nar/gku885
151. Chen H, Li C, Peng X, Zhou Z, Weinstein JN, Liang H, et al. A Pan-Cancer Analysis of Enhancer Expression in Nearly 9000 Patient Samples. *Cell* (2018) 173:386–99.e312. doi: 10.1016/j.cell.2018.03.027
152. Murakawa Y, Yoshihara M, Kawaji H, Nishikawa M, Zayed H, Suzuki H, et al. Enhanced Identification of Transcriptional Enhancers Provides Mechanistic Insights Into Diseases. *Trends Genet* (2016) 32:76–88. doi: 10.1016/j.tig.2015.11.004
153. Schmitt AD, Hu M, Ren B. Genome-Wide Mapping and Analysis of Chromosome Architecture. *Nat Rev Mol Cell Biol* (2016) 17:743–55. doi: 10.1038/nrm.2016.104
154. Zhang Z, Lee JH, Ruan H, Ye Y, Krakowiak J, Hu Q, et al. Transcriptional Landscape and Clinical Utility of Enhancer RNAs for eRNA-Targeted Therapy in Cancer. *Nat Commun* (2019) 10:4562. doi: 10.1038/s41467-019-12543-5
155. Almamun M, Levinson BT, Swaay AC, Johnson NT, McKay SD, Arthur GL, et al. Integrated Methylome and Transcriptome Analysis Reveals Novel Regulatory Elements in Pediatric Acute Lymphoblastic Leukemia. *Epigenetics* (2015) 10:882–90. doi: 10.1080/15592294.2015.1078050
156. Almamun M, Kholod O, Stuckel AJ, Levinson BT, Johnson NT, Johnson GL, et al. Inferring a Role for Methylation of Intergenic DNA in the Regulation of Genes Aberrantly Expressed in Precursor B-Cell Acute Lymphoblastic Leukemia. *Leuk Lymphoma* (2017) 58:1–12. doi: 10.1080/10428194.2016.1272683
157. Teppo S, Laukkanen S, Liuksiala T, Nordlund J, Oittinen M, Teittinen K, et al. Genome-Wide Repression of eRNA and Target Gene Loci by the ETV6-RUNX1 Fusion in Acute Leukemia. *Genome Res* (2016) 26:1468–77. doi: 10.1101/gr.193649.115
158. Park A, Oh S, Jung KL, Choi UY, Lee HR, Rosenfeld MG, et al. Global Epigenomic Analysis of KSHV-Infected Primary Effusion Lymphoma Identifies Functional MYC Superenhancers and Enhancer RNAs. *Proc Natl Acad Sci USA* (2020) 117:21618–27. doi: 10.1073/pnas.1922216117
159. Fatima R, Choudhury SR, Divya TR, Bhaduri U, Rao MRS. A Novel Enhancer RNA, Hmrhl, Positively Regulates Its Host Gene, Phkb, in Chronic Myelogenous Leukemia. *Noncoding RNA Res* (2019) 4:96–108. doi: 10.1016/j.ncrna.2019.08.001
160. Fang K, Huang W, Sun YM, Chen TQ, Zeng ZC, Yang QQ, et al. Cis-Acting lnc-eRNA SEELA Directly Binds Histone H4 to Promote Histone Recognition and Leukemia Progression. *Genome Biol* (2020) 21:269. doi: 10.1186/s13059-020-02186-x
161. Dahan S, Sharma A, Cohen K, Baker M, Taqatqa N, Bentata M, et al. Vegfa's Distal Enhancer Regulates Its Alternative Splicing in CML. *NAR Cancer* (2021) 3:zcab029. doi: 10.1093/narcan/zcab029

162. Yu D, Yang X, Lin J, Cao Z, Lu C, Yang Z, et al. Super-Enhancer Induced IL-20ra Promotes Proliferation/Metastasis and Immune Evasion in Colorectal Cancer. *Front Oncol* (2021) 11:724655. doi: 10.3389/fonc.2021.724655
163. Li Y, He Y, Peng J, Su Z, Li Z, Zhang B, et al. Mutant Kras Co-Opts a Proto-Oncogenic Enhancer Network in Inflammation-Induced Metaplastic Progenitor Cells to Initiate Pancreatic Cancer. *Nat Cancer* (2021) 2:49–. doi: 10.1038/s43018-020-00134-z
164. Xiao J, Liu Y, Yi J, Liu X. LINC02257, an Enhancer RNA of Prognostic Value in Colon Adenocarcinoma, Correlates With Multi-Omics Immunotherapy-Related Analysis in 33 Cancers. *Front Mol Biosci* (2021) 8:646786. doi: 10.3389/fmolb.2021.646786
165. Wang L, Liu J, Tai J, Zhou N, Huang T, Xue Y, et al. A Prospective Study Revealing the Role of an Immune-Related eRNA, WAKMAR2, in Breast Cancer. *Sci Rep* (2021) 11:15328. doi: 10.1038/s41598-021-94784-3
166. Guo XY, Zhong S, Wang ZN, Xie T, Duan H, Zhang JY, et al. Immunogenomic Profiling Demonstrate AC003092.1 as an Immune-Related eRNA in Glioblastoma Multiforme. *Front Genet* (2021) 12:633812. doi: 10.3389/fgene.2021.633812
167. Qin N, Ma Z, Wang C, Zhang E, Li Y, Huang M, et al. Comprehensive Characterization of Functional eRNAs in Lung Adenocarcinoma Reveals Novel Regulators and a Prognosis-Related Molecular Subtype. *Theranostics* (2020) 10:11264–77. doi: 10.7150/thno.47039
168. Ma J, Lin X, Wang X, Min Q, Wang T, Tang C, et al. Reconstruction and Analysis of the Immune-Related LINC00987/A2M Axis in Lung Adenocarcinoma. *Front Mol Biosci* (2021) 8:644557. doi: 10.3389/fmolb.2021.644557
169. Wang Q, Yu X, Yang N, Xu L, Zhou Y. LncRNA AC007255.1, an Immune-Related Prognostic Enhancer RNA in Esophageal Cancer. *PeerJ* (2021) 9: e11698. doi: 10.7717/peerj.11698
170. Gu X, Wang L, Boldrup L, Coates PJ, Fahraeus R, Sgaramella N, et al. AP001056.1, A Prognosis-Related Enhancer RNA in Squamous Cell Carcinoma of the Head and Neck. *Cancers (Basel)* (2019) 11(3):347. doi: 10.3390/cancers11030347
171. Bahr C, Paleske L, Uslu VV, Remeseiro S, Takayama N, Ng SW, et al. A Myc Enhancer Cluster Regulates Normal and Leukaemic Haematopoietic Stem Cell Hierarchies. *Nature* (2018) 553:515–20. doi: 10.1038/nature25193
172. Mansour MR, Abraham BJ, Anders L, Berezovskaya A, Gutierrez A, Durbin AD, et al. Oncogene Regulation. An Oncogenic Super-Enhancer Formed Through Somatic Mutation of a Noncoding Intergenic Element. *Science* (2014) 346:1373–7. doi: 10.1126/science.1259037
173. Zhang X, Choi PS, Francis JM, Imielinski M, Watanabe H, Cherniack AD, et al. Identification of Focally Amplified Lineage-Specific Super-Enhancers in Human Epithelial Cancers. *Nat Genet* (2016) 48:176–82. doi: 10.1038/ng.3470
174. Corces MR, Granja JM, Shams S, Louie BH, Seoane JA, Zhou W, et al. The Chromatin Accessibility Landscape of Primary Human Cancers. *Science* (2018) 362(6413):eaav1898. doi: 10.1126/science.aav1898
175. Ding M, Zhan H, Liao X, Li A, Zhong Y, Gao Q, et al. Enhancer RNA - P2RY2e Induced by Estrogen Promotes Malignant Behaviors of Bladder Cancer. *Int J Biol Sci* (2018) 14:1268–76. doi: 10.7150/ijbs.27151
176. Liang J, Zhou H, Gerdt C, Tan M, Colson T, Kaye KM, et al. Epstein-Barr Virus Super-Enhancer eRNAs Are Essential for MYC Oncogene Expression and Lymphoblast Proliferation. *Proc Natl Acad Sci USA* (2016) 113:14121–6. doi: 10.1073/pnas.1616697113
177. Hamdan FH, Johnsen SA. Perturbing Enhancer Activity in Cancer Therapy. *Cancers (Basel)* (2019) 11 (5):634. doi: 10.3390/cancers11050634
178. Filippakopoulos P, Qi J, Picaud S, Shen Y, Smith WB, Fedorov O, et al. Selective Inhibition of BET Bromodomains. *Nature* (2010) 468:1067–73. doi: 10.1038/nature09504
179. Nicodeme E, Jeffrey KL, Schaefer U, Beinke S, Dewell S, Chung CW, et al. Suppression of Inflammation by a Synthetic Histone Mimic. *Nature* (2010) 468:1119–23. doi: 10.1038/nature09589
180. Belkina AC, Nikolajczyk BS, Denis GV. BET Protein Function Is Required for Inflammation: Brd2 Genetic Disruption and BET Inhibitor JQ1 Impair Mouse Macrophage Inflammatory Responses. *J Immunol* (2013) 190:3670–8. doi: 10.4049/jimmunol.1202838
181. Khan YM, Kirkham P, Barnes PJ, Adcock IM. Brd4 Is Essential for IL-1beta-Induced Inflammation in Human Airway Epithelial Cells. *PloS One* (2014) 9: e95051. doi: 10.1371/journal.pone.0095051
182. Zou Z, Huang B, Wu X, Zhang H, Qi J, Bradner J, et al. Brd4 Maintains Constitutively Active NF-kappaB in Cancer Cells by Binding to Acetylated RelA. *Oncogene* (2014) 33:2395–404. doi: 10.1038/onc.2013.179
183. Brown JD, Lin CY, Duan Q, Griffin G, Federation A, Paranal RM, et al. NF-KappaB Directs Dynamic Super Enhancer Formation in Inflammation and Atherogenesis. *Mol Cell* (2014) 56:219–31. doi: 10.1016/j.molcel.2014.08.024
184. Parua PK, Fisher RP. Dissecting the Pol II Transcription Cycle and Derailing Cancer With CDK Inhibitors. *Nat Chem Biol* (2020) 16:716–24. doi: 10.1038/s41589-020-0563-4
185. Chipumuro E, Marco E, Christensen CL, Kwiatkowski N, Zhang T, Hatheway CM, et al. CDK7 Inhibition Suppresses Super-Enhancer-Linked Oncogenic Transcription in MYCN-Driven Cancer. *Cell* (2014) 159:1126–39. doi: 10.1016/j.cell.2014.10.024
186. Zhang T, Kwiatkowski N, Olson CM, Clarke SED, Abraham BJ, Greifenberg AK, et al. Covalent Targeting of Remote Cysteine Residues to Develop CDK12 and CDK13 Inhibitors. *Nat Chem Biol* (2016) 12:876–84. doi: 10.1038/nchembio.2166
187. Hu S, Marineau JJ, Rajagopal N, Hamman KB, Choi YJ, Schmidt DR, et al. Discovery and Characterization of SY-1365, a Selective, Covalent Inhibitor of CDK7. *Cancer Res* (2019) 79:3479–91. doi: 10.1158/0008-5472.CAN-19-0119
188. Sharifnia T, Wawer MJ, Chen T, Huang QY, Weir BA, Ann Sizemore A, et al. Small-Molecule Targeting of Brachyury Transcription Factor Addiction in Chordoma. *Nat Med* (2019) 25:292–300. doi: 10.1038/s41591-018-0312-3
189. Kwiatkowski N, Zhang T, Rahl PB, Abraham BJ, Reddy J, Ficarro SB, et al. Targeting Transcription Regulation in Cancer With a Covalent CDK7 Inhibitor. *Nature* (2014) 511:616–20. doi: 10.1038/nature13393
190. Schmitz ML, Kracht M. Cyclin-Dependent Kinases as Coregulators of Inflammatory Gene Expression. *Trends Pharmacol Sci* (2016) 37:101–13. doi: 10.1016/j.tips.2015.10.004
191. Wei Y, Li C, Bian H, Qian W, Jin K, Xu T, et al. Targeting CDK7 Suppresses Super Enhancer-Linked Inflammatory Genes and Alleviates CAR T Cell-Induced Cytokine Release Syndrome. *Mol Cancer* (2021) 20:5. doi: 10.1186/s12943-020-01301-7
192. Siebert S, Pratt AG, Stocken DD, Morton M, Cranston A, Cole M, et al. Targeting the Rheumatoid Arthritis Synovial Fibroblast *via* Cyclin Dependent Kinase Inhibition: An Early Phase Trial. *Med (Baltimore)* (2020) 99:e20458. doi: 10.1097/MD.0000000000020458
193. Zhang H, Christensen CL, Dries R, Oser MG, Deng J, Diskin B, et al. CDK7 Inhibition Potentiates Genome Instability Triggering Anti-Tumor Immunity in Small Cell Lung Cancer. *Cancer Cell* (2020) 37:37–54.e39. doi: 10.1016/j.ccell.2019.11.003
194. Cartwright JA, Lucas CD, Rossi AG. Inflammation Resolution and the Induction of Granulocyte Apoptosis by Cyclin-Dependent Kinase Inhibitor Drugs. *Front Pharmacol* (2019) 10:55. doi: 10.3389/fphar.2019.00055
195. Xu YM, Du JY, Lau AT. Posttranslational Modifications of Human Histone H3: An Update. *Proteomics* (2014) 14:2047–60. doi: 10.1002/pmic.201300435
196. Xu B, On DM, Ma A, Parton T, Konze KD, Pattenden SG, et al. Selective Inhibition of EZH2 and EZH1 Enzymatic Activity by a Small Molecule Suppresses MLL-Rearranged Leukemia. *Blood* (2015) 125:346–57. doi: 10.1182/blood-2014-06-581082
197. Huang JP, Ling K. EZH2 and Histone Deacetylase Inhibitors Induce Apoptosis in Triple Negative Breast Cancer Cells by Differentially Increasing H3 Lys(27) Acetylation in the BIM Gene Promoter and Enhancers. *Oncol Lett* (2017) 14:5735–42. doi: 10.3892/ol.2017.6912
198. Sanchez GJ, Richmond PA, Bunker EN, Karman SS, Azofeifa J, Garnett AT, et al. Genome-Wide Dose-Dependent Inhibition of Histone Deacetylases Studies Reveal Their Roles in Enhancer Remodeling and Suppression of Oncogenic Super-Enhancers. *Nucleic Acids Res* (2018) 46:1756–76. doi: 10.1093/nar/gkx1225
199. Mishra VK, Wegwitz F, Kosinsky BL, Sen M, Baumgartner R, Wulff T, et al. Histone Deacetylase Class-I Inhibition Promotes Epithelial Gene Expression in Pancreatic Cancer Cells in a BRD4- and MYC-Dependent Manner. *Nucleic Acids Res* (2017) 45:6334–49. doi: 10.1093/nar/gkx212
200. Maiques-Diaz A, Spencer GJ, Lynch JT, Ciceri F, Williams EL, Amaral FMR, et al. Enhancer Activation by Pharmacologic Displacement of LSD1 From GFI1 Induces Differentiation in Acute Myeloid Leukemia. *Cell Rep* (2018) 22:3641–59. doi: 10.1016/j.celrep.2018.03.012
201. Metzger E, Wissmann M, Yin N, Müller JM, Schneider R, Peters AHFM, et al. LSD1 Demethylates Repressive Histone Marks to Promote Androgen-

Receptor-Dependent Transcription. *Nature* (2005) 437:436–9. doi: 10.1038/nature04020
202. Metzger E, Imhof A, Patel D, Kahl P, Hoffmeyer K, Friedrichs N, et al. Phosphorylation of Histone H3T6 by PKCbeta(I) Controls Demethylation at Histone H3K4. *Nature* (2010) 464:792–6. doi: 10.1038/nature08839
203. Hu Q, Kwon YS, Nunez E, Cardamone MD, Hutt KR, Ohgi KA, et al. Enhancing Nuclear Receptor-Induced Transcription Requires Nuclear Motor and LSD1-Dependent Gene Networking in Interchromatin Granules. *Proc Natl Acad Sci USA* (2008) 105:19199–204. doi: 10.1073/pnas.0810634105

Conflict of Interest: The authors declare that the research was conducted in the absence of any commercial or financial relationships that could be construed as a potential conflict of interest.

Publisher's Note: All claims expressed in this article are solely those of the authors and do not necessarily represent those of their affiliated organizations, or those of the publisher, the editors and the reviewers. Any product that may be evaluated in this article, or claim that may be made by its manufacturer, is not guaranteed or endorsed by the publisher.

frontiers | Frontiers in Immunology

REVIEW
published: 11 May 2022
doi: 10.3389/fimmu.2022.870952

Transient Receptor Potential Vanilloid1 (TRPV1) Channel Opens Sesame of T Cell Responses and T Cell-Mediated Inflammatory Diseases

Tengfei Xiao[1†], *Mingzhong Sun*[1†], *Jingjing Kang*[2] *and Chuanxiang Zhao*[3*]

[1] Department of Clinical Laboratory, The Sixth Affiliated Hospital of Nantong University, Yancheng Third People's Hospital, Yancheng, China, [2] Department of Clinical Laboratory, Affiliated Hospital of Nanjing University Medical School, Yancheng First People's Hospital, Yancheng, China, [3] Institute of Medical Genetics and Reproductive Immunity, School of Medical Science and Laboratory Medicine, Jiangsu College of Nursing, Huai'an, China

Transient receptor potential vanilloid1 (TRPV1) was primarily expressed in sensory neurons, and could be activated by various physical and chemical factors, resulting in the flow of extracellular Ca^{2+} into cells. Accumulating data suggest that the TRPV1 is expressed in some immune cells and is a novel regulator of the immune system. In this review, we highlight the structure and biological features of TRPV1 channel. We also summarize recent findings on its role in modulating T cell activation and differentiation as well as its protective effect in T cell-mediated inflammatory diseases and potential mechanisms.

Keywords: TRPV1, T cell, Ca2+, fever, T cell-mediated inflammatory diseases

OPEN ACCESS

Edited by:
Andrea Baragetti,
University of Milan, Italy

Reviewed by:
Feng Qin,
University at Buffalo, United States
Eva Reali,
University of Milano-Bicocca, Italy

****Correspondence:***
Chuanxiang Zhao
zhao_cx@jscn.edu.cn

[†]These authors have contributed equally to this work and share first authorship

Specialty section:
This article was submitted to Inflammation, a section of the journal Frontiers in Immunology

Received: *07 February 2022*
Accepted: *19 April 2022*
Published: *11 May 2022*

Citation:
Xiao T, Sun M, Kang J and Zhao C (2022) Transient Receptor Potential Vanilloid1 (TRPV1) Channel Opens Sesame of T Cell Responses and T Cell-Mediated Inflammatory Diseases. Front. Immunol. 13:870952. doi: 10.3389/fimmu.2022.870952

INTRODUCTION

Transient receptor potential (TRP) is a large superfamily of nonselective cation channels comprising of 28 members mainly located on the cell membrane. The TRP superfamily can be divided into TRPC (Canonical/Classical), TRPV (Vanilloid) and TRPM (Melastatin) sub-families (1). TRPV sub-families can be activated by vanillic acid compounds consisting of TRPV 1-6 (2). In 1997, TRPV1 was identified as a receptor of capsaicin, the main pungent component in "hot" chilli pepper (3). Over the past few decades, TRPV1 has been widely studied in the nervous system. In the peripheral nervous system, TRPV1 channel was found to be highly expressed in the spinal dorsal root ganglion neurons, the trigeminal ganglion and primary sensory neurons, which mainly mediate pain perception, transmission and regulation process. In the central nervous system, the TRPV channel was mainly involved in the regulation of body temperature, release of synaptic neurotransmitters, synaptic transmission and apoptosis (4). In addition, recent studies have revealed that TRPV1 was widely expressed in non-neuronal cell membranes of the kidney, pancreas, testes, uterus, spleen, stomach, small intestine, lung and liver mucous gland (2). Besides, the TRPV1 channel has been shown to play an important role in the immune system.

In this review, we discuss the structure and biological characteristics of the TRPV1 channel and highlight ecent findings on the roles of the TRPV1 channel in controlling T cell activation and differentiation. We also discuss the protective functions of the TRPV1 in T cell-mediated inflammatory diseases and the underlying potential mechanisms.

THE STRUCTURE AND BIOLOGICAL CHARACTERISTICS OF THE TRPV1 CHANNEL

TRPV1 channel is a coding protein with a molecular weight of 95 kDa, composed of 838 amino acids. Sequence analysis data has shown that the TRPV1 channel is a homologous tetramer composed of four subunits, each of which has six-transmembrane domains with a pore-forming hydrophobic group between the fifth and sixth transmembrane domains (5). Its N-terminal and C-terminal regions are located in the inner side of the cell membrane to regulate the receptor functions. The N-terminal contains several phosphorylation sites and six ankyrin repeat domains, which bind calmodulin and ATP and modulate the sensitivity and functions of the TRPV1 (6, 7). On the other hand, the C-terminal bears a TRP domain, multiple calmodulin binding domains and endogenous substance binding sites, such as phosphatidyl-inositol-4,5-bisphosphate (PIP_2) (8, 9) (**Figure 1**).

The TRPV1 is a multimodal receptor, which is activated and/or allosterically modulated by a range of thermal, mechanical and chemical stimuli (11). Besides capsaicin, TRPV1 channel is also activated by a variety of other plant-derived vanilloids, including camphor and resiniferatoxin (RTX), and putative endogenous vanilloids such as the endocannabinoid, inflammatory mediators such as arachidonic acid (12, 13). The thermal sensitivity of the TRPV1 was shown to be enhanced by various pro-inflammatory factors, such as nerve growth factor (NGF), bradykinin, lipid, prostaglandin and ATP (14). Although many studies have evaluated the role of PIP_2 in the activation of TRPV1, the data still remains controversial. For instance, Yao et al. demonstrated that PIP_2 could fuel the activation of TRPV1 (15, 16), while other studies reported that PIP_2 inhibited the TRPV1 activation (17, 18). Since the membrane is a highly asymmetric lipid bilayer, the contradictory effects of PIP_2 on the TRPV1 may be depending on which leaflet of the cell membrane it interacts with. Insertion of the PIP_2 into the inner leaflet of the plasma membrane enhanced the response of capsaicin in activating the TRPV1, while insertion into both leaflets suppressed the channel activation (19). Other activators of the TRPV1 channel include heat (>43 °C), low pH (< 5.4), static charge and voltage change (13). It has been demonstrated that TRPV1 is intrinsically heat sensitive (18), and temperature sensing is associated with voltage-dependent gating in the heat-sensitive channel TRPV1 (20).

After the TRPV1 activation, extracellular Ca^{2+} flows into the cells, and the intracellular the Ca^{2+} pool releases, resulting in increased concentration of intracellular Ca^{2+} (21). This increased intracellular Ca^{2+} mediates the basic activities of many cells, such as muscle contraction, neuronal activity, transmitter release, cell proliferation and apoptosis. In addition, activated TRPV1 can regulate body temperature and pain (22, 23).

THE ROLE OF THE TRPV1 CHANNEL IN T CELL RESPONSES

Functional Expression and TCR-Mediated Activation of TRPV1 in $CD4^+$ T Cells

Some previous studies analyzed the expression of TRPV1 mRNA and protein in human peripheral blood mononuclear cells (PBMC) (24), and found that they were expressed in mouse and rat thymocytes (25, 26). Thereafter, other studies demonstrated the expression of TRPV1 on human NK and $CD3^+$ T cells (27, 28), as well as in primary mouse and human T cells and human T cell line (Jurkat cells) (24, 28–32). Thus, the TRPV1 channel might play a pivotal role in T cells.

The activation and function of TRPV1 could be modulated by TCR-induced signaling pathway. In resting and TCR-stimulated

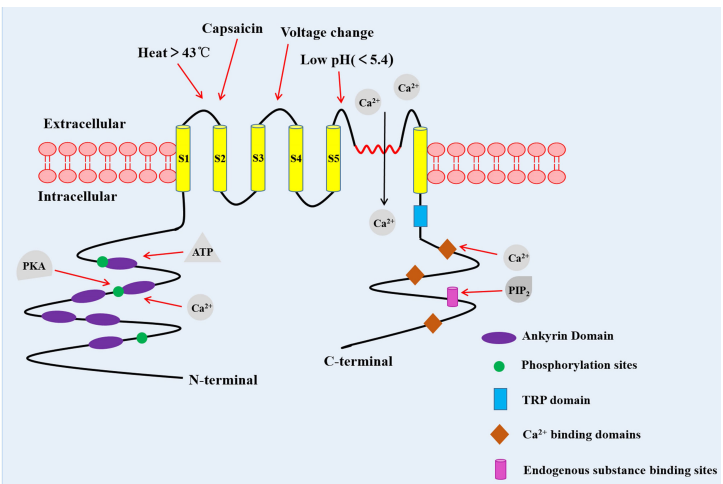

FIGURE 1 | The structure of the TRPV1 channel. TRPV1 channel is a homologous tetramer composed of four subunits, with six-transmembrane domains and a pore-forming hydrophobic group between the fifth and sixth transmembrane domains. The N-terminal contains several phosphorylation sites and six ankyrin repeat domains. The C-terminal has a TRP domain, multiple calmodulin blinding domains and binding sites of endogenous substance. PKA, Protein kinase A (10).

$CD4^+$ T cells, TRPV1 binds TCR co-receptor CD4 and Src-family tyrosine kinase Lck (33). The tyrosine of TRPV1 was rapidly phosphorylated by Lck in response to TCR stimulation leading to inactivation of TRPV1, which was not modified in Lck-deficient T cells (33). In addition, PIP_2 in the intracellular leaflet of the plasma membrane was shown to activate TRPV1. In contrast, PIP_2 located in both leaflets suppressed the activation of the TRPV1 (19). PIP_2 was hydrolyzed into diacylglycerol (DAG) and inositol 1,4,5-trisphosphate (IP_3) by TCR-induced activated phospholipase C gamma 1 (PLC-γ1) (33). The hydrolysis of PIP_2 relieved the PIP_2-mediated inhibition of the TRPV1 (16). Besides, IP_3 binds to its receptor (IP_3R) on endoplasmic reticulum (ER), contributing to the release of Ca^{2+} from the intracellular Ca^{2+} pool (33) (**Figure 2**).

The TCR Signals and TRPV1 Increase Ca^{2+} in $CD4^+$ T Cells

The elevation of intracellular Ca^{2+} is required for T cell activation, proliferation, differentiation and effector functions (34). The engagement of TCR increases the intracellular Ca^{2+} concentration, which results from a dual Ca^{2+} response; Ca^{2+} release from the ER stores and Ca^{2+} influx from the extracellular milieu into the cytosol across the plasma membrane (34). This in turn leads to activation of downstream Ca^{2+}-dependent signaling pathways and nuclear translocation of key transcription factors, which include nuclear factors of activated T-cells (NFAT) and nuclear factor kappa binding (NF-κB) (35). These activities account for T cell responses such as production of various cytokines, as well as proliferation and differentiation into effector cells.

TRPV1 functions as Ca^{2+}-permeable channels on the T cell plasma membrane. For instance, a previous study showed that Capsaicin, a special TRPV1 channel agonist, increased Ca^{2+} influx and intracellular Ca^{2+} concentration in activated $CD4^+$ T cells, but did not affect resting T cells (36, 37). TRPA1 inhibited the TRPV1 channel activity while deletion of TRPA1 in $CD4^+$ T cells increased T-cell receptor-induced Ca^{2+} influx (38). Besides, TRPV1 protein deficiency in $CD4^+$ T cells reduced activation of NFAT and NF-κB in response to TCR stimulation and decreased secretion of IL-2 and IFN-γ (31). Moreover, TRPV1 increased Ca^{2+} influx upon stimulation of phytohemagglutinin (PHA) (39). On the contrary, TRPV1-mediated Ca^{2+} influx was not influenced by ionomycin (a Ca^{2+} ionophore) and thapsigargin (a sarcoplasmic reticulum Ca^{2+}-ATPase pump inhibitor), which is known to mediate TCR-independent Ca^{2+} activation (31). These studies demonstrated that TRPV1 is a non-store-operated Ca^{2+} channel which modulates TCR-induced Ca^{2+} influx in T cells (31) (**Figure 2**).

TRPV1 not only promotes T cell activation, but induces T cell death. Previous studies demonstrated that apoptosis of human peripheral T and Jurkat cells were induced in response to exposure to prolonged and high capsaicin concentration (25, 37). Besides, capsaicin-induced apoptosis was associated with intracellular free Ca^{2+} influx (37). In addition, treatment of thymocytes with capsaicin induced autophagy through ROS-regulated AMPK and Atg4C pathways (26). However, the ROS generation was not associated with Ca^{2+} signaling (37).

Temperature Changes Determine the Fate of $CD4^+$ T Cells *via* TRPV1

Similar to free Ca^{2+}, temperature changes have been shown to activate the immune system (40). Fever is a physiological response to infections, injuries and inflammation. Fever-range temperatures (1°C~4°C above basal body temperature) are rapidly induced in response to an infection, which in turn

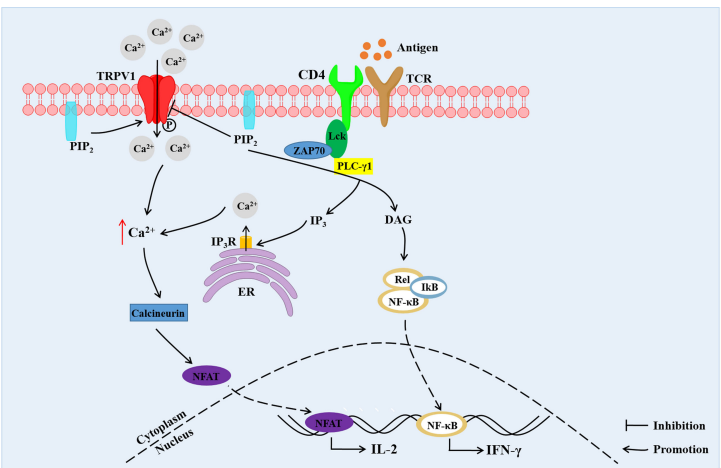

FIGURE 2 | The TCR signals and TRPV1-mediated increase in Ca^{2+} concentration and downstream Ca^{2+}-dependent signaling in $CD4^+$ T cells. TRPV1 is bound with CD4 and Lck. TRPV1 mediates Ca^{2+} influx, and the tyrosine of TRPV1 is phosphorylated by Lck. PIP_2 located in both leaflets suppresses the activation of TRPV1. Hydrolysis of PIP_2 into DAG and IP_3 by PLC-γ1 leads to relieving of PIP_2-mediated inhibition of TRPV1. Besides, IP_3 binds to IP_3R on ER contributing to the release of Ca^{2+} from intracellular Ca^{2+} store. The increased Ca^{2+} concentration promotes migration of NFAT into the nucleus, inducing the expression of IL-2. DAG promotes the entry of NF-κB into the nucleus, resulting in IFN-γ expression. PIP_2, phosphatidylinositol-4,5-bisphosphate; PLC-γ1, phospholipase C gamma 1; IP_3, inositol 1,4,5-trisphosphate; DAG, diacylglycerol; IP_3R, IP_3 receptor; ER, endoplasmic reticulum; NFAT, nuclear factor of activated T-cells; NF-κB, nuclear factor kappa binding (33).

boosts protective immune responses, such as immune surveillance. Two studies showed that fever-range temperatures (38~41°C) could promote lymphocytes homing to secondary lymphoid tissues through enhancement of L-selectin and α4β7 integrin-dependent adhesive interactions between circulating lymphocytes and specialized high endothelial venules, thus increasing immune surveillance (41, 42). Another study revealed that fever promoted trafficking of T cells and enhanced immune surveillance during an infection through heat shock protein 90 (HSP90)-induced α4-integrin activation and increase of α4-intergrin-mediated T cell adhesion (43). Besides, fever-like whole body hyperthermia (WBH) treatment of mice led to increase in tissue T cells with uropods. Besides, the WBH treatment induced reorganization of protein kinase C (PKC) isozymes and increased PKC activity within T cells (44). In addition, mildly elevated temperature range (≤40°C) was shown to strengthen cytotoxic activities of T cells from both adult and cord blood. However, this phenomenon was attenuated on exposure of the T cells to 42°C for 1 hour (45).

On the other hand, temperature changes were shown to affect T cell differentiation. Chen Dong et al. reported that febrile temperature did not influence Th1, Th2 and induced Treg (iTreg) cell differentiation, but selectively and robustly promoted Th17 cell differentiation at 39.5°C. Febrile temperature also elevated Th17 cell cytokine genes (IL-17a, IL-17f and IL-22) and reduced the expression of anti-inflammatory cytokine IL-10 (46). Besides, febrile temperature (38.5°C-39.5°C) fueled the pathogenicity of Th17 cells with a highly pro-inflammatory feature and aggravated experimental allergic encephalomyelitis (EAE) model (46). Mechanistically, febrile-temperature-induced Th17 cell differentiation depended on HSP-70- and HSP-90-related heat shock response and enhanced SUMOylation of SMAD4 transcription factor at its K113 and K159 residues, which facilitated its nuclear localization (46). In sync with the previous findings, Gaublomme and colleagues demonstrated that treatment with anti-fever drugs reduced Th17 cell response *in vivo*, while *in vitro* induced Th17 cells were highly pro-inflammatory in a lung-inflammation model (47) (**Figure 3**). In addition, naïve $CD8^+$ T cells exposed to 39.5°C *in vitro* promoted the rate of synapse formation with APC, which led to differentiation of a greater percentage of $CD8^+$ T cells into effector cells (48). This phenomenon was attributed to an increase in membrane fluidity and clustering of $GM1^+$CD-microdomains, as well as clustering of TCRβ and CD8 co-receptor (48). A recent study showed that fever enhanced production of activated $CD8^+$ T cell cytokines and glycolytic metabolism with a limited effect on the expression of CD69, the activation marker (49). Moreover, febrile temperature promoted protective antitumor effects of $CD8^+$ T cells *via* mitochondrial translation (49). However, data on how the T cells sense subtle temperature changes remain scant.

TRPV1 is a critical regulator of physiological body temperature and fever, outside the central nervous system (50, 51). TRPV1 could be activated at a temperatures threshold near 43°C (52). A previous study demonstrated that fever sensing by $CD4^+$ T cells involve TRPV1 channel during $CD4^+$ T cell differentiation (53). In addition, fever-range temperatures significantly enhanced Th2 differentiation and reduced Th1 commitment at moderate fever temperature (39°C) *in vitro via* a TRPV1 channel-mediated Notch-dependent pathway. This was accompanied by upregulation of Th2-relevant transcription factor GATA3, and reduction of the Th1-relevant transcription factor, T-bet (53) (**Figure 3**). However, both mouse and human naïve $CD4^+$ T cells treatment with temperatures between 37°C and 39°C showed no alterations in the activation, proliferation, or cell survival (53). Samivel R et al. revealed suppression of the production of Th2/Th17 cytokines in $CD4^+$ T cells and Jurkat T cells upon genetic and pharmacological inhibition of TRPV1 (32).

Together, these data demonstrated that TRPV1 functions as a temperature sensor in $CD4^+$ T cells. The temperature changes could regulate $CD4^+$ T cell differentiation through TRPV1.

THE FUNCTIONS OF TRPV1 IN T CELL-MEDIATED INFLAMMATORY DISEASES

Inflammation is the main and common pathophysiological feature of pain, visceral inflammation, hypertension and cancer at different stages of occurrence and development (54). Inflammation is characterized by redness, swelling, heat, pain, tissue injury or organ dysfunction (54). Inflammation has been shown to remove tissue injuries and promote restoration during immune responses (54). Recent studies have shown that TRPV1 plays anti-inflammatory roles by attenuating acute and chronic inflammatory processes as well as enhancing homeostasis, thus, attenuating harmful effects of inflammatory responses. Here, we analyzed how TRPV1 modulates T cell-mediated inflammatory responses, which include multiple sclerosis (MS), pulmonary inflammation, inflammatory skin diseases or inflammatory bowel diseases (IBD) as well as osteoarthritis (OA) (**Figure 4**).

Multiple Sclerosis

Multiple sclerosis (MS) is a complex central nervous system autoimmune disease characterized by autoimmune demyelination and neurodegeneration, which are mediated by Th1 and Th17 cells, macrophages, and immune inflammatory mediators. Previously, TRPV1 mRNA was found to be expressed throughout the central nervous system (CNS), but it was highly expressed in sensory neurons of the dorsal root ganglion (10). The $TRPV1^+$ neurovascular complex, referred to as the blood-CNS barrier, promoted invasion of pathogenic lymphocytes (55). However, SA13353, a TRPV1 agonist, reduced the number of cytokines, including TNF-α, IL-1β, IL-12p40, IL-17, and interferon (IFN)-γ in EAE. In addition, SA13353 attenuated the increase in IL-17-producing cells, demonstrating that SA13353 inhibited the growth of Th17 cells and development of EAE (56). Therefore, TRPV1 channel confers protection by regulating T cells in EAE.

Pulmonary Inflammation

Pulmonary inflammation is caused by infection, physical and chemical factors, immune injury, allergy and drugs, and is

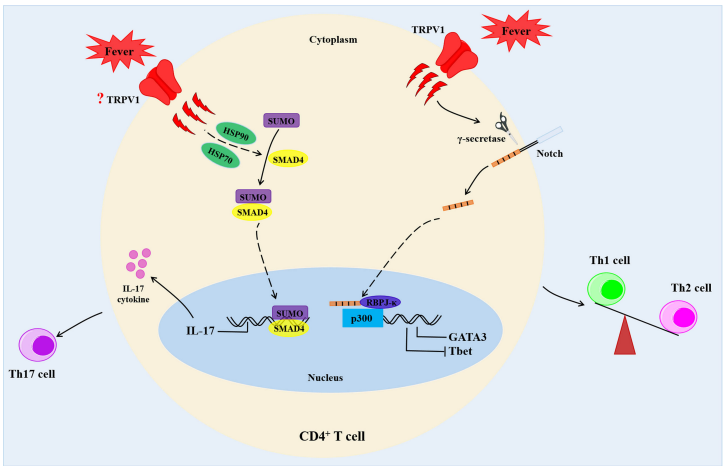

FIGURE 3 | Fever determines the fate of $CD4^+$ T cells. Febrile temperature changes enhance Th2 differentiation and reduce Th1 differentiation *via* a TRPV1-regulated Notch-dependent pathway. In addition, febrile temperature promotes Th17 cell differentiation which depends on HSP-70- and HSP-90-related heat shock response and enhances SUMOylation of SMAD4 transcription factor at its K113 and K159 residues. HSP90, heat shock proteins 90; HSP70, heat shock proteins 70.

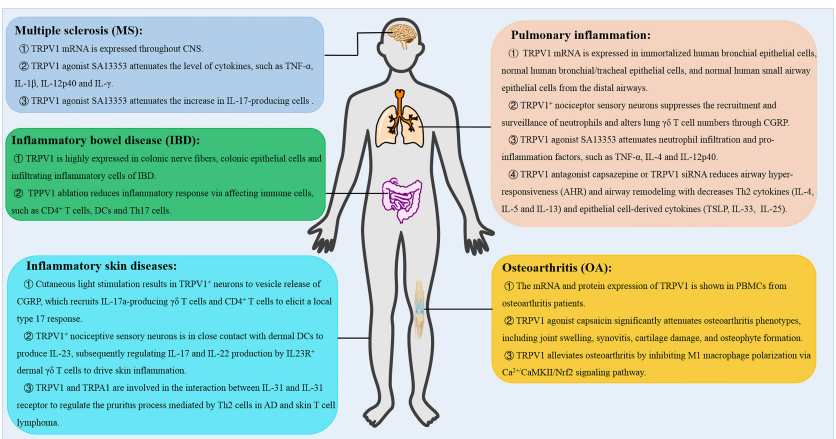

FIGURE 4 | The role of TRPV1 in T cell-mediated inflammatory diseases. TRPV1 regulates the inflammatory responses, such as multiple sclerosis (MS), pulmonary inflammation, inflammatory skin diseases and inflammatory bowel disease (IBD), and osteoarthritis (OA). CNS, central nervous system; AD, atopic dermatitis; CGRP, calcitonin gene-related peptide.

mediated by a variety of inflammatory mediators such as immune cells, chemokines and cytokines. RT-PCR analysis revealed that TRPV1 was expressed in immortalized human bronchial epithelial cells, normal human bronchial/tracheal epithelial cells, and normal human small airway epithelial cells from distal airways (57). In LPS-induced lung injury, SA13353 attenuated neutrophil infiltration and enhanced the TNF-α and CINC-1 levels. In ovalbumin-induced allergic airway inflammation, SA13353 was shown to inhibit leukocyte infiltration and attenuate increase of IL-4 and IL-12p40 (58). Besides, $TRPV1^+$ nociceptor sensory neurons suppressed recruitment and surveillance of neutrophils and altered lung γδ T cells through the release of the neuropeptide calcitonin gene-related peptide (CGRP) (59). In contrast, treatment with TRPV1 antagonist capsazepine or TRPV1 siRNA reduced airway hyper-responsiveness (AHR) and airway remodeling with suppressed Th2 cytokines (IL-4, IL-5 and IL-13) and epithelial cell-derived cytokines (TSLP, IL-33, and IL-25) in ovalbumin-induced chronic asthma (60). Therefore, there is a need for further studies to determine the role of TRPV1 in pneumonia.

Inflammatory Skin Diseases

Inflammatory skin diseases refer to skin diseases caused by various internal and external infectious or non-infectious factors, which include psoriasis, atopic dermatitis, allergic contact dermatitis or irritant contact dermatitis. In the absence

of tissue damage or bacterial invasion, cutaneous light stimulation triggered the release of CGRP from $TRPV1^+$ neurons, which recruited IL-17a-producing γδ T cells and $CD4^+$ T cells. These cells elicited a local type 17 response that augmented host defense to *C. albicans* and *S. aureus* (61). At the same time, the activated neurons could activate $TRPV1^+$ neurons at an adjacent, unstimulated skin through the nerve reflex arc, which provokes the type 17 responses (61). On the other hand, psoriasis is an immune cell-mediated inflammatory skin disease, whose pathogenesis is mediated by IL-23 (62, 63). In imiquimod-induced IL-23-dependent psoriasis-like skin inflammation, $TRPV1^+$ nociceptive sensory neurons were shown to interact with dermal dendritic cells to produce IL-23, thus modulating IL-17 and IL-22 production by $IL23R^+$ dermal γδ T cells, which drive skin inflammation (64). Besides, atopic dermatitis (AD) is a common allergic skin disease characterized by skin barrier dysfunction, inflammation and an intense itch (65). IL-31 is an important inflammatory mediator involved in AD, which is closely associated with pruritus (66). Previous data showed that TRPV1 and TRPA1 were involved in the interaction between IL-31 and IL-31 receptor to regulate the pruritus process, which was mediated by Th2 cells in AD and skin T cell lymphoma (67). Based on the important roles played by TRPV1 in skin inflammation and pruritus, the TRPV1 channel is another potential target for skin diseases.

Inflammatory Bowel Disease (IBD)

The occurrence of IBD is driven by chronic inflammation, which is mainly known as Crohn's disease (CD) and ulcerative colitis (UC). Previous data showed that capsaicin, a TRPV1 agonist, attenuated severe combined immunodeficiency (SCID) T-cell transfer colitis, suggesting that the TRPV1 signaling plays a role in capsaicin-mediated attenuation of colitis (68). It was shown that TRPV1 was highly expressed in colonic nerve fibers of IBD patients (69). Luo *et al.* demonstrated high expression of TRPV1 in colonic epithelial cells and infiltrating inflammatory cells of 60 patients with active IBD (30 cases of UC and 30 cases of CD respectively), which was not associated with severity of the disease (70). Moreover, TRPV1 immunoreactive cells were robustly higher in all intestinal layers from active UC patients (71), which suggested that TRPV1 might be involved in immune cells-mediated pathogenesis of IBD. In the T-cell-mediated colitis model, TRPV1 was shown to promote T cell and intestinal inflammatory responses. Inhibition of TRPV1 in T cells by genetic factors or drugs led to reduction of the symptoms of colitis (31, 38). In addition, TRPV1 played an important role in activating mucosal macrophages and maintaining Th17 immune cells in respond to inflammatory stimuli. Overexpression of TRPV1 significantly increased the susceptibility of DSS-induced colitis and promoted DC activation and cytokine production by enhancing the activation of calcineurin/nuclear factor in activated T cell (NFATc2) signaling, and enhancing DC-mediated Th17 cell differentiation upon inflammatory stimulation (72).

In summary, the data indicated that TRPV1 might be a potential therapeutic target in the treatment of mucosal immunity and IBD.

Osteoarthritis (OA)

Osteoarthritis (OA) is a chronic, painful and degenerative disease that affects all joint tissues and results in loss of articular cartilage. Immune cells such as macrophages and T cells in the synovium participate in stimulating and modulating inflammatory responses in OA (73). The TRPV1 mRNA and protein expression were previously detected in PBMCs from OA patients (74). TRPV1 knockout mice showed attenuated chronic phase (>6 weeks) of RA pain (75). In rat OA model, intra-articular injection of capsaicin significantly attenuated OA phenotypes, such as joint swelling, synovitis, cartilage damage, and osteophyte formation (76). Furthermore, TRPV1 alleviated OA by inhibiting M1 macrophage polarization *via* Ca^{2+}/CaMKII/Nrf2 signaling pathway (76). These findings demonstrated that TRPV1 regulates various cells in OA.

CONCLUSION AND FUTURE PERSPECTIVES

In this review, we analyze recent data on the expression and functions of TRPV1 in T cells and T cell-mediated inflammatory diseases. The data showed that TRPV1 is a Ca^{2+}-permeable channel and mediates TCR-induced Ca^{2+} influx, leading to T cell activation and death as well as differentiation of T cell subsets. However, most of the studies only provided phenotypic observations. Therefore, data on the exact mechanisms underlying the observed phenotypic characteristics is lacking. Besides, whether TRPV1 interacts with other family members or with other channels in T cells remains unclear. In future, scientists should explore interactions between ion channels in T cells, and determine the exact cell-intrinsic roles in T cell development and in different effector T cell subsets.

Furthermore, many studies have demonstrated that TRPV1 can regulate T cell-mediated inflammation and protect the body by regulating production of T cell-related cytokines, such as TNF-α, IL-4 and IL-6. However, due to diverse expression on sensory nerves, immune cells, epithelial cells as well as the consequent activation-induced release of inflammatory mediators, the overall functions of TRPV1 in inflammatory diseases need further evaluation. These data would lay a foundation for future development of new anti-inflammatory drugs targeting TRPV1 in inflammation.

AUTHOR CONTRIBUTIONS

TX and MS wrote the original manuscripts. JK guided on the structure of the manuscript. CZ organized and reviewed the manuscript. CZ and TX provided the funding. All authors contributed to the article and approved the submitted version.

FUNDING

This study received funding from Huai'an Natural Science Research Program (Grant No. HABL202114), the Science and Technology Development Project of Yancheng, China (YK2019108) and the Nantong University Clinical Medicine Special Project, China (2019JZ011).

REFERENCES

1. Montell C. The TRP Superfamily of Cation Channels. *Sci STKE* (2005) 2005 (272):re3. doi: 10.1126/stke.2722005re3
2. Montell C BL, Flockerzi V. The TRP Channels, a Remarkably Functional Family. *Cell* (2002) 108:595–8. doi: 10.1016/s0092-8674(02)00670-0
3. Caterina MJ SM, Tominaga M, Rosen TA, Levine JD, Julius D. The Capsaicin Receptor a Heat-Activated Ion Channel in the Pain Pathway. *Nature* (1997) 389(6653):816–24. doi: 10.1038/39807
4. Talavera K, Nilius B, Voets T. Neuronal TRP Channels: Thermometers, Pathfinders and Life-Savers. *Trends Neurosci* (2008) 31(6):287–95. doi: 10.1016/j.tins.2008.03.002
5. Liao M, Cao E, Julius D, Cheng Y. Structure of the TRPV1 Ion Channel Determined by Electron Cryo-Microscopy. *Nature* (2013) 504(7478):107–12. doi: 10.1038/nature12822
6. Lishko PV, Procko E, Jin X, Phelps CB, Gaudet R. The Ankyrin Repeats of TRPV1 Bind Multiple Ligands and Modulate Channel Sensitivity. *Neuron* (2007) 54(6):905–18. doi: 10.1016/j.neuron.2007.05.027
7. Phelps CB, Procko E, Lishko PV, Wang RR, Gaudet R. Insights Into the Roles of Conserved and Divergent Residues in the Ankyrin Repeats of TRPV Ion Channels. *Channels* (2014) 1(3):148–51. doi: 10.4161/chan.4716
8. Garcia-Sanz N, Fernandez-Carvajal A, Morenilla-Palao C, Planells-Cases R, Fajardo-Sanchez E, Fernandez-Ballester G, et al. Identification of a Tetramerization Domain in the C Terminus of the Vanilloid Receptor. *J Neurosci* (2004) 24(23):5307–14. doi: 10.1523/JNEUROSCI.0202-04.2004
9. Numazaki M TT, Takeuchi K, Murayama N, Toyooka H, Tominaga M. Structural Determinant of TRPV1 Desensitization Interacts With Calmodulin. *Proc Natl Acad Sci USA* (2003) 100(13):8002–6. doi: 10.1073/pnas.1337252100
10. Ho KW, Ward N, Calkins DJ. TRPV1: A Stress Response Protein in the Central Nervous System. *Am J Neurodegener Dis* (2012) 1(1):1–14.
11. Holzer P. The Pharmacological Challenge to Tame the Transient Receptor Potential Vanilloid-1 (TRPV1) Nocisensor. *Br J Pharmacol* (2008) 155 (8):1145–62. doi: 10.1038/bjp.2008.351
12. Chu CJ, Huang SM, De Petrocellis L, Bisogno T, Ewing SA, Miller JD, et al. N-Oleoyldopamine, a Novel Endogenous Capsaicin-Like Lipid That Produces Hyperalgesia. *J Biol Chem* (2003) 278(16):13633–9. doi: 10.1074/jbc.M211231200
13. Meotti FC, Lemos de Andrade E, Calixto JB. TRP Modulation by Natural Compounds. *Handb Exp Pharmacol* (2014) 223:1177–238. doi: 10.1007/978-3-319-05161-1_19
14. Melnick C, Kaviany M. Thermal Actuation in TRPV1: Role of Embedded Lipids and Intracellular Domains. *J Theor Biol* (2018) 444:38–49. doi: 10.1016/j.jtbi.2018.02.004
15. Yao J, Qin F. Interaction With Phosphoinositides Confers Adaptation Onto the TRPV1 Pain Receptor. *PLoS Biol* (2009) 7(2):e46. doi: 10.1371/journal.pbio.1000046
16. Prescott ED, Julius D. A Modular PIP2 Binding Site as a Determinant of Capsaicin Receptor Sensitivity. *Science* (2003) 300(5623):1284–8. doi: 10.1126/science.1083646
17. Ufret-Vincenty CA, Klein RM, Hua L, Angueyra J, Gordon SE. Localization of the PIP2 Sensor of TRPV1 Ion Channels. *J Biol Chem* (2011) 286(11):9688–98. doi: 10.1074/jbc.M110.192526
18. Cao E, Cordero-Morales JF, Liu B, Qin F, Julius D. TRPV1 Channels Are Intrinsically Heat Sensitive and Negatively Regulated by Phosphoinositide Lipids. *Neuron* (2013) 77(4):667–79. doi: 10.1016/j.neuron.2012.12.016
19. Senning EN, Collins MD, Stratiievska A, Ufret-Vincenty CA, Gordon SE. Regulation of TRPV1 Ion Channel by Phosphoinositide (4,5)-Bisphosphate: The Role of Membrane Asymmetry. *J Biol Chem* (2014) 289(16):10999–1006. doi: 10.1074/jbc.M114.553180
20. Voets T, Droogmans G, Wissenbach U, Janssens A, Flockerzi V, Nilius B. The Principle of Temperature-Dependent Gating in Cold- and Heat-Sensitive TRP Channels. *Nature* (2004) 430(7001):748–54. doi: 10.1038/nature02732.
21. Sappington RM, Sidorova T, Long DJ, Calkins DJ. TRPV1: Contribution to Retinal Ganglion Cell Apoptosis and Increased Intracellular Ca2+ With Exposure to Hydrostatic Pressure. *Invest Ophthalmol Vis Sci* (2009) 50 (2):717–28. doi: 10.1167/iovs.08-2321
22. Jeong KY, Seong J. Neonatal Capsaicin Treatment in Rats Affects TRPV1-Related Noxious Heat Sensation and Circadian Body Temperature Rhythm. *J Neurol Sci* (2014) 341(1-2):58–63. doi: 10.1016/j.jns.2014.03.054
23. Negri L, Lattanzi R, Giannini E, Colucci M, Margheriti F, Melchiorri P, et al. Impaired Nociception and Inflammatory Pain Sensation in Mice Lacking the Prokineticin Receptor PKR1: Focus on Interaction Between PKR1 and the Capsaicin Receptor TRPV1 in Pain Behavior. *J Neurosci* (2006) 26(25):6716–27. doi: 10.1523/JNEUROSCI.5403-05.2006
24. Saunders CI, Kunde DA, Crawford A, Geraghty DP. Expression of Transient Receptor Potential Vanilloid 1 (TRPV1) and 2 (TRPV2) in Human Peripheral Blood. *Mol Immunol* (2007) 44(6):1429–35. doi: 10.1016/j.molimm.2006.04.027
25. Amantini C, Mosca M, Lucciarini R, Perfumi M, Morrone S, Piccoli M, et al. Distinct Thymocyte Subsets Express the Vanilloid Receptor VR1 That Mediates Capsaicin-Induced Apoptotic Cell Death. *Cell Death Differ* (2004) 11(12):1342–56. doi: 10.1038/sj.cdd.4401506
26. Farfariello V, Amantini C, Santoni G. Transient Receptor Potential Vanilloid 1 Activation Induces Autophagy in Thymocytes Through ROS-Regulated AMPK and Atg4C Pathways. *J Leukoc Biol* (2012) 92(3):421–31. doi: 10.1189/jlb.0312123
27. Kim HS, Kwon HJ, Kim GE, Cho MH, Yoon SY, Davies AJ, et al. Attenuation of Natural Killer Cell Functions by Capsaicin Through a Direct and TRPV1-Independent Mechanism. *Carcinogenesis* (2014) 35(7):1652–60. doi: 10.1093/carcin/bgu091
28. Majhi RK, Sahoo SS, Yadav M, Pratheek BM, Chattopadhyay S, Goswami C. Functional Expression of TRPV Channels in T Cells and Their Implications in Immune Regulation. *FEBS J* (2015) 282(14):2661–81. doi: 10.1111/febs.13306
29. Wenning AS, Neblung K, Strauss B, Wolfs MJ, Sappok A, Hoth M, et al. TRP Expression Pattern and the Functional Importance of TRPC3 in Primary Human T-Cells. *Biochim Biophys Acta* (2011) 1813(3):412–23. doi: 10.1016/j.bbamcr.2010.12.022
30. Spinsanti G, Zannolli R, Panti C, Ceccarelli I, Marsili L, Bachiocco V, et al. Quantitative Real-Time PCR Detection of TRPV1-4 Gene Expression in Human Leukocytes From Healthy and Hyposensitive Subjects. *Mol Pain* (2008) 4:51. doi: 10.1186/1744-8069-4-51
31. Bertin S, Aoki-Nonaka Y, de Jong PR, Nohara LL, Xu H, Stanwood SR, et al. The Ion Channel TRPV1 Regulates the Activation and Proinflammatory Properties of CD4(+) T Cells. *Nat Immunol* (2014) 15(11):1055–63. doi: 10.1038/ni.3009
32. Samivel R, Kim D, Son HR, Rhee YH, Kim EH, Kim JH, et al. The Role of TRPV1 in the CD4+ T Cell-Mediated Inflammatory Response of Allergic Rhinitis. *Oncotarget* (2016) 7(1):148–60. doi: 10.18632/oncotarget.6653
33. Bertin S, de Jong PR, Jefferies WA, Raz E. Novel Immune Function for the TRPV1 Channel in T Lymphocytes. *Channels (Austin)* (2014) 8(6):479–80. doi: 10.4161/19336950.2014.991640
34. Hogan PG, Lewis RS, Rao A. Molecular Basis of Calcium Signaling in Lymphocytes: STIM and ORAI. *Annu Rev Immunol* (2010) 28:491–533. doi: 10.1146/annurev.immunol.021908.132550
35. Inada H, Iida T, Tominaga M. Different Expression Patterns of TRP Genes in Murine B and T Lymphocytes. *Biochem Biophys Res Commun* (2006) 350 (3):762–7. doi: 10.1016/j.bbrc.2006.09.111
36. Zhang F, Challapalli SC, Smith PJ. Cannabinoid CB(1) Receptor Activation Stimulates Neurite Outgrowth and Inhibits Capsaicin-Induced Ca(2+) Influx in an *In Vitro* Model of Diabetic Neuropathy. *Neuropharmacology* (2009) 57 (2):88–96. doi: 10.1016/j.neuropharm.2009.04.017
37. Macho A CM, Muñoz-Blanco J, Gómez-Díaz C, Gajate C, Mollinedo F, et al. Selective Induction of Apoptosis by Capsaicin in Transformed Cells the Role of Reactive Oxygen Species and Calcium. *Cell Death Differ* (1999) 6(2):155–65. doi: 10.1038/sj.cdd.4400465
38. Bertin S, Aoki-Nonaka Y, Lee J, de Jong PR, Kim P, Han T, et al. The TRPA1 Ion Channel is Expressed in CD4+ T Cells and Restrains T-Cell-Mediated Colitis Through Inhibition of TRPV1. *Gut* (2017) 66(9):1584–96. doi: 10.1136/gutjnl-2015-310710
39. Szallasi A, Cortright DN, Blum CA, Eid SR. The Vanilloid Receptor TRPV1: 10 Years From Channel Cloning to Antagonist Proof-of-Concept. *Nat Rev Drug Discov* (2007) 6(5):357–72. doi: 10.1038/nrd2280
40. Evans SS, Repasky EA, Fisher DT. Fever and the Thermal Regulation of Immunity: The Immune System Feels the Heat. *Nat Rev Immunol* (2015) 15 (6):335–49. doi: 10.1038/nri3843

41. Evans SS WW, Bain MD, Burd R, Ostberg JR, Repasky EA. Fever-Range Hyperthermia Dynamically Regulates Lymphocyte Delivery to High Endothelial Venules. *Blood* (2001) 97(9):2727–33. doi: 10.1182/blood.v97.9.2727
42. Wang WC, Goldman LM, Schleider DM, Appenheimer MM, Subjeck JR, Repasky EA, et al. Fever-Range Hyperthermia Enhances L-Selectin-Dependent Adhesion of Lymphocytes to Vascular Endothelium. *J Immunol* (1998) 160(2):961–9.
43. Lin C, Zhang Y, Zhang K, Zheng Y, Lu L, Chang H, et al. Fever Promotes T Lymphocyte Trafficking *via* a Thermal Sensory Pathway Involving Heat Shock Protein 90 and Alpha4 Integrins. *Immunity* (2019) 50(1):137–51.e6. doi: 10.1016/j.immuni.2018.11.013
44. Wang XY OJ, Repasky EA. Effect of Fever-Like Whole-Body Hyperthermia on Lymphocyte Spectrin Distribution, Protein Kinase C Activity, and Uropod Formation. *J Immunol* (1999) 162(6):3378–87.
45. Shen RN LL, Young P, Shidnia H, Hornback NB, Broxmeyer HE. Influence of Elevated Temperature on Natural Killer Cell Activity, Lymphokine-Activated Killer Cell Activity and Lectin-Dependent Cytotoxicity of Human Umbilical Cord Blood and Adult Blood Cells. *Int J Radiat Oncol Biol Phys* (1994) 29 (4):821–6. doi: 10.1016/0360-3016(94)90571-1
46. Wang X, Ni L, Wan S, Zhao X, Ding X, Dejean A, et al. Febrile Temperature Critically Controls the Differentiation and Pathogenicity of T Helper 17 Cells. *Immunity* (2020) 52(2):328–41.e5. doi: 10.1016/j.immuni.2020.01.006
47. Gaublomme JT, Yosef N, Lee Y, Gertner RS, Yang LV, Wu C, et al. Single-Cell Genomics Unveils Critical Regulators of Th17 Cell Pathogenicity. *Cell* (2015) 163(6):1400–12. doi: 10.1016/j.cell.2015.11.009
48. Mace TA, Zhong L, Kilpatrick C, Zynda E, Lee CT, Capitano M, et al. Differentiation of CD8+ T Cells Into Effector Cells is Enhanced by Physiological Range Hyperthermia. *J Leukoc Biol* (2011) 90(5):951–62. doi: 10.1189/jlb.0511229
49. O'Sullivan D, Stanczak MA, Villa M, Uhl FM, Corrado M, Klein Geltink RI, et al. Fever Supports CD8(+) Effector T Cell Responses by Promoting Mitochondrial Translation. *Proc Natl Acad Sci USA* (2021) 118(25): e2023752118. doi: 10.1073/pnas.2023752118
50. Gavva NR. Body-Temperature Maintenance as the Predominant Function of the Vanilloid Receptor TRPV1. *Trends Pharmacol Sci* (2008) 29(11):550–7. doi: 10.1016/j.tips.2008.08.003
51. Gavva NR, Treanor JJ, Garami A, Fang L, Surapaneni S, Akrami A, et al. Pharmacological Blockade of the Vanilloid Receptor TRPV1 Elicits Marked Hyperthermia in Humans. *Pain* (2008) 136(1-2):202–10. doi: 10.1016/j.pain.2008.01.024
52. Caterina MJ, JuliusD. Thevanilloid Receptor a Molecular Gateway to the Pain Pathway. *Annu Rev Neurosci* (2001) 24:487–517. doi: 10.1146/annurev.neuro.24.1.487.
53. Umar D, Das A, Gupta S, Chattopadhyay S, Sarkar D, Mirji G, et al. Febrile Temperature Change Modulates CD4 T Cell Differentiation *via* a TRPV Channel-Regulated Notch-Dependent Pathway. *Proc Natl Acad Sci USA* (2020) 117(36):22357–66. doi: 10.1073/pnas.1922683117
54. Bousounis P, Bergo V, Trompouki E. Inflammation, Aging and Hematopoiesis: A Complex Relationship. *Cells* (2021) 10(6):1386. doi: 10.3390/cells10061386
55. Paltser G, Liu XJ, Yantha J, Winer S, Tsui H, Wu P, et al. TRPV1 Gates Tissue Access and Sustains Pathogenicity in Autoimmune Encephalitis. *Mol Med* (2013) 19:149–59. doi: 10.2119/molmed.2012.00329
56. Tsuji F, Murai M, Oki K, Seki I, Ueda K, Inoue H, et al. Transient Receptor Potential Vanilloid 1 Agonists as Candidates for Anti-Inflammatory and Immunomodulatory Agents. *Eur J Pharmacol* (2010) 627(1-3):332–9. doi: 10.1016/j.ejphar.2009.10.044
57. Agopyan N, Bhatti T, Yu S, Simon SA. Vanilloid Receptor Activation by 2- and 10-μm Particles Induces Responses Leading to Apoptosis in Human Airway Epithelial Cells. *Toxicol Appl Pharmacol* (2003) 192(1):21–35. doi: 10.1016/s0041-008x(03)00259-x
58. Tsuji F, Murai M, Oki K, Inoue H, Sasano M, Tanaka H, et al. Effects of SA13353, a Transient Receptor Potential Vanilloid 1 Agonist, on Leukocyte Infiltration in Lipopolysaccharide-Induced Acute Lung Injury and Ovalbumin-Induced Allergic Airway Inflammation. *J Pharmacol Sci* (2010) 112(4):487–90. doi: 10.1254/jphs.09295sc
59. Baral P, Umans BD, Li L, Wallrapp A, Bist M, Kirschbaum T, et al. Nociceptor Sensory Neurons Suppress Neutrophil and Gammadelta T Cell Responses in Bacterial Lung Infections and Lethal Pneumonia. *Nat Med* (2018) 24(4):417–26. doi: 10.1038/nm.4501
60. Choi JY, Lee HY, Hur J, Kim KH, Kang JY, Rhee CK, et al. TRPV1 Blocking Alleviates Airway Inflammation and Remodeling in a Chronic Asthma Murine Model. *Allergy Asthma Immunol Res* (2018) 10(3):216–24. doi: 10.4168/aair.2018.10.3.216
61. Cohen JA, Edwards TN, Liu AW, Hirai T, Jones MR, Wu J, et al. Cutaneous TRPV1+ Neurons Trigger Protective Innate Type 17 Anticipatory Immunity. *Cell* (2019) 178(4):919–32.e14. doi: 10.1016/j.cell.2019.06.022
62. Menter A, Krueger GG, Paek SY, Kivelevitch D, Adamopoulos IE, Langley RG. Interleukin-17 and Interleukin-23: A Narrative Review of Mechanisms of Action in Psoriasis and Associated Comorbidities. *Dermatol Ther (Heidelb)* (2021) 11(2):385–400. doi: 10.1007/s13555-021-00483-2
63. Ghoreschi K, Balato A, Enerbäck C, Sabat R. Therapeutics Targeting the IL-23 and IL-17 Pathway in Psoriasis. *Lancet* (2021) 397(10275):754–66. doi: 10.1016/s0140-6736(21)00184-7
64. Riol-Blanco L, Ordovas-Montanes J, Perro M, Naval E, Thiriot A, Alvarez D, et al. Nociceptive Sensory Neurons Drive Interleukin-23-Mediated Psoriasiform Skin Inflammation. *Nature* (2014) 510(7503):157–61. doi: 10.1038/nature13199
65. Nakahara T, Kido-Nakahara M, Tsuji G, Furue M. Basics and Recent Advances in the Pathophysiology of Atopic Dermatitis. *J Dermatol* (2021) 48(2):130–9. doi: 10.1111/1346-8138.15664
66. Imai Y. Interleukin-33 in Atopic Dermatitis. *J Dermatol Sci* (2019) 96(1):2–7. doi: 10.1016/j.jdermsci.2019.08.006
67. Cevikbas F, Wang X, Akiyama T, Kempkes C, Savinko T, Antal A, et al. A Sensory Neuron-Expressed IL-31 Receptor Mediates T Helper Cell-Dependent Itch: Involvement of TRPV1 and TRPA1. *J Allergy Clin Immunol* (2014) 133(2):448–60. doi: 10.1016/j.jaci.2013.10.048
68. Belmaati MS, Diemer S, Hvarness T, Baumann K, Pedersen AE, Christensen RE, et al. Antiproliferative Effects of TRPV1 Ligands on Nonspecific and Enteroantigen-Specific T Cells From Wild-Type and Trpv1 KO Mice. *Inflammation Bowel Dis* (2014) 20(6):1004–14. doi: 10.1097/MIB.0000000000000039
69. Yiangou Y, Facer P, Dyer NH, Chan CL, Knowles C, Williams NS, et al. Vanilloid Receptor 1 Immunoreactivity in Inflamed Human Bowel. *Lancet* (2001) 357(9265):1338–9. doi: 10.1016/s0140-6736(00)04503-7
70. Luo C, Wang Z, Mu J, Zhu M, Zhen Y, Zhang H. Upregulation of the Transient Receptor Potential Vanilloid 1 in Colonic Epithelium of Patients With Active Inflammatory Bowel Disease. *Int J Clin Exp Pathol* (2017) 10(11):11335–44.
71. Toledo-Maurino JJ, Furuzawa-Carballeda J, Villeda-Ramirez MA, Fonseca-Camarillo G, Meza-Guillen D, Barreto-Zuniga R, et al. The Transient Receptor Potential Vanilloid 1 Is Associated With Active Inflammation in Ulcerative Colitis. *Mediators Inflamm* (2018) 2018:6570371. doi: 10.1155/2018/6570371
72. Duo L, Wu T, Ke Z, Hu L, Wang C, Teng G, et al. Gain of Function of Ion Channel TRPV1 Exacerbates Experimental Colitis by Promoting Dendritic Cell Activation. *Mol Ther Nucleic Acids* (2020) 22:924–36. doi: 10.1016/j.omtn.2020.10.006
73. Woodell-May JE, Sommerfeld SD. Role of Inflammation and the Immune System in the Progression of Osteoarthritis. *J Orthop Res* (2020) 38(2):253–7. doi: 10.1002/jor.24457
74. Engler A, Aeschlimann A, Simmen BR, Michel BA, Gay RE, Gay S, et al. Expression of Transient Receptor Potential Vanilloid 1 (TRPV1) in Synovial Fibroblasts From Patients With Osteoarthritis and Rheumatoid Arthritis. *Biochem Biophys Res Commun* (2007) 359(4):884–8. doi: 10.1016/j.bbrc.2007.05.178
75. Hsieh WS, Kung CC, Huang SL, Lin SC, Sun WH. TDAG8, TRPV1, and ASIC3 Involved in Establishing Hyperalgesic Priming in Experimental Rheumatoid Arthritis. *Sci Rep* (2017) 7(1):8870. doi: 10.1038/s41598-017-09200-6
76. Lv Z, Xu X, Sun Z, Yang YX, Guo H, Li J, et al. TRPV1 Alleviates Osteoarthritis by Inhibiting M1 Macrophage Polarization *via* Ca(2+)/CaMKII/Nrf2 Signaling Pathway. *Cell Death Dis* (2021) 12(6):504. doi: 10.1038/s41419-021-03792-8

Conflict of Interest: The authors declare that the research was conducted in the absence of any commercial or financial relationships that could be construed as a potential conflict of interest.

this article, or claim that may be made by its manufacturer, is not guaranteed or endorsed by the publisher.

frontiers | Frontiers in Immunology

ORIGINAL RESEARCH
published: 06 July 2022
doi: 10.3389/fimmu.2022.918636

A Human CD68 Promoter-Driven Inducible Cre-Recombinase Mouse Line Allows Specific Targeting of Tissue Resident Macrophages

Agata N. Rumianek[1], Ben Davies[2], Keith M. Channon[2,3], David R. Greaves[1†] and Gareth S. D. Purvis[1,3*†]*

[1] Sir William Dunn School of Pathology, University of Oxford, Oxford, United Kingdom, [2] Wellcome Trust Centre for Human Genetics, University of Oxford, Oxford, United Kingdom, [3] Division of Cardiovascular Medicine, Radcliffe Department of Medicine, John Radcliffe Hospital, University of Oxford, Oxford, United Kingdom

OPEN ACCESS

Edited by:
Matthias Mack,
University Medical Center Regensburg, Germany

Reviewed by:
Roland Lang,
University Hospital Erlangen, Germany
Morgan Salmon,
University of Michigan, United States

****Correspondence:***
David R. Greaves
david.greaves@path.ox.ac.uk
Gareth S. D. Purvis
gareth.purvis@cardiov.ox.ac.uk

[†]These authors share senior authorship

Specialty section:
This article was submitted to Inflammation, a section of the journal Frontiers in Immunology

Received: *12 April 2022*
Accepted: *07 June 2022*
Published: *06 July 2022*

Citation:
Rumianek AN, Davies B, Channon KM, Greaves DR and Purvis GSD (2022) A Human CD68 Promoter-Driven Inducible Cre-Recombinase Mouse Line Allows Specific Targeting of Tissue Resident Macrophages. Front. Immunol. 13:918636. doi: 10.3389/fimmu.2022.918636

Current genetic tools designed to target macrophages *in vivo* often target cells from all myeloid lineages. Therefore, we sought to generate a novel transgenic mouse which has a tamoxifen inducible Cre-recombinase under the control of the human CD68 promoter (hCD68-CreERT2). To test the efficiency and specificity of the of Cre-recombinase activity we crossed the hCD68-CreERT2 mice with a loxP-flanked STOP cassette red fluorescent protein variant (tdTomato) mouse. We established that orally dosing mice with 2 mg of tamoxifen for 5 consecutive days followed by a 5-day induction period resulted in robust expression of tdTomato in $CD11b^+$ $F4/80^+$ tissue resident macrophages. Using this induction protocol, we demonstrated tdTomato expression within peritoneal, liver and spleen macrophages and blood $Ly6C^{low}$ monocytes. Importantly there was limited or no inducible tdTomato expression within other myeloid cells (neutrophils, monocytes, dendritic cells and eosinophils), T cells ($CD4^+$ and $CD8^+$) and B cells ($CD19^+$). We also demonstrated that the level of tdTomato expression can be used as a marker to identify different populations of peritoneal and liver macrophages. We next assessed the longevity of tdTomato expression in peritoneal macrophages, liver and splenic macrophages and demonstrated high levels of tdTomato expression as long as 6 weeks after the last tamoxifen dose. Importantly, hCD68-CreERT2 expression is more restricted than that of LysM-Cre which has significant expression in major myeloid cell types (monocytes and neutrophils). To demonstrate the utility of this novel macrophage-specific Cre driver line we demonstrated tdTomato expression in recruited $CD11b^+CD64^+F4/80^+$ monocyte-derived macrophages within the atherosclerotic lesions of AAV8-mPCSK9 treated mice, with limited expression in recruited neutrophils. In developing this new hCD68-CreERT2 mouse we have a tool that allows us to target tissue resident macrophages, with the advantage of not targeting other myeloid cells namely neutrophils and inflammatory monocytes.

Keywords: macrophage, Cre/*loxP*, inducible, hCD68, targeting, LysM.

1 INTRODUCTION

Tissue resident macrophages play an important sentinel role, maintaining tissue homeostasis by surveying local tissue niches for pathogen, and regulating the local inflammatory response (1, 2). Macrophages, also play an important role in initiating a programme of wound repair following infection or tissue injury (3). If tissue homeostasis is not fully restored and inflammation resolution not achieved macrophages can promote continued tissue damage and chronic inflammation in diseases such as diabetes, rheumatoid arthritis and atherosclerosis (4–6).

Tissues harbour two main macrophage populations; those seeded during embryonic development and those that are recruited *via* the circulation and are monocyte derived (7). Macrophages are classically defined by flow cytometry as having high expression of CD11b and F4/80, however, the levels of F4/80 between tissues varies considerably. For example, peritoneal macrophages express F4/80 at high levels, whereas capsular macrophages in the liver have relatively low levels of F4/80. This makes identifying tissue-resident macrophages difficult (8), especially if they are not under steady state (9). This problem has been further complicated by large scale sequencing projects that have identified increased heterogeneity within cell surface defined macrophage population (10–12).

Cell surface markers are readily available to discriminate common myeloid cell types such as neutrophils and monocytes from macrophages or dendritic cells in both the mouse and human, however, genetic tools for targeting macrophages are lacking in specificity (13). This is most likely due to the common haemopoietic progenitors which give rise to the common myeloid progenitor which produces neutrophils and monocytes (14), which are the cells that are mostly frequently targeted in so called macrophage specific mouse lines. A common progenitor has been identified for dendritic cells and macrophages which makes discrimination of these two related cells types challenging (15).

More complexity arises in the fact that tissue resident macrophages are thought to be a self-renewing population; however, there is now a bulk of evidence to suggest that with age embryonically seeded tissue resident macrophages are replenished by monocyte-derived macrophages (12, 16). This raises the question as to what a tissue resident macrophage actually is, and what their functions are in different tissues (17, 18). Within the heart tissue resident macrophages have essential and diverse functionality in health; for example in coronary blood and lymphatic vessel development (19, 20) and facilitation of cardiac conduction (21). They also have a critical role in tissue remodelling post injury following myocardial ischaemia (22). In other organs such as skeletal muscle, the eye and the pancreas it is becoming evident that tissue resident macrophages also have unique functions (23, 24). Additionally, within the peritoneal cavity, there is a homogenous population of CD11b and F4/80-expressing peritoneal macrophages but two populations can be identified by size. The large peritoneal macrophages (LPM) which account for approximately 90% of all peritoneal macrophages and are derived embryonically, and small peritoneal macrophages (SPM) which account for around 10% and are derived from circulating monocytes (25).

Human CD68 and its murine homolog, macrosialin (Cd68), are glycosylated type 1 transmembrane proteins that belong to the lysosomal/endosomal-associated membrane glycoprotein (LAMP) family and are widely used as a macrophage marker (26). Although widely cited to be localised to the endocytic compartment its function is not fully elucidated but roles in both antigen processing and as a scavenger receptor have been reported. The murine Cd68 (macrosalin) and human CD68 gene differ in that the first intron (IVS-1) of human CD68 gene region has an additional regulatory element which specifically directs CD68 expression in macrophages, whereas the first intron of the mouse Cd68 gene can direct expression on non-macrophage cells (27, 28). We have previously generated a transgenic reporter mouse line, by expressing a green fluorescent protein gene under the transcriptional control of a hCD68-promoter IVS-1 expression cassette (29). This directs expression of GFP in bone marrow, circulating monocytes and tissue resident and recruited macrophages (30). There is also considerable expression in neutrophils and other myeloid cell linages due the expression of the hCD68-GFP transgene during embryogenesis and haematopoiesis (29).

To better study tissue resident macrophage biology, we wanted to create a more macrophage restricted Cre driver mouse line. To do this we established a novel knock-in mouse line hCD68-CreERT2, which expressed the tamoxifen inducible CreERT2 recombinase under the control of the human CD68 promoter and the regulatory element in IVS-1. We predicted that inducible Cre-recombinase activity would be more restricted to macrophages because it would avoid the early expression profile of CD68 during embryogenesis and haematopoiesis. Our goal was to overcome the limited macrophage specificity seen in available 'macrophage specific' targeting mouse lines.

2 MATERIALS AND METHODS

2.1 Animal Studies

2.1.1 Ethical Statement

All animal experiments were conducted in accordance to the Animal (Scientific Procedures) Act 1986, with procedures reviewed by the Sir William Dunn School of Pathology (SWDSOP) ethical review body (AWERB) and conducted under project **licence** P144E44F2 at the University of Oxford. Animals were housed in individually ventilated cages (between 2 and 6 mice per cage) in specific pathogen free conditions. All animals were provided with standard chow and water ad libitum and, maintained on a 12 h light: 12 h dark cycle at controlled temperature (20–22°C) and humidity. Breeding strategies were optimised to reduce numbers of animals used.

2.1.2 Generation of hCD68-CreERT2 Mouse

A tamoxifen inducible Cre recombinase cDNA (CreERT2) was cloned downstream of a CD68 promoter, consisting of 2.9 kb of CD68 5' flanking sequence with the 83-bp first intron (IVS-1) of the CD68 gene (PMID 11454064), together with a rabbit beta-globin polyadenylation sequence. This transgenic cassette was

subcloned into the pExchange4-CB9 vector suitable for PhiC31 integrase mediated cassette exchange at the Gt(ROSA)26Sor locus (PMID 21853122). The resulting vector, CB9-CD68-CreERT2 contains a promoterless neomycin phosphotransferase cassette, upstream of CD68-CreERT2-pA and the whole array is flanked by PhiC31 attP sites.

CB9-CD68-CreERT2 DNA (5 μg) was electroporated into 1 × 106 RS-PhiC embryonic stem cells, a C57BL/6N JM8F6 derived line (PMID 26369329), using the Neon transfection system (Life Technologies) (3 × 1400 V, 10 ms), and selected in 210 μg/ml G418 for 7 days. Resistant colonies were isolated, expanded and screened for correct cassette exchange at the Gt(ROSA)26Sor locus using primers CAG-F (5′-CAGCCATTGCCTTTTATGGT-3) and ExNeo2 (5′-GTTGTGCCCAGTCATAGCCGAATAG-3′) to verify the 5' integration event and att-F1 (5′-GCACTAGTTC TAGAGCGATCCCC-3') and 3HR-R1 (5′-CGGGAGAAATGG ATATGAAGTACTGGGC-3′) to verify the 3' integration event. Recombinant ES cells were injected into albino C57BL/6J blastocysts, and the resulting chimeras were bred with albino C57BL/6J mice to confirm germline transmission.

2.1.3 Generation of hCD68-CreERT2 LSL-tdTomato Mice

Gt(ROSA)26Sortm27.1(CAG-COP4*H134R/tdTomato) (LSL-tdTomato) mice were bought from The Jackson Laboratory and maintained in-house and genotype confirmed using PCR. LSL-tdTomato heterozygous females were crossed with hCD68-CreERT2 heterozygous males. Off-spring were then genotyped to confirm presence of transgenes. Mice which were heterozygous for both transgenes, hCD68-CreERT2 LSL-tdTomato (hCD68-tdTom) were used to assess Cre-recombinase efficacy in further experiments. Littermates were used as negative controls.

2.1.4 Tamoxifen Preparation

Tamoxifen (catalog #156738; MP Biomedicals) was dissolved in 100% ethanol followed by dilution in peanut oil (catalog #P2144; Sigma-Aldrich) at the final concentration of 10 mg/ml.

2.1.5 Cre-Recombinase Induction Protocol

8 to 13-week-old male and female mice were given tamoxifen (2 mg; for 5 days; *via* oral gavage) or peanut oil as vehicle control. Mice were killed humanely and tissues harvested 5 days or 6 weeks and 5 days after the final dose; refer to **Figures 1** and **5** for timeline.

2.2 Flow Cytometry

Cells were washed in FACS buffer (0.05% BSA, 2 mM EDTA in PBS, pH 7.4) blocked using anti-CD16/32 (1 μg; Biolegend) for 15 mins at 4°C, followed by 30 min antibody staining for the surface markers with isotype controls. Cells were again washed and resuspended in 200 μL of FACS buffer without fixation. Antibodies used are listed in **Table 1**, all bought from BioLegend apart from FITC-CD8a, which was bought from BD Biosciences.

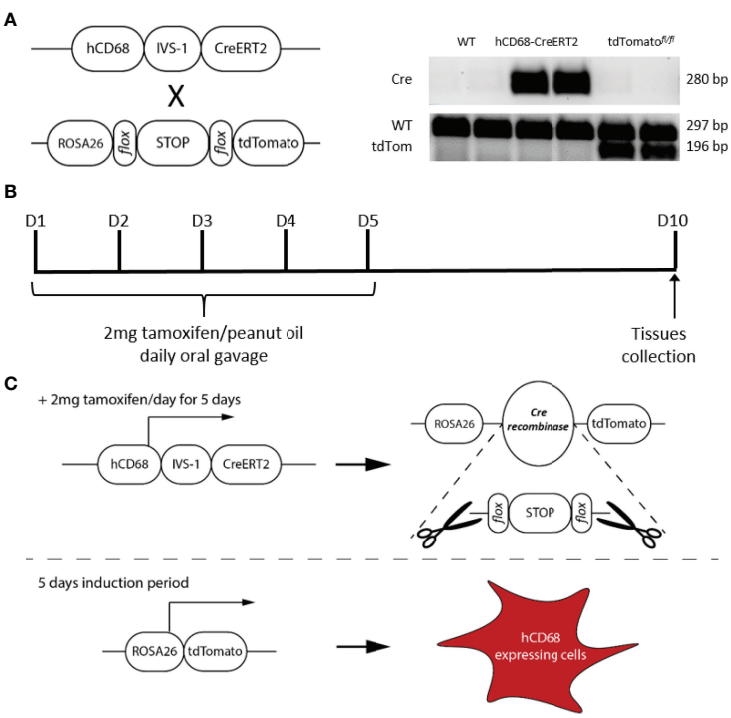

FIGURE 1 | Design and generation of the inducible hCD68-CreERT2 model. **(A)** Presence of Cre recombinase and tdTomato genes was confirmed by extracting DNA from ear notches, a standard PCR amplification and running side-by-side on an agarose gel for all genotypes available for het x het breeding strategy (see methods for details). **(B)** Tamoxifen dosing protocol for induction of Cre recombinase activity in hCD68-CreERT2 model. **(C)** Principles of the human CD68 promoter-driven tamoxifen inducible Cre recombinase activation; not to scale.

TABLE 1 | List of flow cytometry antibodies used in this study.

Marker	Fluorophore	Isotype	Clone
CD3	Brilliant Violet 510	Armenian Hamster IgG	145-2C11
CD4	PE/Cyanine7	Rat IgG2b	GK1.5
CD8a	FITC	Rat IgG2a	53-6.7
CD8a	PE	Rat IgG2a	53-6.7
CD11b	Brilliant Violet 421	Rat IgG2b	M1/70
CD11c	Brilliant Violet 650	Armenian Hamster IgG	N418
CD11c	PE/Cyanine7	Armenian Hamster IgG	N418
CD19	Pacific Blue	Rat IgG2a	6D5
CD45	APC/Cyanine7	Rat IgG2b	30-F11
CD45R/B220	APC	Rat IgG2a	RA3-6B2
CD68	PE	Rat IgG2a	FA-11
CD68	APC/Cyanine7	Rat IgG2a	FA-11
CD115	PE/Cyanine7	Rat IgG2a	AFS98
CD170 (Siglec-F)	APC	Rat IgG2a	S17007L
Ly-6C	FITC	Rat IgG2c	HK1.4
Ly-6C	PerCP/Cyanine5.5	Rat IgG2c	HK1.4
Ly-6C	PE	Rat IgG2c	HK1.4
Ly-6G	Brilliant Violet 510	Rat IgG2a	1A8
F4/80	PE	Rat IgG2a	BM8
F4/80	APC	Rat IgG2a	BM8
F4/80	FITC	Rat IgG2a	BM8
F4/80	APC/Cyanine7	Rat IgG2a	BM8
I-A/I-E (MHCII)	FITC	Rat IgG2b	M5/114.15.2
I-A/I-E (MHCII)	PE	Rat IgG2b	M5/114.15.2
CLEC4F	Alexa Fluor 647	Mouse IgG1	3E3F9
Tim-4	PE/Cyanine7	Rat IgG2a	RMT4-54

Intracellular staining was performed as per manufacturer's instructions using eBioscience FOXP3/Transcription Factor Staining Buffer Set (invitrogen). Briefly, after the last wash of the extracellular staining protocol, cells were fixed in Fixation/ Permeabilization Buffer for 30 min at room temperature. Cells were washed and resuspended in Permeabilization Buffer; intracellular antibodies were added for 30 min in room temperature. Cells were again washed in Permeabilization Buffer and resuspended in FACS buffer for flow cytometric analysis.

Data were acquired using BD Fortessa X20 cytometer and Diva software (BD Biosciences) and then analysed using FlowJo (Tree Star Inc, USA) software. Fluorescence minus One (FMO) controls were used for gating and single stains for compensation were obtained using UltraComp eBeads™ Compensation Beads (InVitrogen) for liver, spleen and blood panels and single stained cell samples for peritoneal cells.

2.3 Fluorescent Microscopy

Mice were perfused with 10-20 mL of cold PBS and organs were harvested into 4% paraformaldehyde and incubated at 4oC for 6 hours before transferring into 30% sucrose overnight to dehydrate. Samples were then embedded OCT matrix and sectioned at –20oC at 5 µm per section. Sections were then countered-stained with DAPI. Images were taken using Live Cell Olympus Confocal Microscope.

2.4 Hyperlipidaemia Model

hCD68-tdTom male and female mice and their control littermates were injected intravenously once with AAVmPCSK9 (AAV.8TBGmPCSK9D377Y, Penn Vector Core) at 5×1011 viral particles/mouse and placed onto a high fat and cholesterol diet (SDS 829108 Western RD diet) for 16 weeks. After 16 weeks mice were orally gavaged with 2 mg of tamoxifen or peanut oil as a vehicle control for 5 consecutive days and tissues were collected 5 days later; refer to **Figure 7** for timeline.

2.5 Oil Red O Staining

Perfusion fixed frozen hearts were embedded in OCT and cut in 5 µm sections. Sections were brought to room temperature, washed with 60% isopropanol, then saturated with Oil Red O (1% w/v, 60% isopropanol) for 15 min, washed in 60% isopropanol and rinsed in distilled water. Sections were then counterstained with haematoxylin. Coverslips were applied in aqueous mounting medium.

2.6 Aortic Digestion

All enzymes were purchased from Sigma-Aldrich, unless stated otherwise. Tissues were isolated in 5% FBS in RPMI-1640 (Gibco). Tissues were cut into small pieces and digested in the enzyme cocktail (450 U/ml collagenase I, 125 U/ml collagenase XI 60 U/ml hyaluronidase and 60 U/ml DNase I (ThermoFisher Scientific)) at 37 °C in shaker for 50 min. The cells were retrieved by passing tissue pieces through a 70 µm cell strainer (Greiner Bio-One) and processed for immunofluorescent staining for flow cytometry (31).

2.7 Statistical Analysis

All experiments were designed, where possible, to generate groups of equal size. Where possible, blinding and randomisation protocols were used. All data in the text and figures are presented as mean ± standard error mean (SEM) of n observations, where n represents the number of animals studied (*in vivo*) or independent values, not technical replicates (*in vitro*). All statistical analysis was calculated using GraphPad Prism 9 (GraphPad Software, San Diego, California, USA; RRID : SCR_002798). When the mean of two experimental groups were compared, a two-tailed Students t-test was performed. Normally distributed data without repeated measurements were assessed by a one-way ANOVA followed by Bonferroni correction if the F value reached significance; two-way ANOVA was used for comparing control and experimental mice across two separate conditions In all cases a $P < 0.05$ was considered significant.

3 RESULTS

3.1 Generation of hCD68-CreERT2-tdTomato Reporter Mouse

To exploit the macrophage targeting activity of the human CD68 promoter which includes the regulatory element IVS-1 (28, 32) we engineered a DNA construct that encoded a tamoxifen inducible Cre recombinase (33) under the hCD68 promoter regulatory region, this was then inserted into the ROSA26 locus of embryonic stem cells before being injected into albino C57BL/6J blastocysts yielding hCD68-CreERT2 chimeric

founders. Mice were fertile and produced an expected Mendelian ratio of transgenic and non-transgenic litter mates with no obvious developmental defects. Genotype was confirmed by PCR. Heterozygous offspring were then bred with LSL-tdTomato mice to generate double transgenic experimental mice (hCD68-tdTom) (**Figure 1A**), littermates carrying no transgenes, or a single transgene were used as controls; out of 444 pups born during this study 109 were heterozygous for both alleles, 101 mice were heterozygous for hCD68-CreERT2 only, 102 mice were heterozygous for tdTomato only and 132 mice were wild-typed for both alleles. The optimal Cre recombinase induction protocol was determined to be administration of tamoxifen (2 mg per mouse; p.o.) for 5 days, and collection of cells and tissues 5 days later (**Figure 1B**).

3.2 The hCD68 Promotor Drives Inducible Cre-Recombinase in Tissue Resident Macrophages

In order to assess the pattern of inducible Cre activity in tamoxifen treated hCD68-tdTom mice in different tissue resident macrophage populations we used flow cytometry with panels of well characterised monoclonal antibodies. When compared to vehicle treated hCD68-tdTom mice, tamoxifen treated hCD68-tdTom mice had robust expression of tdTomato in $CD11b^+F4/80^+$ peritoneal resident macrophages (**Figures 2A–C**). We further investigated the level of tdTomato expression in two known peritoneal macrophage populations (**Supplementary Figure 1**). When compared to vehicle treated hCD68-tdTom mice, in tamoxifen treated hCD68-tdTom mice ~40% of LPM displayed tdTomato expression, while ~ 20% of SPM displayed tdTomato expression, moreover, the level of tdTomato expression (MFI) was significantly lower in SPM compared to LPM.

Within the spleen of tamoxifen treated hCD68-tdTom mice there was robust expression of tdTomato in $CD11b^+F4/80^+$ macrophages (**Figures 2D–F**). As the spleen is a reservoir for multiple myeloid cell types tdTomato expression was quantified in other myeloid cell populations within the spleen. Monocytes were sub-divided into $Ly6C^{hi}$ ($CD11b^+CD115^+Ly6C^{hi}$) and $Ly6C^{low}$ ($CD11b^+CD115^+Ly6C^{low}$) (**Supplementary Figure 2A**). Importantly, <5% of $Ly6C^{hi}$ monocytes had tdTomato expression (**Supplementary Figure 2B**) while ~27% of the splenic $Ly6C^{low}$ monocytes expressed tdTomato (**Supplementary Figure 2C**). On the other hand, < 4% of neutrophils ($CD11b^+Cd115^-Ly6G^+$) expressed tdTomato (**Supplementary Figure 2D**). We also found that ~20% of splenic dendritic cells ($CD45^+CD11c^+MHCII^+$) had tdTomato expression (**Supplementary Figures 2E/F**). In the non-myeloid cells ~ 2.5% of splenic T-cells ($CD45^+CD11b^-CD3^+$) (**Supplementary Figure 2E/G**) and 5% B-cells ($CD45^+CD11b^-B220^+$) expressed tdTomato (**Supplementary Figure 2E/H**).

The liver has a large and heterogenous population of tissue resident macrophages (34). When compared to vehicle-treated hCD68-tdTom mice, tamoxifen treated hCD68-tdTom mice had robust expression of tdTomato in all liver macrophage populations. Within the liver ~80% of $CD11b^{hi}F4/80^{hi}$ macrophages from tamoxifen treated hCD68-tdTom mice expressed high levels of tdTomato (**Figure 2G-I**). However, within the liver there is significant heterogeneity within the macrophage population (**Supplementary Figure 3**); we therefore wanted to further investigate hCD68 promoter driven Cre activity within different macrophage subsets. The populations assessed were lipid-associated macrophages (LAMs; $CD11b^{hi}Ly6C^+CD11c^-MHCII^+CLEC4F^{low}$; **Supplementary Figure 3B**), monocyte-derived Kupffer cells (Mono-KC; $CD11b^{hi}Ly6C^+CD11c^-MHCII^+CLEC4F^+$; **Supplementary Figure 2C**), capsular macrophages (CM; $CD11b^{low}F4/80^{int}TIM4^-MHCII^+$; **Supplementary Figure 3D**); Kupffer cells (KC; $CD11b^+F4/80^{hi}CLEC4F^{hi}TIM4^{hi}$; **Supplementary Figure 3E**). All liver macrophage populations in tamoxifen treated hCD68-tdTom mice expressed tdTomato, however the intensity of tdTomato was different between subsets of liver macrophage (**Supplementary Figure 3F**). Mono-KCs expressed the highest levels of tdTomato, while CMs expressed the lowest level (**Supplementary Figure 3F**).

To confirm flow cytometry results we used fluorescent microscopy to visualize endogenous tdTomato expression in the spleen and liver. Control spleens (**Figure 2J**) and liver (**Figure 2K**) displayed no expression of tdTomato. However, tamoxifen treated hCD68-tdTom mice displayed a discrete expression pattern of tdTomato within the spleens (**Figure 2J**) and liver (**Figure 2K**) that was consistent with data obtained using flow cytometry.

3.3 The hCD68 Promotor Drives Limited Inducible Cre-Recombinase Expression in Circulating Leukocytes

Previously the hCD68 protomer was used to drive green fluorescent protein and was shown to have robust expression profiles in non-macrophage myeloid cell populations namely, monocytes and neutrophils (29, 30). Therefore, Cre-recombinase activity was assessed in circulating myeloid and non-myeloid leukocyte populations. There was no detectable tdTomato expression in circulating $CD11b^+CD115^+$ monocytes from control mice, however, tamoxifen treated hCD68-tdTom mice had a small but significant increase in the number of tdTomato expressing cells (**Figure 3B**). We further assessed the level of tdTomato expression in $Ly6C^{high}$ and $Ly6C^{low}$ monocytes. Interestingly, we only saw evidence of td-Tomato expression in $Ly6C^{low}$ monocytes, suggesting that the inducible hCD68 promotor driven Cre-recombinase has activity in patrolling $Ly6C^{low}$ monocytes (**Figure 3C**). Other myeloid Cre driver lines have significant activity in neutrophils. We therefore wanted to ascertain if the inducible hCD68 driven Cre recombinase had any activity in circulating neutrophils. Tamoxifen treated hCD68-tdTom mice had no or very low expression of tdTomato (<2%) in $CD11b^+CD115^-Ly6G^+$ neutrophils (**Figure 3D**). Similarly, there was <5% expression of tdTomato in dendritic cells from tamoxifen treated hCD68-tdTom mice and <1% tdTomato expression in eosinophils from tamoxifen treated hCD68-tdTom mice (**Figures 3F, G** respectively). Additionally, there was almost no tdTomato expression in $CD4^+$, $CD8^+$ T-cells or in circulating B-cells in tamoxifen treated hCD68-tdTom mice (**Figures 3I-K**

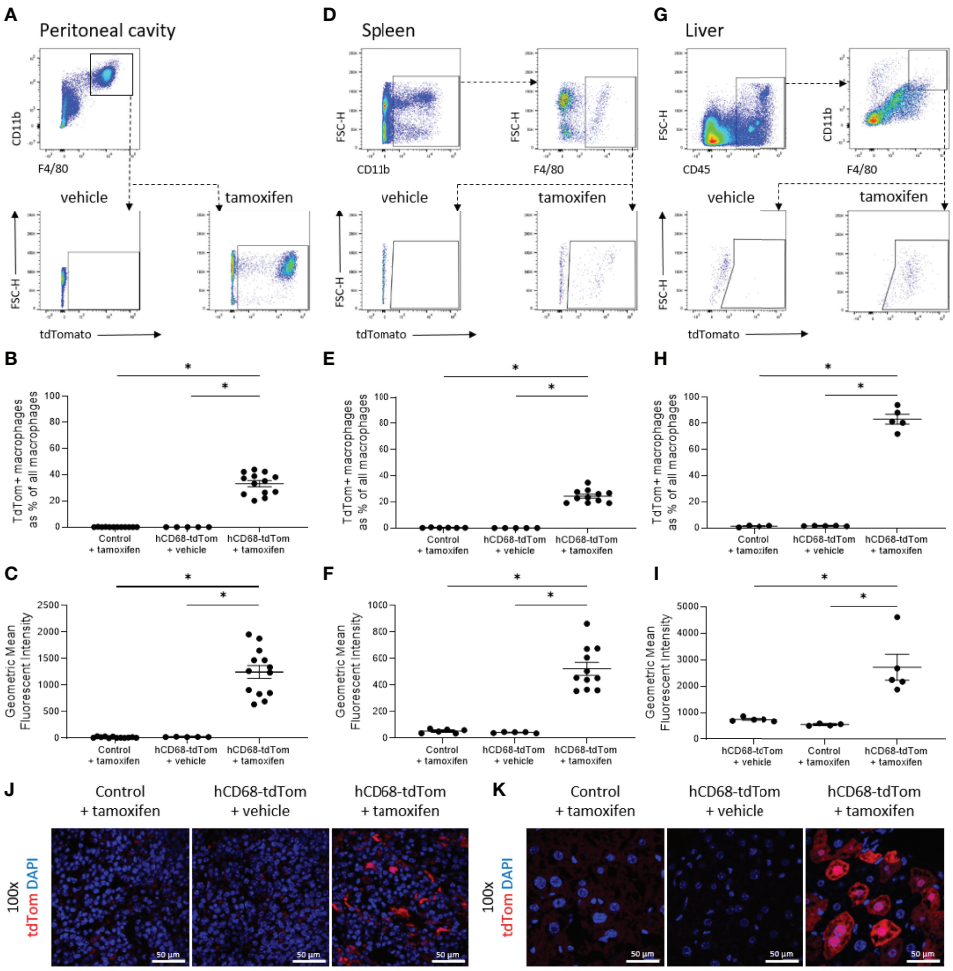

FIGURE 2 | The hCD68 promoter driven inducible Cre recombinase has high activity levels in tissue resident macrophages. Tissue-resident macrophage populations in **(A)** peritoneal cavity, **(D)** spleen and **(G)** liver were defined as CD11b$^+$ and F4/80$^+$ cells (gating strategy shown by representative dot plots) with the corresponding frequency of tdTomato-expressing macrophages as a proportion of all macrophages shown in **(B)** peritoneal cavity, **(E)** spleen and **(H)** liver and with respective mean fluorescence intensity values of tdTomato expression in the whole macrophage population in **(C)**, **(F)** and **(I)**; one-way ANOVA (* = $p < 0.05$). Representative immunofluorescence images of endogenous tdTomato expression in **(J)** the spleen and **(K)** the liver at 100x magnification with DAPI in blue and tdTomato in red; scale bar = 50µm.

respectively). Taken together, these results demonstrate that hCD68 driven inducible Cre recombinase is highly selective for macrophage populations *in vivo* and has little activity in circulating myeloid and lymphoid cell populations.

3.4 The Human CD68 Promoter Has Higher Macrophage Specificity Compared to Endogenous Murine Cd68 Expression

Having shown that hCD68 driven inducible Cre recombinase has selective activity in macrophage populations, versus other myeloid cell populations, we postulated that this could mirror differing levels of the murine Cd68 expression. Even though all CD11b$^+$F4/80$^+$ tissue resident peritoneal macrophages express murine Cd68 (**Figures 4C**), only around ~30% of the same population express tdTomato (**Figure 4D/E**). In the circulation (**Figure 4F**), murine Cd68 was highly expressed by all neutrophils (CD11b$^+$CD115$^-$ Ly6G$^+$) (**Figure 4G**), Ly6C^{high} (**Figure 4H**) and Ly6C^{low} (**Figure 4I**) monocytes, but they expressed low to undetectable levels of tdTomato. These results show that the human CD68 promoter has increased lineage specificity for macrophages compared to expression of the murine Cd68/macrosialin.

3.5 TdTomato Expression in Tissue Resident Macrophages Is Maintained for at Least 6 Weeks After Cre Recombinase Activation

To test the longevity of tdTom expression following hCD68 driven Cre recombinase induction a 6-week protocol was used; baseline tdTom expression was determined 5 days after the last tamoxifen dose and a second group of mice (+ 6 weeks) was harvested after 6 weeks later (**Figure 5A**). tdTomato expression was assessed in macrophage populations within the peritoneal

cavity, spleen and liver macrophages and in circulating leukocytes at baseline and + 6 weeks. There was no decrease in the number of tdTomato expressing macrophages in the peritoneal cavity (**Figure 5B**), spleen (**Figure 5D**) and liver (**Figure 5F**) in the +6 weeks group, however, there was increase in the intensity of tdTomato expression in the peritoneal cavity (**Figure 5C**) and spleen (**Figure 5E**) compared to baseline. Within circulating immune cell populations there was no expression of tdTomato in circulating neutrophils (**Figure 5H**) or Ly6C^{hi} monocytes (**Figure 5I**) and in the +6 weeks group and there was a significant decrease in the number of tdTomato expressing Ly6C^{low} monocytes (**Figure 5J**) compared to baseline.

3.6 The Human CD68 Promotor-Driven Inducible Cre Recombinase Improves Targeting of Liver Macrophages Compared to LysM-Cre.

The LysM-Cre is one of the most widely used macrophage Cre driver mice. We therefore, wanted to compare tdTomato expression in tamoxifen treated hCD68-tdTom mice with constitutively activated LyM-Cre-tdTom mice. Cre activation in both hCD68-tdTom and LysM-Cre-tdTom resulted in tdTomato expression in macrophages in the peritoneal cavity (**Figure 6A/B**), spleen (**Figure 6C/D**) and liver (**Figure 6E/F**). Peritoneal cavity macrophages from LysM-Cre-tdTom mice, also had higher levels of tdTom expression (**Figure 6B**), while no difference in MFI was seen in splenic macrophages (**Figure 6D**). Livers from tamoxifen treated hCD68-tdTom had significantly more tdTomato expressing macrophages than livers from LysM-Cre-tdTom mice (**Figure 6E**), however, there was no difference in MFI (**Figure 6F**). Fluorescent microscopy to visualize tdTomato expression and confirmed flow cytometry results in the spleen (**Figure 6G**) and liver (**Figure 6H**).

We next wanted to examine the specificity of the hCD68-CreERT2 expression by assessing tdTomato in circulating leukocyte populations. We demonstrated that tamoxifen treated hCD68-tdTom mice have almost no expression of tdTomato on blood neutrophils (**Figure 6I**); however, ~90% of circulating neutrophils in LysM-Cre-tdTom mice expressed tdTom (**Figure 6I**). A similar result was seen in blood Ly6C^{hi} monocytes; only ~2.5% of Ly6C^{hi} monocytes in tamoxifen treated hCD68-tdTom expressed tdTomato, whereas ~66% of Ly6C^{hi} monocytes from LysM-Cre-tdTom mice expressed tdTomato (**Figure 6J**). Additionally, ~20% of Ly6C^{low} monocytes from tamoxifen treated hCD68-tdTom expressed tdTomato, whereas ~83% of Ly6C^{low} monocytes from LysM-Cre-tdTom mice expressed tdTomato (**Figure 6K**).

3.7 The Human CD68 Promotor-Driven Inducible Cre Recombinase Targets Recruited Macrophages in Atherosclerotic Lesions

Lipid laden macrophages within arterial walls are a key driver of the pathophysiology in cardiovascular disease. To induce hyperlipidaemia hCD68-tdTom and control mice were injected with a gain-of-function mutant PCSK9 adeno-associated virus vector (AAV) or a control viral vector (35). Mice given a single intravenous injection of AAV8-mPCSK9 or control AAV were placed on a high fat diet (HFD). After 16 weeks of HFD feeding hCD68-tdTom mice or control were given tamoxifen to induce Cre recombinase activity (**Figure 7A**). As expected, mice given a single injection of AAV8-mPCSK9 but not a control AAV developed atherosclerotic lesions in the aortic sinus as shown by increased Oil Red O staining (**Figure 7B**). We next looked for tdTomato expression within atherosclerotic lesions in tamoxifen treated hCD68-tdTom mice. AAV8-mPCSK9 injected hCD68-tdTom mice treated with tamoxifen expressed high levels of tdTomato within the atherosclerotic plaque. (**Figure 7C**). TdTomato expressing macrophages were distinguishable from auto fluorescent lipid drops, due to the proximal co-localisation of DAPI stained nuclei (**Supplementary Figure 4A**).

To further assess the tdTom expression in the immune cells compartment of the atherosclerotic lesion we preformed aortic digests followed by flow cytometry (**Supplementary Figure 4B**). As expected, there was a large population of CD11b^{+}F4/80^{+}CD64^{+} macrophages in AAV8-mPCSK9 injected mice. Importantly, when these mice were treated with tamoxifen to induce Cre recombinase activity there was significant induction in expression of tdTomato (**Figure 7D**). We observed tdTomato expression in ~25% of all Ly6C^{+} monocyte derived macrophages within in the atherosclerotic lesion (**Supplementary Figure 4C**), and reassuringly there was no tdTomato expression in recruited neutrophils (**Supplementary Figure 4D**). As expected within the blood (**Supplementary Table 1**) and the spleen (**Supplementary Table 2**) there was limited td-tomato expression in all major leukocyte populations except Ly6C^{low} monocytes in AAV8-mPCSK9 injected hCD68-tdTom mice treated with tamoxifen.

Of note when compared to baseline, AAV8-mPCSK9 injected hCD68-tdTom mice treated with tamoxifen and fed a HFD for 16 weeks did not have different levels of tdTomato expression in the peritoneal cavity (**Supplementary Figure 5A/B**) or spleen macrophages (**Supplementary Figure 5C/D**). Additionally, as expected, in the blood there was no difference in td-Tomato expression in neutrophils (**Supplementary Figure 5E/F**), Ly6C^{high} (**Supplementary Figure 5G/H**) and Ly6C^{lo} monocytes (**Supplementary 5Figure I/J**). Of note, there was a higher number of td-Tomato expressing Ly6C^{hi} monocytes within the spleen of atherogenic mice (4.25 ± 0.54 vs 13.50 ± 2.69; **Supplementary Table 3**). Collectively, these results demonstrate that the human CD68 promoter-driven inducible Cre recombinase can specifically target macrophages with atherosclerotic lesions, with limited targeting to plaque associated neutrophils.

4 DISCUSSION

We have generated and characterised a novel transgenic reporter mouse expressing tamoxifen inducible Cre recombinase under the control of the human CD68 promoter. To assess the efficiency of Cre recombinase activation we crossed the

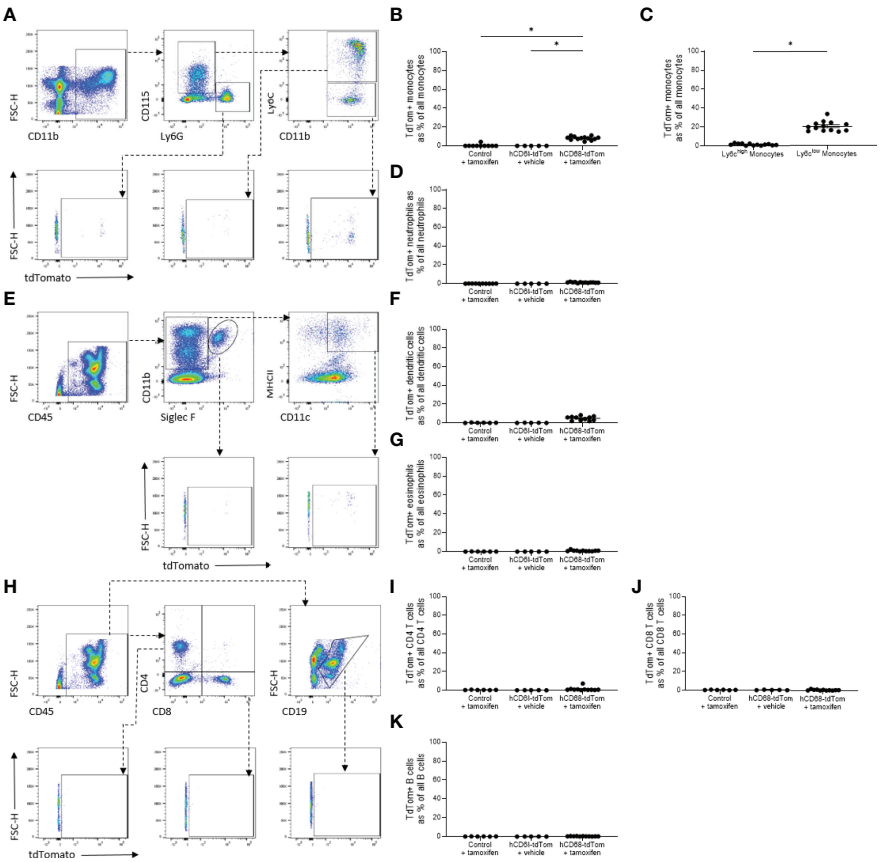

FIGURE 3 | The hCD68 promoter driven inducible Cre recombinase has limited activity in circulating leukocytes. **(A)** Representative dot plots of the gating strategy for neutrophils ($CD11b^+$, $CD115^-$, $Ly6G^+$), total monocytes ($CD11b^+$, $CD115^+$, $Ly6G^-$), $Ly6C^{high}$ and $Ly6C^{low}$ monocytes ($CD11b^+$, $CD115^+$, $Ly6G^-$, $Ly6C^+$ and $CD11b^+$, $CD115^+$, $Ly6G^-$, $Ly6C^-$ respectively). **B)** Frequency of tdTomato-expressing monocytes as a proportion of all monocytes. **(C)** Frequency of tdTomato-expressing $Ly6C^{high}$ and $Ly6C^{low}$ monocytes. **(D)** Frequency of tdTomato-expressing neutrophils as a proportion of all neutrophils. **(E)** Representative dot plots of the gating strategy for dendritic cells ($CD45^+$, $CD11b^+$, Siglec F^-, $MHCII^+$, $CD11c^+$) and eosinophils ($CD45^+$, $CD11b^+$, Siglec F^+). **(F)** Frequency of tdTomato-expressing dendritic cells as a proportion of all dendritic cells. **(G)** Frequency of tdTomato-expressing eosinophils as a proportion of all eosinophils. **(H)** Representative dot plots of the gating strategy for CD4 T cells ($CD45^+$, $CD4^+$, $CD8^-$), CD8 T cells ($CD45^+$, $CD4^-$, $CD8^+$) and B cells ($CD45^+$, $CD19^+$). **(I)** Frequency of tdTomato-expressing CD4 T cells as a proportion of all CD4 T cells. **(J)** Frequency of tdTomato-expressing CD8 T cells as a proportion of all CD8 T cells. **(K)** Frequency of tdTomato-expressing B cells as a proportion of all B cells; one-way ANOVA or student t-test as appropriate, (* = $p < 0.05$).

hCD68-CreERT2 mice with commercially available $TdTomato^{flox/flox}$ mice, a standard way of phenotyping new transgenic Cre driver lines. TdTomato-expressing cells were detected using flow cytometry and confocal microscopy in resident macrophage populations in the peritoneal cavity, spleen and liver (**Figure 2**). Detailed analysis showed that inducible tdTomato expression is restricted to tissue-resident macrophages, absent from the circulating leukocytes and independent from murine Cd68 expression (**Figures 3** and **4** respectively). We tested the longevity of Cre recombinase targeting by allowing 6 weeks wash-out period following the usual dosing protocol and showed no decline in tdTomato expression in tissue-resident macrophage populations (**Figure 5**). Additionally, we performed a side-by-side comparison with LysM-Cre mice (using the same $tdTomato^{flox/flox}$ mouse colony for breeding) and showed better macrophage lineage-restricted expression of tdTomato in our model (**Figure 6**). As a proof-of-concept experiment, we induced atherosclerotic lesions in hCD68-tdTom mice using the PCSK9 model (35) and showed that it is possible to target macrophages recruited to the plaques with our model (**Figure 7**). Taken together, our experiments show that hCD68-CreERT2 mouse line allows efficient and specific targeting of tissue-resident macrophage populations and can be used in long term studies and disease models.

The search for a truly 'macrophage-specific' transgene targeting has so far been unsuccessful, most likely due to all myeloid cells expressing very similar markers at various stages of development (36, 37). CD68 is a classical macrophage-defining marker, frequently used to identify macrophages in histological sections (38). In our new mouse line, tdTomato expression in circulating leukocytes of myeloid origins (neutrophils, monocytes and dendritic cells) is extremely low (**Figure 3**). This is a crucial difference to our earlier work, where we used the hCD68 promoter

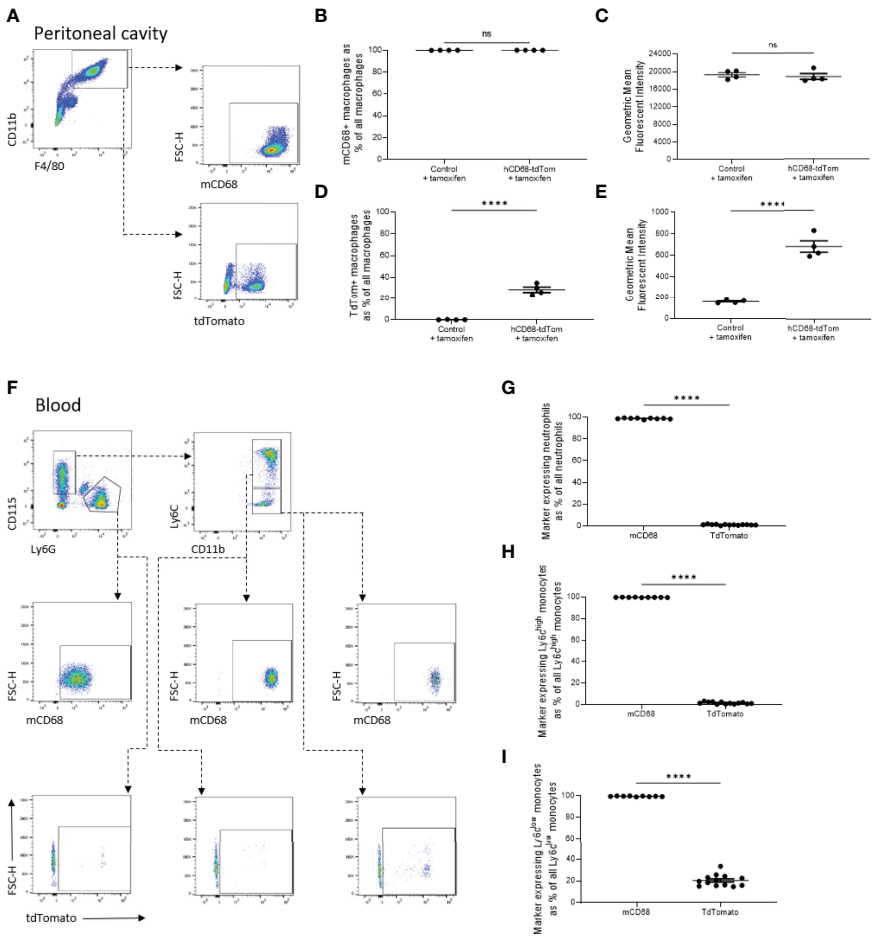

FIGURE 4 | The transgenic human CD68 promoter has higher macrophage specificity compared to endogenous murine Cd68 expression. **(A)** Representative dot plots of the gating strategy for peritoneal macrophages ($CD11b^+$, $F4/80^+$) and their expression of tdTomato and murine CD68 (mCD68). **(B)** Frequency of tdTomato-expressing peritoneal macrophages as a proportion of all peritoneal macrophages with corresponding mean fluorescence intensity in **(C)**. **(D)** Frequency of mCD68-expressing macrophages as a proportion of all peritoneal macrophages with corresponding mean fluorescence intensity in **(E)**. **(F)** Representative dot plots of the gating strategy for blood neutrophils ($CD115^-$, $Ly6G^+$), $Ly6C^{high}$ and $Ly6C^{low}$ monocytes ($CD115^+$, $Ly6G^-$, $Ly6C^+$ and $CD115^+$, $Ly6G^-$, $Ly6C^-$ respectively) and their expression of tdTomato and mCD68. **(G)** Comparison of frequency of neutrophils expressing mCD68 and tdTomato. **(H)** Comparison of frequency of $Ly6C^{high}$ monocytes expressing mCD68 and tdTomato. **(I)** Comparison of frequency of $Ly6C^{low}$ monocytes expressing mCD68 and tdTomato; for panels **(G–I)** mCD68 was quantified for control mice without tamoxifen, tdTom was measured for hCD68-tdTom + tamoxifen mice, student t-test (**** = $p < 0.0001$). ns, not significant.

IVS-1 cassette and saw constitutive expression of green fluorescent protein in neutrophils, monocytes and macrophages alike (29). We hypothesised that the difference in transgene expression might result from differential expression of murine Cd68 across the myeloid populations in the blood. Contrary to our hypothesis, we saw that macrosialin was highly expressed in all myeloid populations in the peritoneum and blood, including the neutrophils (**Figure 4**). It has been previously reported that monocytes and a subset of human blood neutrophils can express CD68, but not to the extent we saw in our study (39). The human CD68 promoter and IVS-1 intron expression cassette has been shown to be a very potent driver for macrophage targeting when used in a constitutive GFP transgenic mouse (29). However, due to the nature of this cassette, when activated embryonically it targets other myeloid cell types with efficiency comparable to macrophage targeting, in line with Cd68 being expressed by other myeloid cell types. Iqbal *et al.* demonstrated that hCD68-GFP protein was detected as early as day E8.5, which is before distinct hematopoietic progeny are present and the emergence of *bone fide* macrophages within the hematogenic endothelium between E10.5 and E12.5. Similar results have been seen in other inducible hCD68 promoter-driven mice models, where reported expression in blood leukocytes was lower than in other macrophage targeting Cre lines (13, 40). This suggests that human CD68 promoter cassette when activated in adult animals is highly specific for mature tissue resident macrophages, unlike the endogenous expression pattern of murine Cd68.

The main limitation of our transgenic model lies in the fact that we do not achieve full targeting in all tissue resident macrophage populations. This is however unsurprising given that none of the previously published macrophage targeting inducible Cre models achieved full expression in desired cell

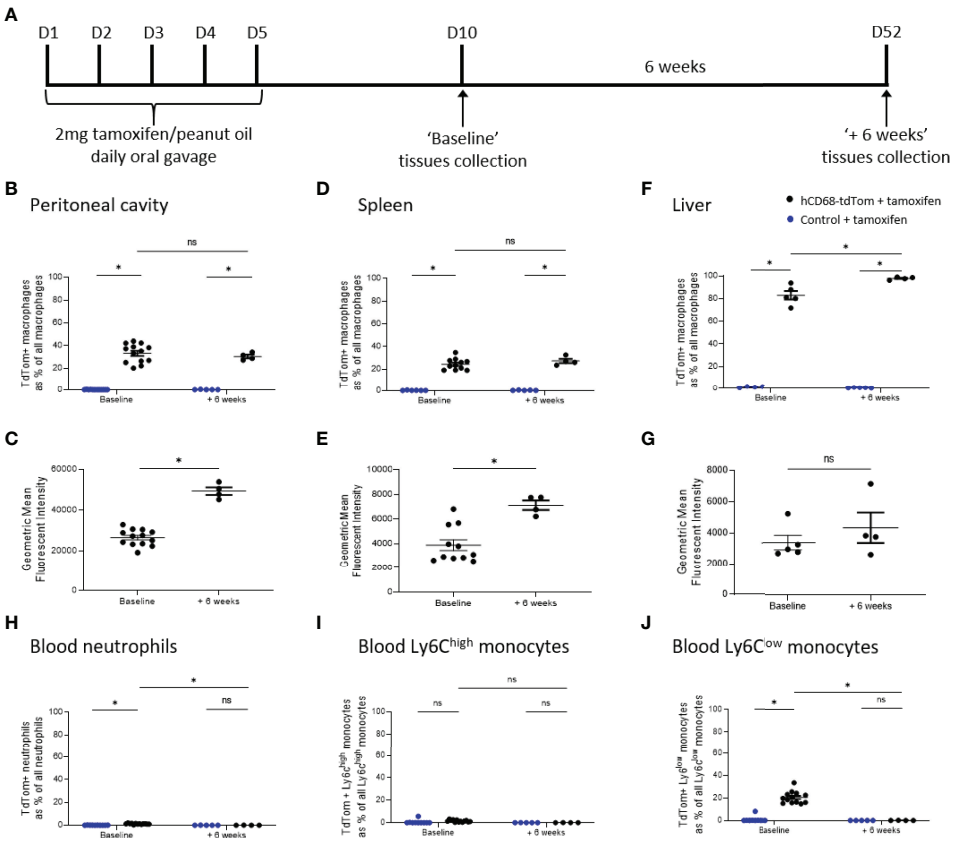

FIGURE 5 | TdTomato expression in tissue resident macrophages is maintained for at least 6 weeks after Cre recombinase activation. In panels **(B, D, F, H–J)** control + tamoxifen mice are marked as blue dots; hCD68-tdTom + tamoxifen mice are marked as black dots. In all panels mice with the usual 5 days wash out period are marked 'Baseline', while mice with an additional 6 weeks wait are marked '+ 6 weeks'. **(A)** Tamoxifen dosing protocol for induction of Cre recombinase activity and assessment of targeting efficiency 6 weeks post-induction in hCD68-CreERT2 model. Frequency of tdTomato-expressing macrophages as a proportion of all macrophages in **(B)** peritoneal cavity **(D)** spleen and **(F)** liver with corresponding mean fluorescence intensity of tdTomato$^+$ macrophages for 'Baseline' and '+6 weeks' groups in **(C, E, G)**. Frequency of tdTomato-expressing blood **(H)** neutrophils, **(I)** Ly6C^{high} monocytes and **(J)** Ly6C^{low} monocytes as a proportion of all blood leukocytes of the given type for 'Baseline' and '+6 weeks' groups; two-way ANOVA in panels **(B, D, F, H–J)**, student t-test in panels **(C, E, G)**, (* = $p < 0.05$). ns, not significant.

populations (13, 40, 41). We achieved the highest efficiency of targeting in the liver, which might be due to tamoxifen being metabolised in the liver to its active form (4-hydroxy tamoxifen) and therefore having the highest bioavailability in that tissue (42). Our mouse line achieved better expression in liver macrophages in comparison to LysM Cre mice, which are the gold standard of macrophage targeting lines (**Figure 6**). Moreover, we were able to discriminate between different sub-populations of liver macrophages and show that Cre recombinase activation varies between them in terms of efficiency of targeting as well as intensity of expression (**Supplementary Figure 3**). Kupffer cells were the highest expressors of tdTomato in the liver with much lower values in the monocyte-derived sub-populations and in capsular macrophages, reinforcing the idea that hCD68-CreERT2 mouse line preferentially targets tissue resident macrophages. Moreover, we were able to distinguish between macrophage subsets based on significant differences in their mean fluorescence intensity values (34). Encouragingly, we saw no decline in tdTomato expression 6 weeks post-targeting (**Figure 5**), which further points to the targeting of tissue-resident macrophages, which are known to have a slow turnover (43). In contrast, after the 6 weeks wash-out period there was no expression of tdTomato in the blood at all, since circulating blood cells tend to be short-lived (44).

In a proof of concept experiment we were able to target recruited monocytes and macrophages in a widely used animal model of atherosclerosis. We were able to show that aortic-resident and recruited monocyte-derived macrophages expressed tdTomato, proving the possibility of using our system to study macrophage biology in pathological states (**Figure 7** and **Supplementary Figure 4**). The relatively high level of monocyte targeting compared to homeostatic state in other tissues and in blood could be because monocytes that have migrated into the aortic tissue have most likely started the phenotypic shift towards macrophages and therefore upregulated the expression of hCD68 promoter cassette.

Cre driver mouse lines which are referred to as macrophage-targeting are driven by five main gene expression cassettes, LysM, Csf1r, Cx3cr1, CD11b and F4/80, however none of them are truly

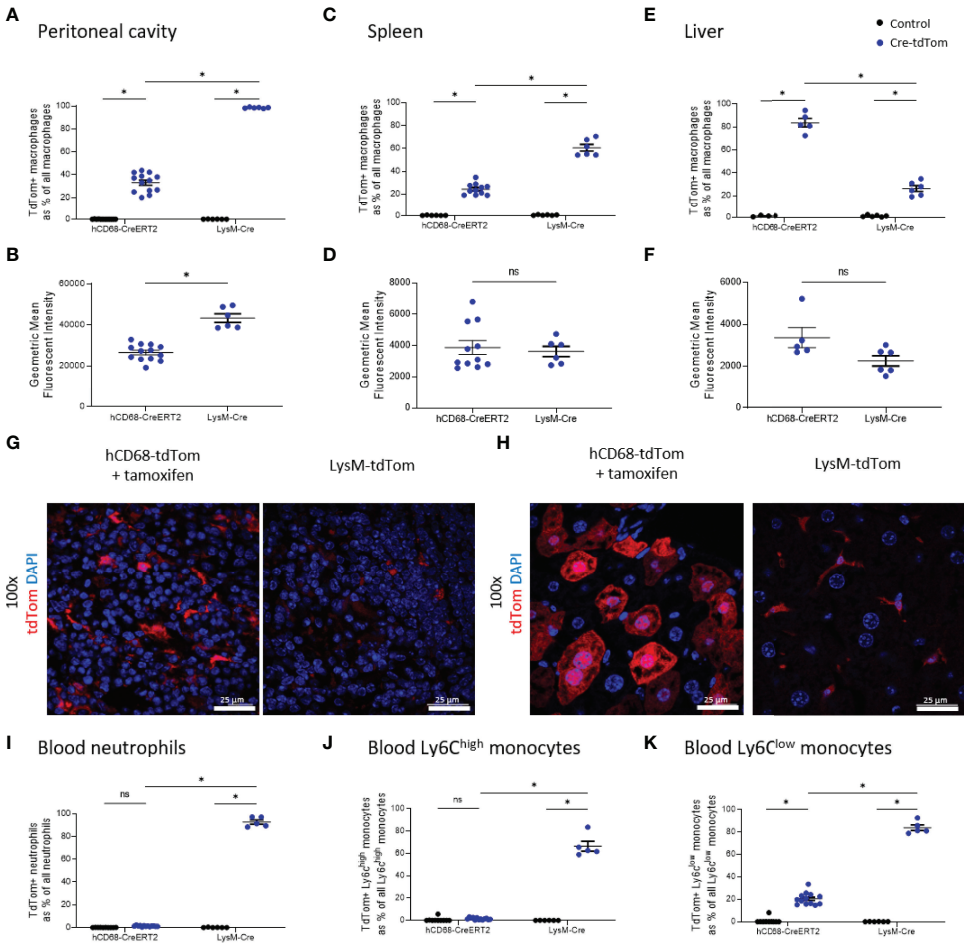

FIGURE 6 | The hCD68 promoter driven inducible Cre recombinase improves targeting of liver macrophages compared to LysM-Cre. In all panels control mice (littermates of hCD68-tdTom mice that were given tamoxifen or littermates of LysM-tdTom mice) are marked as black dots; Cre-tdTom mice (hCD68-tdTom + tamoxifen or LysM-tdTom mice) are marked as blue dots. Frequency of tdTomato-expressing macrophages as a proportion of all macrophages in **(A)** peritoneal cavity **(C)** spleen and **(E)** liver with corresponding mean fluorescence intensity of tdTomato^{+} macrophages for hCD68-CreERT2 and LysM-Cre mice in **(B, D, F)**. Representative immunofluorescence images of endogenous tdTomato expression in **(G)** the spleen and **(H)** the liver of hCD68-tdTom and LysM-tdTom mice at 100x magnification with DAPI in blue and tdTomato in red; scale bar = 25 µm. Frequency of tdTomato-expressing blood **(I)** neutrophils, **(J)** Ly6C^{high} monocytes and **(K)** Ly6C^{low} monocytes as a proportion of all blood leukocytes of the given type for hCD68-CreERT2 and LysM-Cre mice.; two-way ANOVA in panels **(A, C, E, I–K)**, student t-test in panels **(B, D, F)**, (* = $p < 0.05$). ns, not significant.

macrophage-specific. LysM-Cre was shown by us and others to target all myeloid populations, whilst having relatively low levels of expression in tissue-resident macrophages in spleen and liver (45). Csf1r-Cre mouse was noted to target at least 50% of neutrophils and T cells alongside bone-marrow derived macrophages, while other fluorescent reporter mice driven by Csf1r gene were shown to have high levels of targeting in megakaryocytes and dendritic cells (41, 46). Cx3cr1 promoter cassette has been used to create both constitutive and tamoxifen-inducible Cre mouse lines, however in comparative analysis with other macrophage targeting Cre lines showed that Cx3cr1-Cre had relatively low efficiency of targeting tissue-resident macrophages in the spleen and the lungs whilst having significant spill-over expression into mast cells and dendritic cells (8, 47). CD11b is a pan-myeloid marker and therefore, as expected, induced very high expression in all cells of myeloid lineage, while F4/80 was shown to target only selected tissue-resident macrophage populations due to differences the level of expression of F4/80 between tissues, making both of these mice a fairly rare choice for studying tissue resident macrophages (48, 49).

As we are gaining a better understanding of tissue-resident macrophages, their origins and ways to replenish them, it is crucial to develop more macrophage specific models that can be used for *in vivo* investigations. So far, the most detailed descriptions of heterogeneous macrophage populations have come from single cell studies, which have their own limitations and constraints in terms of availability to researchers and experimental design. Currently available macrophage-targeting mouse models offer little reassurance that circulating monocytes and neutrophils will not be equally well targeted. In this study we

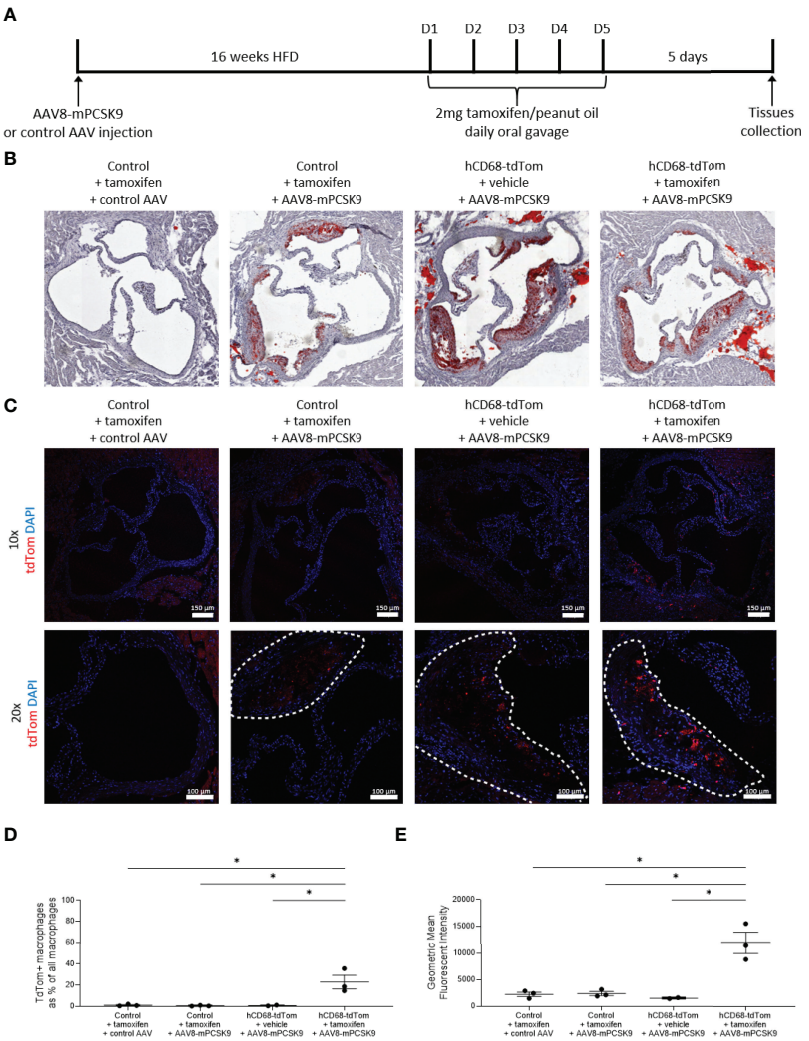

FIGURE 7 | The hCD68 promoter driven inducible Cre recombinase targets recruited macrophages in the atherosclerotic lesion. **(A)** Timeline of the inducible PCSK9 atherosclerosis model and induction of Cre recombinase in hCD68-CreERT2 mice. **(B)** Representative images of Oil Red O staining of the aortic roots confirm the induction of atherosclerotic plaques in the AAV8-mPCSK9 injected groups. **(C)** Representative immunofluorescence images of endogenous tdTomato expression in the aortic roots at 10x (whole aortic root) and 20x (plaque close-up with plaque edges outlined with the dashed line) magnification with DAPI in blue and tdTomato in red; scale bar = 150 µm in 10x images and 100 µm in 20x images. **(D)** Frequency of tdTomato-expressing aortic macrophages as a proportion of all aortic macrophages with the corresponding mean fluorescent intensity of total aortic macrophages in **(E)**; one-way ANOVA (* = $p < 0.05$).

present a novel human CD68 promoter cassette driven inducible CreERT2 mouse model with the potential to improve tissue resident macrophage targeting *in vivo*. At the steady state, we showed improved specificity of targeting macrophages and minimal off-target effects in the blood, compared to other published mouse Cre driver lines. Moreover, we showed stable targeting over long periods of time and that it is possible to induce the Cre recombinase expression in disease models without disrupting the model itself. We believe that the hCD68-CreERT2 mice will find multiple applications in studying tissue-resident macrophage populations and their heterogeneity in health and disease.

DATA AVAILABILITY STATEMENT

The original contributions presented in the study are included in the article/**Supplementary Material**. Further inquiries can be directed to the corresponding authors.

ETHICS STATEMENT

The animal study was reviewed and approved by Sir William Dunn School of Pathology (SWDSOP) ethical review body (AWERB), University of Oxford.

AUTHOR CONTRIBUTIONS

AR, DG, and GP designed the research. BD generated the hCD68-CreERT2 line. AR performed experiments with help from GP, AR analyzed the data. All authors contributed to the article and approved the submitted version.

FUNDING

DG acknowledges support from the BHF Centre of Regenerative Medicine, Oxford (RM/13/3/30159). This work was funded by British Heart Foundation (BHF) Programme Grant awards to DG and KC (RG/15/10/31485 and RG/17/10/32859) and a BHF Chair Award (CH/16/1/32013) to KC. DG, KC. and G.P are members of the MeRIAD consortium which is supported by a Novo Nordisk Foundation (NNF) grant (NNF15CC0018346) to the University of Oxford, University of Copenhagen (UCPH), and Karolinska Institute. AR is the recipient of a BHF graduate studentship FS/17/68/33478.

ACKNOWLEDGMENTS

We would like to acknowledge the support of Prof Paul Riley, who gave his assessment of the data and feedback at various stages throughout the project. We would also like acknowledge Dr Gillian Douglas who kindly provided the AAV.8TBGmPCSK9D377Y vector.

SUPPLEMENTARY MATERIAL

The Supplementary Material for this article can be found online at: https://www.frontiersin.org/articles/10.3389/fimmu.2022.918636/full#supplementary-material

REFERENCES

1. Wynn TA, Chawla A, Pollard JW. Macrophage Biology in Development, Homeostasis and Disease. *Nat* (2013) 496:445–55. doi: 10.1038/nature12034
2. Mosser DM, Hamidzadeh K, Goncalves R. Macrophages and the Maintenance of Homeostasis. *Cell Mol Immunol* (2020) 18:579–87. doi: 10.1038/s41423-020-00541-3
3. Wynn TA, Vannella KM. Macrophages in Tissue Repair, Regeneration, and Fibrosis. *Immunity* (2016) 44:450–62. doi: 10.1016/j.immuni.2016.02.015
4. Wentworth JM, Naselli G, Brown WA, Doyle L, Phipson B, Smyth GK, et al. Pro-Inflammatory CD11c+CD206+ Adipose Tissue Macrophages Are Associated With Insulin Resistance in Human Obesity. *Diabetes* (2010) 59:1648–56. doi: 10.2337/db09-0287
5. Nathan C, Ding A. Nonresolving Inflammation. *Cell* (2010) 140:871–82. doi: 10.1016/j.cell.2010.02.029
6. Barrett TJ. Macrophages in Atherosclerosis Regression. *Arterioscler Thromb Vasc Biol* (2020) 40:20–33. doi: 10.1161/ATVBAHA.119.312802
7. Hettinger J, Richards DM, Hansson J, Barra MM, Joschko A-C, Krijgsveld J, et al. Origin of Monocytes and Macrophages in a Committed Progenitor. *Nat Immunol* (2013) 14:821–30. doi: 10.1038/ni.2638
8. Yona S, Kim K-W, Wolf Y, Mildner A, Varol D, Breker M, et al. Fate Mapping Reveals Origins and Dynamics of Monocytes and Tissue Macrophages Under Homeostasis. *Immunity* (2013) 38:79–91. doi: 10.1016/j.immuni.2012.12.001
9. Gosselin D, Link VM, Romanoski CE, Fonseca GJ, Eichenfield DZ, Spann NJ, et al. Environment Drives Selection and Function of Enhancers Controlling Tissue-Specific Macrophage Identities. *Cell* (2014) 159:1327–40. doi: 10.1016/j.cell.2014.11.023
10. Summers KM, Bush SJ, Hume DA. Network Analysis of Transcriptomic Diversity Amongst Resident Tissue Macrophages and Dendritic Cells in the Mouse Mononuclear Phagocyte System. *PloS Biol* (2020) 18:e3000859. doi: 10.1371/JOURNAL.PBIO.3000859
11. Hildreth AD, Ma F, Wong YY, Sun R, Pellegrini M, O'Sullivan TE. Single-Cell Sequencing of Human White Adipose Tissue Identifies New Cell States in Health and Obesity. *Nat Immunol* (2021) 22:639–53. doi: 10.1038/s41590-021-00922-4
12. Evren E, Ringqvist E, Tripathi KP, Sleiers N, Rives IC, Alisjahbana A, et al. Distinct Developmental Pathways From Blood Monocytes Generate Human Lung Macrophage Diversity. *Immunity* (2021) 54:259–275.e7. doi: 10.1016/j.immuni.2020.12.003
13. McCubbrey AL, Barthel L, Mould KJ, Mohning MP, Redente EF, Janssen WJ. Selective and Inducible Targeting of CD11b+ Mononuclear Phagocytes in the Murine Lung With Hcd68-rtTA Transgenic Systems. *Am J Physiol Lung Cell Mol Physiol* (2016) 311:L87–L100. doi: 10.1152/ajplung.00141.2016
14. Iwasaki H, Akashi K. Myeloid Lineage Commitment From the Hematopoietic Stem Cell. *Immunity* (2007) 26:726–40. doi: 10.1016/j.immuni.2007.06.004
15. Fogg DK, Sibon C, Miled C, Jung S, Aucouturier P, Littman DR, et al. A Clonogenic Bone Marrow Progenitor Specific for Macrophages and Dendritic Cells. *Science* (2006) 311:83–7. doi: 10.1126/science.1117729
16. Gibbings SL, Thomas SM, Atif SM, McCubbrey AL, Desch AN, Danhorn T, et al. Three Unique Interstitial Macrophages in the Murine Lung at Steady State. *Am J Respir Cell Mol Biol* (2017) 57:66–76. doi: 10.1165/rcmb.2016-0361OC
17. Nahrendorf M, Swirski FK. Abandoning M1/M2 for a Network Model of Macrophage Function. *Circ Res* (2016) 119:414–7. doi: 10.1161/CIRCRESAHA.116.309194
18. Xue J, Schmidt SV, Sander J, Draffehn A, Krebs W, Quester I, et al. Transcriptome-Based Network Analysis Reveals a Spectrum Model of Human Macrophage Activation. *Immunity* (2014) 40:274–88. doi: 10.1016/j.immuni.2014.01.006
19. Leid J, Carrelha J, Boukarabila H, Epelman S, Jacobsen SEW, Lavine KJ. Primitive Embryonic Macrophages Are Required for Coronary Development and Maturation. *Circ Res* (2016) 118:1498–511. doi: 10.1161/CIRCRESAHA.115.308270
20. Cahill TJ, Sun X, Ravaud C, Villa Del Campo C, Klaourakis K, Lupu I-E, et al. Tissue-Resident Macrophages Regulate Lymphatic Vessel Growth and Patterning in the Developing Heart. *Development* (2021) 148(3): dev194563. doi: 10.1242/dev.194563
21. Hulsmans M, Clauss S, Xiao L, Aguirre AD, King KR, Hanley A, et al. Macrophages Facilitate Electrical Conduction in the Heart. *Cell* (2017) 169:510–522.e20. doi: 10.1016/j.cell.2017.03.050
22. Wong NR, Mohan J, Kopecky BJ, Guo S, Du L, Leid J, et al. Resident Cardiac Macrophages Mediate Adaptive Myocardial Remodeling. *Immunity* (2021) 54:2072–2088.e7. doi: 10.1016/j.immuni.2021.07.003
23. Chazaud B. Inflammation and Skeletal Muscle Regeneration: Leave It to the Macrophages! *Trends Immunol* (2020) 41:481–92. doi: 10.1016/j.it.2020.04.006
24. Wang Z, Koenig AL, Lavine KJ, Apte RS. Macrophage Plasticity and Function in the Eye and Heart. *Trends Immunol* (2019) 40:825–41. doi: 10.1016/j.it.2019.07.002
25. Bou Ghosn EE, Cassado AA, Govoni GR, Fukuhara T, Yang Y, Monack DM, et al. Two Physically, Functionally, and Developmentally Distinct Peritoneal Macrophage Subsets. *Proc Natl Acad Sci USA* (2010) 107:2568–73. doi: 10.1073/PNAS.0915000107/SUPPL_FILE/PNAS.200915000SI.PDF
26. Holness CL, Da Silva RP, Fawcett J, Gordon S, Simmons DL. Macrosialin, a Mouse Macrophage-Restricted Glycoprotein, Is a Member of the Lamp/Lgp Family. *J Biol Chem* (1993) 268:9661–6. doi: 10.1016/S0021-9258(18)98400-0

27. Greaves DR, Quinn CM, Seldin MF, Gordon S. Functional Comparison of the Murine Macrosialin and Human CD68 Promoters in Macrophage and Nonmacrophage Cell Lines. *Genomics* (1998) 54:165–8. doi: 10.1006/geno.1998.5546
28. Gough PJ, Gordon S, Greaves DR. The Use of Human CD68 Transcriptional Regulatory Sequences to Direct High-Level Expression of Class A Scavenger Receptor in Macrophages *In Vitro* and *In Vivo*. *Immunology* (2001) 103:351–61. doi: 10.1046/j.1365-2567.2001.01256.x
29. Iqbal AJ, McNeill E, Kapellos TS, Regan-Komito D, Norman S, Burd S, et al. Human CD68 Promoter GFP Transgenic Mice Allow Analysis of Monocyte to Macrophage Differentiation *In Vivo*. *Blood* (2014) 124:e33–44. doi: 10.1182/blood-2014-04-568691
30. McNeill E, Iqbal AJ, Jones D, Patel J, Coutinho P, Taylor L, et al. Tracking Monocyte Recruitment and Macrophage Accumulation in Atherosclerotic Plaque Progression Using a Novel Hcd68gfp/ApoE-/- Reporter Mouse-Brief Report. *Arterioscler Thromb Vasc Biol* (2017) 37:258–63. doi: 10.1161/ATVBAHA.116.308367
31. Park I, Goddard ME, Cole JE, Zanin N, Lyytikäinen L-P, Lehtimäki T, et al. C-Type Lectin Receptor CLEC4A2 Promotes Tissue Adaptation of Macrophages and Protects Against Atherosclerosis. *Nat Commun* (2022) 13:215. doi: 10.1038/s41467-021-27862-9
32. Lang R, Rutschman RL, Greaves DR, Murray PJ. Autocrine Deactivation of Macrophages in Transgenic Mice Constitutively Overexpressing IL-10 Under Control of the Human CD68 Promoter. *J Immunol* (2002) 168:3402–11. doi: 10.4049/JIMMUNOL.168.7.3402
33. Metzger D, Clifford J, Chiba H, Chambon P. Conditional Site-Specific Recombination in Mammalian Cells Using a Ligand-Dependent Chimeric Cre Recombinase. *Proc Natl Acad Sci USA* (1995) 92:6991–5. doi: 10.1073/PNAS.92.15.6991
34. Blériot C, Ginhoux F. Understanding the Heterogeneity of Resident Liver Macrophages. *Front Immunol* (2019) 10:2694. doi: 10.3389/fimmu.2019.02694
35. Lu H, Howatt DA, Balakrishnan A, Graham MJ, Mullick AE, Daugherty A. Hypercholesterolemia Induced by a PCSK9 Gain-Of-Function Mutation Augments Angiotensin II–Induced Abdominal Aortic Aneurysms in C57BL/6 Mice—Brief Report. *Arterioscler Thromb Vasc Biol* (2016) 36:1753–7. doi: 10.1161/ATVBAHA.116.307613
36. Gordon S, Taylor PR. Monocyte and Macrophage Heterogeneity. *Nat Rev Immunol* (2005) 5:953–64. doi: 10.1038/nri1733
37. Guilliams M, Mildner A, Yona S. Developmental and Functional Heterogeneity of Monocytes. *Immunity* (2018) 49:595–613. doi: 10.1016/J.IMMUNI.2018.10.005
38. Chistiakov DA, Killingsworth MC, Myasoedova VA, Orekhov AN, Bobryshev YV. CD68/macrosialin: Not Just a Histochemical Marker. *Lab Investig* (2016) 97:4–13. doi: 10.1038/labinvest.2016.116
39. Amanzada A, Ahmed Malik I, Blaschke M, Khan S, Rahman H, Ramadori G, et al. Identification of CD68+ Neutrophil Granulocytes in *In Vitro* Model of Acute Inflammation and Inflammatory Bowel Disease. *Int J Clin Exp Pathol* (2013) 6:561. doi: 10.1055/s-0033-1352657
40. Pillai MM, Hayes B, Torok-Storb B. Inducible Transgenes Under the Control of the Hcd68 Promoter Identifies Mouse Macrophages With a Distribution That Differs From the F4/80 and CSF-1R Expressing Populations. *Exp Hematol* (2009) 37:1387. doi: 10.1016/J.EXPHEM.2009.09.003
41. Grabert K, Sehgal A, Irvine KM, Wollscheid-Lengeling E, Ozdemir DD, Stables J, et al. A Transgenic Line That Reports CSF1R Protein Expression Provides a Definitive Marker for the Mouse Mononuclear Phagocyte System. *J Immunol* (2020) 205:3154–66. doi: 10.4049/jimmunol.2000835
42. Jahn HM, Kasakow CV, Helfer A, Michely J, Verkhratsky A, Maurer HH, et al. Refined Protocols of Tamoxifen Injection for Inducible DNA Recombination in Mouse Astroglia. *Sci Rep* (2018) 8:1–11. doi: 10.1038/s41598-018-24085-9
43. Hashimoto D, Chow A, Noizat C, Teo P, Beasley MB, Leboeuf M, et al. Tissue-Resident Macrophages Self-Maintain Locally Throughout Adult Life With Minimal Contribution From Circulating Monocytes. *Immunity* (2013) 38:792–804. doi: 10.1016/J.IMMUNI.2013.04.004
44. Kline DL, Cliffton EE. LifesPan of Lezlcocytes in Man. *J App Physiol* (1952) 5 (2):79–84. doi: 10.1152/jappl.1952.5.2.79
45. Clausen BE, Burkhardt C, Reith W, Renkawitz R, Förster I. Conditional Gene Targeting in Macrophages and Granulocytes Using LysMcre Mice. *Transgenic Res* (1999) 8:265–77. doi: 10.1023/A:1008942828960
46. Deng L, Zhou JF, Sellers RS, Li JF, Nguyen AV, Wang Y, et al. A Novel Mouse Model of Inflammatory Bowel Disease Links Mammalian Target of Rapamycin-Dependent Hyperproliferation of Colonic Epithelium to Inflammation-Associated Tumorigenesis. *Am J Pathol* (2010) 176:952–67. doi: 10.2353/AJPATH.2010.090622
47. Abram CL, Roberge GL, Hu Y, Lowell CA. Comparative Analysis of the Efficiency and Specificity of Myeloid-Cre Deleting Strains Using ROSA-EYFP Reporter Mice. *J Immunol Methods* (2014) 408:89–100. doi: 10.1016/j.jim.2014.05.009
48. Ferron M, Vacher J. Targeted Expression of Cre Recombinase in Macrophages and Osteoclasts in Transgenic Mice. *genesis* (2005) 41:138–45. doi: 10.1002/GENE.20108
49. Schaller E, Macfarlane AJ, Rupec RA, Gordon S, McKnight AJ, Pfeffer K. Inactivation of the F4/80 Glycoprotein in the Mouse Germ Line. *Mol Cell Biol* (2002) 22:8035–43. doi: 10.1128/MCB.22.22.8035-8043.2002

Conflict of Interest: The authors declare that the research was conducted in the absence of any commercial or financial relationships that could be construed as a potential conflict of interest.

frontiers | Frontiers in Immunology

REVIEW
published: 14 July 2022
doi: 10.3389/fimmu.2022.944142

The Delivery of Extracellular "Danger" Signals to Cytosolic Sensors in Phagocytes

Gerone A. Gonzales[1] *and Johnathan Canton*[2,3]*

[1] Department of Biochemistry and Molecular Biology, Cumming School of Medicine, University of Calgary, Calgary, AB, Canada, [2] Faculty of Veterinary Medicine, University of Calgary, Calgary, AB, Canada, [3] Calvin, Joan and Phoebe Snyder Institute for Chronic Diseases, University of Calgary, Calgary, AB, Canada

Phagocytes, such as macrophages and dendritic cells, possess the ability to ingest large quantities of exogenous material into membrane-bound endocytic organelles such as macropinosomes and phagosomes. Typically, the ingested material, which consists of diverse macromolecules such as proteins and nucleic acids, is delivered to lysosomes where it is digested into smaller molecules like amino acids and nucleosides. These smaller molecules can then be exported out of the lysosomes by transmembrane transporters for incorporation into the cell's metabolic pathways or for export from the cell. There are, however, exceptional instances when undigested macromolecules escape degradation and are instead delivered across the membrane of endocytic organelles into the cytosol of the phagocyte. For example, double stranded DNA, a damage associated molecular pattern shed by necrotic tumor cells, is endocytosed by phagocytes in the tumor microenvironment and delivered to the cytosol for detection by the cytosolic "danger" sensor cGAS. Other macromolecular "danger" signals including lipopolysaccharide, intact proteins, and peptidoglycans can also be actively transferred from within endocytic organelles to the cytosol. Despite the obvious biological importance of these processes, we know relatively little of how macromolecular "danger" signals are transferred across endocytic organelle membranes for detection by cytosolic sensors. Here we review the emerging evidence for the active cytosolic transfer of diverse macromolecular "danger" signals across endocytic organelle membranes. We will highlight developing trends and discuss the potential molecular mechanisms driving this emerging phenomenon.

Keywords: phagocyte, dendritic cell, macrophage, pattern recognition receptor, endocytic organelle, DAMP, PAMP, phagocytosis

OPEN ACCESS

Edited by:
Pedro Elias Marques,
KU Leuven, Belgium

Reviewed by:
Jean-Philippe Pellois,
Texas A&M University, United States
Warrison A. Andrade,
University of São Paulo, Brazil
Hisaaki Hirose,
Kyoto University, Japan

***Correspondence:**
Johnathan Canton
Johnathan.canton@ucalgary.ca

Specialty section:
This article was submitted to Inflammation, a section of the journal Frontiers in Immunology

Received: *14 May 2022*
Accepted: *23 June 2022*
Published: *14 July 2022*

Citation:
Gonzales GA and Canton J (2022) The Delivery of Extracellular "Danger" Signals to Cytosolic Sensors in Phagocytes. Front. Immunol. 13:944142. doi: 10.3389/fimmu.2022.944142

INTRODUCTION

Phagocytes serve a central role in the maintenance of organismal homeostasis and immunity. Through their ability to ingest large quantities of extracellular material *via* the specialized endocytic processes of macropinocytosis and phagocytosis, phagocytes can scavenge cellular debris, such as apoptotic cells or material derived from necrotic cells, ingest and kill invading pathogens and survey

the environment for signs of potential "danger". Both phagocytosis and macropinocytosis are active processes and the constitutive ingestion of exogenous material represents a significant metabolic burden. For example, phagocytosis of an apoptotic cell results in the acquisition of macromolecules including proteins, nucleic acids, lipids and carbohydrates (1). As such, phagocytes have in place machinery for the breakdown and recycling of phagocytic and macropinocytic cargo. Phagosomes undergo sequential interactions with endocytic organelles and lysosomes and also acquire v-ATPases which results in the gradual acidification of the lumen and the simultaneous acquisition of degradative enzymes with acidic pH optima. Whereas macropinosomes undergo membrane crenation and shrinkage events that allow for the recycling of membrane back to the plasma membrane as well as for their cargo to be delivered to lysosomes where it can be digested (2, 3). Endocytosed macromolecules are therefore digested into smaller molecules such as amino acids and nucleosides which can be exported to the cytosol *via* transmembrane transporters for incorporation into the phagocyte's metabolic pathways or for altogether export from the cell *via* plasma membrane transporters (4).

There are, however, exceptions – not all macromolecules ingested by phagocytes are digested in phagosomes and macropinosomes. In some cases, intact macromolecules are exported to the cytosol (**Figure 1**). For example, it has been known for decades that, in dendritic cells, intact endocytosed proteins can be transferred across the phagosomal membrane to the cytosol where they are processed for antigen cross-presentation [reviewed in (5–7)]. Cross-presentation is fundamental to the ability of immune cells to detect potential "danger" in the form of pathogen-derived proteins and neoantigens and to instigate immunity. Organisms deficient in cross-presentation become dangerously susceptible to infection and tumor challenge (5–13). More recently, there is mounting evidence that in addition to proteins, many other macromolecules are actively transported across phagosomal membranes. In the tumor microenvironment, double stranded DNA (dsDNA) in tumor cell debris is phagocytosed by dendritic cells and macrophages and transferred to the cytosol where it activates the cGAS-STING pathway (14–16). Similarly, during bacterial infection, macrophages distal to the site of infection macropinocytose lipopolysaccharide (LPS) and transfer it to the cytosol for inflammatory signalling (17–20). Despite the obvious importance of these processes to the ability of macrophages and dendritic cells to detect "danger" and to instigate immunity, our understanding of how macromolecules are delivered to the cytosol of phagocytes is in its infancy.

Here we review the evidence for the newly emerging concept of phagocyte-concerted transfer of endocytosed macromolecules to the cytosol. We discuss the physiological consequences of and attempt to provide perspectives on potential mechanisms for the cytosolic transfer of endocytosed macromolecules by phagocytes.

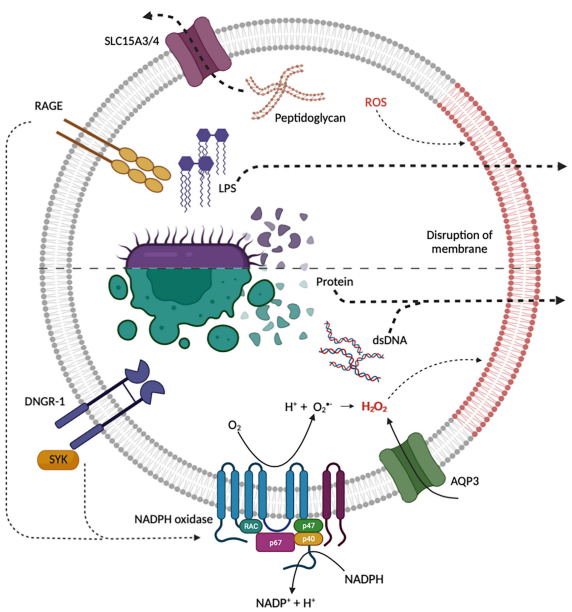

FIGURE 1 | Current proposed mechanisms for the endosomal escape of diverse macromolecular "danger" signals from endocytic organelles. Internalized bacteria can release peptidoglycan, LPS and bacterial protein which may gain access to the cytosol through transporters or induced membrane destabilization. Both RAGE and DNGR-1 induce NADPH oxidase ROS production, triggering ROS mediated membrane damage and the release of protein, dsDNA and LPS. NADPH oxidase and AQP3 may be recruited to endocytic organelles to induce ROS-dependent membrane damage and lipid peroxidation. Red lipids indicate disruption of endosomal membrane by ROS. Created with BioRender.com.

DELIVERING ENDOCYTOSED PROTEINS TO THE CYTOSOL

Some of the earliest evidence for the transfer of endocytosed macromolecules to the cytosol came from the study of antigen cross-presentation. Antigen cross-presentation is the process by which antigen presenting cells, primarily dendritic cells, initiate cytotoxic T lymphocyte responses to many types of viruses and tumors (21–23). There are believed to be two pathways for cross-presentation. In the first, referred to as the vacuolar pathway, exogenous proteins are processed into peptides and loaded onto histocompatibility complex class I (MHC-I) molecules within the lumen of endocytic organelles (24–26). The peptide-MHC-I complexes are then transported to the cell surface where they can serve as a ligand for T cell receptors on CD8 T cells. In the second pathway, known as the cytosolic pathway of antigen cross-presentation, intact or partially degraded proteins are transferred from within endocytic organelles, including phagosomes and macropinosomes, to the cytosol (27–30). Evidence for the transfer of intact or partially degraded proteins come from the finding that enzymes retain their enzymatic activity upon transfer to the cytosol (31–33). Once in the cytosol, the proteins are processed into peptides by the proteasome (27, 34, 35). The peptides are finally loaded onto MHC-I molecules in the endoplasmic reticulum and transported to the cell surface to activate CD8+ T lymphocytes (5). But exactly how proteins escape degradation in endocytic organelles and are then transported across endocytic organelle membranes to the cytosol remains unclear (6).

Although several phagocytes can perform cross-presentation *in vitro*, dendritic cells excel at cross-presentation relative to other cell types and most of the *in vivo* evidence points to dendritic cells as the primary cross-presenting cells (7, 9, 10). It is therefore conceivable that dendritic cells may express specific antigen export machinery that allows for the transfer of endocytosed proteins to the cytosol. This notion is bolstered by several seminal findings. For example, when cytochrome *c* is injected into the blood stream of mice, it results in the selective depletion of a group of cross-presenting dendritic cells known as classical (or sometimes also referred to as conventional) dendritic cells type 1 (cDC1) (32). The implication is that cytochrome c is endocytosed by these cells and subsequently transferred from within endocytic organelles to the cytosol where it induces APAF-1-dependent cell death (32). Importantly, this selective depletion of cDC1s completely ablates *in vivo* cross-presentation. Similarly, in mice lacking the transcription factor BATF3, *in vivo* cross-presentation of protein antigens from virally infected cells and tumor cells is completely lost (10). BATF3 is required for the development of cDC1s and the loss of cross-presentation is likely due to the complete absence of cDC1s, although other BATF3-dependent functions may also contribute. It is also worth noting that very recently another group of spleen-resident phagocytes, known as red pulp macrophages, have also been shown to be capable of cross-presenting model protein antigens *in vivo (*36). Together, these findings suggest that dendritic cells, particularly cDC1s, and perhaps some types of macrophages are specialized in cross-presentation and may express unique machinery for the transfer of intact proteins across endocytic organelle membranes. But what might this specialized machinery look like?

Several hypotheses exist for the transfer of endocytosed proteins across endocytic organelle membranes. One hypothesis that has been extensively studied is the "transporter hypothesis". The transporter hypothesis states that the translocation of proteins from within endocytic organelles to the cytosol is mediated by a protein transporter (5, 6). Early evidence from proteomics analyses of phagosomes (37), which was later corroborated by high resolution microscopy (31, 38, 39), found that phagosomes in dendritic cells and macrophages contain components of the endoplasmic reticulum including proteins involved in endoplasmic reticulum-associated degradation (ERAD) (40). This led to a series of studies describing a role for the endoplasmic reticulum-resident trimeric protein channel SEC61 in the translocation of proteins from within endocytic organelles, including phagosomes, to the cytosol. SEC61 is an ERAD protein that is believed to be responsible for the retro-translocation of peptides from the lumen of the endoplasmic reticulum to the cytosol for subsequent degradation (41). Inhibition of SEC61 with the bacterial toxin exotoxin A [ExoA (41)] results in reduced cross-presentation. Similarly, the knockdown of SEC61 with siRNA, as well as the exclusion of SEC61 from endocytic organelles with an ER-retaining intrabody diminishes cross-presentation. Cells transfected with a dominant-negative form of the p97 AAA ATPase, a hexametric protein that interacts with proteins undergoing translocation *via* SEC61, failed to export luciferase from within endocytic organelles to the cytosol and failed to cross-present exogenous antigen (39, 42). Altogether, these findings point to a potential role for the SEC61 translocon in the export of endocytosed proteins from endocytic organelles to the cytosol.

The precise role played by SEC61 in the delivery of endocytosed proteins to the cytosol for cross-presentation is nevertheless difficult to deduce. Indeed, much of the work on SEC61 in cross-presentation has been performed using tools that result in the chronic inhibition or mislocalization of SEC61 or other ERAD proteins. Such chronic inhibition may result in the inhibition of MHC-I-dependent presentation by other off-target effects that are not related to protein export from endocytic organelles. For example, SEC61 inhibition can result in reduced trafficking of MHC-I from the endoplasmic reticulum to the plasma membrane (43). To circumvent this limitation, a very recent study employed a newly described tool – mycolactone – for potent and acute SEC61 inhibition (43). Acute inhibition of SEC61 with mycolactone did reduce cross-presentation, however, contrary to previous findings, it did not correlate with the inhibition of the endosome-to-cytosol export of endocytosed proteins (43). Instead, the inhibition of cross-presentation by SEC61 resulted from the diminished expression of proteins required for cross-presentation, including MHC-I. These findings directly contradict SEC61-mediated protein translocation out of endocytic organelles

(43). It is therefore unclear at present what role, if any at all, the ERAD machinery has in the transport of endocytosed proteins to the cytosol.

In the last five years, another model for the transfer of endocytosed proteins to the cytosol has been gaining traction. The "indigestion model" was first described nearly thirty years ago by Reis e Sousa and Germain (28). This model states that destabilization of endocytic organelle membranes leads to rupture and the subsequent release of cargo, including protein antigens, into the cytosol (28). One proposed mechanism of membrane destabilization is through the peroxidation of lipids in the limiting membrane of endocytic organelles by reactive oxygen species (ROS) (**Figure 1**). ROS can modify lipid bilayers through the direct oxidization of polyunsaturated lipid tails. Oxidized lipid tails bend towards the water phase and this conformational change affects the thickness, fluidity, and permeability of the bilayer (44–46). Studies by Dingjan et al. suggest that endosomal ROS produced by the NOX2-containing NADPH-oxidase can cause lipid peroxidation (47, 48). When cells are stimulated with lipopolysaccharide (LPS), a pathogen-associated molecular pattern (PAMP) that is known to promote NADPH oxidase activity, there is an increase in peroxidation of lipids on endocytic organelles resulting in rupture and the leakage of endocytosed proteins to the cytosol (47). Similarly, α-Tocopherol, an antioxidant which scavenges the ROS produced by the NADPH oxidase, reduces ROS-induced lipid peroxidation as well as the release of endocytosed proteins into the cytosol (47). Further evidence in support of ROS-induced membrane destabilization was provided by Nalle et al. who demonstrated that aquaporin-3 (AQP3) transports hydrogen peroxide into endocytic organelles where it contributes to lipid peroxidation, membrane destabilization and protein release to the cytosol (49). It is worth mentioning, that apart from ROS-dependent lipid modification, other lipid modifications on endocytic organelles, such as the accumulation of sphingosine-based lipids, have been proposed although there is no direct evidence for these modifications in the escape of endocytosed proteins into the cytosol as yet [reviewed in (50)].

As ROS-induced destabilization of endocytic organelle membranes may induce cellular toxicity, it is likely that the process is tightly regulated. Evidence for regulation of this sort was recently provided in a study on the dendritic cell receptor DNGR-1 (11, 51). DNGR-1, also known as CLEC9A, is a transmembrane C-type lectin receptor on the surface of cDC1s (12). The ligand for DNGR-1 is filamentous (F-)actin and myosin complexes associated with dead cell debris (11, 12, 52). When DNGR-1 binds to its ligand it recruits and activates the kinase SYK to phagosomes harboring dead cell debris (11). DNGR-1-SYK signalling results in NADPH oxidase-dependent ROS production in phagosomes leading to phagosomal rupture and the efflux of proteins from the lumen of the phagosome to the cytosol (11) (**Figure 1**). Using three-dimensional (3D) corelative light and electron microscopy (CLEM) and serial block face (SBF) scanning electron microscopy (SEM), the rupture of the phagosome was visualized, showing a hole with a diameter between 1-1.5 μm (11). This process is believed to regulate the cross-presentation of dead cell associated proteins by cDC1s (11, 13, 51).

The observation that endocytic organelle rupture is regulated by receptors that sense "danger" suggests that rupture or endocytic organelle "indigestion" is inducible - a likely adaptation to guard against unnecessary or constitutive damage to endocytic organelles. Any toxicity associated with endocytic organelle damage may also be offset by mechanisms of membrane repair such as the endosomal sorting complex required for transport (ESCRT) machinery or galectins both of which mediate the repair of damaged endocytic organelles (53–55). The kinetics and regulation of endocytic organelle membrane destabilization have yet to be fully elucidated.

In summary, phagocytes exert mechanisms for the active transfer of endocytosed proteins to the cytosol. This has primarily been studied in the context of cross-presentation and the most recent evidence points to inducible mechanisms that allow for the nonselective delivery of endocytic organelle cargo to the cytosol. This implies that other endocytosed macromolecules may also be released through these pathways. In the next section, we discuss the evidence for the release of another endocytosed macromolecule - double stranded DNA (dsDNA) - to the cytosol.

DELIVERING ENDOCYTOSED DOUBLE STRANDED DNA TO THE CYTOSOL

Double stranded DNA (dsDNA) is often shed by dead and dying pathogens or damaged cells at sites of tissue damage (**Figure 1**). Immune cells harbor pattern recognition receptors that recognize dsDNA as a "danger" signal. For example, in dendritic cells present in the necrotic core of tumors, the cytosolic dsDNA receptor cyclic GMP-AMP synthase (cGAS) is activated by tumor cell-derived dsDNA which leads to stimulator of interferon genes (STING)-dependent inflammatory signalling (14–16). The activation of dendritic cells in this way is critical – impairment of this pathway in dendritic cells renders organisms dangerously susceptible to tumor challenge (14, 16). But how does dsDNA, a macromolecule shed by dead or dying tumor cells, end up in the cytosol of dendritic cells to activate the cGAS-STING pathway?

Recent evidence suggests that the delivery of dsDNA to the cytosol of dendritic cells is likely a two-step process involving first the internalization of extracellular dsDNA into endocytic organelles and second the escape of dsDNA to the cytosol. In line with this, dsDNA shed by dying cells forms complexes with proteins that serve to both prevent its degradation by extracellular DNase-I and to facilitate its endocytosis by phagocytes. For example, the antimicrobial peptide LL37 (also known as CAMP) facilitates the endocytosis of extracellular dsDNA by dendritic cells (56, 57). The interaction between dsDNA and LL37 converts non-stimulatory self-dsDNA into an effective "danger" signal which stimulates inflammatory signalling in phagocytes including dendritic cells and

monocytes (56, 57). In monocytes in particular, LL37-dsDNA complexes escape from endocytic organelles to activate the cGAS-STING pathway. Interestingly, LL37-dsDNA escape into the cytosol is enhanced in the presence of the V-ATPase inhibitor bafilomycin (57). The relationship between V-ATPase activity, which acidifies the lumen of endocytic organelles, and the escape of macromolecules is unclear. It is, however, conceivable that bafilomycin impairs the degradation of endocytosed dsDNA by DNase II, which functions optimally under acidic conditions.

More recently, other proteins have been shown to complex with extracellular dsDNA to facilitate its endocytosis and subsequent release to the cytosol. High mobility group box 1 (HMGB1) and other HMGB proteins function as sentinels for extracellular nucleic acids (58). HMGB1 forms complexes with dsDNA leading to its endocytosis (59, 60). Although TLR2 and TLR4 have been implicated in the endocytosis of HMGB1-dsDNA complexes by phagocytes, the exact mechanism and receptor(s) involved remain unclear. HMGB1-dsDNA uptake does however appear to be regulated by the inhibitory receptor T cell immunoglobulin and mucin domain containing (TIM)-3 in dendritic cells, as TIM-3 blockade results in increased endocytosis of extracellular HMGB1-dsDNA complexes (14). Endocytosis of HMGB1-dsDNA complexes results in the transfer of dsDNA to the cytosol where it activates the cGAS-STING pathway in the dendritic cells (14). HMGB1-dependent dsDNA uptake and cytosolic transfer appears to be particularly important in the context of tumors where necrotic tumor cells shed dsDNA which is taken up in the form of HMGB1-dsDNA complexes. The subsequent triggering of the cGAS-STING pathway in the dendritic cells leads to robust anti-tumor immunity (14, 16).

Finally, dsDNA present in neutrophil extracellular traps (NETs) can also trigger the cytosolic cGAS-STING pathway in macrophages (61, 62). Neutrophils release NETs through a specialized form of cell death known as NETosis. These NETs physically trap and kill microbes in a web-like complex of neutrophil derived antimicrobial peptides, granular proteins, neutrophil elastase and dsDNA (61, 62). After NETosis has occurred, macrophages phagocytose the NETs and NET-derived dsDNA escapes the phagosome into the cytosol to activate cGAS (62). Ultrastructural analysis revealed that NETs interact with cGAS after escaping from phagosomes (62). Although the mechanism of dsDNA escape into the cytosol following the phagocytosis of NETs remains unclear, it appears to involve neutrophil elastase, a protein which is abundant in NETs and that can bind to dsDNA. How neutrophil elastase may promote the phagosomal escape of dsDNA is not yet known (62).

In summary, there is growing evidence that phagocytes can endocytose and subsequently deliver dsDNA to the cytosol for the activation of cGAS. This results in inflammatory signalling and is already emerging as an important feature in the generation of anti-tumor immunity. Nevertheless, how dsDNA, a membrane impermeant macromolecule, can cross endocytic organelle membranes to gain access to cytosolic danger sensors is a mystery. Findings thus far suggest that dsDNA requires complexing with protein chaperones to trigger robust cytosolic recognition and to elicit inflammatory signalling, but there has yet to be any proposed mechanisms on how these chaperones allow dsDNA to gain access to the cytosol. Interestingly, the delivery if dsDNA to the cytosol from within endocytic organelles results in the activation of dendritic cells and the upregulation of costimulatory molecules and cytokines such as type I interferons (15). This in turn promotes the cross-presentation of protein antigens (15). It is tempting to speculate that the mechanism(s) governing the release of protein antigens and the release of dsDNA from endocytic organelles are related and perhaps interconnected. To the best of our knowledge, there are no studies investigating whether NADPH oxidase-dependent ROS production and peroxidation of the limiting membranes of endocytic organelles also regulates the escape of endocytosed dsDNA to the cytosol in phagocytes.

OTHER MACROMOLECULAR "DANGER" SIGNALS THAT ARE DELIVERED TO THE CYTOSOL OF PHAGOCYTES

In addition to proteins and dsDNA, there is growing evidence that other macromolecular "danger" signals can be endocytosed and subsequently transferred to the cytosol of phagocytes to instigate inflammatory signal. This has mostly been observed in the context of infection. For example, in a bacterial infection, pathogen-derived peptidoglycan, flagellin, and lipopolysaccharide (LPS) are delivered to the cytosol where they are detected by cytosolic pattern recognition receptors (**Figure 1**). In some instances, this is due to pathogen-concerted mechanisms, such as cell penetrating peptides or secretion systems and toxins, that allow for cytosolic invasion. These processes will not be discussed here as it has been recently reviewed elsewhere [see (63–66)]. Instead, we discuss the emerging evidence for the active or phagocyte-concerted transfer of endocytosed PAMPs to the cytosol.

Peptidoglycan is a major component of the cell wall of gram-positive bacteria. It is recognized as a "danger" signal and serves as a ligand for the cytosolic pattern recognition receptors nucleotide-binding oligomerization domain (NOD)-like receptors (NLRs), NOD1 and NOD2 (67). The activation of NOD1 and NOD2 leads to pro-inflammatory signalling *via* the activation of NF-κB and mitogen-activated protein kinase (MAPK) (67). During an infection, peptidoglycan is internalized by phagocytes either by phagocytosis of the pathogenic bacteria or by the macropinocytosis of peptidoglycan derivatives, such as muramyl dipeptide, shed by invading bacteria. As the resultant phagosomes and macropinosomes mature, they acquire V-ATPases which acidify the lumen. The proton gradient generated by acidification facilitates the transport of peptidoglycan derivatives to the cytosol *via* proton-coupled oligopeptide transporters (POT) also known as solute carrier family 15 (SLC15), including SLC15A3 and SLC15A4 - both of which are highly expressed in macrophages and dendritic cells (68–70) (**Figure 1**). Of note, and similar to the cytosolic translocation of proteins and dsDNA described above,

internalization of peptidoglycan into an endocytic organelle is a prerequisite for its delivery to the cytosol. This two-step process for the detection of peptidoglycan has recently been used to link the constitutive macropinocytosis of macrophages and dendritic cells to their immune surveillance function (71). Indeed, blockade of constitutive macropinocytosis in primary human macrophages renders them incapable of sensing extracellular peptidoglycan derivatives (71). Whether constitutive macropinocytosis contributes significantly to the delivery of other extracellular "danger" signals is currently not known.

Another extracellular PAMP that is actively delivered to cytosolic pattern recognition receptors is LPS. LPS, also known as endotoxin, is a major component of the cell wall of gram-negative bacteria. LPS is well known to elicit inflammatory signalling that is dependent upon its recognition by the transmembrane pattern recognition receptor TLR4. However, it has recently been demonstrated that endocytosed LPS is also delivered to the cytosol where it can bind and activate caspase-11, which cleaves gasdermin D (GSDMD) (17–20, 72, 73). When activated, GSDMD assembles into a pore on the plasma membrane which cause pyroptosis, a lytic form of cell death (72, 73). But how is LPS actively delivered to cytosolic pattern recognition receptors? Interestingly, the mechanism involved in delivering LPS to the cytosol shares several features with the delivery of dsDNA to the cytosol. During a state of sepsis, HMGB1 released from hepatocytes complexes with extracellular LPS. The HMGB1-LPS complexes bind to receptors for advanced glycation end-products (RAGE) on the surface of macrophages and are subsequently internalized into endocytic organelles and delivered to lysosomes (19). In the acidic environment of lysosomes, HMGB1-LPS complexes destabilize and ultimately permeabilize the limiting membrane of the lysosomes. This leads to the leakage of HMGB1-LPS complexes into the cytosol and to the activation of caspase-11 (19). Although it is currently unclear how HMGB1-LPS complexes result in membrane permeabilization, whole-cell patch clamping revealed an HMGB1-dependent inward current presumably caused by HMGB1-dependent membrane permeabilization (19). In addition to the similarities between the delivery of LPS and dsDNA to the cytosol, it is worth noting that the requirement of engagement of the receptor RAGE for subsequent delivery of LPS to the cytosol shares some similarities with the DNGR-1-dependent endocytic organelle destabilization discussed above. Both RAGE and DNGR-1 trigger robust NADPH oxidase-dependent ROS production (11, 74–76) (**Figure 1**). However, whether ROS production downstream of RAGE engagement contributes to the observed lysosome membrane destabilization that results in LPS release to the cytosol remains to be determined.

Apart from HMGB1-dependent membrane permeabilization other pathways have been described for the delivery of endocytosed LPS to the cytosol. Guanylate binding proteins (GBPs) are interferon-γ-inducible GTPases capable of restricting the replication of bacteria and promoting noncanonical inflammasome activation (77–82). GBPs can bind directly to cytosolic pathogens, but can also be recruited to pathogen-containing phagosomes where they instigate phagosomal rupture (77). Phagosomal rupture leads to the delivery of pathogen-derived LPS to the host cytosol. Once in the cytosol LPS activates caspase-11 and downstream inflammatory signalling (77, 78). Although the lysis of pathogen-containing phagosomes by GBPs is well-documented, the molecular mechanism(s) by which GBPs discern "self" endomembranes from the limiting membranes of pathogen-containing phagosomes remains to be determined. It is tempting to speculate that receptors may survey the luminal contents of the phagosomes for PAMPs or DAMPs and initiate signalling that in some way marks the limiting membrane for detection by GBPs and is a promising avenue for future investigation.

Apart from peptidoglycan and LPS, other pathogen-derived PAMPs which actively delivered to the cytosol of phagocytes are being studied. For example, flagellin, the principal structural component in flagella, is shed by some types of bacteria in structures called outer membrane vesicles (OMVs) (83). The OMVs are subsequently endocytosed by macrophages and the flagellin is delivered to the cytosol where it is detected by the cytosolic sensor neuronal apoptosis inhibitory protein 5 (NAIP5). When bound to flagellin, the flagellin-NAIP5 complex assembles with NOD-like receptor family, caspase activation recruitment domain (CARD) domain-containing protein 4 (NLRC4) to form a pro-inflammatory signalling complex called the inflammasome (83, 84). Although less is known about how flagellin gains access to the cytosol, it is likely to involve an HMGB1-RAGE-dependent pathway as OMVs also contain LPS and have been shown to facilitate the cytosolic delivery of LPS (17).

CONCLUSION

The phagocyte-concerted delivery of extracellular, seemingly membrane impermeant, "danger" signals to the cytosol to activate cytosolic pattern recognition receptors is emerging as a fundamental mechanism by which phagocytes carry out their immune surveillance function. Nevertheless, the molecular mechanisms by which this occurs remain unclear. This process is likely to be highly regulated. We propose that the cytosolic delivery of macromolecular extracellular "danger" signals to cytosolic sensors is regulated at three key stages. First, entry into the host cell occurs *via* receptor-mediated endocytosis. Dedicated receptors on the surface of phagocytes either bind directly to the "danger" signal, or indirectly *via* protein bridges or chaperones such as HMGB1 and LL37. This serves to regulate the type of cargo being delivered to the cytosol, but also, by virtue of selective expression of the receptors, serves to target the "danger" signals to sentinel cells such as macrophages and dendritic cells. Second, receptor signaling results in the destabilization of the endocytic organelle membrane by mechanisms such as, but not limited to, NADPH dependent-ROS production. Both DNGR-1 and RAGE induce robust NADPH oxidase-dependent ROS production which may directly destabilize the limiting membranes of endocytic organelles or may in some way mark the endocytic organelles for destabilization by other protein effectors. Receptor-

engagement provides an added layer of regulation resulting in the selective and inducible destabilization of endocytic organelles carrying "danger" signals. Finally, membrane destabilization results in the delivery of the "danger" signal to the cytosol for detection by cytosolic sensors. Although currently unknown, we anticipate that such membrane destabilization is transient and is likely repaired by membrane repair machinery such as the ESCRT pathway. Similarly, damaged organelles may also be replenished *via* organelle biogenesis (85–87). With already defined roles in tumor immunity, sepsis and antigen presentation, the detection of extracellular "danger" signals by cytosolic sensors will continue to emerge as a fundamental mechanism by which sentinel cells such as macrophages and dendritic cells achieve their roles in immunity and homeostasis. Understanding the mechanisms driving these processes is therefore of critical importance.

AUTHOR CONTRIBUTIONS

GG and JC wrote the manuscript. All authors contributed to the article and approved the submitted version.

ACKNOWLEDGEMENTS

We thank the reviewers for their critical reading of this manuscript.

REFERENCES

1. Han CZ, Ravichandran KS. Metabolic Connections During Apoptotic Cell Engulfment. *Cell* (2011) 147:1442–5. doi: 10.1016/j.cell.2011.12.006
2. Freeman SA, Grinstein S. Resolution of Macropinosomes, Phagosomes and Autolysosomes: Osmotically Driven Shrinkage Enables Tubulation and Vesiculation. *Traffic* (2018) 19:965–74. doi: 10.1111/tra.12614
3. Freeman SA, Uderhardt S, Saric A, Collins RF, Buckley CM, Mylvaganam S, et al. Lipid-Gated Monovalent Ion Fluxes Regulate Endocytic Traffic and Support Immune Surveillance. *Science* (2020) 367:301–5. doi: 10.1126/science.aaw9544
4. Levin R, Grinstein S, Canton J. The Life Cycle of Phagosomes: Formation, Maturation, and Resolution. *Immunol Rev* (2016) 273:156–79. doi: 10.1111/imr.12439
5. Blum JS, Wearsch PA, Cresswell P. Pathways of Antigen Processing. *Annu Rev Immunol* (2013) 31:443–73. doi: 10.1146/annurev-immunol-032712-095910
6. Grotzke JE, Sengupta D, Lu Q, Cresswell P. The Ongoing Saga of the Mechanism(s) of MHC Class I-Restricted Cross-Presentation. *Curr Opin Immunol* (2017) 46:89–96. doi: 10.1016/j.coi.2017.03.015
7. Theisen D, Murphy K. The Role of Cdc1s *In Vivo*: CD8 T Cell Priming Through Cross-Presentation. *F1000Res* (2017) 6:98. doi: 10.12688/f1000research.9997.1
8. Murphy TL, Murphy KM. Dendritic Cells in Cancer Immunology. *Cell Mol Immunol* (2022) 19:3–13. doi: 10.1038/s41423-021-00741-5
9. Theisen DJ, et al. WDFY4 is Required for Cross-Presentation in Response to Viral and Tumor Antigens. *Science* (2018) 362:694–9. doi: 10.1126/science.aat5030
10. Hildner K, Edelson BT, Purtha WE, Diamond M, Matsushita H, Kohyama M, et al. Batf3 Deficiency Reveals a Critical Role for CD8α+ Dendritic Cells in Cytotoxic T Cell Immunity. *Science* (2008) 322:1097–100. doi: 10.1126/science.1164206
11. Canton J, Blees H, Henry CM, Buck MD, Schulz O, Rogers NC, et al. The Receptor DNGR-1 Signals for Phagosomal Rupture to Promote Cross-Presentation of Dead-Cell-Associated Antigens. *Nat Immunol* (2021) 22:140–53. doi: 10.1038/s41590-020-00824-x
12. ancho D, Joffre OP, Keller AM, Rogers NC, Martínez D, Hernanz-Falcón P, et al. Identification of a Dendritic Cell Receptor That Couples Sensing of Necrosis to Immunity. *Nature* (2009) 458:899–903. doi: 10.1038/nature07750
13. Giampazolias E, Schulz O, Lim KHJ, Rogers NC, Chakravarty P, Srinivasan N, et al. Secreted Gelsolin Inhibits DNGR-1-Dependent Cross-Presentation and Cancer Immunity. *Cell* (2021) 184:4016–31.e22. doi: 10.1016/j.cell.2021.05.021
14. de Mingo Pulido Á, Hänggi K, Celias DP, Gardner A, Li J, Batista-Bittencourt B, et al. The Inhibitory Receptor TIM-3 Limits Activation of the cGAS-STING Pathway in Intra-Tumoral Dendritic Cells by Suppressing Extracellular DNA Uptake. *Immunity* (2021) 54:1154–67.e7. doi: 10.1016/j.immuni.2021.04.019
15. Ahn J, Xia T, Rabasa Capote A, Betancourt D, Barber GN. Extrinsic Phagocyte-Dependent STING Signaling Dictates the Immunogenicity of Dying Cells. *Cancer Cell* (2018) 33:862–73.e5. doi: 10.1016/j.ccell.2018.03.027
16. Woo S-R, Fuertes MB, Corrales L, Spranger S, Furdyna MJ, Leung MYK, et al. STING-Dependent Cytosolic DNA Sensing Mediates Innate Immune Recognition of Immunogenic Tumors. *Immunity* (2014) 41:830–42. doi: 10.1016/j.immuni.2014.10.017
17. Vanaja SK, Russo AJ, Behl B, Banerjee I, Yankova M, Deshmukh SD, et al. Bacterial Outer Membrane Vesicles Mediate Cytosolic Localization of LPS and Caspase-11 Activation. *Cell* (2016) 165:1106–19. doi: 10.1016/j.cell.2016.04.015
18. Vasudevan SO, Russo AJ, Kumari P, Vanaja SK. & Rathinam, V. A. A TLR4-Independent Critical Role for CD14 in Intracellular LPS Sensing. *Cell Rep* (2022) 39:110755. doi: 10.1016/j.celrep.2022.110755
19. Deng M, Tang Y, Li W, Wang X, Zhang R, Zhang X, et al. The Endotoxin Delivery Protein HMGB1 Mediates Caspase-11-Dependent Lethality in Sepsis. *Immunity* (2018) 49:740–53.e7. doi: 10.1016/j.immuni.2018.08.016
20. Tang Y, Wang X, Li Z, He Z, Yang X, Cheng X, et al. Heparin Prevents Caspase-11-Dependent Septic Lethality Independent of Anticoagulant Properties. *Immunity* (2021) 54:454–67.e6. doi: 10.1016/j.immuni.2021.01.007
21. Huang AYC, Golumbek P, Ahmadzadeh M, Jaffee E, Pardoll D, Levitsky H. Role of Bone Marrow-Derived Cells in Presenting MHC Class I-Restricted Tumor Antigens. *Science* (1994) 264:961–5. doi: 10.1126/science.7513904
22. Sigal LJ, Crotty S, Andino R, Rock KL. Cytotoxic T-Cell Immunity to Virus-Infected non-Haematopoietic Cells Requires Presentation of Exogenous Antigen. *Nature* (1999) 398:77–80. doi: 10.1038/18038
23. den Haan JMM, Bevan MJ. Antigen Presentation to CD8+ T Cells: Cross-Priming in Infectious Diseases. *Curr Opin Immunol* (2001) 13:437–41. doi: 10.1016/S0952-7915(00)00238-7
24. Harding CV, Song R. Phagocytic Processing of Exogenous Particulate Antigens by Macrophages for Presentation by Class I MHC Molecules. *J Immunol* (1994) 153:4925–33.
25. Song R, Harding CV. Roles of Proteasomes, Transporter for Antigen Presentation (TAP), and Beta 2-Microglobulin in the Processing of Bacterial or Particulate Antigens *via* an Alternate Class I MHC Processing Pathway. *J Immunol* (1996) 156:4182–90.
26. Pfeifer JD, Wick MJ, Roberts RL, Findlay K, Normark SJ, Harding CV. Phagocytic Processing of Bacterial Antigens for Class I MHC Presentation to T Cells. *Nature* (1993) 361:359–62. doi: 10.1038/361359a0
27. Kovacsovics-Bankowski M. & Rock, K. L. A Phagosome-to-Cytosol Pathway for Exogenous Antigens Presented on MHC Class I Molecules. *Science* (1995) 267:243–6. doi: 10.1126/science.7809629
28. Reis e Sousa C, Germain RN. Major Histocompatibility Complex Class I Presentation of Peptides Derived From Soluble Exogenous Antigen by a Subset of Cells Engaged in Phagocytosis. *J Exp Med* (1995) 182:841–51. doi: 10.1084/jem.182.3.841
29. Oh YK, Harding CV, Swanson JA. The Efficiency of Antigen Delivery From Macrophage Phagosomes Into Cytoplasm for MHC Class I-Restricted

Antigen Presentation. *Vaccine* (1997) 15:511–8. doi: 10.1016/S0264-410X(97)00221-1
30. Norbury CC, Hewlett LJ, Prescott AR, Shastri N, Watts C. Class I MHC Presentation of Exogenous Soluble Antigen *via* Macropinocytosis in Bone Marrow Macrophages. *Immunity* (1995) 3:783–91. doi: 10.1016/1074-7613(95)90067-5
31. Cebrian I, Visentin G, Blanchard N, Jouve M, Bobard A, Moita C, et al. Sec22b Regulates Phagosomal Maturation and Antigen Crosspresentation by Dendritic Cells. *Cell* (2011) 147:1355–68. doi: 10.1016/j.cell.2011.11.021
32. Lin ML, Zhan Y, Proietto AI, Prato S, Wu L, Heath WR, et al. Selective Suicide of Cross-Presenting CD8+ Dendritic Cells by Cytochrome C Injection Shows Functional Heterogeneity Within This Subset. *Proc Natl Acad Sci U.S.A.* (2008) 105:3029–34. doi: 10.1073/pnas.0712394105
33. Giodini A, Cresswell P. Hsp90-Mediated Cytosolic Refolding of Exogenous Proteins Internalized by Dendritic Cells. *EMBO J* (2008) 27:201–11. doi: 10.1038/sj.emboj.7601941
34. Ackerman AL, Kyritsis C, Tampé R, Cresswell P. Early Phagosomes in Dendritic Cells Form a Cellular Compartment Sufficient for Cross Presentation of Exogenous Antigens. *Proc Natl Acad Sci U.S.A.* (2003) 100:12889–94. doi: 10.1073/pnas.1735556100
35. Palmowski MJ, Gileadi U, Salio M, Gallimore A, Millrain M, James E, et al. Role of Immunoproteasomes in Cross-Presentation. *J Immunol* (2006) 177:983–90. doi: 10.4049/jimmunol.177.2.983
36. Enders M, Franken L, Philipp MS, Kessler N, Baumgart AK, Eichler M, et al. Splenic Red Pulp Macrophages Cross-Prime Early Effector CTL That Provide Rapid Defense Against Viral Infections. *J Immunol* (2020) 204:87–100. doi: 10.4049/jimmunol.1900021
37. Garin J, Diez R, Kieffer S, Dermine JF, Duclos S, Gagnon E, et al. The Phagosome Proteome. *J Cell Biol* (2001) 152:165–80. doi: 10.1083/jcb.152.1.165
38. Alloatti A, Rookhuizen DC, Joannas L, Carpier JM, Iborra S, Magalhaes JG, et al. Critical Role for Sec22b-Dependent Antigen Cross-Presentation in Antitumor Immunity. *J Exp Med* (2017) 214:2231–41. doi: 10.1084/jem.20170229
39. Zehner M, Marschall AL, Bos E, Schloetel JG, Kreer C, Fehrenschild D, et al. The Translocon Protein Sec61 Mediates Antigen Transport From Endosomes in the Cytosol for Cross-Presentation to CD8+ T Cells. *Immunity* (2015) 42:850–63. doi: 10.1016/j.immuni.2015.04.008
40. Grotzke JE, Cresswell P. Are ERAD Components Involved in Cross-Presentation? *Mol Immunol* (2015) 68:112–5. doi: 10.1016/j.molimm.2015.05.002
41. Koopmann J-O, Albring J, Hüter E, Bulbuc N, Spee P, Neefjes J, et al. Export of Antigenic Peptides From the Endoplasmic Reticulum Intersects With Retrograde Protein Translocation Through the Sec61p Channel. *Immunity* (2000) 13:117–27. doi: 10.1016/S1074-7613(00)00013-3
42. Ackerman AL, Giodini A. & Cresswell, P. A Role for the Endoplasmic Reticulum Protein Retrotranslocation Machinery During Crosspresentation by Dendritic Cells. *Immunity* (2006) 25:607–17. doi: 10.1016/j.immuni.2006.08.017
43. Grotzke JE, Kozik P, Morel JD, Impens F, Pietrosemoli N, Cresswell P, et al. Sec61 Blockade by Mycolactone Inhibits Antigen Cross-Presentation Independently of Endosome-to-Cytosol Export. *Proc Natl Acad Sci* (2017) 114:E5910–9. doi: 10.1073/pnas.1705242114
44. Leibowitz ME, Johkson MC. Relation of Lipid Peroxidation to Loss of Cations Trapped in Liposomes. *J Lipid Res* (1971) 12:662–70. doi: 10.1016/S0022-2275(20)39453-0
45. Stark G. The Effect of Ionizing Radiation on Lipid Membranes. *Biochim Biophys Acta (BBA) - Rev Biomembranes* (1991) 1071:103–22. doi: 10.1016/0304-4157(91)90020-W
46. Wong-ekkabut J, Xu Z, Triampo W, Tang IM, Tieleman DP, Monticelli L. Effect of Lipid Peroxidation on the Properties of Lipid Bilayers: A Molecular Dynamics Study. *Biophys J* (2007) 93:4225–36. doi: 10.1529/biophysj.107.112565
47. Dingjan I, Verboogen DR, Paardekooper LM, Revelo NH, Sittig SP, Visser LJ, et al. Lipid Peroxidation Causes Endosomal Antigen Release for Cross-Presentation. *Sci Rep* (2016) 6:22064. doi: 10.1038/srep22064
48. Dingjan I, Paardekooper LM, Verboogen DRJ, von Mollard GF, Ter Beest M, van den Bogaart G. VAMP8-Mediated NOX2 Recruitment to Endosomes is Necessary for Antigen Release. *Eur J Cell Biol* (2017) 96:705–14. doi: 10.1016/j.ejcb.2017.06.007
49. Nalle SC, Barreira da Silva R, Zhang H, Decker M, Chalouni C, Xu M, et al. Aquaporin-3 Regulates Endosome-to-Cytosol Transfer *via* Lipid Peroxidation for Cross Presentation. *PloS One* (2020) 15:e0238484. doi: 10.1371/journal.pone.0238484
50. Gros M, Amigorena S. Regulation of Antigen Export to the Cytosol During Cross-Presentation. *Front Immunol* (2019) 10:. doi: 10.3389/fimmu.2019.00041
51. Hatinguais R, Brown GD. Cross-Presentation is Getting DNGRous. *Nat Immunol* (2021) 22:108–10. doi: 10.1038/s41590-020-00831-y
52. Schulz O, Hanč P, Böttcher JP, Hoogeboom R, Diebold SS, Tolar P, et al. Myosin II Synergizes With F-Actin to Promote DNGR-1-Dependent Cross-Presentation of Dead Cell-Associated Antigens. *Cell Rep* (2018) 24:419–28. doi: 10.1016/j.celrep.2018.06.038
53. Childs E, Henry CM, Canton J, Reis e Sousa C. Maintenance and Loss of Endocytic Organelle Integrity: Mechanisms and Implications for Antigen Cross-Presentation. *Open Biol* (2021) 11:210194. doi: 10.1098/rsob.210194
54. Radulovic M, Schink KO, Wenzel EM, Nähse V, Bongiovanni A, Lafont F, et al. ESCRT-Mediated Lysosome Repair Precedes Lysophagy and Promotes Cell Survival. *EMBO J* (2018) 37:e99753. doi: 10.15252/embj.201899753
55. Skowyra ML, Schlesinger PH, Naismith TV, Hanson PI. Triggered Recruitment of ESCRT Machinery Promotes Endolysosomal Repair. *Sci 360 Eaar5078* (2018) 360:eaar5078. doi: 10.1126/science.aar5078
56. Lande R, Gregorio J, Facchinetti V, Chatterjee B, Wang YH, Homey B, et al. Plasmacytoid Dendritic Cells Sense Self-DNA Coupled With Antimicrobial Peptide. *Nature* (2007) 449:564–9. doi: 10.1038/nature06116
57. Chamilos G, Gregorio J, Meller S, Lande R, Kontoyiannis DP, Modlin RL, et al. Cytosolic Sensing of Extracellular Self-DNA Transported Into Monocytes by the Antimicrobial Peptide LL37. *Blood* (2012) 120:3699–707. doi: 10.1182/blood-2012-01-401364
58. Yanai H, Ban T, Wang Z, Choi MK, Kawamura T, Negishi H, et al. HMGB Proteins Function as Universal Sentinels for Nucleic-Acid-Mediated Innate Immune Responses. *Nature* (2009) 462:99–103. doi: 10.1038/nature08512
59. Li X, Yue Y, Zhu Y, Xiong S. Extracellular, But Not Intracellular HMGB1, Facilitates Self-DNA Induced Macrophage Activation *via* Promoting DNA Accumulation in Endosomes and Contributes to the Pathogenesis of Lupus Nephritis. *Mol Immunol* (2015) 65:177–88. doi: 10.1016/j.molimm.2015.01.023
60. Lu J, Yue Y, Xiong S. Extracellular HMGB1 Augments Macrophage Inflammation by Facilitating the Endosomal Accumulation of ALD-DNA *via* TLR2/4-Mediated Endocytosis. *Biochim Biophys Acta (BBA) - Mol Basis Dis* (2021) 1867:166184. doi: 10.1016/j.bbadis.2021.166184
61. Lande R, Ganguly D, Facchinetti V, Frasca L, Conrad C, Gregorio J, et al. Neutrophils Activate Plasmacytoid Dendritic Cells by Releasing Self-DNA–Peptide Complexes in Systemic Lupus Erythematosus. *Sci Trans Med* (2011) 3:73ra19–9. doi: 10.1126/scitranslmed.3001180
62. Apel F, Andreeva L, Knackstedt LS, Streeck R, Frese CK, Goosmann C, et al. The Cytosolic DNA Sensor cGAS Recognizes Neutrophil Extracellular Traps. *Sci Signaling 14 Eaax7942* (2021) 14:eaax7942. doi: 10.1126/scisignal.aax7942
63. GUO Z, PENG H, KANG J, SUN D. Cell-Penetrating Peptides: Possible Transduction Mechanisms and Therapeutic Applications. *BioMed Rep* (2016) 4:528–34. doi: 10.3892/br.2016.639
64. Ruseska I, Zimmer A. Internalization Mechanisms of Cell-Penetrating Peptides. *Beilstein J Nanotechnol* (2020) 11:101–23. doi: 10.3762/bjnano.11.10
65. Brubaker SW, Bonham KS, Zanoni I, Kagan JC. Innate Immune Pattern Recognition: A Cell Biological Perspective. *Annu Rev Immunol* (2015) 33:257–90. doi: 10.1146/annurev-immunol-032414-112240
66. Ragland SA, Kagan JC. Cytosolic Detection of Phagosomal Bacteria-Mechanisms Underlying PAMP Exodus From the Phagosome Into the Cytosol. *Mol Microbiol* (2021) 116:1420–32. doi: 10.1111/mmi.14841
67. Trindade BC, Chen GY. NOD1 and NOD2 in Inflammatory and Infectious Diseases. *Immunol Rev* (2020) 297:139–61. doi: 10.1111/imr.12902
68. Lee J, Tattoli I, Wojtal KA, Vavricka SR, Philpott DJ, Girardin SE. pH-Dependent Internalization of Muramyl Peptides From Early Endosomes Enables Nod1 and Nod2 Signaling. *J Biol Chem* (2009) 284:23818–29. doi: 10.1074/jbc.M109.033670

69. Nakamura N, Lill JR, Phung Q, Jiang Z, Bakalarski C, de Mazière A, et al. Endosomes are Specialized Platforms for Bacterial Sensing and NOD2 Signalling. *Nature* (2014) 509:240–4. doi: 10.1038/nature13133
70. Hu Y, Song F, Jiang H, Nuñez G, Smith DE. SLC15A2 and SLC15A4 Mediate the Transport of Bacterially Derived Di/Tripeptides To Enhance the Nucleotide-Binding Oligomerization Domain-Dependent Immune Response in Mouse Bone Marrow-Derived Macrophages. *J Immunol* (2018) 201:652–62. doi: 10.4049/jimmunol.1800210
71. Canton J, Schlam D, Breuer C, Gütschow M, Glogauer M, Grinstein S. Calcium-Sensing Receptors Signal Constitutive Macropinocytosis and Facilitate the Uptake of NOD2 Ligands in Macrophages. *Nat Commun* (2016) 7:1–12. doi: 10.1038/ncomms11284
72. He W, Wan H, Hu L, Chen P, Wang X, Huang Z, et al. Gasdermin D is an Executor of Pyroptosis and Required for Interleukin-1β Secretion. *Cell Res* (2015) 25:1285–98. doi: 10.1038/cr.2015.139
73. Cheng KT, Xiong S, Ye Z, Hong Z, Di A, Tsang KM, et al. Caspase-11–Mediated Endothelial Pyroptosis Underlies Endotoxemia-Induced Lung Injury. *J Clin Invest* (2017) 127:4124–35. doi: 10.1172/JCI94495
74. Piras S, Furfaro AL, Domenicotti C, Traverso N, Marinari UM, Pronzato MA, et al. RAGE Expression and ROS Generation in Neurons: Differentiation Versus Damage. *Oxid Med Cell Longev* (2016) 2016:9348651. doi: 10.1155/2016/9348651
75. Yao D, Brownlee M. Hyperglycemia-Induced Reactive Oxygen Species Increase Expression of the Receptor for Advanced Glycation End Products (RAGE) and RAGE Ligands. *Diabetes* (2010) 59:249–55. doi: 10.2337/db09-0801
76. Wautier MP, Chappey O, Corda S, Stern DM, Schmidt AM, Wautier JL, et al. Activation of NADPH Oxidase by AGE Links Oxidant Stress to Altered Gene Expression *via* RAGE. *Am J Physiol Endocrinol Metab* (2001) 280:E685–94. doi: 10.1152/ajpendo.2001.280.5.E685
77. Meunier E, Dick MS, Dreier RF, Schürmann N, Kenzelmann Broz D, Warming S, et al. Caspase-11 Activation Requires Lysis of Pathogen-Containing Vacuoles by IFN-Induced GTPases. *Nature* (2014) 509:366–70. doi: 10.1038/nature13157
78. Finethy R, Luoma S, Orench-Rivera N, Feeley EM, Haldar AK, Yamamoto M, et al. Inflammasome Activation by Bacterial Outer Membrane Vesicles Requires Guanylate Binding Proteins. *mBio* (2017) 8:e01188–17. doi: 10.1128/mBio.01188-17
79. Fisch D, Bando H, Clough B, Hornung V, Yamamoto M, Shenoy AR, et al. Human GBP1 is a Microbe-Specific Gatekeeper of Macrophage Apoptosis and Pyroptosis. *EMBO J* (2019) 38:e100926. doi: 10.15252/embj.2018100926
80. Wandel MP, Kim BH, Park ES, Boyle KB, Nayak K, Lagrange B, et al. Guanylate-Binding Proteins Convert Cytosolic Bacteria Into Caspase-4 Signaling Platforms. *Nat Immunol* (2020) 21:880–91. doi: 10.1038/s41590-020-0697-2
81. Santos JC, Boucher D, Schneider LK, Demarco B, Dilucca M, Shkarina K, et al. Human GBP1 Binds LPS to Initiate Assembly of a Caspase-4 Activating Platform on Cytosolic Bacteria. *Nat Commun* (2020) 11:3276. doi: 10.1038/s41467-020-16889-z
82. Santos JC, Broz P. Sensing of Invading Pathogens by GBPs: At the Crossroads Between Cell-Autonomous and Innate Immunity. *J Leuk Biol* (2018) 104:729–35. doi: 10.1002/JLB.4MR0118-038R
83. Yang J, Hwang I, Lee E, Shin SJ, Lee EJ, Rhee JH, et al. Bacterial Outer Membrane Vesicle-Mediated Cytosolic Delivery of Flagellin Triggers Host NLRC4 Canonical Inflammasome Signaling. *Front Immunol* (2020) 11. doi: 10.3389/fimmu.2020.581165
84. Tenthorey JL, Haloupek N, López-Blanco JR, Grob P, Adamson E, Hartenian E, et al. The Structural Basis of Flagellin Detection by NAIP5: A Strategy to Limit Pathogen Immune Evasion. *Science* (2017) 358:888–93. doi: 10.1126/science.aao1140
85. Saftig P, Klumperman J. Lysosome Biogenesis and Lysosomal Membrane Proteins: Trafficking Meets Function. *Nat Rev Mol Cell Biol* (2009) 10:623–35. doi: 10.1038/nrm2745
86. Idone V, Tam C, Andrews NW. Two-Way Traffic on the Road to Plasma Membrane Repair. *Trends Cell Biol* (2008) 18:552–9. doi: 10.1016/j.tcb.2008.09.001
87. Roy D, Liston DR, Idone VJ, Di A, Nelson DJ, Pujol C, et al. A Process for Controlling Intracellular Bacterial Infections Induced by Membrane Injury. *Science* (2004) 304:1515–8. doi: 10.1126/science.1098371

Conflict of Interest: The authors declare that the research was conducted in the absence of any commercial or financial relationships that could be construed as a potential conflict of interest.

frontiers | Frontiers in Immunology

ORIGINAL RESEARCH
published: 28 July 2022
doi: 10.3389/fimmu.2022.892114

Susceptibility to Infections During Acute Liver Injury Depends on Transient Disruption of Liver Macrophage Niche

Mateus Eustáquio Lopes[1*], *Brenda Naemi Nakagaki*[1†], *Matheus Silvério Mattos*[1†], *Gabriel Henrique Campolina-Silva*[2,3], *Raquel de Oliveira Meira*[4], *Pierre Henrique de Menezes Paixão*[4], *André Gustavo Oliveira*[5], *Lucas D. Faustino*[6], *Ricardo Gonçalves*[4] *and Gustavo Batista Menezes*[1*]

[1] Center for Gastrointestinal Biology, Departamento de Morfologia, Instituto de Ciências Biológicas, Universidade Federal de Minas Gerais (UFMG), Belo Horizonte, Brazil, [2] Department of Biochemistry and Immunology, Instituto de Ciências Biológicas, Universidade Federal de Minas Gerais (UFMG), Belo Horizonte, Brazil, [3] Centre de Recherche du Centre Hospitalier Universitaire de Québec, Université Laval, Québec, QC, Canada, [4] Macrophage and Monocyte Biology Laboratory, Department of Pathology, Instituto de Ciências Biológicas, Universidade Federal de Minas Gerais (UFMG), Belo Horizonte, Brazil, [5] Department of Physiology and Biophysics, Instituto de Ciências Biológicas, Universidade Federal de Minas Gerais (UFMG), Belo Horizonte, Brazil, [6] Center for Immunology and Inflammatory Diseases, Division of Rheumatology, Allergy and Immunology, Massachusetts General Hospital, Harvard Medical School, Boston, MA, United States

Kupffer cells are the primary liver resident immune cell responsible for the liver firewall function, including clearance of bacterial infection from the circulation, as they are strategically positioned inside the liver sinusoid with intimate contact with the blood. Disruption in the tissue-resident macrophage niche, such as in Kupffer cells, can lead to a window of susceptibility to systemic infections, which represents a significant cause of mortality in patients with acetaminophen (APAP) overdose-induced acute liver injury (ALI). However, how Kupffer cell niche disruption increases susceptibility to systemic infections in ALI is not fully understood. Using a mouse model of ALI induced by APAP overdose, we found that Kupffer cells upregulated the apoptotic cell death program and were markedly reduced in the necrotic areas during the early stages of ALI, opening the niche for the infiltration of neutrophils and monocyte subsets. In addition, during the resolution phase of ALI, the remaining tissue macrophages with a Kupffer cell morphology were observed forming replicating cell clusters closer to necrotic areas devoid of Kupffer cells. Interestingly, mice with APAP-induced liver injury were still susceptible to infections despite the dual cellular input of circulating monocytes and proliferation of remaining Kupffer cells in the damaged liver. Therapy with bone marrow-derived macrophages (BMDM) was shown to be effective in occupying the niche devoid of Kupffer cells following APAP-induced ALI. The rapid BMDM migration to the liver and their positioning within necrotic areas enhanced the healing of the tissue and restored the liver firewall function after BMDM therapy. Therefore, we showed that disruption in the Kupffer cell niche and its

OPEN ACCESS

Edited by:
Andrea Baragetti,
University of Milan, Italy

Reviewed by:
Cheryl Rockwell,
Michigan State University, United States
Fabrizia Bonacina,
University of Milan, Italy
Mattia Albiero,
Università degli Studi di Padova, Italy

***Correspondence:**
Mateus Eustáquio Lopes
mateusedml@gmail.com
Gustavo Batista Menezes
menezesgb@ufmg.br

[†]These authors have contributed equally to this work

Specialty section:
This article was submitted to Inflammation, a section of the journal Frontiers in Immunology

Received: *08 March 2022*
Accepted: *20 June 2022*
Published: *28 July 2022*

Citation:
Lopes ME, Nakagaki BN, Mattos MS, Campolina-Silva GH, Meira RO, Paixão PHM, Oliveira AG;, Faustino LD, Gonçalves R and Menezes GB (2022) Susceptibility to Infections During Acute Liver Injury Depends on Transient Disruption of Liver Macrophage Niche. Front. Immunol. 13:892114. doi: 10.3389/fimmu.2022.892114

impaired function during acute liver injury are key factors for the susceptibility to systemic bacterial infections. In addition, modulation of the liver macrophage niche was shown to be a promising therapeutic strategy for liver injuries that reduce the Kupffer cell number and compromise the organ function.

Keywords: Kupffer cell, Macrophage niche, Acute liver injury, Inflammation, Cell therapy, Systemic infection

INTRODUCTION

The liver is a complex organ that plays a pivotal role in body physiology. Liver resident macrophages, named Kupffer cells (KCs), are an essential liver component (1, 2), comprising one of the largest tissue-resident macrophage populations in adult mammals (3–5). These cells originate from erythro-myeloid progenitor from yolk-sac, migrate to the fetal liver during embryogenesis where they further differentiate, and become mature macrophages after birth (6–8). During adulthood, hepatic tissue factors, such as macrophage colony-stimulating factor (CSF-1), TGF-β, and desmosterol, maintain the KCs niche within the liver (9, 10). These tissue factors are responsible for preserving the population pool by self-renewal with minimal input from the circulating monocytes (11). In addition, the strategic positioning of KCs inside the liver sinusoids, promoting direct contact with the circulation, is a fundamental feature for iron recycling, lipid metabolism, debris removal, as well as phagocytosis and elimination of circulating or gut-derived pathogens (1). However, such KCs niche might be disrupted in several liver inflammatory conditions, and those functions might be ultimately lost (12–15).

Acetaminophen (APAP) overdose is the leading cause of acute liver injury (ALI) in humans (16, 17). The hepatotoxic effects of APAP bioactivation involve the accumulation of N-acetyl-p-benzoquinone imine (NAPQI) inside hepatocytes, which drive a harmful intracellular oxidative stress response, leading to necrotic hepatocyte death and release of damage-associated patterns (DAMPs), such as DNA, histones, and HMGB1 (18). APAP overdose induces a robust inflammatory response in the liver dominated by an influx of neutrophils and subtypes of myeloid cells. Neutrophils are the predominant immune cell type in the first hours and have been described to be directly involved in the increase in tissue damage (18, 19). Also, ALI leads to a massive reduction in the KCs population, causing a major impairment in the liver firewall function (20, 21). Concomitantly, circulating monocytes are recruited to the liver in a time-dependent manner. Infiltration of the pro-inflammatory monocyte subset, characterized by the expression of the glycoprotein Ly6C, is thought to amplify ALI in early stages (22), whereas - at a later time point - a pro-resolutive monocyte subset ($Ly6C^-$) is thought to restrains the inflammatory response, which is a crucial step to in restoring liver homeostasis (20, 23). Although the recruitment of inflammatory cells is critical for tissue repair, uncontrolled inflammation can evolve to a systemic inflammatory response and, ultimately, acute liver failure (ALF) (24). Such disease outcomes are problematic as therapeutic options for APAP-induced liver injury are very limited. Administration of N-acetylcysteine (NAC) is the only treatment available, but its efficacy is limited to the first 12h after APAP overdose (16, 24). As an aggravating factor for the lack of treatment, patients with ALF are often affected by systemic infections, which result in increased mortality and morbidity rates (24–26).

The reduction in the KC population and their functional impairment during ALI is a strong candidate for the increased mortality rates in these patients (20, 21, 27). Despite the rapid recruitment of monocytes in the acute phase of the lesion, several immune-related liver functions are severely impaired (27). In addition, the dynamics of the KC niche and how these cells are recovered after organ damage are still unclear. It is well accepted that infiltrating monocytes can differentiate into liver resident macrophages in the resolution phase of liver injuries (12, 28). On the other hand, the remaining KCs may also contribute to a new macrophage pool through proliferation in the resolution phase (20). Also, the program for the liver macrophage niche replacement seems to depend on the type of inflammation, and the extension of reduction in the KC population, impacting ultimately the kinetics of the organ return to homeostasis (29). Considering that the major part of these risks arises from a malfunction of resident macrophages, therapy with bone marrow-derived macrophages (BMDM) emerges as a potential therapy for ALI (30). In fact, it has been demonstrated that intravenous injection of BMDM rescues liver fibrosis, promoting a proper healing response after chronic injuries (31). Also, it has been shown that therapy with BMDM that were polarized to an alternative activation profile accelerates and improves the resolution phase of ALI and reduces liver failure. In this case, newly transferred macrophages displayed high phagocytic capacity and released pro-regenerative mediators (32), although the effects of BMDM therapy on the acute phase of ALI or ALF remain elusive.

In this work, we hypothesized that transient disruption in the Kupffer cell niche during ALI is responsible for the susceptibility to systemic infections. We revealed that APAP-mediated liver damage led to a massive KCs apoptosis and death, which triggered time-dependent recruitment of monocyte subsets that transiently occupied the empty KC niche. We showed that proliferation of KCs and infiltration of monocyte-derived macrophages restored the hepatic macrophage population following ALI and remained in the liver during the organ healing phase. Notably, during KC niche disruption and transient liver macrophage recovery create an open window for systemic infections, shown by increased circulating bacteria after infection. Ultimately, by employing a BMDM therapy to accelerate hepatic macrophage niche occupation, we found that

transferred BMDM were strategically positioned in the necrotic areas of the liver, where KCs were absent during ALI. These engrafted BMDM partially restored the liver bacterial clearance ability, which was lost in the acute phase of the acute liver injury model.

MATERIALS AND METHODS

Mice

C57BL/6J female mice aged 8-10 weeks were acquired from Centro de Bioterismo do Instituto de Ciências Biológicas – UFMG (CEBIO/UFMG). CX3CR1$^{+/GFP^+}$CCR2$^{+/rfp}$ 8-10 weeks of old female mice were obtained from the animal facility of Laboratório de Imunofarmacologia - ICB/UFMG crossing the CX3CR1$^{GFP^+}$/GFP$^+$ (B6.129P(Cg)-*Cx3cr1^{tmLitt}*/J) mice with CCR2$^{rfp/rfp}$ (B6.129S4-*Ccr2^{tm1lfc}*/J). LysM$^{+/cre}$Rosa26$^{+/tdTomato}$ female mice of 4-6 weeks were obtained from the animal facility of Laboratório de Imunofarmacologia - ICB/UFMG crossing the LysM$^{cre/cre}$ (B6.129P2-*Lys2$^{tm1(cre)lfo}$*/J) with the Rosa26$^{tdTomato/tdTomato}$ lineage (B6.Cg-*Gt(Rosa)26Sor$^{tm14(CAG-tdTomato)Hze}$*/J). Mice were kept in the animal facility of Laboratório de Imunofarmacologia - ICB/UFMG using mouse microisolator (Alesco, Monte Mor, SP, BR) under controlled conditions of temperature, 23°C, light/dark cycle of 12/12h with sterile water and food (Nuvilab, Curitiba, PR, BR) *ad libitum*. All procedures were approved by CEUA/UFMG 377/2016 and 076/2020 protocols.

Acute Liver Injury Model Induced by Acetaminophen Overdose

Mice were fasted for 15 hours before oral gavage of acetaminophen (APAP, Sigma-Aldrich-, St. Louis, MO, USA), 600mg/kg, or 0.9% saline solution (33). APAP was diluted in a pre-warmed saline solution. ALI kinetics was observed at 12, 24, 72 hours, 7, and 15 days post oral gavage to perform the following assays. The survival rate was checked in a 6 hours intervals from starting point to 15 days.

Histopathologic Analysis

Liver fragments were collected for histology. The tissue was fixed in 4% paraformaldehyde in phosphate buffer saline (PBS, Sigma-Aldrich), then dehydrated in alcohol and embedded in paraffin. Sections of 4μm thicknesses were stained for hematoxylin and eosin (H&E). Images were acquired using a 4x objective lens in a Nikon Ti A1R microscope (Nikon, Shinagawa, Tokyo, Japan).

Alanine Aminotransferase (ALT) Assay

Serum alanine aminotransferase (ALT) activity was performed using a kinetic test (Bioclin, Belo Horizonte, MG, Brazil). Serum was acquired after blood harvest, followed by 1500x *g* 10 minutes centrifugation. Briefly, the enzymatic assay was performed in 96 well-plate (Corning, New York, NY, USA) where pure serum or sequentially dilute was added. Substrates and coenzymes provided and specified in the kit were added at 37°C after 1 min plate was read in a spectrophotometer (Versamax, Molecular Devices, San Jose, CA, USA) at 37°C every 1 min for 4 min.

Indocyanine Green Depuration Assay

The Indocyanine green (ICG, Sigma-Aldrich) assay measures the liver depuration capacity (34). Mice received a single intravenous injection of ICG (20mg/kg); 20 min later, blood samples were collected, and the serum was obtained following centrifugation 1500x *g* 10 minutes. ICG concentration was determined by spectrophotometry (Molecular Devices) at 800nm.

Liver Non-Parenchymal Cells Isolation

To isolate non-parenchymal cells (NPC), first, mice were anesthetized subcutaneously with a mixture of ketamine (60mg/kg, Syntec, Tamboré, SP, BR) and xylazine (15mg/kg, Syntec) then the blood was collected by exsanguination *via* the femoral vein. The peritoneal cavity was exposed, and the liver was harvested and fragmented into small pieces followed by enzymatic digestion with collagenase VII (1mg/ml, Sigma-Aldrich) in RPMI-1640 medium (Gibco, Billings, MT, USA) for 60 minutes in constant agitation at 37°C. Next, liver homogenates were filtered using a 70μm cell strainer to remove undigested tissue. Then, a series of differential centrifugation, 400x *g* 5 min, 60x *g* 3 min, 400x *g* 5 *min*, was performed. Finally, red blood cells were lysate Ammonium Chloride solution (ACK) for a clean NPC suspension. The cell suspension was counted, and 10^6 cells were used for the Flow Cytometry assay.

Flow Cytometry

NPCs suspension, when applied, was first stained for viability with Fixable Viability Stain 510, 1μL per million cells, for 15 minutes at room temperature. Then, the staining was performed for 30 min at 4°C using Fc block Fc-γ III/II CD16/32 (clone 2.4G2; BD Biosciences, Franklin Lakes, New Jersey, USA), anti-CD45 (clone 30-F11, BD Biosciences), anti-F4/80 (clone T45-2342, BD Biosciences), anti-CD11b (clone M1/70, BD Biosciences), anti-Ly6C (clone AL-21, BD Biosciences), anti-Ly6G (clone 1A8, BD Biosciences). Anti-Clec4F was not used to detect Kupffer cells because it was not reliable in intravital confocal microscopy. For cell death program staining, Annexin V (Biolegend, San Diego, CA, USA) and Propidium Iodide (Life Technologies, Carlsbad, CA, USA) staining was performed after surface staining as previously described (35). Finally, flow cytometry was performed using CytoFlex (Beckman Coulter, Indianapolis, IN, USA) or Accuri™ C6 (BD Biosciences).

Escherichia Coli Cultivation

The *Escherichia coli* transfected with a plasmid containing green fluorescent protein (GFP$^+$, ATCC®25922GFP$^+$) and Ampicillin dependent promoter was gently provided by Dr. Shirong Liu (Harvard Medical School, Boston, USA). First, the bacteria culture was performed using Luria-Bertani broth (Sigma-Aldrich) containing Ampicillin for 12 hours under agitation at 37°C. Next, the culture was washed at 1500x *g* for 15 min. Finally, bacterial amounts were determined by optical density at 600nm in the

spectrophotometer (Molecular Devices), being that OD_{600} = 1 corresponds to $8x10^8$ bacteria/ml.

Bacterial Challenging and Colony-Forming Units (CFU) Assay

Mice received *E. coli* GFP^+ $5x10^5$ bacteria/20g intravenously in 50µl. After the E. coli challenge, the control and 24 hours group survival rates were evaluated by monitoring mice every 3 hours for 30 hours. For CFU assay, 24 hours after the challenging mice were anesthetized, blood and liver were harvested, processed, and cultivated for 24h in Luria-Bertani agar (Sigma-Aldrich) containing ampicillin at 37°C. Next, CFUs were quantified, adjusting to blood volume (ml) and liver weight (g).

Blood Clearance Assay

To evaluate the bacterial removal from blood, mice received intravenously *E. coli* GFP^+ $5x10^6$ bacteria/20g in 50µl. After 5 min, mice were anesthetized, blood was collected from the hepatic vein diluted in PBS, and bacteria count was analyzed using Accuri™ C6 (BD Biosciences). The result was represented as the number of events per blood volume (µl).

Escherichia Coli Tracking in the Liver

The real-time behavior and displacement of *E. coli* GFP^+ were performed by tracking the bacteria in the liver using Intravital Microscopy. See the specific section for IVM. Briefly, mice placed in the microscope received $5x10^7$ bacteria/20g in 50µl after film acquisition started. Bacteria reach the liver in the first 20 seconds, and individualized events were followed for 5 minutes. The tracking of each *E. coli* GFP^+ was performed by the NIS-Elements Advanced Research software using the NIS.ai module (Nikon). The circular graph contains an internal circle of 400 µm and an outer circle of 800 µm.

Pharmacological Depletion of Kupffer Cells

Depletion of Kupffer cells was performed by intravenous injection of 50 µl, 125 µl, or 200 µl of Clodronate Liposomes (50mg/ml, Liposoma, Amsterdam, NL) (36) to achieve a depletion grade. The Control group received 0.9% saline solution in the same volumes. Flow Cytometry and Intravital Microscopy were used to accomplish the depletion. Mice were also submitted to blood clearance assay.

Intravital Microscopy

Intravital microscopy (IVM) of the liver is powerful in seeing the biological phenomena *in vivo* and in real-time (37). Here, the Nikon Ti A1R confocal microscope (Nikon) was used. Before the surgical procedure, mice, when specified, received anti-F4/80 (clone T45-2342, BD Biosciences), anti-CD31 (clone 390, Biolegend) intravenously, and waited 20 minutes. Then, when discriminated, immediately before the anesthesia, mice received intravenously Sytox green (250nmol/kg, Invitrogen, Waltham, MA, USA). Next, mice were anesthetized as previously described (Liver non-parenchymal cells isolation section), followed by a midline laparoscopy to expose the liver for imaging. Mice were placed over an acrylic plate and then adequately positioned in the microscope. Finally, the positive staining was confirmed by injecting proper isotypes controls (IgG) for each staining. Movies and images were acquired using the NIS-Elements Advanced Research software using the NIS.ai module (Nikon).

Immunofluorescence

Liver fragments were collected from the Control, 12, 24, and 72 hours groups and first, fixed overnight in PFA 4%, dehydrated in a sucrose gradient (10%-30%, weight/volume in PBS), and then embedded in Tissue-Tek ® O.C.T compound (Sakura, Torrance, CA, USA). Cryosections of 15µm thickness were generated for each sample. For immunostaining, cryosections were permeabilized with 0.5% Triton X-100/PBS for 15 min and then incubated for 1 hour in the blocking solution (PBS containing 5% goat serum and 5 µg/ml mouse BD Fc Block). Targets were labeled overnight at 4°C using rat anti-F4/80 (clone T45-2342, BD Biosciences), rabbit anti-cleaved caspase 3 (clone 5A1, Cell Signaling Technology, Danvers, MA, USA), rabbit anti-Ki67 (Abcam, Cambridge, UK) primary antibodies, diluted 1:100 in PBS containing 0.05% Triton X-100. After washing in PBS, sections were incubated for 90 min at room temperature with the Alexa Fluor 488 conjugated goat anti-rabbit antibody (polyclonal, Invitrogen) at 1:200 dilution in PBS. Cell nuclei were stained with 4′,6-diamidino-2-phenylindole (DAPI, Sigma-Aldrich). Images were acquired using the Nikon Ti A1R confocal microscope (Nikon) and the NIS-Elements Advanced Research software (Nikon).

Bone Marrow-Derived Macrophages Culture and Activation

Bone marrow precursors were harvested from femurs of LysM-TdTomato and wild-type mice, washed and differentiated into macrophages in a culture dish containing DMEM-F12 (Gibco) supplemented with 10% FBS (Gibco), 2mM of L-glutamine (Gibco), 100 µg/ml streptomycin (Gibco), 100 U/l penicillin (Gibco), 25mM HEPES (Sigma-Aldrich), and 20% of supernatant from L929 cell culture as previously described (38). After 7 days of differentiation at 37°C, 5% CO_2 incubator, cells were harvested and stimulated overnight with IL-4 (20ng/ml, Peprotech, Rocky Hill, NJ, USA) to achieve the alternative activation (BMDM A.A). The activation status was analyzed by mRNA expression using real-time PCR.

Analysis of mRNA Expression by Real-Time PCR

Total mRNA was extracted from BMDM, steady-state (BMDM ϕ) and alternatively activated (BMDM A.A) after overnight incubation using the ReliaPrep RNA Miniprep System (Promega, Madison, WI, USA) following the kit instructions. Then, total mRNA was quantified using a Nanodrop Lite (Thermo Fisher, Waltham, MA, USA) followed by reverse transcription using the iScript cDNA Synthesis kit (Bio-rad, Hercules, CA, USA) in a Rotor-Gene Q (Qiagen, Hilden, Germany) using manufacturer's instructions. The amplification was performed using the Rotor-Gene Q (Qiagen), and the results were analyzed by the comparative threshold cycle method using $2^{-\Delta\Delta CT}$ to determine the fold increase. Evaluated genes and their

TABLE 1 | Primers sequence.

Gene	Foward	Reverse
actinb	5'-AGGTGTGCACCTTTTATTGGTCTCAA-3'	5'-TGTATGAAGGTTTGGTCTCCCT-3'
chil3	5'-AGAAGGGAGTTCAAACCTGGT-3'	5'-GTCTTGCTCATGTGTGTAAGTGA-3'
rentla	5'-AATCCAGCTAACTATCCCTCCA -3'	5'-CAGTAGCAGRCATCCCAGCA-3'
arg1	5'-CTGGCAGTTGGAAGCATCTCT-3'	5'-CTGGCAGTTGGAAGCATCTCT-3'

sequences are described in **Table 1**. Each gene expression was normalized to *actinb* (β-actin) mRNA expression as endogenous control and non-stimulated cells (BMDM ϕ).

Cell Therapy

Mice in the Acute Liver Injury model received the BMDM cell therapy intravenously 16 hours after APAP overdose. Cell suspension, $1x10^6$ cells in 100 µl, were administrated by orbital plexus that allows the rapid delivery to the liver (Data not shown, patronized by fluorescent beads administration). PBS was used as a vehicle, and the Control group received its volume. Flow Cytometry confirmed the cell delivery. Finally, control, 24 hours, BMDM ϕ, and BMDM A.A were analyzed at 24 hours after lesion induction (8 hours after treatment) by Flow Cytometry, Liver Histology, Intravital Microscopy, and Blood clearance assay.

Data and Statistical Analysis

Biochemical assays were analyzed using SoftMax v5.4.1 (Molecular Devices). The NIS-Elements Advanced Research software was used to analyze and export all image, movie, and 3D data. The videos were generated using Sony Vegas Pro 16 (Sony, Tokyo, Japan). The Flow cytometry data were analyzed using FlowJo v10 (BD Biosciences). Data were analyzed using GraphPad Prism 8.0 (GraphPad Software, San Diego, CA, USA) and submitted for normality testing. The parametric data were shown as mean ± SEM and non-parametric as Median ± SD. In two-group comparisons, t-student or Mann-Whitney tests were performed. For kinetic or multiple groups assays, we performed One-way Anova followed by Tukey post-test in parametric data and Kruskal-Wallis followed by Dunn's multiple comparison test for non-parametric data. Differences were considered statistically significant when $p < 0.05$.

RESULTS

APAP Overdose Induces Liver Damage and Alteration in Myeloid Cell Composition

Acetaminophen (APAP) is one of the most common causes of human acute liver injury and acute liver failure that can result in death (24). Here, we used a well-established mouse model of acute liver injury (ALI) (16, 33, 39) to investigate alterations in the myeloid cell compartment during liver damage. To induce ALI, C57BL/6 female mice were fasted for 15h and given oral gavage with 600 mg/kg of APAP diluted in warm saline **(Figure 1A).** In this model, APAP led to a 25% mortality in the first 24h **(Figure 1B)**, a similar mortality rate (28%) found in human acute liver failure induced by APAP overdose (24). Liver histopathology showed extensive necrotic areas during the acute phase, between 12h and 24h, followed by significant tissue regeneration after 72h of APAP administration, as indicated by the arrows in the respective histological sections of the liver **(Figure 1C)** and histopathologic score **(Figure 1D)**. According to liver histopathology, mice showed increased serum alanine aminotransferase (ALT) levels in the acute phase, which returned to baseline levels 72h after APAP administration and remained undetectable thereafter **(Figure 1E)**. The tissue damage caused by APAP overdose led to an impairment in liver function measured by an increase in indocyanine green (ICG) in the serum due to a reduced depuration rate 24h after APAP administration **(Figure 1F)**. Following 72h, the serum ICG levels were reduced to similar levels found in the non-treated control group **(Figure 1F)** in line with the regenerative process of the disease (24, 39, 40). To get an insight into the impact of the inflammatory response in the myeloid cell compartment, we assessed the influx of neutrophils in the liver and changes in the myeloid cell populations, including liver resident Kupffer cells (KCs), monocyte subsets **(Supplementary Figure 1A)**. We found that, during the acute phase of APAP overdose, the liver underwent a massive reduction of KCs, which was associated with a pronounced liver neutrophil infiltration and a significant increase in the $Ly6C^{hi}$ monocytes and a slight decrease in $Ly6C^{lo}$ monocytes **(Figure 1G** and **Supplementary Figure 1B)**. Taken together, our mouse model of ALI induced by APAP overdose was consistent with the human ALI disease outcome, showing induction of tissue damage and liver dysfunction associated with neutrophilic inflammation and substantial changes in liver myeloid cell composition.

Reduction in Kupffer Cell Population During ALI Disrupts an Essential Niche in the Liver

Kupffer cells represent the biggest tissue-resident macrophage niche in adult mammals (5). These cells play a diverse and essential role in the liver, including iron metabolism and removal of gut-derived pathogens (2). Given the essential role of KCs in liver physiology and function, we characterized their phenotype, morphology, and positioning in liver-specific niche during the induction, progression and regeneration of the liver damage induced by APAP overdose. To visualize the alterations in the KCs morphology in a liver-specific niche during ALI, we used intravital microscopy of the liver in mice previously injected i.v. with fluorescent monoclonal antibodies (mAb) targeting the macrophage surface marker F4/80, as well as necrotic cells (DNA labeling by Sytox green) and liver vasculature using anti-CD31. **(Supplementary Figure 2A)**. Unbiased quantification of the

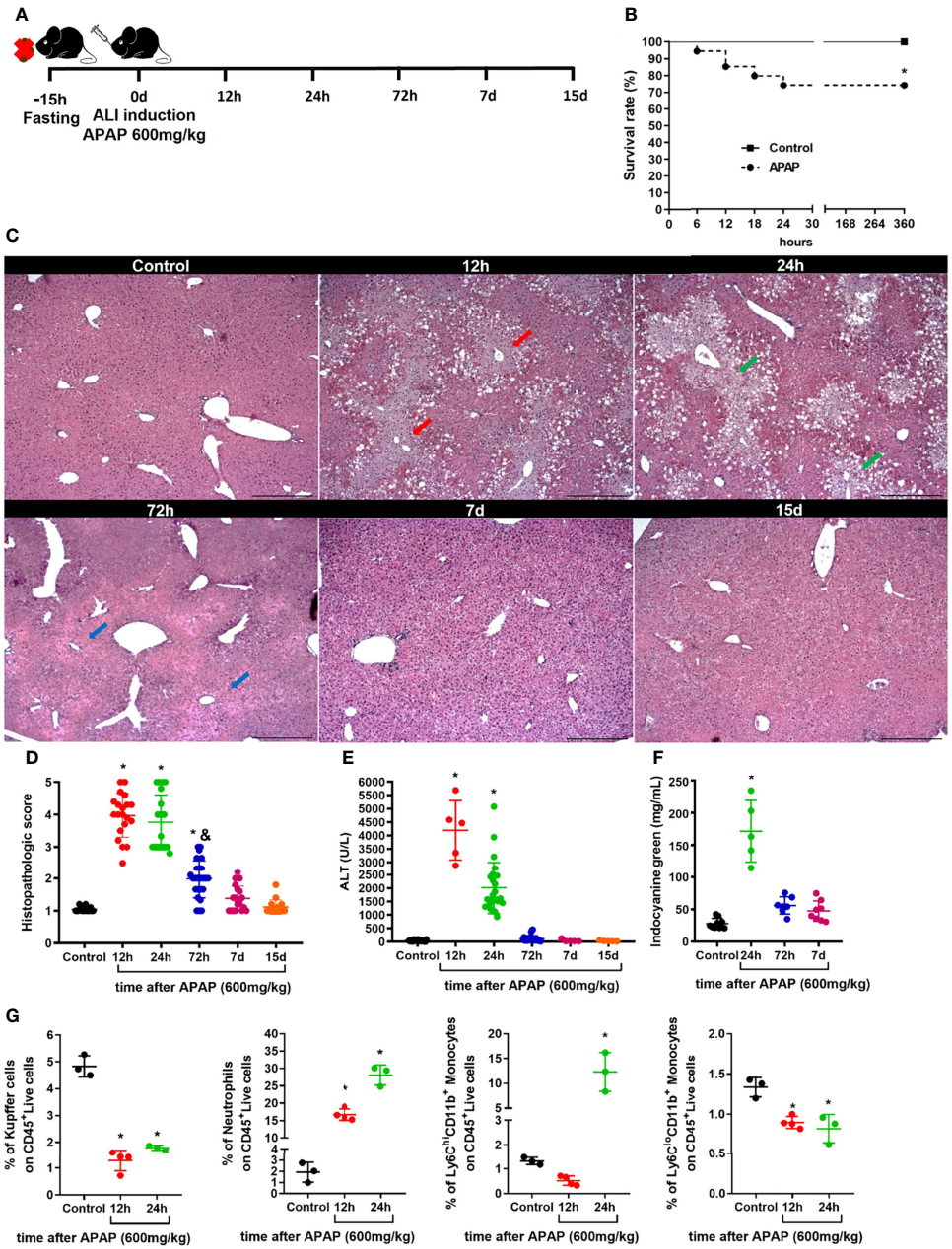

FIGURE 1 | Acute liver injury induced by APAP overdose induces tissue damage and myeloid cell alterations. **(A)** Scheme for Acute Liver Injury (ALI) induced by Acetaminophen (APAP; 600mg/kg) overdose on 8-10 weeks old C57BL/6J mice. **(B)** Mice survival rate (%) after ALI induction; n ≥ 9 mice per group. **(C)** Representative liver histology of ALI kinetics stained with Hematoxylin and Eosin (H&E); scale bar = 500 µm. **(D)** Time-course of ALI tissue damage measured by the histopathologic score of liver sections; n = 8-15 mice per group. **(E)** Measurement of liver injury by serum levels of alanine aminotransferase (ALT); n = 5-15 mice per group. **(F)** Liver dysfunction showed by indocyanine green depuration from the serum; n = 5-9 mice per group. **(G)** Percentage (%) of different populations of myeloid cells within the $CD45^+$ live cell pool during acute liver inflammation obtained by flow cytometry; n = 3-5 mice per group; Representative of 3 independent experiments. Data are presented as mean ± SEM. * indicates statistical difference to the control group using Mantel-Cox survival test **(B)** and one-way ANOVA followed and Tukey post-test **(D-G)** (* = $p < 0.05$). & indicates statistical difference compared to the 24h group using one-way ANOVA followed and Tukey post-test (& = $p < 0.05$).

KC morphology did not find a significant difference in KCs area (**Supplementary Figure 2B**), length (**Supplementary Figure 2C**), elongation (**Supplementary Figure 2D**), and circularity (**Supplementary Figure 2D**) during the course of ALI. At steady-state, the liver parenchyma (blue, autofluorescence to 405nm laser) and the vasculature (white) was healthy with $F4/80^+$ KCs (red) located inside the vasculature with projections to parenchyma (**Figure 2A** and

Supplementary Figure 3). In contrast, ALI was characterized by necrosis of the parenchyma after 12h and 24h of APAP overdose characterized by marked deposition of extracellular DNA in the necrotic areas (**Figure 2A**). Moreover, both the liver vasculature structure and KCs were dramatically disrupted, especially in the necrotic areas (**Figure 2A**). Seventy-two hours after APAP administration, the extracellular DNA deposition was completely cleared while the numbers of KCs and the liver parenchyma and vasculature structure started to show a process of restoration when compared to the Control group (**Figures 2A, B**). On days 7 and 15 after ALI induction, all parameters resembled the Control group (**Figures 2A, B**). These data demonstrate that APAP overdose causes a transient disruption in specific liver

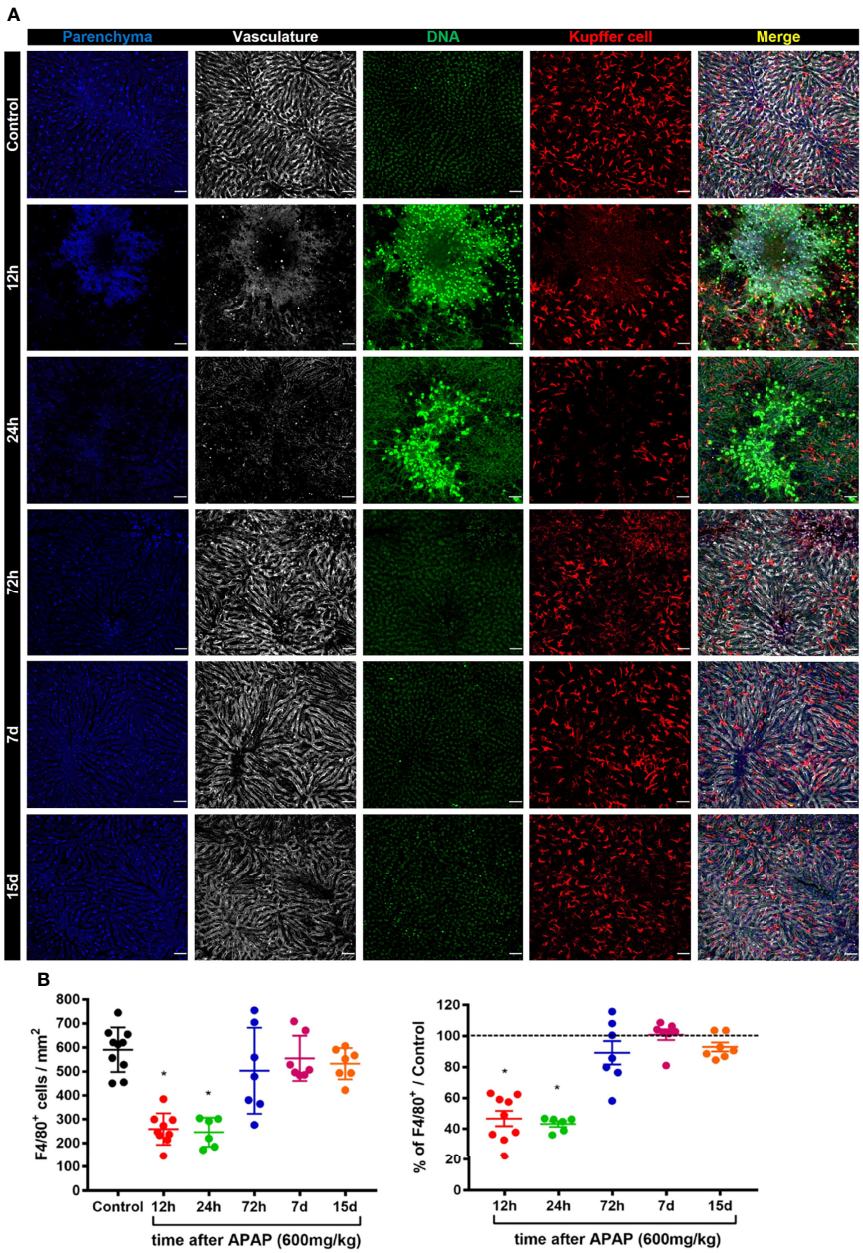

FIGURE 2 | ALI causes a dramatic reduction in the Kupffer cell population and disrupts an essential niche in the liver. **(A)** Representative intravital microscopy (IVM) images acquired during ALI to characterize liver architecture and Kupffer cell population; Parenchyma is represented by liver auto-fluorescence (blue); Vasculature is stained by anti-CD31 PE antibody (white); Kupffer cell is stained by anti-F4/80 APC (red); DNA is stained Sytox green (green). Representative of 2 independent experiments; scale bar = 50 μm. **(B)** Kupffer cell quantification (Left panel) and the percentage based on Control (Right panel; —— = 100%); n ≥ 5 mice per group and 10 images per mice. Data are presented as mean ± SD. * indicates statistical difference compared to the control group using one-way ANOVA followed and Tukey post-test (* = $p < 0.05$).

niches with a reduction in the number of KC during ALI, which can lead to increased susceptibility to infections.

To better understand the biology of the KC disappearance in liver-specific niches during ALI, we investigate the cell death program of KCs. We first assessed whether KCs underwent apoptosis and cell death by flow cytometry using Annexin V and Propidium iodide (PI) staining of F4/80$^+$ cells in the liver **(Supplementary Figure 4A)**. We found an increase in the percentage of apoptotic cells (Annexin V$^+$PI$^-$) 12h and 24h after APAP overdose and in the percentage of necrotic (Annexin V$^-$PI$^+$) and necroptotic cells (Annexin V$^+$PI$^+$) at 12h. **(Figure 3A)**. As expected, there was a reduction of live (Annexin V$^-$PI$^-$) F4/80$^+$ cells at 12h and 24h of ALI **(Figure 3A)**. Furthermore, immunofluorescence of the liver for cleaved Caspase-3 (green), an intracellular cascade activated in cells undergoing apoptosis (41), revealed the activation of the apoptotic program in F4/80$^+$ KC (red) in the first 12h and 24h of ALI **(Figure 3B)** and a significant increase in Caspase-3$^+$ KC in the liver compared to the Control group **(Figure 3C)**. Therefore, Kupffer cell disappearance observed in ALI following APAP overdose occurs through an induction of an apoptotic and cell death program.

A dual-input of cells occupies the liver macrophage niche during the resolutive phase

In homeostasis, liver macrophage niche maintenance occurs by self-renewal of the KCs with minimal input of monocyte-derived macrophages (11). However, monocyte-derived macrophages can contribute to niche recovery after a reduction in the KCs population (9). In **Figure 2** we showed that the KC niche starts to recover 72h after APAP overdose. During intravital microscopy imaging of the liver, we often observed the presence of cell clusters being formed in the resolutive stage, 72h after APAP overdose, with significant amounts of KC clusters (F4/80$^+$ cells) per field of view **(Figure 4A)**. Therefore, KCs self-renewal was initially analyzed to address its contribution to the niche recovery. To do so, KCs proliferation was assessed by analysis of the intracellular marker of active cell proliferation Ki67 by immunofluorescence of the liver. Replicating Ki67$^+$ KCs were detected 72h after APAP overdose with a significant increase over the Control **(Figures 4B, C)**, indicating a contribution of self-renewing Kupffer cells to niche recovery. Next, we looked at the monocyte infiltration and their positioning in the liver during ALI, as they could contribute to niche replacement as monocyte-derived macrophages. As previously described, there is a phenotypic and functional transition of different subtypes of monocytes until they reach the Kupffer cell niche and differentiate into monocyte-derived macrophages after ALI (20) or myeloid cell depletion (9). To investigate the monocytic transition and location during ALI, we used dual reporter CX3CR1$^{+/GFP^+}$CCR2$^{+/rfp}$ mice in our mouse model of ALI induced by the APAP overdose **(Figure 4D)**. As expected, APAP administration led to an increased serum ALT levels, a sign of liver injury, at 24h, which returns to basal levels at 72h post-APAP overdose **(Figure 4E)**. Intravital microscopy analysis of CX3CR1$^{+/GFP^+}$CCR2$^{+/rfp}$ mice also showed considerable parenchyma damage (blue) indicating necrotic areas after 24h of APAP overdose **(Figure 4F)**, similar to our findings in wild-type mice in **Figure 2**. More interestingly, there was an extensive infiltration of inflammatory monocytes (CX3CR1$^-$CCR2$^+$) and patrolling monocytes (CX3CR1$^+$CCR2$^-$) and fewer monocytes with a transitory phenotype (CX3CR1$^+$CCR2$^+$) in the liver after 24h **(Figures 4F, G)**. Seventy-two hours after APAP overdose, we observed a significant reduction in the inflammatory monocyte population compared to the acute phase, at 24h, while the transitory and patrolling monocyte populations were unaltered **(Figures 4F, G)**. It is worth highlighting that these different monocyte populations found in the acute and resolution phase were positioned in the necrotic areas represented by disrupted parenchyma **(Figure 4F)**. Moreover, we did not find KCs within the necrotic areas. Therefore, in addition to the proliferation of remaining KC (Ki67$^+$ KC), monocytes strategically located in damaged areas can give rise to new macrophages during ALI, supporting the notion of a KCs/monocyte-derived macrophage dual-input in liver regeneration.

Liver firewall function is impaired during ALI, increasing the susceptibility to bacterial infections

Liver firewall function is one of the primary immunological functions of the liver, which consist of removing gut-derived compounds, exogenous molecules, or pathogens from the bloodstream (42). Indeed, it has been reported that patients diagnosed with ALI often develop systemic infection by bacteria or fungi (25), indicating an impairment of liver function. Thus, we hypothesized that disruption of the hepatic tissue and myeloid cell niche alteration could increase the susceptibility to infections. To test this hypothesis, mice were challenged with intravenous injection of *E. coli* expressing GFP$^+$ during ALI **(Figure 5A)**. First, we measured the mortality rate in mice injected with a low dose of *E. coli* (5x10^5 bacteria/20g) without or with APAP overdose. While 100% of mice without APAP administration survived after *E. coli* infection, we found a 40% mortality rate in mice treated with APAP, showing increased susceptibility to systemic infection in the APAP overdose group **(Figure 5B)**. Next, we addressed the ability of the liver to clear circulating *E. coli*. To do so, mice treated with APAP overdose were injected with 5x10^5 *E. coli*/20g in different time points (12h, 24h, 72h, 7d, and 15d) and, 24h later, a CFU assay was performed. CFUs were only detected in blood samples from mice 12h and 24h after APAP overdose when liver injury peaks **(Figure 5C).** Accordingly, liver samples from 12h and 24h post-APAP overdose groups displayed the highest increase in CFU **(Figure 5D)**, indicating an inability to control the bacterial growth. Surprisingly, 72 hours and 7 days post-APAP overdose, when both liver ALT and histopathology were diminished or returned to baseline, we still detect enhanced CFUs in the liver **(Figure 5D)**, suggesting that an extended period might be necessary for the hepatic immune system to return into homeostasis as observed when mice were infected at day 15.

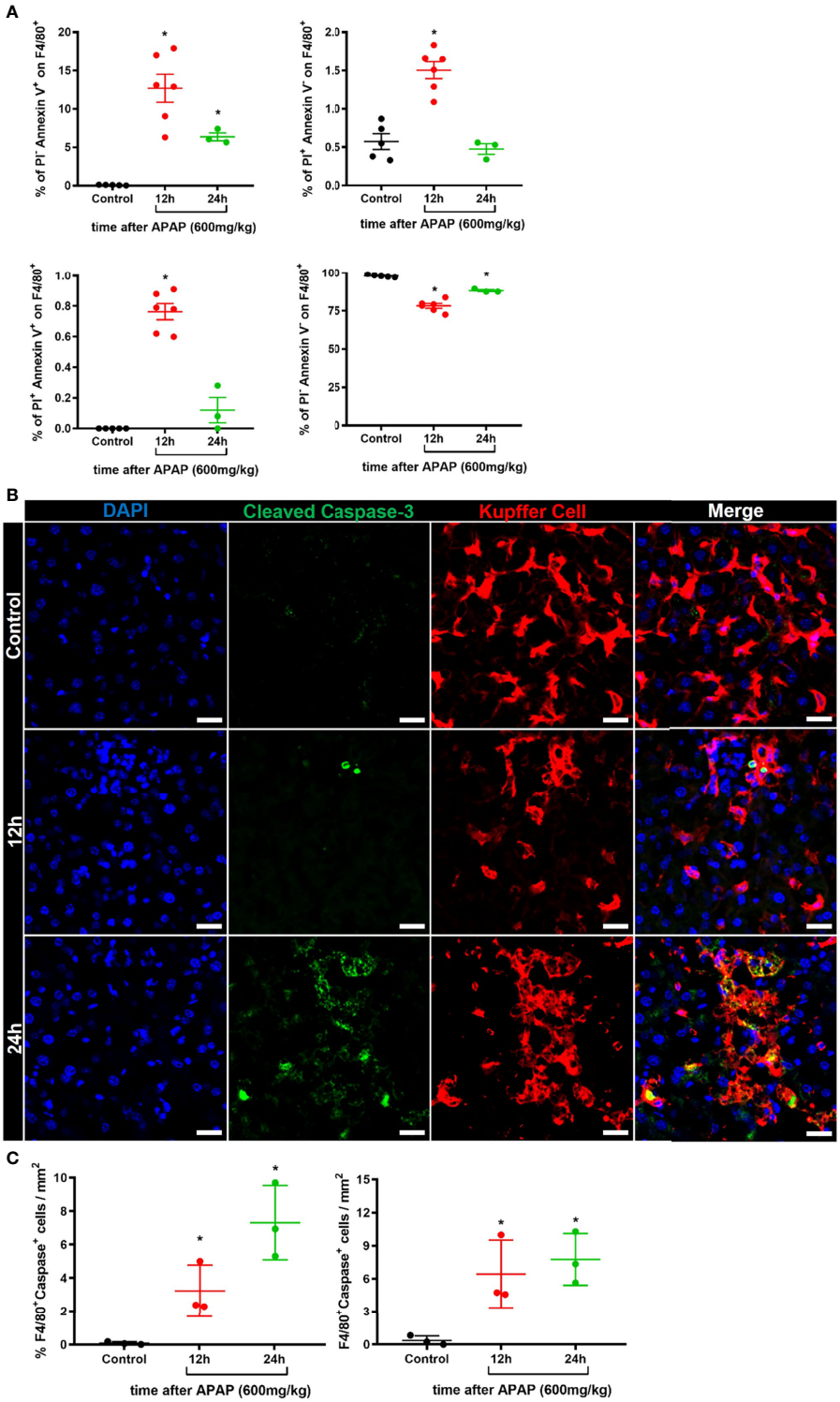

FIGURE 3 | Kupffer cell disappearance occurs by induction of an apoptotic and cell death program during ALI. **(A)** Percentage of different Kupffer cell status of cell death: apoptosis (Upper left, Annexin V^+PI^-), necrosis (Upper right, Annexin V^-PI^+), necroptosis (Bottom left, Annexin V^+PI^+), and live cells (Bottom left, Annexin V^-PI^-); n ≥ 3 mice per group; Representative of 2 independent experiments. **(B)** Representative immunofluorescence images of liver sections stained for DAPI (Blue), Cleaved Caspase 3 (Green), and Kupffer cell (Red, anti-F4/80); scale bar = 20μm. **(C)** Quantification of the percentage (Left panel) and number (Right panel) of F4/80$^+$Caspase-3$^+$ Kupffer cells in liver sections; n ≥ 3 mice per group and 10 images per mice. Data are presented as mean ± SEM. * indicates statistical difference compared to the control group using one-way ANOVA followed and Tukey post-test (* = $p < 0.05$).

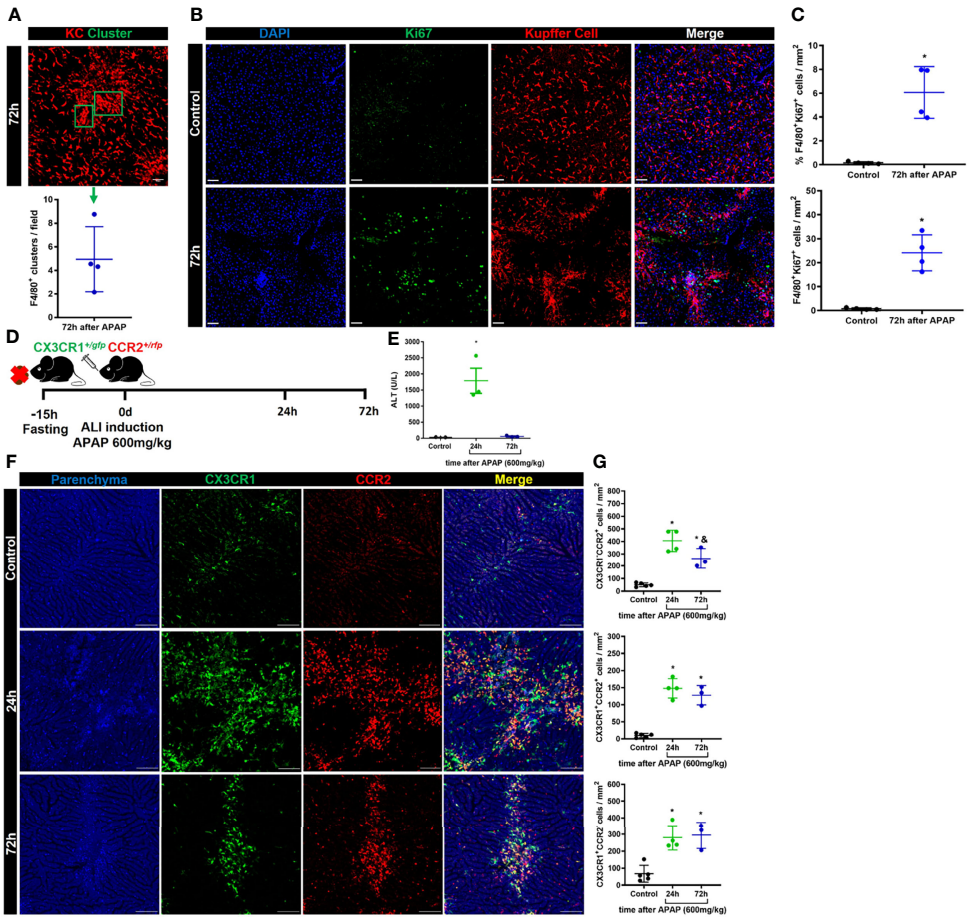

FIGURE 4 | Kupffer cell proliferation and infiltration of monocyte-derived cells promote liver niche restoration. **(A)** Representative IVM image illustrating the Kupffer cell clusters and their quantification per field in the resolution phase, 72h after APAP administration; scale bar = 50 µm; n = 4 mice per group and 10 images per mice; representative of 2 independent experiments. **(B)** Evaluation of Kupffer cell proliferation during ALI resolution phase by immunofluorescence stained for DAPI (Blue), Ki67 (green), and F4/80 (Red); Representative images of 2 independent experiments; scale bar = 50 µm. **(C)** Quantification of % (Upper panel) and numbers (bottom panel) of Kupffer cell/Cluster co-localized with Ki67 staining; n = 4 mice per group and 10 images per mice; representative of 2 independent experiments. **(D)** Scheme of ALI induction by oral gavage administration of APAP 600mg/kg in 8–10-weeks old $CX3CR1^{/+GFP+}CCR2^{/+rfp}$ female mice. **(E)** Measurement of liver injury by serum levels of Alanine aminotransferase (ALT); n =3 mice per group; representative data for 2 experiments. **(F)** Representative images of IVM assay during ALI to characterize liver architecture (Parenchyma) and monocyte populations; Parenchyma is represented by liver auto-fluorescence (blue); monocytes $CX3CR1^{+}CCR2^{+}$ are represented by yellow cells; monocytes $CX3CR1^{+}CCR2^{-}$ are represented by green cells; monocytes $CX3CR1^{-}CCR2^{+}$ are represented by red cells; scale bar = 100 µm. **(G)** Quantification of each monocyte subset: monocytes $CX3CR1^{-}CCR2^{+}$ (Upper panel), monocytes $CX3CR1^{+}CCR2^{+}$ (Middle panel), and monocytes $CX3CR1^{+}CCR2^{-}$ (Bottom panel); n ≥ 3 mice per group and 10 images per mice; representative of 2 independent experiments. Data are presented as mean ± SEM. * indicates statistical difference to the control group using one-way ANOVA followed and Tukey post-test (* = $p < 0.05$). & Indicates statistical difference compared to the 24h group using one-way ANOVA followed and Tukey post-test (& = $p < 0.05$).

Next, to evaluate how ALI affects the bacterial clearance from the blood by the liver, mice received an i.v injection of $5x10^6$ *E. coli* GFP^+/20g, and 5 minutes later, the blood was collected from the hepatic vein, and then GFP^+ events were counted by flow cytometry (**Supplementary Figure 5**). In line with our previous results, we found an impairment in bacterial clearance from the blood during the acute phase (12h and 24h) of ALI, as showed by increased amounts of circulating GFP^{++} bacteria, approximately a five-fold increase over the control group (**Figure 5E**). During the resolution phase, 72h post-APAP administration, we observed an efficient clearance of circulating bacteria by the liver, comparable to the uninfected control group (**Figure 5E**). To evaluate the real-time behavior of circulating bacteria in the liver, we performed IVM to track the bacteria *in vivo* after i.v injection of $5x10^7$ *E. coli* GFP^+/20g. Consistent with the impaired clearance capacity in the acute phase of ALI, *E. coli* real-time tracking using IVM assay revealed a higher bacterial displacement 12h and 24h after APAP-induced liver injury (**Figure 5F**). On the other hand, tracking *E. coli* at later time points, starting at 72h post-APAP, showed limited bacterial displacement in the liver (**Figure 5F**), indicating a rapid capture of bacteria by liver phagocytes. Thus, impaired blood clearance of pathogens by the liver during acute stages of ALI

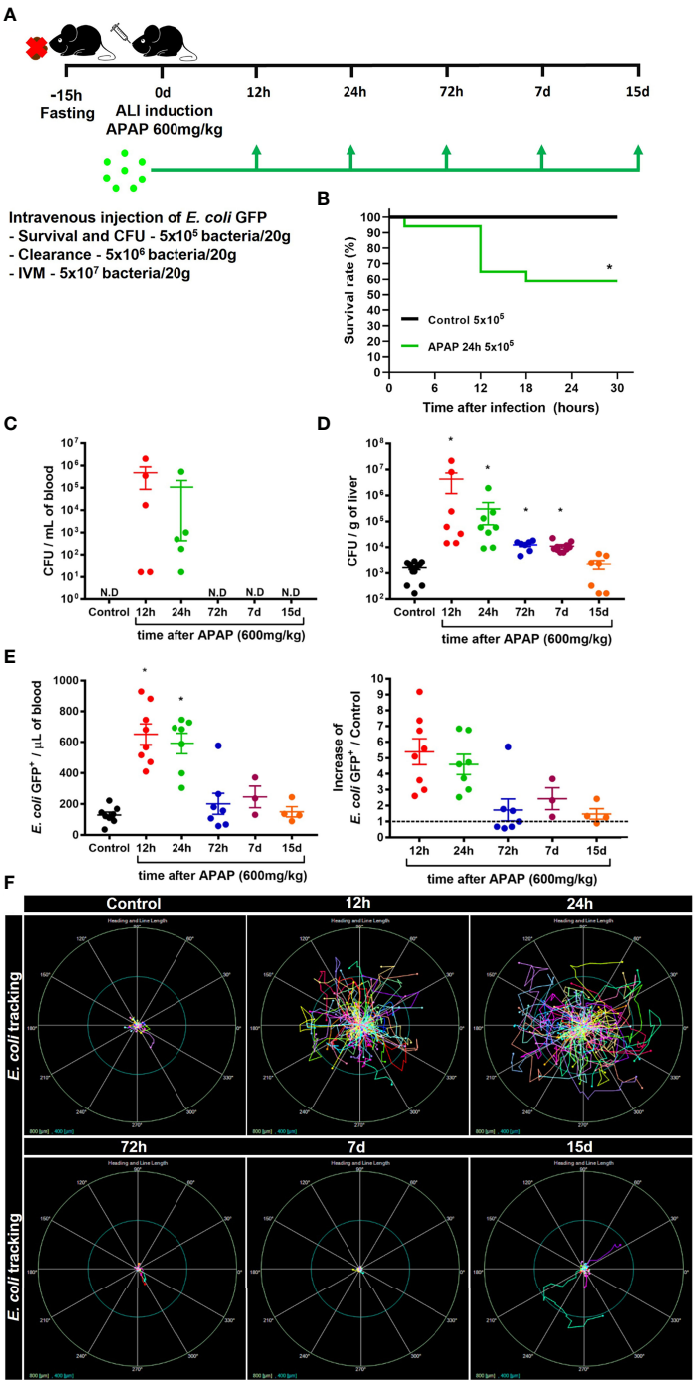

FIGURE 5 | ALI impairs liver firewall function and promotes susceptibility to bacterial infection. **(A)** Scheme for intravenous (i.v) injection of *E. coli* bacteria during the time-course of ALI on 8-10 weeks old C57BL/6J mice. **(B)** Mice survival rate (%) after infection with $5x10^5$ bacteria/20g in APAP untreated control mice or in mice 24h after APAP overdose (APAP 24h group); n ≥ 5 mice per group. Quantification of Colony-forming units (CFU) of *E. coli* in the blood **(C)** and liver **(D)** 24h after infection with $5x10^5$ bacteria/20g; n ≥ 9 mice per group; Representative of 3 independent experiments. **(E)** Measurement of liver firewall function by quantification of GFP^+ bacterial events from blood samples (Left panel) by Flow cytometry and determination of the blood clearance ability (Right panel; Increase over the control (– – – – – – = 1) 5 minutes after infection with $5x10^6$ bacteria/20g; n ≥ 3 mice per group; Representative of 3 independent experiments. **(F)** In vivo real-time tracking of *E. coli* by Intravital Microscopy (IVM) during the first 5 minutes after infection with $5x10^7$ bacteria/20g; Representative bacterial displacement graphs for each group; scale = 800 µm; n ≥ 5 mice per group. Representative of 2 independent experiments. Data are presented as mean ± SEM. * indicates statistical difference compared to the control group using Mantel-Cox for survival test **(B)**, non-parametric Kruskal Wallis test followed by Dunn's multiple comparisons tests **(C, D)**, and one-way ANOVA followed and Tukey post-test **(E)** (* = $p < 0.05$).

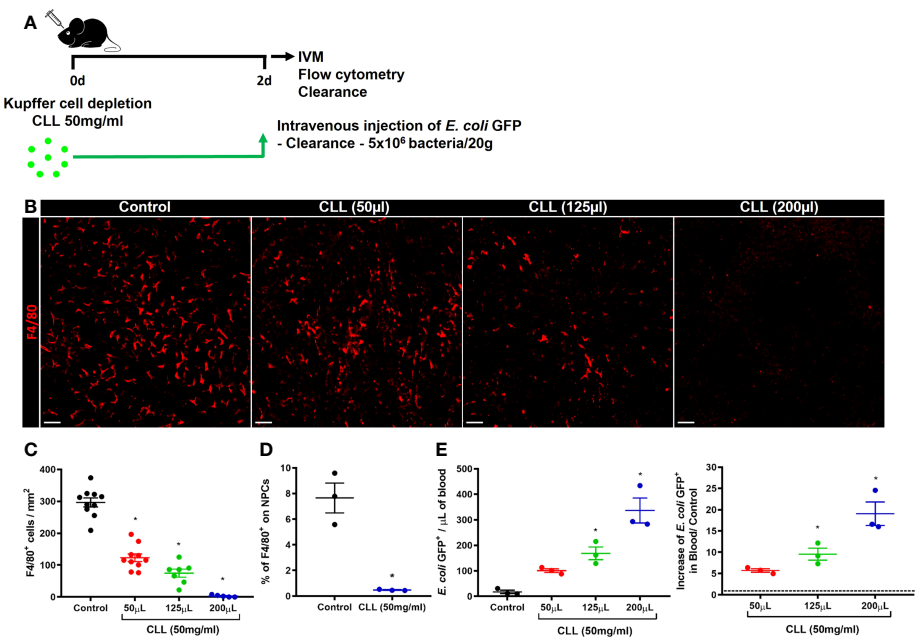

FIGURE 6 | Kupffer cells are essential for bacterial clearance and liver firewall function. **(A)** Scheme for Kupffer cell depletion using i.v injection of Clodronate Liposomes (CCL; 50mg/ml) in different volumes (50 µL, 125µL, and 200 µL). **(B)** Representative IVM images in mice intravenously injected with anti-F4/80 (Kupffer cells in red) 20 minutes before surgery; scale bar = 100 µm. **(C)** Quantification of Kupffer cells per mm^2; n ≥ 5 mice per group and 10 images per mice. **(D)** Percentage of F4/80$^+$ cells in liver non-parenchymal cells (NPCs) measured by Flow Cytometry. n = 3 mice per group; Representative of 2 independent experiments. **(E)** Quantification of *E. coli* GFP$^+$ events from blood samples (left panel) by flow cytometry and determination of the blood clearance ability (right panel); n ≥ 3 mice per group; Representative of 2 independent experiments. Data are presented as mean ± SEM. * indicates statistical difference compared to the control group using T-Student test **(D)** and one-way ANOVA followed and Tukey post-test **(C, E)** (* = $p < 0.05$).

suggests a susceptibility window for systemic infections during liver damage induced by APAP overdose.

Kupffer Cells are Essential for the Liver Firewall Function, Which is Reduced During Acute Liver Injury

Phagocytes are critical for the capture and elimination of pathogens. In the liver, KCs are the primary phagocyte responsible for those functions (42). To test whether the impairment in bacterial clearance during the acute stages of ALI was due to the reduced number of KCs, we pharmacologically depleted liver phagocytes by using intravenous injection of Clodronate Liposomes (CLL) (**Figure 6A**). Although *in vivo* CLL treatment can deplete phagocytes other than KCs, this method is still reliable for studies on Kupffer cell biology (34). IVM and flow cytometry analyses showed a dose-dependent depletion of KCs in the liver 48h after treatment (**Figures 6B–D**). The reduced number of KCs in the liver was inversely related to the increase in bacterial load in the blood, as showed by the increase in *E. coli* GFP$^+$ events in blood samples measured by flow cytometry (**Figure 6E**). These data demonstrate a critical role of liver phagocytes, in which KCs are the most abundant, in blood bacterial clearance and liver firewall function.

We next evaluated the phagocytosis capacity of KCs during ALI. For this purpose, *in vivo* real-time catching of intravenously injected *E. coli* GFP$^+$ by KCs during the time-course of ALI was assessed by IVM (**Figure 7A**). During homeostasis, KCs rapidly phagocytosed circulating bacteria. This capacity is visible reduced 12h and 24h after APAP-induced lesion, but begins to be restored after 72h and normalized 7 and 15 days after APAP overdose (**Supplementary Video 1**). With this approach, we confirmed that KCs play a vital role in the clearance of circulating pathogens, such as *E. coli*. We also quantified the percentage of KCs that captured circulating *E. coli* GFP$^+$ during the acute phase of ALI. We found that the percentage of KCs that phagocytosed *E. coli* GFP$^+$ (F4/80$^+$*E. coli* GFP^{++} cells) was significatively reduced in the first 12h and 24h of APAP overdose, which returned to a similar percentage after 72h (**Figures 7B, C**). In addition, KCs from mice 12h and 24h after APAP overdose internalize fewer circulating bacteria, showed as a mean of *E. coli* GFP^{++} per F4/80$^+$*E. coli* GFP^{++} cells. The number of internalized bacteria by KCs from mice at 72h, 7d and 15d after APA-induced ALI was comparable to control mice (**Figures 7D, E** and **Supplementary Video 2**). Altogether, these data showed that KCs play a critical role in bacterial clearance from the blood due to their high phagocytic capacity and suggest that disruption of the Kupffer cell niche by APAP overdose is an important cause of increased susceptibility to infections during ALI.

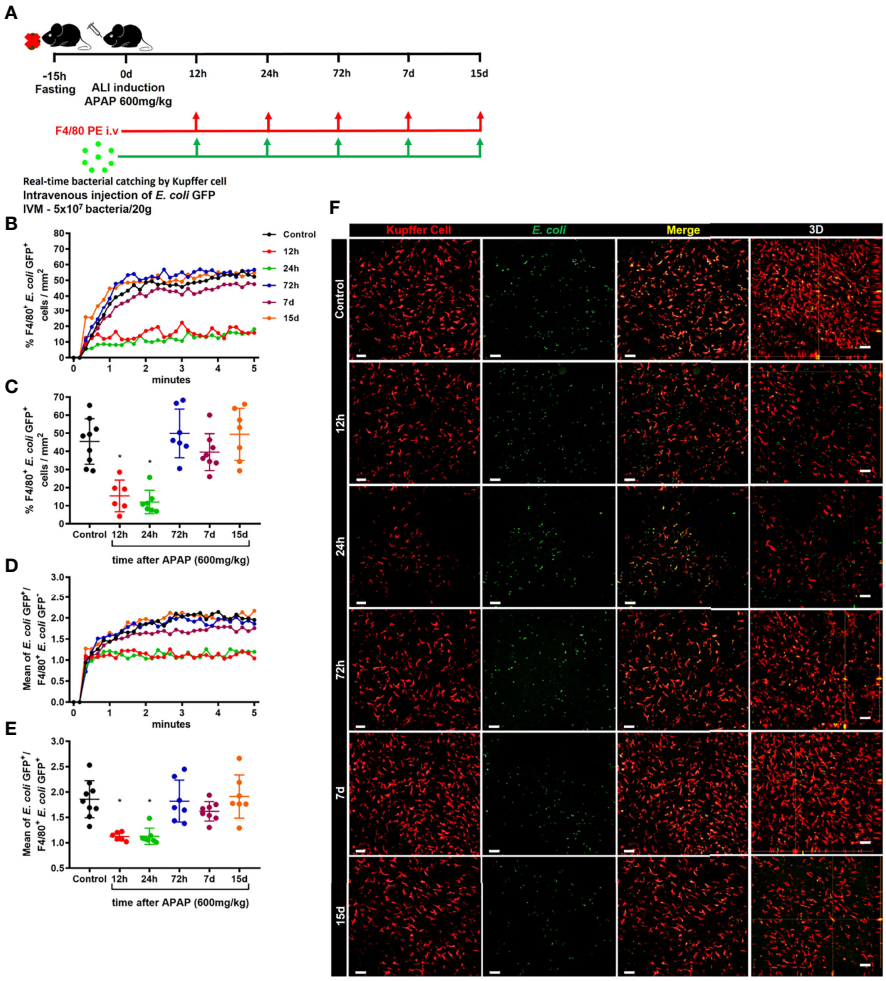

FIGURE 7 | Kupffer cell phagocytic ability is strongly reduced in the early stage of ALI. **(A)** Scheme of real-time *E. coli* phagocytosis by Kupffer cells in 5 minutes after i.v injection of 5x10^7 bacteria/20g. Measurement of real-time *E. coli* phagocytosis by Kupffer cell every 10 seconds during the first 5 minutes **(B)** after injection and at the end of 5 minutes **(C)**; n ≥ 6 mice per group; representative of 2 independent experiments. Mean of *E. coli* GFP$^+$ numbers per Kupffer cell GFP$^+$ quantified during the first 5 minutes **(D)** after injection and at the end of 5 minutes **(E)**; n ≥ 6 mice per group; representative of 2 independent experiments. **(F)** Representative images at minute 5 and 3D slice (fourth column) for each group; *E. coli* is green; Kupffer cell is stained by anti-F4/80 PE (red) and *E. coli* merged with Kupffer cell in yellow; scale bar = 50 µm. Data are presented as mean ± SD. * indicates statistical difference compared to the control group using one-way ANOVA followed and Tukey post-test (* = $p < 0.05$).

Bone Marrow-Derived Macrophage Therapy Reduces Liver Necrosis and Improves the Liver Firewall Function During ALI

Liver macrophage niche replacement and organ recovery by cell therapy with bone marrow-derived macrophages have been proposed as a promising treatment for liver fibrosis and APAP overdose (31, 32). We, therefore, hypothesized that the liver macrophage niche recovery or replacement during the first 24h of ALI could reduce the susceptibility to infection from circulating pathogens. Thus, we treated mice intravenously with 1x10^6 bone marrow-derived macrophages at steady-state (BMDM ϕ) or after alternative activation with IL-4 (BMDM A.A) 16h after APAP-induced liver injury. The effect of the therapy with bone marrow-derived macrophages in liver recovery was analyzed during the peak of ALI, 24h after APAP overdose administration (**Figure 8A**). First, we assessed the BMDM activation status by real-time PCR. We found that IL-4 by itself was enough to induce an alternative activation profile in (BMDM A.A) as showed by increased mRNA expression of *chil3*, *retnla*, and *arg1* when compared to BMDM ϕ (**Supplementary Figure 6A**). Next, we confirmed by flow cytometry that the transferred fluorescent-reporter BMDMs reached the target organ, the liver (**Figure 8B**). We found that both BMDM ϕ and BMDM A.A equally arrived in the organ (**Figure 8C** and **Supplementary Figure 6B**), and the BMDMs were localized in the liver 8h after cell transfer.

We also evaluated the myeloid cell compartment and the neutrophilic inflammation in the liver of APAP-treated mice by

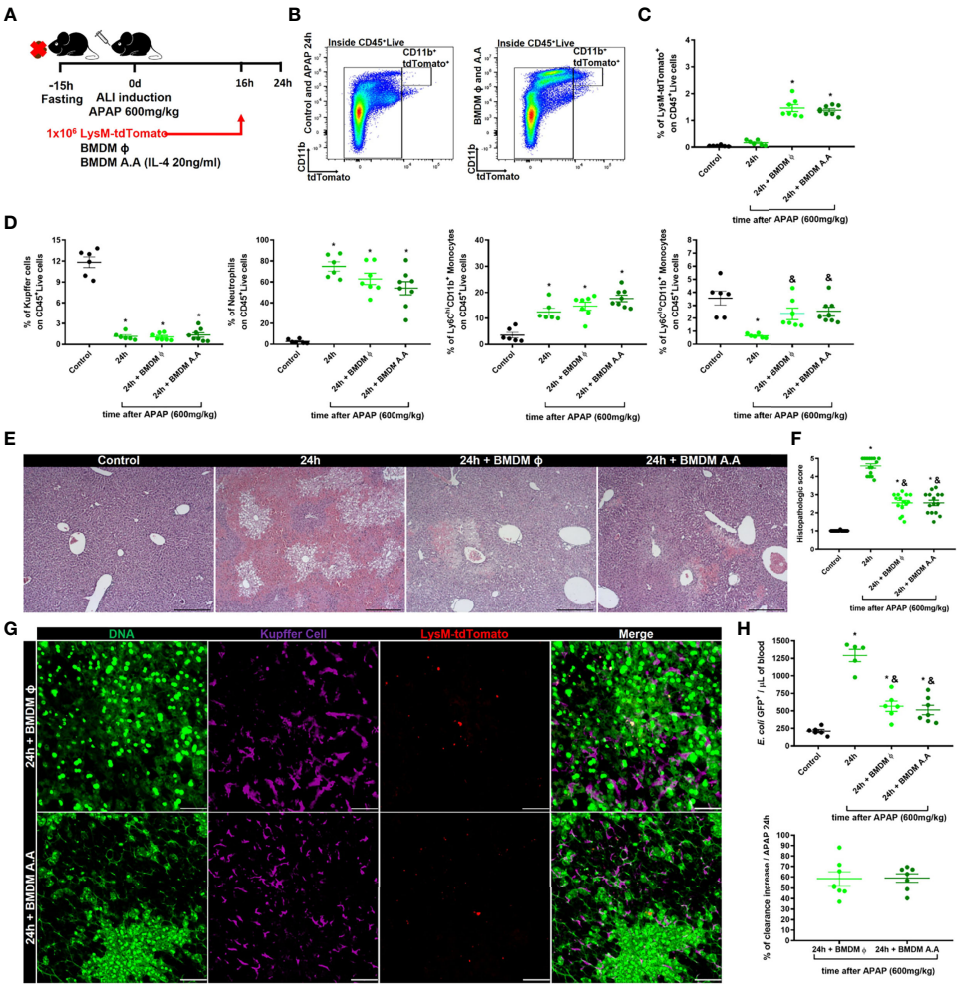

FIGURE 8 | Cellular therapy with bone marrow-derived macrophages reduce liver necrosis and rescues liver blood clearance. **(A)** Scheme for bone marrow-derived macrophage (BMDM) therapy during ALI, 16h after APAP administration. $1x10^6$ BMDC from $LysM^{cre/+}Rosa26^{tdTomato/+}$ mice that were non-activated (BMDM ϕ) or alternatively activated with IL-4 (BMDM A.A) were transferred into recipient mice 16h after APAP administration. **(B)** Flow cytometry gate strategy of inoculated $LysM^{cre/+}Rosa26^{tdTomato/+}$ BMDM ϕ and BMDM A.A in CD45+ live cell gate detected in the liver 8h after BMDM therapy (24h post-APAP administration). **(C)** Percentage of $LysM^{cre/+}Rosa26^{tdTomato/+}$ in liver samples; n ≥ 5 mice; representative of 2 independent experiments. **(D)** Evaluation of myeloid cell niche after BMDM cell therapy by flow cytometry showing the percentage (%) of myeloid cell subtypes; n ≥ 5 mice; representative of 2 independent experiments. **(E)** Representative liver histopathology of all four groups stained with Hematoxylin and Eosin (H&E); scale bar = 500 µm. **(F)** Tissue damage measured by the histopathologic score of the liver; n = 8-15 mice per group. **(G)** Representative IVM images of treated groups (BMDM A.A and BMDM ϕ) showing extracellular DNA (green, Sytox green), Kupffer cell (purple, anti-F4/80), and $LysM^{cre/+}Rosa26^{tdTomato/+}$ (red); scale bar = 100 µm; n = 2 mice per group. **(H)** Measurement of liver firewall function by quantification of *E. coli* GFP^+ events per ul of blood (Upper panel) by Flow cytometry and determination of the blood clearance ability (Bottom panel; % increase over the APAP at 24h) 5 minutes after infection with $5x10^6$ bacteria/20g; n ≥ 5 mice per group; Representative of 2 independent experiments. Data are presented as mean ± SEM. * indicates statistical difference compared to the control group using one-way ANOVA followed and Tukey post-test (* = $p < 0.05$). & indicates statistical difference compared to the 24h group (not treated with BMDM) using one-way ANOVA followed and Tukey post-test (& = $p < 0.05$).

flow cytometry 8h after BMDM transfer. BMDM therapy did not alter the percentage and the absolute number of Kupffer cells, neutrophils, and inflammatory monocytes ($Ly6C^{hi}CD11b^+$ cells) compared to APAP-treated mice that did not receive BMDM transplantation (**Figure 8D** and **Supplementary Figure 6C**). However, the BMDM therapy in APAP-treated mice did recover the percentage (**Figure 8D**) and number (**SupplementaryFigure 6C**) of patrolling monocytes ($Ly6C^{lo}CD11b^+$ cells) in the liver to levels comparable to the APAP-untreated Control group. Patrolling monocytes are often characterized as having a pro-regenerative phenotype (43), acting in the resolution phase of ALI (20). Thus, we investigated whether the increased numbers of patrolling monocytes ($Ly6C^{lo}CD11b^+$ cells) reduced the liver damage caused by APAP overdose. Histopathologic analysis of the liver showed reduced necrotic areas around centrilobular veins in BMDM ϕ and BMDM A.A groups and those areas did not connect to adjacent necrotic areas, as was seen in mice that did

not receive BMDM therapy (**Figure 8E**). In addition, the therapy with both the steady-state and alternatively activated macrophages reduced the histopathologic score due to the reduction of necrotic areas and increased regeneration of the damaged organ compared to the non-treated group (**Figures 8E, F**). Intriguingly, we did not observe a significant change in levels of ALT in the serum (**Supplementary Figure 6C**), as has been previously observed by another group (32). We next evaluated the positioning of the transferred BMDMs in the liver during ALI using IVM. We found that BMDM ϕ and BMDM A.A were positioned in the necrotic areas, characterized by deposition of extracellular DNA, where the number of KCs were reduced (**Figure 8G**), suggesting that BMDM ϕ and BMDM A.A occupied the niche opened by KCs death during ALI. Finally, we evaluated the liver firewall function using the *in vivo* assay of bacterial clearance from the blood. We found that therapy with both BMDM ϕ and BMDM A.A in mice intravenously infected with *E. coli* GFP^+ reduced the number of bacteria in the blood compared to *E. coli* GFP^+ infected mice without BMDM therapy (**Figure 8H**, upper panel), promoting an increase of 60% in liver blood clearance capacity (**Figure 8H**, bottom panel). Taken together, these data demonstrated that therapy with BMDMs, which occupy the open niche in the liver caused by KCs death after APAP overdose, improves the regeneration of the damaged liver during ALI, decreasing the susceptibility to systemic infections.

DISCUSSION

Acetaminophen overdose induces a complex acute inflammation initiated by hepatocyte necrosis, leading to massive parenchyma damage (16). Consequently, intracellular components are released within the liver and can reach the systemic circulation acting as DAMPS. In addition, since the liver is an extremely vascularized organ, hepatic microcirculation – together with other resident immune cells – is profoundly disturbed during ALI (19, 33). These events lead to inflammation that, if not controlled, can evolve into a fatal outcome (24). Patients that survived the acute metabolic damage due to liver necrosis but have subsequent systemic infections are responsible for a significant percentage of the mortality rate of those patients (25, 44). These conditions are mainly related to the loss of blood clearance by the liver, which is crucial for restraining the circulation of pathogens. A key liver component for such firewall function are KCs (3, 42), and it is becoming increasingly clear that disruption in their number or function are a hallmark of liver failure.

Liver necrosis results in an abrupt release of intracellular components, such as ALT, which are used for laboratory diagnosis of liver damage. However, several intracellular molecules, which comprise a large group of damage-associated molecular patterns (DAMPs), are also released (18). In fact, DNA, HMGB-1 (high mobility group box protein 1), and histones are not only responsible for acute inflammation, but also for direct endothelial cell death (45), damaging the hepatic sinusoidal network. Therefore, necrosis-derived DAMPs could consequently trigger KCs death since they are mainly located inside liver sinusoids. In sharp contrast, the disappearance of tissue-resident macrophages during local inflammation has been also discussed as "intentional" cell death, which could avoid over inflammation and further tissue damage (46, 47). The KCs death phenomenon also occurs in various liver inflammatory processes, such as viral or bacterial infection and sterile inflammation caused by non-alcoholic steatohepatitis (12, 14, 15). In ALI induced by APAP overdose, KC death occurs through an apoptotic program, which a marked characteristic of this program is the reduced amplification of local inflammation (48). However, in the absence of KCs, the ALI outcome is worse, indicating a crucial role of those cells in restraining the onset of APAP overdose-induced disease (49, 50). In addition, KCs also are known to participate in the resolution of the inflammation and to contribute to organ regeneration by removing debris and stimulating angiogenesis, respectively (51, 52). Thus, in the absence of functional KCs, tissue damage during ALI may worsen and organ regeneration may be delayed.

Phagocytosis and the elimination of pathogens are primary KC functions (3). Here, we highlighted the importance of this function during the ALI. Following APAP-induced liver injury, we observed a reduction in the KC population and a reduced percentage of cells in the liver with the ability to capture circulating bacteria. This defect in host liver-resident immune cell ability to clear blood-born bacteria remained impaired up to 7 days post-APAP overdose. Therefore, the loss of such vital liver function might open a window for systemic infections in patients with ALF induced by ALI (24). We have previously shown that mice treated with APAP had no detectable bacteria in blood and liver samples, suggesting that APAP-induced liver injury does not promote microbiota translocation by itself but rather would predispose patients to systemic infections following exposure to an infectious pathogen (Marques et al, 2015). Indeed, approximately 50% of ALF patients are affected by systemic infections, with a 40% of mortality rate (24, 25, 44). Thus, disruption of the KC niche appears to be a determinant factor for worse outcomes in patients with ALF.

During an acute inflammatory response in the liver, the KCs replenishment kinetics must be increased relative to the steady-state (6) as the rapid resolution of inflammation and the return of the organ to homeostasis are essential for the organism. KCs depletion caused by liver inflammation can create an environment for a proper liver resident macrophage replenishment (29, 53). However, the origin of these new cells depends on the inflammatory insult and extension of the tissue damage and inflammation. It has been proposed that KCs replicate in the resolution phase of ALI and contribute to niche replacement (20), although this does not exclude the possibility of a dual input of liver cell replenishment, one from replicating KCs and another from infiltrating monocytes. Moreover, the transcriptional profile transitioned from the $Ly6C^{hi}$ monocytes to $Ly6C^{lo}$ monocytes and then to KC at 72 hours, indicating a phenotype changing from first to the last. Here, we showed that replicating KCs that remained in the liver

formed cell clusters in necrotic areas. We also found a massive infiltration of Ly6C^{hi} and Ly6C^{lo} monocytes early in ALI that lasted until the resolution phase and were strategically positioned in areas devoid of KCs. Differentiation of circulating monocytes into liver resident macrophages has been described for other liver disease models (9, 12, 28, 49). Another study described a possible competition by the open liver macrophage niche between the remaining KCs and the infiltrated monocytes (29). In our study we were not able to definitively determine whether the recovery in KCs population in the resolution phase of ALI was due to replication of remaining liver KCs, infiltration of monocytes and their differentiation into new KCs, or both. An approach that could address this is the fate-mapping model *via* Ms4a3, which allows the tracking of monocyte-derived cells (11). Therefore, further studies are still necessary to definitively determine the KC replication and monocyte differentiation rate in the liver macrophage niche replenishment during ALI.

Differentiation of monocytes into functionally competent KCs requires a period to adapt to the tissue environment, including the acquisition of specific transcriptional and phenotypic characteristics and their positioning in specific organ niches (9, 10, 29, 54, 55). Infiltrating monocytes are transiently immature compared to KCs with signaling pathways related to phagocytosis and elimination of pathogens, such as FcγR signaling, complement receptors and their downstream cascade, phagosome and lysosome, downregulated in both Ly6C^{hi} and Ly6C^{lo} monocyte subsets (20). Thus, even with the KC niche transiently occupied by infiltrating monocytes, there is an increased susceptibility to systemic infections due to their inability to appropriately deal with circulating bacteria. Even though professional phagocytes internalize pathogens, the latter disposes of mechanisms to evade the cellular immune response (56). Pathogens, including bacteria, commonly use three strategies: I) escape of phagosome mechanisms; II) inhibition of the fusion between phagosome and lysosome; III) capacity to resist inside the phagolysosome (57, 58). This could explain why, in our system, the *E. coli* titers were increased in the liver 7 days after APAP overdose. In addition, despite the presence of remaining KCs in the injured liver, their failure to adequately phagocytose and eliminate pathogens could be explained by increased demand for removal of cell debris due to liver necrosis (51, 59, 60). Therefore, the infiltration of monocytes with an immature phenotype added to insufficient response by remaining KCs may result in impaired antimicrobial response during ALI, which can contribute to the enhanced susceptibility to infections (61).

The difficulty of proper and early diagnosis of the ALI and ALF reduces their treatment. However, a cell-based therapeutic possibility recently emerged as an alternative for managing hepatic diseases. In the last decade, macrophage therapy has been shown effective anti-fibrotic and pro-regenerative results (30, 31). In fact, treatment of APAP overdose using bone marrow-derived macrophages, generated by CSF-1 stimuli into precursors in culture, significantly improved the recovery of the injured liver. Also, alternatively activated BMDM (BMDM A.A), an anti-inflammatory activation profile (62), accelerated the resolution of inflammation by clearance of the necrotic areas and stimulation of hepatocellular proliferation when analyzed 36h after APAP-induced tissue lesion (32). Indeed, BMDM A.A. is highly phagocytic and expresses a pro-regenerative profile, such as IL-10, TGF-β, YM1, and FIZZ1 (32). Here, we extended the BMDM therapy effects to the acute phase of ALI. We found that the engrafted BMDM migrated to the liver, reduced liver necrosis, and improved the blood bacterial clearance capacity by the liver. However, therapy with BMDM alternatively activated did not differ from the therapy with conventional BMDM, suggesting that BMDM A.A. may not be necessary for the acute phase as they are for the resolution stage. Importantly, although the BMDM therapy did not immediately replenish KCs during ALI, it can support and maintain some KC functions while the repopulation and maturation processes occur. It is important to note that macrophage maturation and education (mainly due to tissue factors) can be a long-term process (30-60 days in mice) and, in some cases, may not fully restore the original macrophage identity. Therefore, despite of some limitations, BMDM therapy appears as a promising treatment for ALI and ALF in during both early and later stages.

In summary, we found that the liver macrophage niche is essential for restraining ALI and that BMDM therapy improves the resolution of liver inflammation and damage, as well as reduces the susceptibility of the host to infections. Thus, therapies targeting the Kupffer cell niche can add to the current treatment of the ALI and ALF symptoms in order to enhance liver healing and improve the recovery of organ function. Such a therapeutic strategy that can be extended to other diseases with disruption of tissue-resident macrophage populations.

ETHICS STATEMENT

The animal study was reviewed and approved by Comissão Ética de Utilização Animal (CEUA), Universidade Federal de Minas Gerais (UFMG), protocols number 377/2016 and 076/2020.

AUTHOR CONTRIBUTIONS

ML conceptualized the project, designed and performed the experiments, analyzed and interpreted data, and wrote the manuscript. BN designed and performed the experiments, interpreted data, and wrote the manuscript. MM performed the experiments, interpreted data, and wrote the manuscript. GCS designed and performed the experiments. RM performed the experiments. PM performed the experiments. AO designed and performed the experiments and interpreted data. LF reviewed and wrote the manuscript. RG designed and supervised the experiments and interpreted data. GM conceptualized the project, supervised the experiments, interpreted data, and wrote the manuscript.

FUNDING

This study was financed by CNPq, CAPES, and FAPEMIG (Universal 2018, Rede Mineira de Imunobiológicos) agencies.

ACKNOWLEDGMENTS

The authors are indebted to Dra. Cristina de Paula for exquisite lab managing work at the Center for Gastrointestinal Biology; members of Macrophage and Monocyte Biology Laboratory/UFMG; Professor Leda Vieira for opening the Laboratory of Gnotobiology and Immunology to space and equipment usage; Dr. Matheus Batista Carneiro for all scientific discussions.

SUPPLEMENTARY MATERIAL

The Supplementary Material for this article can be found online at: https://www.frontiersin.org/articles/10.3389/fimmu.2022.892114/full#supplementary-material

REFERENCES

1. Krenkel O, Tacke F. Liver Macrophages in Tissue Homeostasis and Disease. *Nat Rev Immunol* (2017) 17(5):306–21. doi: 10.1038/nri.2017.11
2. Wen Y, Lambrecht J, Ju C, Tacke F. Hepatic Macrophages in Liver Homeostasis and Diseases-Diversity, Plasticity and Therapeutic Opportunities. *Cell Mol Immunol* (2021) 18(1):45–56. doi: 10.1038/s41423-020-00558-8
3. Bilzer M, Roggel F, Gerbes AL. Role of Kupffer Cells in Host Defense and Liver Disease. *Liver Int* (2006) 26(10):1175–86. doi: 10.1111/j.1478-3231.2006.01342.x
4. Gregory SH, Wing EJ. Accessory Function of Kupffer Cells in the Antigen-Specific Blastogenic Response of an L3t4+ T-Lymphocyte Clone to Listeria Monocytogenes. *Infect Immun* (1990) 58(7):2313–9. doi: 10.1128/IAI.58.7.2313-2319.1990
5. Guilliams M, Bonnardel J, Haest B, Vanderborght B, Wagner C, Remmerie A, et al. Spatial Proteogenomics Reveals Distinct and Evolutionarily Conserved Hepatic Macrophage Niches. *Cell* (2022) 185(2):379–96 e38. doi: 10.1016/j.cell.2021.12.018
6. Gomez Perdiguero E, Klapproth K, Schulz C, Busch K, Azzoni E, Crozet L, et al. Tissue-Resident Macrophages Originate From Yolk-Sac-Derived Erythro-Myeloid Progenitors. *Nature* (2015) 518(7540):547–51. doi: 10.1038/nature13989
7. Mass E, Ballesteros I, Farlik M, Halbritter F, Gunther P, Crozet L, et al. Specification of Tissue-Resident Macrophages During Organogenesis. *Science* (2016) 353(6304). doi: 10.1126/science.aaf4238
8. Nakagaki BN, Mafra K, de Carvalho E, Lopes ME, Carvalho-Gontijo R, de Castro-Oliveira HM, et al. Immune and Metabolic Shifts During Neonatal Development Reprogram Liver Identity and Function. *J Hepatol* (2018) 69(6):1294–307. doi: 10.1016/j.jhep.2018.08.018
9. Bonnardel J, T'Jonck W, Gaublomme D, Browaeys R, Scott CL, Martens L, et al. Stellate Cells, Hepatocytes, and Endothelial Cells Imprint the Kupffer Cell Identity on Monocytes Colonizing the Liver Macrophage Niche. *Immunity* (2019) 51(4):638–54 e9. doi: 10.1016/j.immuni.2019.08.017
10. Sakai M, Troutman TD, Seidman JS, Ouyang Z, Spann NJ, Abe Y, et al. Liver-Derived Signals Sequentially Reprogram Myeloid Enhancers to Initiate and Maintain Kupffer Cell Identity. *Immunity* (2019) 51(4):655–70.e8. doi: 10.1016/j.immuni.2019.09.002
11. Liu Z, Gu Y, Chakarov S, Bleriot C, Kwok I, Chen X, et al. Fate Mapping *Via* Ms4a3-Expression History Traces Monocyte-Derived Cells. *Cell* (2019) 178(6):1509–25.e19. doi: 10.1016/j.cell.2019.08.009
12. Bleriot C, Dupuis T, Jouvion G, Eberl G, Disson O, Lecuit M. Liver-Resident Macrophage Necroptosis Orchestrates Type 1 Microbicidal Inflammation and Type-2-Mediated Tissue Repair During Bacterial Infection. *Immunity* (2015) 42(1):145–58. doi: 10.1016/j.immuni.2014.12.020
13. Borst K, Frenz T, Spanier J, Tegtmeyer PK, Chhatbar C, Skerra J, et al. Type I Interferon Receptor Signaling Delays Kupffer Cell Replenishment During Acute Fulminant Viral Hepatitis. *J Hepatol* (2017) 68(4):682–90. doi: 10.1016/j.jhep.2017.11.029
14. Lai SM, Sheng J, Gupta P, Renia L, Duan K, Zolezzi F, et al. Organ-Specific Fate, Recruitment, and Refilling Dynamics of Tissue-Resident Macrophages During Blood-Stage Malaria. *Cell Rep* (2018) 25(11):3099–109.e3. doi: 10.1016/j.celrep.2018.11.059
15. Remmerie A, Martens L, Thone T, Castoldi A, Seurinck R, Pavie B, et al. Osteopontin Expression Identifies a Subset of Recruited Macrophages Distinct From Kupffer Cells in the Fatty Liver. *Immunity* (2020) 53(3):641–57.e14. doi: 10.1016/j.immuni.2020.08.004
16. Lee WM. Acetaminophen (Apap) Hepatotoxicity-Isn't It Time for Apap to Go Away? *J Hepatol* (2017) 67(6):1324–31. doi: 10.1016/j.jhep.2017.07.005
17. Asrani SK, Devarbhavi H, Eaton J, Kamath PS. Burden of Liver Diseases in the World. *J Hepatol* (2019) 70(1):151–71. doi: 10.1016/j.jhep.2018.09.014
18. Yang R, Tonnesseen TI. Damps and Sterile Inflammation in Drug Hepatotoxicity. *Hepatol Int* (2019) 13(1):42–50. doi: 10.1007/s12072-018-9911-9
19. Jaeschke H, Ramachandran A. Mechanisms and Pathophysiological Significance of Sterile Inflammation During Acetaminophen Hepatotoxicity. *Food Chem Toxicol* (2020) 138:111240. doi: 10.1016/j.fct.2020.111240
20. Zigmond E, Samia-Grinberg S, Pasmanik-Chor M, Brazowski E, Shibolet O, Halpern Z, et al. Infiltrating Monocyte-Derived Macrophages and Resident Kupffer Cells Display Different Ontogeny and Functions in Acute Liver Injury. *J Immunol* (2014) 193(1):344–53. doi: 10.4049/jimmunol.1400574
21. Shan Z, Ju C. Hepatic Macrophages in Liver Injury. *Front Immunol* (2020) 11:322. doi: 10.3389/fimmu.2020.00322
22. Mossanen JC, Krenkel O, Ergen C, Govaere O, Liepelt A, Puengel T, et al. Chemokine (C-C Motif) Receptor 2-Positive Monocytes Aggravate the Early Phase of Acetaminophen-Induced Acute Liver Injury. *Hepatology* (2016) 64(5):1667–82. doi: 10.1002/hep.28682
23. Graubardt N, Vugman M, Mouhadeb O, Caliari G, Pasmanik-Chor M, Reuveni D, et al. Ly6c(Hi) Monocytes and Their Macrophage Descendants Regulate Neutrophil Function and Clearance in Acetaminophen-Induced Liver Injury. *Front Immunol* (2017) 8:626. doi: 10.3389/fimmu.2017.00626
24. Stravitz RT, Lee WM. Acute Liver Failure. *Lancet* (2019) 394(10201):869–81. doi: 10.1016/S0140-6736(19)31894-X
25. Rolando N, Philpott-Howard J, Williams R. Bacterial and Fungal Infection in Acute Liver Failure. *Semin Liver Dis* (1996) 16(4):389–402. doi: 10.1055/s-2007-1007252
26. Karvellas CJ, Pink F, McPhail M, Cross T, Auzinger G, Bernal W, et al. Predictors of Bacteraemia and Mortality in Patients With Acute Liver Failure. *Intensive Care Med* (2009) 35(8):1390–6. doi: 10.1007/s00134-009-1472-x
27. Triantafyllou E, Gudd CL, Mawhin MA, Husbyn HC, Trovato FM, Siggins MK, et al. Pd-1 Blockade Improves Kupffer Cell Bacterial Clearance in Acute Liver Injury. *J Clin Invest* (2021) 131(4). doi: 10.1172/JCI140196
28. Scott CL, Zheng F, De Baetselier P, Martens L, Saeys Y, De Prijck S, et al. Bone Marrow-Derived Monocytes Give Rise to Self-Renewing and Fully Differentiated Kupffer Cells. *Nat Commun* (2016) 7:10321. doi: 10.1038/ncomms10321
29. Guilliams M, Scott CL. Does Niche Competition Determine the Origin of Tissue-Resident Macrophages? *Nat Rev Immunol* (2017) 17(7):451–60. doi: 10.1038/nri.2017.42
30. Starkey Lewis PJ, Moroni F, Forbes SJ. Macrophages as a Cell-Based Therapy for Liver Disease. *Semin Liver Dis* (2019) 39(4):442–51. doi: 10.1055/s-0039-1688502

31. Thomas JA, Pope C, Wojtacha D, Robson AJ, Gordon-Walker TT, Hartland S, et al. Macrophage Therapy for Murine Liver Fibrosis Recruits Host Effector Cells Improving Fibrosis, Regeneration, and Function. *Hepatology* (2011) 53 (6):2003–15. doi: 10.1002/hep.24315
32. Lewis PS, Campana L, Aleksieva N, Cartwright JA, Mackinnon A, O'Duibhir E, et al. Alternatively Activated Macrophages Promote Resolution of Necrosis Following Acute Liver Injury. *J Hepatol* (2020) 73(20):349–60. doi: 10.1016/j.jhep.2020.02.031
33. Marques PE, Oliveira AG, Pereira RV, David BA, Gomides LF, Saraiva AM, et al. Hepatic DNA Deposition Drives Drug-Induced Liver Injury and Inflammation in Mice. *Hepatology* (2015) 61(1):348–60. doi: 10.1002/hep.27216
34. David BA, Rezende RM, Antunes MM, Santos MM, Freitas Lopes MA, Diniz AB, et al. Combination of Mass Cytometry and Imaging Analysis Reveals Origin, Location, and Functional Repopulation of Liver Myeloid Cells in Mice. *Gastroenterology* (2016) 151(6):1176–91. doi: 10.1053/j.gastro.2016.08.024
35. Crowley LC, Marfell BJ, Scott AP, Waterhouse NJ. Quantitation of Apoptosis and Necrosis by Annexin V Binding, Propidium Iodide Uptake, and Flow Cytometry. *Cold Spring Harb Protoc* (2016) 2016(11). doi: 10.1101/pdb.prot087288
36. Van Rooijen N, Sanders A. Kupffer Cell Depletion by Liposome-Delivered Drugs: Comparative Activity of Intracellular Clodronate, Propamidine, and Ethylenediaminetetraacetic Acid. *Hepatology* (1996) 23(5):1239–43. doi: 10.1053/jhep.1996.v23.pm0008621159
37. Marques PE, Antunes MM, David BA, Pereira RV, Teixeira MM, Menezes GB. Imaging Liver Biology in Vivo Using Conventional Confocal Microscopy. *Nat Protoc* (2015) 10(2):258–68. doi: 10.1038/nprot.2015.006
38. Gonçalves R, Mosser DM. The Isolation and Characterization of Murine Macrophages. *Curr Protoc Immunol* (2015), 111:14.1.1–16. doi: 10.1002/0471142735.im1401s111
39. Mattos MS, Lopes ME, de Araujo AM, Alvarenga DM, Nakagaki BN, Mafra K, et al. Prolonged Neutrophil Survival at Necrotic Sites Is a Fundamental Feature for Tissue Recovery and Resolution of Hepatic Inflammation. *J leuk Biol* (2020) 108(4):1199–213. doi: 10.1002/JLB.1MA0420-634R
40. Marques PE, Vandendriessche S, Oliveira TH, Crijns H, Lopes ME, Blanter M, et al. Inhibition of Drug-Induced Liver Injury in Mice Using a Positively Charged Peptide That Binds DNA. *Hepatol Commun* (2021) 5(10):1737–54. doi: 10.1002/hep4.1759
41. Schwabe RF, Luedde T. Apoptosis and Necroptosis in the Liver: A Matter of Life and Death. *Nat Rev Gastroenterol Hepatol* (2018) 15(12):738–52. doi: 10.1038/s41575-018-0065-y
42. Balmer ML, Slack E, de Gottardi A, Lawson MA, Hapfelmeier S, Miele L, et al. The Liver May Act as a Firewall Mediating Mutualism Between the Host and Its Gut Commensal Microbiota. *Sci Trans Med* (2014) 6(237):237ra66. doi: 10.1126/scitranslmed.3008618
43. Yang W, Zhao X, Tao Y, Wu Y, He F, Tang L. Proteomic Analysis Reveals a Protective Role of Specific Macrophage Subsets in Liver Repair. *Sci Rep* (2019) 9(1):2953. doi: 10.1038/s41598-019-39007-6
44. Rolando N, Harvey F, Brahm J, Philpott-Howard J, Alexander G, Gimson A, et al. Prospective Study of Bacterial Infection in Acute Liver Failure: An Analysis of Fifty Patients. *Hepatology* (1990) 11(1):49–53. doi: 10.1002/hep.1840110110
45. Yang R, Zou X, Tenhunen J, Tonnessen TI. Hmgb1 and Extracellular Histones Significantly Contribute to Systemic Inflammation and Multiple Organ Failure in Acute Liver Failure. *Mediators Inflammation* (2017) 2017:5928078. doi: 10.1155/2017/5928078
46. Di Paolo NC, Doronin K, Baldwin LK, Papayannopoulou T, Shayakhmetov DM. The Transcription Factor Irf3 Triggers "Defensive Suicide" Necrosis in Response to Viral and Bacterial Pathogens. *Cell Rep* (2013) 3(6):1840–6. doi: 10.1016/j.celrep.2013.05.025
47. Ginhoux F, Bleriot C, Lecuit M. Dying for a Cause: Regulated Necrosis of Tissue-Resident Macrophages Upon Infection. *Trends Immunol* (2017) 38 (10):693–5. doi: 10.1016/j.it.2017.05.009
48. Li Z, Weinman SA. Regulation of Hepatic Inflammation *Via* Macrophage Cell Death. *Semin Liver Dis* (2018) 38(4):340–50. doi: 10.1055/s-0038-1670674
49. David BA, Rubino S, Moreira TG, Freitas-Lopes MA, Araujo AM, Paul NE, et al. Isolation and High-Dimensional Phenotyping of Gastrointestinal Immune Cells. *Immunology* (2017) 151(1):56–70. doi: 10.1111/imm.12706
50. Holt MP, Cheng L, Ju C. Identification and Characterization of Infiltrating Macrophages in Acetaminophen-Induced Liver Injury. *J leuk Biol* (2008) 84 (6):1410–21. doi: 10.1189/jlb.0308173
51. Triantafyllou E, Pop OT, Possamai LA, Wilhelm A, Liaskou E, Singanayagam A, et al. Mertk Expressing Hepatic Macrophages Promote the Resolution of Inflammation in Acute Liver Failure. *Gut* (2018) 67(2):333–47. doi: 10.1136/gutjnl-2016-313615
52. You Q, Holt M, Yin H, Li G, Hu CJ, Ju C. Role of Hepatic Resident and Infiltrating Macrophages in Liver Repair After Acute Injury. *Biochem Pharmacol* (2013) 86(6):836–43. doi: 10.1016/j.bcp.2013.07.006
53. Guilliams M, Thierry GR, Bonnardel J, Bajenoff M. Establishment and Maintenance of the Macrophage Niche. *Immunity* (2020) 52(3):434–51. doi: 10.1016/j.immuni.2020.02.015
54. van de Laar L, Saelens W, De Prijck S, Martens L, Scott CL, Van Isterdael G, et al. Yolk Sac Macrophages, Fetal Liver, and Adult Monocytes Can Colonize an Empty Niche and Develop Into Functional Tissue-Resident Macrophages. *Immunity* (2016) 44(4):755–68. doi: 10.1016/j.immuni.2016.02.017
55. Bleriot C, Chakarov S, Ginhoux F. Determinants of Resident Tissue Macrophage Identity and Function. *Immunity* (2020) 52(6):957–70. doi: 10.1016/j.immuni.2020.05.014
56. Kaufmann SHE, Dorhoi A. Molecular Determinants in Phagocyte-Bacteria Interactions. *Immunity* (2016) 44(3):476–91. doi: 10.1016/j.immuni.2016.02.014
57. Thakur A, Mikkelsen H, Jungersen G. Intracellular Pathogens: Host Immunity and Microbial Persistence Strategies. *J Immunol Res* (2019) 2019:1356540. doi: 10.1155/2019/1356540
58. Baxt LA, Garza-Mayers AC, Goldberg MB. Bacterial Subversion of Host Innate Immune Pathways. *Science* (2013) 340(6133):697–701. doi: 10.1126/science.1235771
59. Horst AK, Tiegs G, Diehl L. Contribution of Macrophage Efferocytosis to Liver Homeostasis and Disease. *Front Immunol* (2019) 10:2670. doi: 10.3389/fimmu.2019.02670
60. Boada-Romero E, Martinez J, Heckmann BL, Green DR. The Clearance of Dead Cells by Efferocytosis. *Nat Rev Mol Cell Biol* (2020) 21(7):398–414. doi: 10.1038/s41580-020-0232-1
61. Triantafyllou E, Woollard KJ, McPhail MJW, Antoniades CG, Possamai LA. The Role of Monocytes and Macrophages in Acute and Acute-On-Chronic Liver Failure. *Front Immunol* (2018) 9:2948. doi: 10.3389/fimmu.2018.02948
62. Murray PJ, Allen JE, Biswas SK, Fisher EA, Gilroy DW, Goerdt S, et al. Macrophage Activation and Polarization: Nomenclature and Experimental Guidelines. *Immunity* (2014) 41(1):14–20. doi: 10.1016/j.immuni.2014.06.008

Conflict of Interest: ML is a CNPq fellow. MM was a CAPES fellow and is currently an EILF-EASL Sheila Sherlock Postdoctoral fellow. BN is a CNPq fellow. RM is a CAPES. GCS was a CAPES fellow and is currently FRQS postdoctoral fellowship. PM is a CNPq fellow. AO is a FAPEMIG and CNPq fellow. RG is a FAPEMIG fellow (RED-00313-16; REMETTEC-RED 00570-16). GM is currently a CNPq fellow.

The authors declare that the research was conducted without any commercial or financial relationships that could be construed as a potential conflict of interest.

frontiers | Frontiers in Immunology

TYPE Correction
PUBLISHED 14 October 2022
DOI 10.3389/fimmu.2022.1038067

OPEN ACCESS

APPROVED BY
Frontiers Editorial Office,
Frontiers Media SA, Switzerland

*CORRESPONDENCE
Mateus Eustáquio Lopes
mateusedml@gmail.com
Gustavo Batista Menezes
menezesgb@ufmg.br

†These authors have contributed equally to this work

SPECIALTY SECTION
This article was submitted to Inflammation, a section of the journal Frontiers in Immunology

RECEIVED 06 September 2022
ACCEPTED 03 October 2022
PUBLISHED 14 October 2022

CITATION
Lopes ME, Nakagaki BN, Mattos MS, Campolina-Silva GH, Meira RdO, Paixão PHdM, Oliveira AG, Faustino LD, Gonçalves R and Menezes GB (2022) Corrigendum: Susceptibility to infections during acute liver injury depends on transient disruption of liver macrophage niche. *Front. Immunol.* 13:1038067. doi: 10.3389/fimmu.2022.1038067

Corrigendum: Susceptibility to infections during acute liver injury depends on transient disruption of liver macrophage niche

Mateus Eustáquio Lopes[1*], Brenda Naemi Nakagaki[1†], Matheus Silvério Mattos[1†], Gabriel Henrique Campolina-Silva[2,3], Raquel de Oliveira Meira[4], Pierre Henrique de Menezes Paixão[4], André Gustavo Oliveira[5], Lucas D. Faustino[6], Ricardo Gonçalves[4] and Gustavo Batista Menezes[1*]

[1]Center for Gastrointestinal Biology, Departamento de Morfologia, Instituto de Ciências Biológicas, Universidade Federal de Minas Gerais (UFMG), Belo Horizonte, Brazil, [2]Department of Biochemistry and Immunology, Instituto de Ciências Biológicas, Universidade Federal de Minas Gerais (UFMG), Belo Horizonte, Brazil, [3]Centre de Recherche du Centre Hospitalier Universitaire de Québec, Université Laval, Québec, QC, Canada, [4]Macrophage and Monocyte Biology Laboratory, Department of Pathology, Instituto de Ciências Biológicas, Universidade Federal de Minas Gerais (UFMG), Belo Horizonte, Brazil, [5]Department of Physiology and Biophysics, Instituto de Ciências Biológicas, Universidade Federal de Minas Gerais (UFMG), Belo Horizonte, Brazil, [6]Center for Immunology and Inflammatory Diseases, Division of Rheumatology, Allergy and Immunology, Massachusetts General Hospital, Harvard Medical School, Boston, MA, United States

KEYWORDS

Kupffer cell, Macrophage niche, Acute liver injury, Inflammation, Cell therapy, Systemic infection

A Corrigendum on

Susceptibility to infections during acute liver injury depends on transient disruption of liver macrophage niche

by Lopes ME, Nakagaki BN, Mattos MS, Campolina-Silva GH, Meira RdO, Paixão P H M, Oliveira A G, Faustino L D, Gonçalves R and Menezes GB (2022) Front. Immunol. 13:892114. doi: 10.3389/fimmu.2022.892114

In the published article, there was an error in affiliations 1, 2, 4 and 5. Instead of "Center for Gastrointestinal Biology, Department of Morphology, Institute of Biological Sciences, Federal University of Minas Gerais, Belo Horizonte, Brazil", "Department of Biochemistry and Immunology, Institute of Biological Sciences, Federal University of Minas Gerais, Belo Horizonte, Brazil", "Macrophage and Monocyte Biology Laboratory, Department of Pathology, Institute of Biological Sciences, Federal University of Minas Gerais, Belo

Horizonte, Brazil" and "Department of Physiology and Biophysics, Institute of Biological Sciences, Federal University of Minas Gerais, Belo Horizonte, Brazil", it should be "Center for Gastrointestinal Biology, Departamento de Morfologia, Instituto de Ciências Biológicas, Universidade Federal de Minas Gerais (UFMG), Belo Horizonte, Brazil", "Department of Biochemistry and Immunology, Instituto de Ciências Biológicas, Universidade Federal de Minas Gerais (UFMG), Belo Horizonte, Brazil", "Macrophage and Monocyte Biology Laboratory, Department of Pathology, Instituto de Ciências Biológicas, Universidade Federal de Minas Gerais (UFMG), Belo Horizonte, Brazil" and "Department of Physiology and Biophysics, Instituto de Ciências Biológicas, Universidade Federal de Minas Gerais (UFMG), Belo Horizonte, Brazil".

The authors apologize for this error and state that this does not change the scientific conclusions of the article in any way. The original article has been updated.

Publisher's note

frontiers | Frontiers in Immunology

TYPE Original Research
PUBLISHED 11 August 2022
DOI 10.3389/fimmu.2022.937201

OPEN ACCESS

EDITED BY
Andrea Baragetti,
University of Milan, Italy

REVIEWED BY
Roberto Scicali,
Garibaldi Hospital, Italy
Federica Fogacci,
University of Bologna, Italy
Maria Giovanna Lupo,
University of Padua, Italy

*CORRESPONDENCE
Najiao Hong
drnjhong@yahoo.com
Sixin Xie
ljtnc2021@gmail.com

SPECIALTY SECTION
This article was submitted to Inflammation, a section of the journal Frontiers in Immunology

RECEIVED 05 May 2022
ACCEPTED 07 July 2022
PUBLISHED 11 August 2022

CITATION
Hong N, Lin Y, Ye Z, Yang C, Huang Y, Duan Q and Xie S (2022) The relationship between dyslipidemia and inflammation among adults in east coast China: A cross-sectional study. *Front. Immunol.* 13:937201. doi: 10.3389/fimmu.2022.937201

The relationship between dyslipidemia and inflammation among adults in east coast China: A cross-sectional study

Najiao Hong[1*], Yongjun Lin[1], Zhirong Ye[1], Chunbaixue Yang[2], Yulong Huang[1], Qi Duan[1] and Sixin Xie[1*]

[1]Department of General Medicine, The First Hospital of Quanzhou affiliated to Fujian Medical University, Quanzhou, China, [2]Department of Mathematics, Virginia Tech, Blacksburg, VA, United States

Objective: Dyslipidemia is one of the major public health problems in China. It is characterized by multisystem dysregulation and inflammation, and oxidant/antioxidant balance has been suggested as an important factor for its initiation and progression. The objective of this study was to determine the relationship between prevalence of dyslipidemia and measured changes in the levels of proinflammatory cytokines (IL-6, TNF-a, and MCP-1), thiobarbituric acid-reactant substances (TBARS), and serum total antioxidant capacity (TAC) in serum samples.

Study design: A cross-sectional survey with a purposive sampling of 2,631 enrolled participants (age 18–85 years) was performed using the adult population of long-term residents of the municipality of east coast China in Fujian province between the years 2017 and 2019. Information on general health status, dyslipidemia prevalence, and selected mediators of inflammation was collected through a two-stage probability sampling design according to socioeconomic level, sex, and age.

Methods: The lipid profile was conducted by measuring the levels of total cholesterol (TC), high-density lipoprotein cholesterol (HDL-C), low-density lipoprotein cholesterol (LDL-C), and triglycerides (TG) with an autoanalyzer. Dyslipidemia was defined according to National Cholesterol Education Program Adult Treatment Panel III diagnostic criteria, and patients with it were identified by means of a computerized database. Serum parameters including IL-6/TNF-a/MCP-1, TBARS, and TAC were measured in three consecutive years. Familial history, education level, risk factors, etc. were determined. The association between dyslipidemia and serum parameters was explored using multivariable logistic regression models. Sociodemographic, age, and risk factors were also investigated among all participants.

Results: The mean prevalence of various dyslipidemia in the population at baseline (2017) was as follows: dyslipidemias, 28.50%; hypercholesterolemia, 26.33%; high LDL-C, 26.10%; low HDL-C, 24.44%; and hypertriglyceridemia,

27.77%. A significant effect of aging was found among all male and female participants. The mean levels of serum Il-6/TNF-a/MCP-1 were significantly higher in all the types of dyslipidemia among male participants. Female participants with all types of dyslipidemia but low HDL-C showed an elevation of IL-6 and MCP-1 levels, and those with dyslipidemias and hypercholesterolemia presented higher levels of TNF-a compared to the normal participants. The oxidative stress marker TBARS increased among all types of dyslipidemia except hypertriglyceridemia. All participants with different types of dyslipidemia had a lower total antioxidant capacity. Correlation analysis showed that cytokines and TBARS were positively associated with age, obesity, and diabetes mellitus, but not sex, sedentary leisure lifestyle, hypertension, and CVD/CHD history. The activity of TAC was negatively associated with the above parameters.

Conclusions: The correlation between the prevalence of dyslipidemia and the modification of inflammation status was statistically significant. The levels of proinflammatory cytokines, oxidative stress, and antioxidant capacity in serum may reflect the severity of the lipid abnormalities. These promising results further warrant a thorough medical screening in enhanced anti-inflammatory and reduced oxidative stress to better diagnose and comprehensively treat dyslipidemia at an early stage.

KEYWORDS

dyslipidemia, IL-6, TNF-a, MCP-1, TBARS, TAC

Introduction

Dyslipidemia is recognized worldwide as one important risk factor in cardiovascular disease, morbidity, and mortality. Some studies suggested an independent correlation between dyslipidemia and the risk of cardiovascular and encephalovascular events (1, 2). It is characterized by a systemic abnormal lipid profile in which the level of serum cholesterol, triglycerides, or both is elevated, or the level of high-density lipoprotein cholesterol (HDL-C) is reduced (1, 2).

The occurrences and developments of some lipid disorders are often associated with excessive induction of proinflammatory cytokine production. Previous studies showed that cytokines such as TNF-α were involved in the severity of the lipid disturbance. Certain proinflammatory cytokines not only are involved in regulating energy balance, proliferation, and apoptosis of adipocytes, but also regulate lipolysis, inhibit lipid synthesis, and lower blood lipids, among others. Many reports indicated that proinflammatory cytokines may significantly influence the development of lipid metabolism of obesity, atherosclerosis, steatohepatitis, hyperlipoproteinemia, and type 2 diabetes (3, 4). The study by Scicali et al. (5) observed the biomarker role of S100A12, a molecule expressed primarily by neutrophils in familial hypercholesterolemia (FH) in which the level of serum S100A12 was correlated not only with age and genetic mutation but also with pulse wave velocity. Another study (6) indicated that the ligation of S100A12 with its receptor-advanced glycation end products (RAGE) occurs downstream of activation of intracellular signal cascades, e.g., MAP-kinase and nuclear factor (NF)-κB, resulting in production of proinflammatory cytokines such as TNF-α and IL-1β, and high expression of adhesion molecules such as intercellular adhesion molecule (ICAM)-1 and vascular cell adhesion molecule (VCAM)-1. A recent report by Kim et al. (7) demonstrated a correlation between serum S100A12 levels and the vascular calcification score, suggesting the progression of atherosclerotic vascular complications consequent to the induction of systemic inflammation. A clinical study by Kroon et al. (8) indicated the evidence of an increased arterial wall inflammation in familial dysbetalipoproteinemia (FD) accompanied by elevated lipid accumulation in monocytes and higher expression of surface integrins (CD11b, CD11c, and CD18). Overall, these findings imply that inflammation is a key regulatory process that hitches the immune system and hypercholesterolemia, which contributes to the increased cardiovascular disease risk.

Several studies have shown an imbalance between oxidants and antioxidants in impaired lipid metabolism due to the altered lipid peroxidation and antioxidant enzyme activities (9–12). According to the hypothesis of allostasis by McEwen et al. (13), it is possible that prolonged oxidative stress, as the mediators of allostatic load, may induce a long-term alteration in lipid profile concomitant with altered antioxidant status, resulting in severe consequence such as atherosclerosis.

In the last two decades, many reports have shown the estimated prevalence of dyslipidemia with the following difference rates: 59.74% in the state of São Paulo of Brazil (2014) (14), 53% in U.S. (2006) (15), 88.9% in Thailand (16). 79.55% in Turkey (2014) (17), 79.00% in India (2014) (18), 56.50% in Japan (2015) (19), and 19.05% in China (2006) (20).

In China, the east coast has been undergoing rapid socioeconomic development and urbanization in the past four decades. In the 21st century, an increase in industrialization and an acceleration of rural-to-urban migration are occurring along east coast provinces, which are now confronted with a major public health challenge, especially the growing disease burden attributable to environmental conditions, food and nutrition, and lifestyle choices (21).

While China is known to have a rapidly increasing epidemiology of lipid metabolic dysfunction, there have been few effective studies on complete evaluation of proinflammation and oxidative stress to assess the magnitude of the dyslipidemia profile among the adults in east coast. The evidence of the prevalence of dyslipidemia and trends of proinflammatory markers and oxidative stress within a distinct group representative of east coast urban population will undoubtedly ensure proper guidelines of healthcare resources for both primary and secondary prevention of cardiovascular disease and atherosclerosis (22–26).

The present study aimed to determine a 3-year change in the levels of proinflammatory markers, oxidative stress, antioxidant capacity, and the prevalence of dyslipidemias from a large representative sample of the urban population ≥18 years old residing in east coast urban, Fujian province, China. The correlations among the serum markers, e.g., IL-6, TNF-α, MCP-1, TBARS, and TAC, and lipid disorders were explored as one of changing times and public health significance.

Methods

Study population and sample

Our cross-sectional study was carried out through a two-stage stratified sampling method in which a representative sample was selected among the general population aged ≥ 18 years in east coast, Fujian, China. According to the method by Yang et al. (26), the first level of sampling in the study population was stratified by indicated geographical regions of the east coast. The selected areas encompassed six urban districts —Fuzhou, Xiamen, Quanzhou, Zhangzhou, Putian, and Ningde. For the second stage of sampling, classified factors included sex, age distribution, education level, and socioeconomic strata based on Fujian urban districts data published in the year of 2016. According to Kish selection table (27) and the government (Fujian Provincial Bureau of Statistics) household registration profile, especially the data on the household and residential compositions, eligible households and its adult members were randomly chosen on each listed street/avenue/road of 89 units with probability proportional to population size. The representative participants were qualified from urban civilian adults who had been living in their current city for ≥5 years. Any participants who may not be available due to personal reasons were replaced by other eligible households within a similar local community during the recruiting time. In the second level of sampling, participants were stratified according to ages, sex, general health status, and educational status as well as social status.

Ethical approval and consent to all participants and the study was approved by the hospital Ethical Committee of Quanzhou in accordance with the Declaration of Helsinki. The health survey that the current study conducted was adopted by the Chinese Resident Health Literacy Scale (CRHLS), which was developed by the Chinese Ministry of Health. The scale's reliability and construct validity were assessed by using a population-based sample from South China by Shen et al. (28) and others (29, 30). It was prepared in simplified Chinese and consisted of 64 selected items based on classical test theory and item response theory. A pre-test pertinent to field test, consultation process, and plain language examination was displayed in a pilot group recruited from five cities. It was noticeable that the test was time-consuming because it took 25–35 min for a participant to complete and even longer for those with limited literacy or other conditions. The scales showed not only a balance between complexity and quantity of questions in different categories of the questionnaire but also a good psychometric property with construct validity, reliability, and acceptability. The overall performance of existing CRHLS in the current study was a qualified tool in accuracy of predictive performance during the home interview. In detail, the participants needed to complete a survey questionnaire about demographic features, socioeconomic status, lifestyle, health/medical history especially hypertension, atherosclerosis, and diabetes, smoking, and alcohol consumption. Exclusion criteria included those who showed very low literacy or poor communication skills, those with severe organic or neurologic pathology, and those unable to process an interview due to psychiatric disorders. Participants who met the exclusion criteria should be replaced by other eligible participants recruited within a similar community. The criterion of smoking was defined as continuous use of tobacco or quit within 4 months. The

criterion of drinking was defined as having 30 g/week of alcohol intake for the past 12 months or quit within 4 months. The physical activity levels were classified as regular physical activity and sedentary leisure based on the global physical activity questionnaire. Education levels were graded as lower or college/high school, and occupation was categorized as white-collar workers, blue-collar workers, and unemployed/unskilled/housewives. As suggested by Fujian Bureau of Statistics, the average annual income per capita of the participant's household in five consecutive years (expressed in US dollars) was classified into three major categories: low (<$6,030), medium ($6,030–10,960), and high (>$10,960).

Participant characteristics

Table 1 shows the demographic and socioeconomic strata among the selected participants in six age groups compared to the whole east coast urban adults in Fujian province and the overall urban population of the province based on Fujian 2016 census data (31). Fujian province has a population of about 76 hundred million, out of which 38.1 million people live in six major cities along the east coast, namely, Fuzhou, Xiamen, Quanzhou, Zhangzhou, Putian, and Ningde.

A total of 2,631 individuals (1,368 male and 1,266 female individuals) aged 18 to 85 years between 2017 and 2019 were selected before registration in the study. There was an overall response rate of 91.1% (2,397), 88.6% (1,209) among male adults and 93.8% (1,188) among female adults. In the year of the original investigation, 31 participants opted out of the study for various reasons, and the replacement rate was 1.3%. A total of 2,001 participants with an 83.46% overall response rate entered the first year of the follow-up study. Thirty (1.5%) participants had to discontinue their interest in the second year of follow-up. By the end of 2019, 1,962 individuals with 963 men and 999 women were invited to complete the investigation. During the three years, registered participants had three analyses in each calendar year.

Collection of blood samples

As the second step, a series of clinical examinations were carried out: health-related questionnaire, blood pressure, fasting blood glucose, lipid profiles, proinflammatory markers, and oxidative stress.

The serum samples were later analyzed for serum lipids. Eighty milliliters of fasting blood was obtained after 12 h overnight fasting and kept for 30 min to allow the blood to clot. All the serum samples were separated and stored at −70°C. The biochemical analyses and methods were performed for the following parameters: glycemia by blood gas analyzer (Bayer 865, NY), and lipid including total cholesterol, serum triglycerides, and HDL-C by the enzymatic method [Hitachi 7600 auto-analyzer (Hitachi, Japan)].

Lipid level analysis

Serum LDL-C was estimated by using the Friedewald formula: LDL-C = TC − HDL-C − TG/5. The value of non-HDL-C was calculated through the equation: non-HDL-C (mg/dl) = TC - HDL-C. It was suggested by NCEP-ATP III guidelines that dyslipidemia was characterized within four lipid components as hypercholesterolemia (TC ≥ 240 mg/dl) or hypertriglyceridemia (TG ≥ 160 mg/dl) or low HDL-C (≤40 mg/dl), or high LDL-C (≥160 mg/dl).

Proinflammatory marker measurement

The levels of serum proinflammatory markers—interleukin-6, monocyte chemoattractant protein-1, and tumor necrosis factor-α—were detected by using enzyme-linked immunosorbent assay (ELISA) (MultiSciences Biotech Co., Ltd.) according to the manufacturer's protocol. As suggested by the ELISA kit, a mixture of 50 µl of serum samples, twofold diluted standard, and diluted detection antibody were incubated at room temperature for 1 h and 45 min on a microplate shaker set at 300 rpm. After careful washing, 100 µl of diluted streptavidin-horseradish peroxidase was added. Then, progressive development of a colored complex in the plates was produced by using a substrate solution. The intensity of the produced colored complex was directly proportional to the concentration of the markers in the samples. The absorbance of the complex is finally measured and calculated by plotting against the expected concentration, forming a standard curve.

Thiobarbituric acid reactive substance measurement

Determination of serum TBARS was tested by thiobarbituric acid assay according to the method by Kamal et al. (32). First, 50 µl of serum samples was purified with butylated hydroxytoluene in 10% trichloroacetic acid. Then, 0.6% thiobarbituric acid in 0.44 M phosphoric acid was added; after 45-min incubation at 90°C, the pink color complex was developed. Finally, the absorbance of the complex was measured and calculated by plotting against the 1,1,3,3 tetramethoxypropane standard curve.

Total antioxidant capacity measurement

Total antioxidant capacity was assessed by a spectrophotometric method. First, the diluted serum sample [1:25 in phosphate buffer

TABLE 1 Distribution of demographic characteristics and general socioeconomic indicators among different urban populations.

Characteristic	The population in the current study			Fujian coast urban population	Fujian urban Population
	1st year (2017)	Follow-up I (2018)	Follow-up II (2019)		
Total number	15,397	12,144	11,762	9,936,850	3,495,356
Age distribution (years) (%)					
18–29	14.9	14.1	14.2	15.8	16.1
30–39	17.7	17.0	17.1	18.5	17.4
40–49	19.8	20.5	19.7	21.4	19.5
50–59	20.8	21.0	20.6	19.2	20.2
60–69	17.1	17.8	18.9	15.5	17.3
≥70	9.7	9.6	9.5	9.6	9.5
Median (years)	41.8	41.9	42.0	41.1	42.2
Sex					
Male	50.08	49.90	49.82	50.12	50.88
Female	49.92	50.10	50.18	49.88	49.12
Education					
Lower	53.02	52.90	51.91	53.89	65.26
College/high school	46.98	47.10	48.09	46.11	34.74
Occupation					
White-collar workers	34.1	33.9	33.1	34.0	32.6
Blue-collar workers	42.2	41.5	41.8	44.9	42.6
Unemployed, retired and housewives	23.7	24.6	25.1	21.1	24.8
Income					
Low	20.1	19.3	18.3	21.2	29.5
Medium	63.0	63.6	64.1	62.4	57.3
High	16.9	17.1	17.6	16.4	13.2
Marital status					
Married	73.1	72.5	70.9	74.3	74.7
Single	26.9	27.5	29.1	25.7	25.3

saline (pH = 7.4)] was mixed with 0.1 mM 2,2 diphenyl-1-picrylhydrazyl reagent. Then, the mixture was incubated in a dark room for 30 min. After centrifuging at 14,000 rpm, the absorbance was measured and finally calculated by plotting against the standard curve.

Statistical analysis

Demographics, health-related and medical histories, social status, and biomedical parameters were tested by SPSS 21.0 software (SPSS, Inc.). Means and standard deviations (SDs) were described for continuous variables including levels of biomedical markers within each group or each lipid abnormality class. Means and confidence interval (CI) were used for evaluating the prevalence of dyslipidemias within group/class. ANOVA was used to analyze multiple comparisons. Logistic regression analysis was applied for the relationship between the independent variables (e.g., age and proinflammatory cytokines, TBARS, and IAC) and the response variables (e.g., lipid abnormality). Pearson correlation coefficients were calculated for the association between biomedical marker parameters and lipid abnormalities. A two-tailed p-value of <0.05 was considered to be significant.

Results

As shown in Table 1, our participant sample was composed of 1,397 adults living in the east coast, Fujian, China, whose baseline ages ranged from 18 to 83, 50.08% men and 49.92% women, and the mean age was 40.6 ± 13.8 years in men and 42.9 ± 12.9 years in women. The consecutive 3-year visits (from 2017 to 2019) yielded demographic characteristics and general socioeconomic indicators among them.

To probe the normality of the samples, we applied the Anderson–Darling test to delineate three probability plots through the overall parameters, time (years), and sex, respectively. The result showed that the data followed a normal distribution. Table 2 indicates the levels of serum lipid profile in the consecutive years. Higher serum levels of total cholesterol, LDL-C, and triglycerides were significantly

TABLE 2 Means and standard deviations of the serum levels of cholesterol, LDL cholesterol, HDL cholesterol, and triglycerides among adults in East Coast, Fujian, China.

Gender	Group (years)	Serum Cholesterol (mg/dl)*									Serum Triglycerides (mg/dl)*		
		Non-HDL-C			LDL-C			HDL-C					
		1st year (2017) X ± SD	Follow-up I (2018) X ± SD	Follow-up II (2019) X ± SD	1st year (2017) X ± SD	Follow-up I (2018) X ± SD	Follow-up II (2019) X ± SD	1st year (2017) X ± SD	Follow-up I (2018) X ± SD	Follow-up II (2019) X ± SD	1st year (2017) X ± SD	Follow-up I (2018) X ± SD	Follow-up II (2019) X ± SD
Male													
Total	18–29	142.0 ± 22.4	144.9 ± 26.1	145.3 ± 22.5	108.8 ± 20.8	109.4 ± 19.1	110.3 ± 20.7	57.5 ± 9.6	57.2 ± 10.1	56.8 ± 7.9	190.9 ± 20.6	191.1 ± 20.1	194.1 ± 27.1
	30–39	144.9 ± 21.9	145.8 ± 23.8	150.9 ± 23.4	110.1 ± 20.3	110.6 ± 19.9	112.9 ± 20.6	56.7 ± 8.8	56.7 ± 9.4	57.0 ± 7.4	191.6 ± 21.2	193.0 ± 22.6	195.4 ± 21.4
	40–49	153.3 ± 23.5	155.7 ± 22.6	157.3 ± 24.3	111.5 ± 20.3	113.2 ± 20.1	117.4 ± 21.1	52.1 ± 9.0	52.0 ± 9.9	51.9 ± 8.8	194.1 ± 22.7	196.7 ± 20.6	200.5 ± 28.8
	50–59	156.4 ± 21.8	159.4 ± 25.5	163.1 ± 20.9	121.9 ± 21.3	124.3 ± 20.3	127.9 ± 20.3	53.3 ± 7.8	54.0 ± 8.7	53.0 ± 9.9	188.7 ± 23.3	191.9 ± 23.6	195.4 ± 25.5
	60–69	157.2 ± 23.4	160.9 ± 24.5	163.5 ± 22.5	132.0 ± 20.7	133.0 ± 20.1	136.6 ± 19.5	52.9 ± 8.9	53.0 ± 8.5	52.4 ± 8.3	168.3 ± 25.6	171.9 ± 22.5	175.0 ± 20.4
	≥70	152.6 ± 25.2	155.9 ± 26.8	162.8 ± 21.1	135.5 ± 20.1	137.1 ± 19.2	141.0 ± 18.8	58.6 ± 9.1	58.0 ± 8.3	55.5 ± 9.5	158.0 ± 22.1	162.0 ± 22.9	165.1 ± 21.1
		153.8 ± 20.8	156.8 ± 21.4	160.7 ± 22.7	123.3 ± 19.9	123.7 ± 22.7	134.6 ± 21.6	55.4 ± 7.7	54.5 ± 8.5	53.9 ± 7.8	190.2 ± 24.1	194.6 ± 23.3	196.6 ± 22.8
p-values for linear trend		<0.001	<0.001	<0.001	<0.001	<0.001	<0.001	0.09	0.06	0.08	<0.001	<0.001	<0.001
Female													
Total	18–29	130.1± 22.8	130.2 ± 24.1	132.3 ± 24.6	109.2 ± 19.8	111.3 ± 19.3	112.5 ± 20.5	60.6 ± 6.6	60.3 ± 8.2	59.5 ± 8.9	159.8 ± 20.1	160.7 ± 26.5	165.4 ± 23.8
	30–39	131.0 ± 19.9	131.7 ± 24.4	135.4 ± 23.6	109.4 ± 18.5	111.6 ± 17.7	112.6 ± 18.7	60.6 ± 7.1	60.2 ± 8.6	59.2 ± 9.9	160.1 ± 23.5	161.4 ± 26.6	166.6 ± 25.7
	40–49	134.0 ± 22.6	135.9 ± 21.1	139.4 ± 22.6	113.4 ± 23.3	116.2 ± 18.6	122.9 ± 20.3	61.1 ± 7.4	60.1 ± 7.6	60.3 ± 7.7	160.5 ± 23.5	162.4 ± 25.5	167.0 ± 24.9
	50–59	137.0 ± 22.1	142.9 ± 22.6	150.8 ± 25.8	117.4 ± 22.5	119.1 ± 16.9	126.4 ± 20.6	59.6 ± 7.9	59.3 ± 7.7	58.8 ± 8.4	167.0 ± 22.1	167.1 ± 23.8	170.7 ± 22.1
	60–69	147.2 ± 24.4	149.1 ± 25.2	157.7 ± 26.1	121.2 ± 21.5	123.9 ± 22.6	130.8 ± 19.3	56.4 ± 8.5	56.1 ± 8.2	55.3 ± 10.1	177.2 ± 22.1	179.5 ± 25.8	184.1 ± 23.8
	≥70	148.8 ± 24.7	153.3 ± 22.4	158.2 ± 22.6	121.2 ± 21.6	123.9 ± 23.7	131.9 ± 17.7	56.1 ± 7.4	56.4 ± 9.9	55.4 ± 9.5	175.0 ± 23.1	179.3 ± 25.4	183.8 ± 22.4
		127.0 ± 22.2	129.8 ± 23.9	135.9 ± 24.9	101.4 ± 20.5	102.9 ± 17.7	107.9 ± 19.1	51.1 ± 7.3	51.4 ± 8.1	51.3 ± 9.6	145.9 ± 22.1	147.8 ± 24.4	153.1 ± 24.6
p-values for linear trend		<0.001	<0.001	<0.001	<0.001	<0.001	<0.001	0.06	<0.01	0.06	<0.001	<0.001	<0.001

X, mean; SD, standard deviation. Values expressed in mg/dl [n = 15,397 (2017), 12,144 (2018), and 11,762 (2019)]. HDL indicates high-density lipoprotein; LDL, low-density lipoprotein.
*To convert from milligrams per deciliter to millimoles per liter divided by 38.67 for total, HDL, and LDL cholesterol and by 88.574 for triglycerides.

associated with aging among men and women. No significant change was observed in the 3 years within each age group.

We examined the distribution of lipid abnormalities among urban adults (Table 3). Results showed that within each lipid profile, participants present decreases in borderline levels compared to high/very high levels over time. Table 4 indicates the mean prevalence of various lipid profiles within the three consecutive years. A higher prevalence of dyslipidemia was significantly associated with male participants, family history, unhealthy habits (alcohol drinking and sedentary leisure activity), body weight (high waist circumference, overweight, and obesity), and health-related history (CHD, CVD, hypertension, and diabetes). The prevalence of other various cholesterols and TG was significantly higher among the participants with higher-than-average body weight (high waist circumference, overweight, and/or obese) and with a history of CVD and diabetes. The male-specific prevalence was found in high LDL cholesterol. There was a clear influence of history of

TABLE 3 Distribution of lipid abnormalities among adults in East Coast, Fujian, China in 2017 and 2-year follow-up.

			Prevalence, * % (95% CI)								
			1st year (2017)			Follow-up I (2018)			Follow-up II (2019)		
			Overall	Male	Female	Overall	Male	Female	Overall	Male	Female
Sample size			15,397	7,829	7,568	12,144	6,047	6,097	11,762	5,776	5,986
Lipid	**Value**	**Grading**									
Serum Non-HDL-C (mg/dl)	<130	Optimum	17.2 (15.3–19.1)	15.9 (14.1–19.8)	17.5 (15.9–19.5)	16.5 (15.1–18.0)	15.1 (11.4–18.8)	17.5 (15.9–19.5)	16.0 (15.1–17.0)	14.7 (12.5–16.9)	16.5 (14.9–18.2)
	130–159	Desirable	28.3 (25.5–31.1)	25.9 (23.3–29.9)	31.7 (27.5–33.5)	23.1 (25.5–31.1)	22.9 (21.3–24.6)	24.8 (22.5–27.2)	21.3 (19.5–23.1)	21.4 (20.3–22.6)	24.0 (22.0–26.1)
	160–189	Borderline	21.3 (19.6–23.2)	23.2 (21.1–25.5)	19.5 (15.7–22.3)	23.3 (19.6–23.2)	25.0 (22.6–27.5)	19.5 (15.7–22.3)	23.5 (20.6–26.4)	24.7 (22.6–26.8)	19.4 (16.7–22.2)
	190–219	High	26.2 (23.2–29.2)	28.2 (24.2–32.2)	24.2 (20.3–28.1)	29.2 (32.1–26.7)	29.6 (33.1–26.8)	28.8 (32.9–25.7)	29.0 (27.0–31.1)	28.6 (33.4–26.1)	29.3 (33.1–26.1)
	≥220	Very high	7.0 (4.1–10.0)	6.8 (4.3–9.3)	7.1 (4.1–10.1)	7.9 (10.1–6.1)	7.4 (9.3–5.5)	8.4 (11.6–5.2)	10.2 (13.1–7.3)	10.6 (13.1–7.2)	9.8 (11.7–8.3)
Serum LDL-C (mg/dl)	<100	Optimum	20.8 (17.7–23.9)	20.7 (17.9–23.8)	20.8 (17.7–23.9)	19.6 (17.7–21.9)	19.6 (17.6–21.6)	19.5 (17.9–21.1)	18.9 (16.1–20.7)	18.5 (16.1–20.9)	19.3 (16.1–20.7)
	100–129	Desirable	28.6 (26.3–30.9)	28.8 (25.7–31.7)	28.5 (26.2–30.8)	28.5 (26.5–30.5)	28.6 (26.5–30.7)	28.4 (26.5–30.5)	26.5 (23.7–29.3)	26.4 (23.4–29.4)	26.6 (23.7–29.3)
	130–159	Borderline	24.7 (21.9–27.5)	25.0 (23.1–27.1)	24.4 (21.8–27.6)	24.6 (21.7–27.5)	24.7 (21.9–27.5)	24.6 (21.7–27.5)	23.1 (21.4–24.8)	23.1 (21.2–24.9)	23.1 (21.5–24.7)
	160–189	High	18.6 (16.4–21.0)	18.7 (17.2–21.0)	18.5 (15.1–21.8)	18.6 (17.6–20.6)	18.8 (16.8–20.9)	18.4 (16.0–20.8)	25.1 (23.3–27.7)	24.5 (22.3–26.7)	25.7 (23.9-27.5)
	≥190	Very high	7.3 (4.7–10.1)	6.8 (5.1–8.6)	7.8 (6.6–9.1)	8.7 (7.5–9.9)	8.3 (6.5–9.9)	9.1 (7.3–11.0)	6.4 (4.8–8.2)	7.5 (6.1–9.0)	5.3 (3.1-7.7)
Serum HDL-C (mg/dl)	≥60	High	16.5 (14.2–18.8)	16.1 (13.7–18.5)	16.9 (13.9–19.9)	16.2 (14.0–18.4)	15.9 (14.0–17.8)	17.5 (14.1–20.9)	15.0 (13.7–16.3)	14.5 (13.2–15.8)	15.5 (13.0–18.0)
	40–59	Borderline	58.2 (56.1–60.3)	57.8 (55.8–59.8)	58.6 (55.2–61.0)	58.1 (55.9–60.3)	58.0 (55.2–60.8)	58.2 (55.4–61.0)	57.3 (55.3–59.3)	56.9 (55.0–57.8)	57.7 (56.1–59.3)
	<40	Low	25.3 (23.7–27.1)	26.1 (23.7–28.7)	24.5 (21.9–27.1)	25.7 (22.9–28.6)	26.1 (24.3–28.1)	25.3 (22.0–28.8)	27.7 (25.4–29.8)	28.6 (26.4–30.8)	26.8 (24.8-28.9)
Serum TG (mg/dl)	<150	Optimum	40.7 (38.1–43.3)	40.5 (38.0–43.0)	40.9 (38.1–43.7)	40.0 (38.0–42.0)	39.9 (38.0–42.0)	40.1 (38.0–42.2)	39.0 (37.7–40.3)	38.7 (37.7–40.3)	39.3 (37.2–41.4)
	150–199	Borderline	31.4 (29.8–33.0)	31.4 (29.6–33.2)	31.3 (29.5–33.1)	31.0 (29.1–32.9)	30.9 (29.1–32.9)	31.1 (29.0–33.2)	30.9 (29.0–32.8)	30.8 (29.0–32.8)	31.0 (28.8–33.2)
	200–499	High	21.0 (19.5–23.4)	22.0 (20.8–23.1)	19.9 (13.3–22.1)	22.0 (18.5–25.6)	22.7 (20.8–24.6)	21.3 (19.9–23.2)	22.6 (20.9–24.1)	23.6 (21.9–25.8)	21.6 (19.7-24.2)
	≥500	Very high	6.9 (5.1–8.8)	6.1 (4.7–7.8)	7.9 (5.9–9.9)	7.0 (5.2–8.9)	6.5 (5.1–8.0)	7.5 (5.8–9.3)	7.5 (5.0–9.1)	6.9 (5.3–8.6)	8.1 (6.1-10.1)
Total	From Optimum/ low to Borderline*		67.3 (61.9-72.7)	66.2 (62.7–69.5)	68.4 (63.2–73.6)	65.4 (61.1–69.7)	64.2 (59.5–68.9)	66.6 (61.2–72.0)	63.6 (58.1–68.5)	62.1 (57.7–66.5)	65.5 (60.3–70.7)
	High and Very high		32.7 (30.1-34.8)	33.8 (31.1–35.8)	31.6 (30.0–33.3)	34.6 (31.1–37.5)	35.8 (33.9–37.8)	33.4 (30.0–36.6)	36.4 (32.9–39.9)	37.9 (35.9–39.9)	34.5 (32.9–36.8)

*Prevalence (%) adjusted for age according to data from Chinese population estimates for the year 2017, 2018, and 2019 according to ATP III—Third Report of the Expert Panel on Detection, Evaluation, and Treatment of High Blood Cholesterol in Adults; CI, confidence interval; LDL, low-density lipoprotein; HDL, high-density lipoprotein. *$p < 0.01$ (χ^2 test).

smoking and hypertension on the prevalence of high triglyceride and low HDL cholesterol. There was no impact of educational level on the lipid profiles.

Figures 1, 2 show the age-specific prevalence of various lipid profiles in male and female participants, respectively. Overall, there was a significant aging trend of stable increases in prevalence of all lipid abnormalities from the young to the old group in both sexes. Maximum prevalence of dyslipidemia was in the sixth decade of life in both sexes. The prevalence of abnormal total cholesterol had a significant increase after the observed years among male participants ≥70 years of age onwards, whereas the levels were greater between 40 and 69 years in female participants. The prevalence of high LDL-C was found to significantly increase after the 3 years among the group of 40–59 years in male participants and the group of 40–49 years in female participants.

TABLE 4 Mean prevalence of dyslipidemias according to demographic and socioeconomic variables and familial history among adults in East Coast, Fujian, China.

Prevalence, * % (95% CI)					
	Dyslipidemia[#]	**High total cholesterol**	**High LDL-C**	**High TG**	**Low HDL-C**
Male	39.54 (35.87–43.21)	34.31 (30.79–37.82)	29.33 (25.89–32.77)	29.67 (26.51–32.84)	26.10 (22.97–29.56)
Female	31.97 (28.85–34.99)	28.85 (25.79–31.92)	28.97 (25.95–31.99)	28.93 (25.92–31.92)	24.54 (22.87–26.21)
P	0.04	0.06	0.20	0.20	0.18
Dyslipidemia in family					
Yes	44.31 (39.15–47.99)	11.14 (8.69–13.59)	11.01 (8.24–13.80)	30.61 (25.99–35.26)	20.96 (17.29–24.91)
No	32.23 (29.99–33.02)	7.46 (5.90–8.92)	7.31 (6.58–7.71)	20.52 (16.86–23.76)	17.24 (14.39–20.09)
p	<0.01	0.06	<0.01	0.02	0.08
Education level					
Low education	40.56 (35.21–45.92)	10.01 (7.40–12.63)	9.52 (8.41–9.65)	26.11 (22.03–26.19)	18.01 (16.02–19.99)
College/higher education	36.03 (33.01–40.05)	8.49 (5.99–10.47)	8.78 (7.99–9.58)	25.02 (21.94–28.92)	20.20 (18.06–22.39)
p (Linear tread)	0.10	0.13	0.18	0.09	0.21
History of smoking ^					
Yes	42.91 (37.64–46.41)	9.93 (6.91–10.99)	9.89 (7.99–9.81)	29.12 (25.21–33.03)	26.25 (23.01–29.50)
No	33.69 (29.41–38.69)	8.61 (6.36–10.86)	8.42(7.11–9.14)	22.03 (18.96–25.02)	11.99 (9.98–13.99)
p	0.06	0.25	0.08	0.03	0.01
Alcohol drinking†					
Yes	42.08 (38.87–45.29)	9.84 (7.97–11.71)	10.07 (7.91–8.99)	30.76 (26.99–34.53)	27.59 (23.86–30.93)
No	34.45 (30.21–38.70)	8.71 (5.99–11.48)	8.24 (7.61–9.87)	20.42 (17.82–23.02)	10.65 (9.02–12.29)
p	0.04	0.13	0.07	0.03	0.01
Overweight§					
Yes	46.57 (39.86–53.28)	10.82 (8.89–12.25)	10.54 (8.95–12.13)	30.99 (27.98–34.99)	22.19 (18.97–25.39)
No	29.95 (25.03–34.97)	7.75 (5.90–9.61)	7.77 (6.59–8.91)	20.15 (17.96–22.34)	16.07 (14.76–17.37)
p	<0.001	<0.001	0.01	<0.001	<0.01
Obesity					
Yes	53.22 (41.98–64.57)	12.12 (10.01–14.23)	12.14 (10.97–13.35)	31.35 (28.99–33.31)	21.25 (18.89–23.66)
No	23.31 (21.44–25.23)	6.44 (5.01–7.87)	6.17 (5.49–6.85)	19.77 (17.91–21.63)	17.05 (16.21–17.89)
p	<0.001	<0.001	<0.001	<0.001	0.01
Waist circumference ¶					
High	49.77 (45.03–53.57)	12.38 (10.25–14.54)	12.39 (11.03–14.60)	29.75 (26.11–34.97)	23.91 (18.99–28.04)
Normal	26.83 (22.86–30.81)	6.23 (5.15–7.31)	5.94 (5.11–7.03)	21.43 (18.76–24.88)	14.36 (11.21–17.11)
p	<0.001	<0.001	<0.001	<0.001	0.01
Lifestyle					
Regular physical activity ~	29.84 (24.59–35.01)	7.01 (5.14–8.88)	7.11 (5.23–8.98)	21.05 (19.76–22.74)	17.42 (14.95–19.86)
Sedentary Leisure	46.69 (41.86–51.53)	11.54 (8.99–14.09)	11.25 (9.20–13.02)	30.96 (15.78–19.14)	20.81 (17.65–23.99)
p	<0.001	0.01	0.01	0.01	0.09
History of CHD					
Yes	40.71 (38.51–43.01)	9.28 (7.21–11.26)	10.11 (8.84–11.51)	27.39 (24.94–29.84)	17.25 (14.21–19.32)
No	35.82 (33.58–38.06)	9.23 (7.75–10.72)	8.14 (7.01–9.27)	23.72 (20.53–26.92)	20.98 (17.99–24.22)
p	0.01	0.12	0.06	0.10	0.10
History of CVD					
Yes	40.85 (38.22–43.48)	11.96 (9.15–15.81)	11.71 (9.02–14.41)	29.85 (24.93–35.08)	23.98 (18.90–29.10)
No	35.71 (32.29–38.21)	6.53 (4.81–8.25)	7.50 (6.01–8.99)	21.31 (19.65–23.65)	14.22 (11.13–17.04)
p	0.01	<0.001	0.01	0.01	0.01
Hypertension					
Yes	44.87 (41.02–48.67)	11.77 (9.01–14.61)	8.61 (7.22–9.98)	32.85 (29.40–35.73)	24.77 (19.99–29.67)
No	31.73 (28.83–34.71)	6.79 (5.02–8.68)	9.66 (7.86–10.42)	18.34 (16.30–20.80)	13.43 (10.81–16.05)
p	<0.001	0.01	0.15	<0.001	<0.01

(Continued)

TABLE 4 Continued

Prevalence, * % (95% CI)

	Dyslipidemia#	High total cholesterol	High LDL-C	High TG	Low HDL-C
Diabetes Mellitus					
Yes	46.23 (41.99–50.47)	13.74 (11.09–16.54)	12.73 (10.04–15.23)	31.15 (28.02–34.29)	25.51 (21.34–29.69)
No	30.27 (27.82–32.73)	4.83 (3.99–5.77)	5.53 (4.02–7.04)	20.03 (16.44–23.64)	12.72 (9.69–15.79)
p	<0.001	<0.001	<0.001	<0.001	<0.001

*Mean percentages (95% confidence interval) were shown and based on the overall values within the 3 years. CVD indicates cardiovascular disease; CHD, coronary heart disease; BP, blood pressure; LDL, low-density lipoprotein; and HDL, high-density lipoprotein.
#Dyslipidemia was defined as total cholesterol 240 mg/dl, and/or triglyceride ≥160 mg/dl, and/or LDL cholesterol 160 mg/dl, and/or HDL cholesterol 40 mg/dl, and/or use of lipid-lowering medications.
^Smoking was defined as current daily smoking or quit less than 5 years; Non-smoking is defined as never smoking cigarettes daily or quit smoking more than 5 years.
†Alcohol drinking was defined as consumption of 30 g of alcohol per week for 1 year.
§Overweight was defined as a body mass index (kg/m^2) value of 24 or more; Obesity was defined as a body mass index (kg/m^2) value of 28 and above. High circumference is defined as a waist circumference over 85 cm for men and over 80 cm for women.
~ Defined as an exercise of moderate or vigorous activity at least for 30 min per day with 3 days per week.

Dyslipidemia appeared much higher within the group of 60–69 years compared to others within the male population.

We examined the average levels of proinflammatory cytokines and oxidative status (TBARS and TAC) among the participants and the effects of general demographic and socioeconomic factors on the molecules (Tables 5, 6). There was no difference in overall mean levels of cytokines and oxidative molecules between male and female participants. While both male and female participants had a small change of molecule levels after the observed 3 years, the majority of the participants exhibited a significant trend in favor of their age. Increases in serum IL-6, TNF-α, MCP-1, and TBARS, and reduction in serum TAC was statistically associated with the history of dyslipidemia, diabetes, and obesity.

To determine the effect of different lipid abnormalities on serum proinflammatory cytokines and oxidative status, we measured average serum levels of IL-6, TNF-α, MCP-1, TBARS, and TAC on each lipid-specific group (Figures 3, 4). Compared to the normal baseline, IL-6 level was significantly higher among the groups with high total cholesterol, LDL-C,

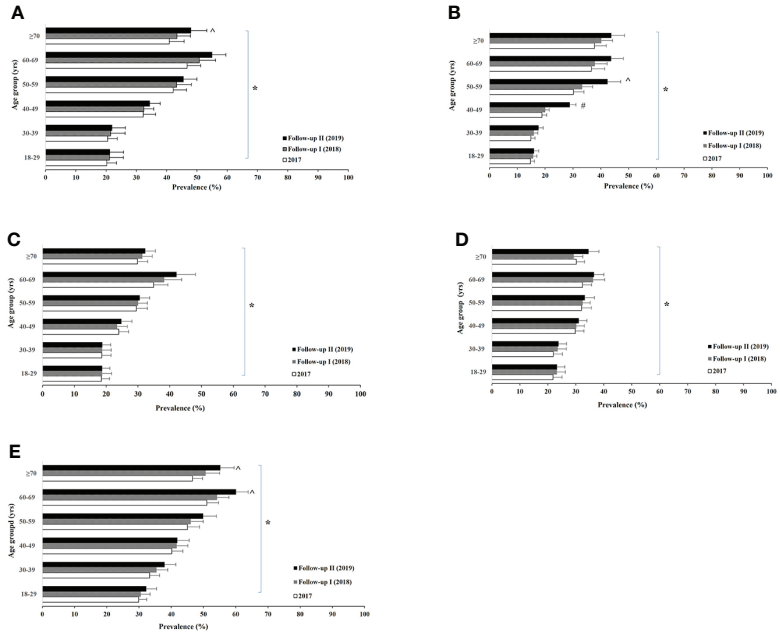

FIGURE 1
Male age-specific prevalence of high total (non-HDL) cholesterol **(A)**, high low-density lipoprotein cholesterol **(B)**, low high-density lipoprotein **(C)**, high triglyceride **(D)**, and dyslipidemias **(E)** among urban adults in East Coast, Fujian, China between 2017 and 2019. Logistic regression analysis indicated: * aging trend within each lipid abnormality **(A)** $p < 0.005$; **(B)** $p < 0.001$; **(C)** $p < 0.001$; **(D)** $p = 0.003$; **(E)** $p < 0.001$, and ^ for time trend within the age group **(B)** $p < 0.001$.

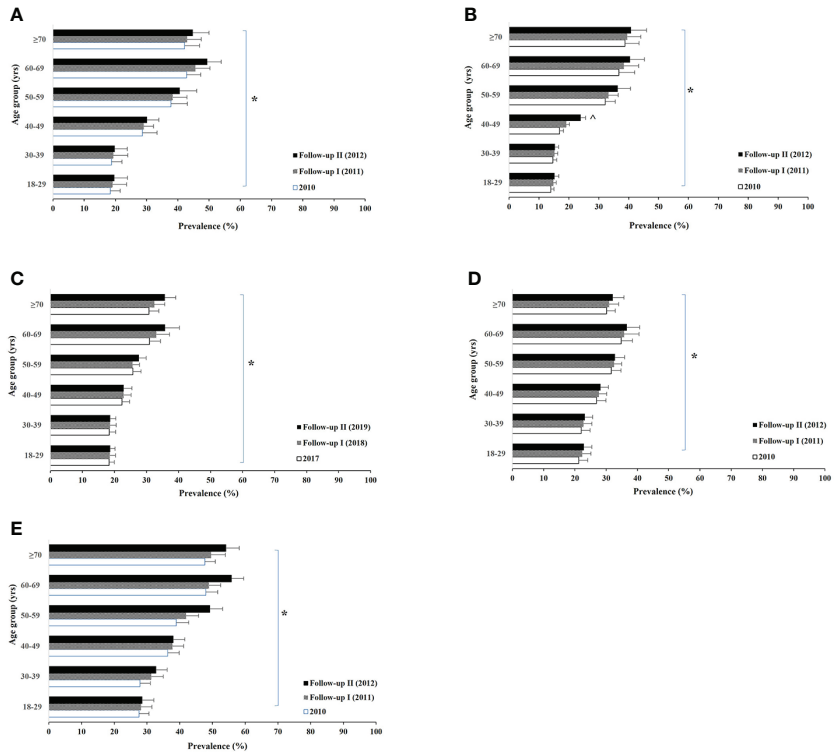

FIGURE 2
Female age-specific prevalence of high total (non-HDL) cholesterol **(A)**, high low-density lipoprotein cholesterol **(B)**, low high-density lipoprotein **(C)**, high triglyceride **(D)**, and dyslipidemias **(E)** among urban adults in East Coast, Fujian, China between 2017 and 2019. Logistic regression analysis indicated: * aging trend within each lipid abnormality **(A)** $p < 0.01$; **(B)** $p < 0.001$; **(C)** $p < 0.001$; **(D)** $p = 0.002$; **(E)** $p < 0.001$, and ^ for time trend within the age group **(B)** $p < 0.001$.

TG, and dyslipidemia. TNF-α and MCP-1 appeared to be higher for all groups with lipid abnormalities in male participants. Among female participants, TNF-α increased in groups of high total cholesterol and dyslipidemia; MCP-1 remained unchanged in the group of low HDL-C but not in other groups. Similarly, the oxidative stress representative molecule TBARS was statistically higher in groups with high total cholesterol, LDL-C, and dyslipidemia. It also increased in the male group with low HDL-C and female participants with high TG. The level of total antioxidant capacity was lower in all different abnormal lipid groups than the normal. No change of any molecular level was observed within any group during the three consecutive years.

Table 7 demonstrates significant correlations between serum proinflammatory cytokine levels and the participant's age and degrees of all types of dyslipidemia except low HDL-C. Similarly, such positive correlation was seen between the cytokines and obesity or diabetes but not hypertension, CVD, and CHD. TBARS level was positively correlated with age, degrees of majority of all dyslipidemia groups, with dyslipidemia in family history, and diabetes. In contrast, a negative significant correlation was found between total antioxidant capacity and age or all types of dyslipidemia.

Discussion

The aim of the 3-year cross-sectional investigation was to obtain the overall profile of the prevalence of dyslipidemia, serum proinflammatory cytokines, and oxidative stress among the participants representing urban adults in east coast China. Such calculations were valued through subpopulating samples matched within categorical variables such as age, sex, family income, and education level. The finding of an elevated trend in the prevalence of dyslipidemia in the 21st century among urban populations is consistent with previous studies (20, 33, 34) in other areas of China. In our study, from 2017 to 2019, the TC levels in male participants increased by 10.4% (6.6%–14.3%). Based on clinical documentation of the association between a 10% difference in serum cholesterol and 15% difference in the risk of CHD, it is predicted that the incidence of CVD in urban east coast may increase by 17.3% in the 2020s.

The result showed an age-specific increase in the prevalence of all dyslipidemia subtypes including hypercholesterolemia, high LDL-C, hypertriglyceridemia, and low HDL-C, suggesting the possibility of more cases of CVD/CHD and diabetes as their ages advance. Such a growing public health problem was also

TABLE 5 The serum levels of proinflammatory cytokines according to demographic and socioeconomic variables among adults in East Coast, Fujian, China.

Serum inflammatory marker*										
		IL-6 (pg/ml)			TNF-a (pg/ml)			MCP-1 (pg/ml)		
		1st year (2017)	Follow-up I (2018)	Follow-up II (2019)	1st year (2017)	Follow-up I (2018)	Follow-up II (2019)	1st year (2017)	Follow-up I (2018)	Follow-up II (2019)
Sex	Age (years)	X ± SD *	X ± SD	X ± SD	X ± SD	X ± SD	X ± SD	X ± SD	X ± SD	X ± SD
Male										
	18–29	23.6 ± 2.1	23.9 ± 2.4	23.8 ± 2.2	81.9 ± 8.2	81.8 ± 8.0	82.5 ± 8.1	86.0 ± 8.7	85.8 ± 8.4	86.1± 8.5
	30–39	23.4 ± 2.4	23.6 ± 2.2	23.9 ± 3.1	82.6 ± 8.4	82.9 ± 9.2	83.2 ± 9.2	86.2 ± 9.2	86.7± 8.6	87.1± 8.4
	40–49	23.8 ± 2.6	24.1 ± 2.6	24.4 ± 2.4	82.2 ± 8.3	83.2 ± 9.2	83.9 ± 9.1	87.1 ± 9.3	87.9 ± 9.0	88.2 ± 9.1
	50–59	23.9 ± 2.1	24.7 ± 2.4	24.6 ± 2.6	82.1 ± 8.2	82.6 ± 9.1	83.1 ± 8.9	88.2 ± 9.2	89.2 ± 9.9	90.5 ± 9.3
	60–69	24.8 ± 2.6	25.5 ± 2.5	26.0 ± 2.7	82.7 ± 8.6	83.5 ± 8.8	84.6 ± 9.0	88.1 ± 9.0	88.9 ± 9.4	89.2 ± 9.7
	≥70	25.7 ± 2.7	26.4 ± 2.4	27.9 ± 3.1	83.3 ± 8.6	85.2 ± 8.6	88.1 ± 9.0	89.5 ± 8.8	90.8 ± 10.0	91.1 ± 9.7
Total										
Mean		24.2 ± 3.0	24.6 ± 3.1	25.1 ± 3.2	82.5 ± 8.6	83.2 ± 8.4	84.2 ± 8.9	87.5 ± 8.9	88.2 ± 8.9	88.7 ± 8.8
p for linear trend		<0.01	<0.01	<0.01	<0.01	<0.01	<0.005	<0.01	<0.005	<0.005
Female										
	18–29	23.8 ± 2.3	23.5 ± 2.3	24.2 ± 2.3	81.4 ± 8.1	81.7 ± 8.2	82.1 ± 8.2	85.2 ± 8.1	85.9 ± 8.1	85.5 ± 8.7
	30–39	23.2 ± 2.4	23.9 ± 2.4	23.9 ± 2.1	82.9 ± 9.0	82.7± 9.0	82.9± 8.4	85.8 ± 8.8	86.6 ± 8.7	86.8 ± 8.8
	40–49	23.9 ± 2.1	24.7 ± 3.0	24.9 ± 2.9	82.0 ± 7.4	82.9 ± 8.4	83.3 ± 8.5	86.9 ± 8.9	86.8 ± 8.1	87.7 ± 8.8
	50–59	23.2 ± 2.3	24.4 ± 2.5	25.0 ± 3.1	82.9 ± 8.3	83.6 ± 8.9	83.9 ± 8.8	88.0 ± 9.0	88.9 ± 8.5	89.6 ± 9.1
	60–69	24.7 ± 2.5	25.0 ± 2.4	25.9 ± 2.6	82.8 ± 8.7	83.4 ± 9.1	84.1 ± 8.7	87.9 ± 8.6	88.3 ± 8.8	88.9 ± 8.8
	≥70	25.6 ± 2.7	26.8 ± 3.0	27.1 ± 2.7	83.6 ± 8.7	84.2 ± 9.1	85.6 ± 8.6	89.9 ± 8.7	92.3 ± 9.1	92.1 ± 9.1
Total										
Mean		24.1 ± 2.9	24.7 ± 2.6	25.2 ± 2.7	82.6 ± 8.8	83.1 ± 8.9	83.7 ± 8.8	87.3 ± 9.0	88.2 ± 9.1	88.3 ± 9.6
p for linear trend		<0.01	<0.01	<0.01	<0.01	<0.01	<0.01	<0.01	<0.005	<0.005
Dyslipidemia in family										
	Yes	26.3 ± 2.9	26.3 ± 2.8	27.9 ± 3.0	94.9 ± 8.9	91.9 ± 9.2	92.9 ± 9.2	93.1 ± 9.6	93.1± 9.3	93.9 ± 9.1
	No	22.1 ± 2.5	23.1 ± 2.4	24.1 ± 3.0	81.1 ± 8.1	84.1 ± 8.5	82.3 ± 8.3	87.3 ± 8.7	88.5 ± 8.9	87.1 ± 8.0
	p	0.08	0.10	0.09	0.07	0.09	0.07	0.10	0.10	0.09
Education level										
	Low education	24.9 ± 3.3	25.0 ± 3.0	26.9 ± 3.0	88.7 ± 9.2	87.7 ± 9.0	88.7 ± 9.3	89.1 ± 9.7	90.1 ± 9.1	91.1 ± 9.1
	College/higher education	23.6 ± 3.2	24.8 ± 3.2	23.9 ± 3.0	83.3 ± 9.0	82.2 ± 9.0	82.3 ± 9.1	84.5 ± 9.3	82.5 ± 8.9	81.5 ± 8.8
	p	0.12	0.15	0.10	0.10	0.10	0.10	0.10	0.10	0.10
History of smoking ^										
	Yes	28.8 ± 3.6	29.1 ± 3.3	29.0 ± 3.3	89.7 ± 9.2	90.7 ± 9.2	92.7 ± 9.3	90.1 ± 9.9	88.1 ± 9.1	87.1 ± 9.11
	No	23.2 ± 3.9	23.1 ± 3.0	23.9 ± 3.0	81.3 ± 9.0	81.3 ± 9.0	82.3 ± 9.1	84.5 ± 8.3	82.5 ± 7.9	83.5 ± 8.7
	p	0.13	0.10	0.10	0.10	0.10	0.10	0.10	0.10	0.15
Alcohol drinking †										
	Yes	27.3 ± 3.3	27.9 ± 3.1	27.9 ± 3.3	89.7 ± 8.7	91.7 ± 9.2	91.9 ± 9.1	90.9 ± 9.1	89.9 ± 9.1	91.5 ± 9.1
	No	23.6 ± 3.4	22.9 ± 3.3	22.9 ± 3.2	80.3 ± 8.5	80.9 ± 8.6	82.3 ± 8.9	82.5 ± 8.5	81.5 ± 8.4	82.5 ± 8.7
	p	0.11	0.09	0.09	0.08	0.07	0.10	0.09	0.11	0.10
Overweight §										
	Yes	29.9 ± 3.5	30.6 ± 3.0	32.2 ± 3.9	93.7 ± 8.2	96.7 ± 8.3	98.7 ± 9.1	94.9 ± 7.8	95.7 ± 8.6	97.5 ± 9.0
	No	22.0 ± 3.1	22.6 ± 3.5	23.1 ± 3.0	78.2 ± 8.1	79.1 ± 7.9	79.7 ± 8.6	79.8 ± 7.3	78.8 ± 7.7	80.3 ± 7.9
	p	0.01	0.01	0.01	0.01	0.01	0.01	0.01	0.01	0.01

(Continued)

TABLE 5 Continued

Serum inflammatory marker*

	IL-6 (pg/ml)			TNF-a (pg/ml)			MCP-1 (pg/ml)		
	1st year (2017)	Follow-up I (2018)	Follow-up II (2019)	1st year (2017)	Follow-up I (2018)	Follow-up II (2019)	1st year (2017)	Follow-up I (2018)	Follow-up II (2019)
Sex Age (years)	**X ± SD ***	**X ± SD**	**X ± SD**	**X ± SD**	**X ± SD**	**X ± SD**	**X ± SD**	**X ± SD**	**X ± SD**
Obesity									
Yes	29.7 ± 3.3	31.4 ± 4.1	30.1 ± 3.9	95.7 ± 8.2	94.9 ± 8.2	95.5 ± 7.3	96.9 ± 8.9	97.2 ± 9.0	98.7 ± 9.0
No	22.0 ± 3.5	22.9 ± 3.2	22.8 ± 3.4	80.1 ± 8.0	80.1 ± 7.8	81.1 ± 8.1	78.0 ± 7.8	80.1 ± 8.2	82.2 ± 7.4
p	0.01	0.01	0.01	0.01	0.01	0.01	0.01	0.01	0.01
Waist circumference ¶									
High	28.8 ± 3.7	28.0 ± 3.0	27.9 ± 3.5	87.7 ± 9.1	89.7 ± 9.0	92.7 ± 9.3	92.1 ± 9.3	89.1 ± 9.1	94.1 ± 9.1
Normal	23.9 ± 3.2	25.8 ± 3.4	24.9 ± 3.0	83.3 ± 8.9	83.9 ± 9.0	84.3 ± 9.1	83.5 ± 8.5	83.5 ± 8.7	83.5 ± 7.9
p	0.08	0.11	0.10	0.09	0.10	0.07	0.06	0.10	0.06
Lifestyle									
Regular physical activity ~	27.1 ± 3.4	28.0 ± 3.4	26.9 ± 3.9	89.7 ± 9.2	91.7 ± 9.2	90.9 ± 9.0	92.9 ± 9.9	92.1 ± 9.10	93.6 ± 8.7
Sedentary Leisure	25.2 ± 3.5	26.1 ± 3.5	29.9 ± 3.4	80.3 ± 9.0	81.3 ± 9.0	80.8 ± 9.1	86.5 ± 10.3	85.6 ± 7.9	84.4 ± 7.9
p	0.12	0.20	0.25	0.15	0.15	0.15	0.15	0.15	0.15
History of CHD									
Yes	28.3 ± 3.4	29.0 ± 3.9	29.0 ± 3.9	89.7 ± 9.2	89.9 ± 9.2	92.7 ± 9.3	94.1 ± 9.9	90.1 ± 7.10	94.1 ± 9.0
No	22.8 ± 3.2	22.8 ± 3.9	23.9 ± 3.4	81.3 ± 9.0	82.3 ± 9.0	85.3 ± 9.1	83.5 ± 7.6	82.5 ± 8.0	82.3 ± 8.0
p	0.10	0.10	0.25	0.10	0.15	0.15	0.15	0.15	0.15
History of CVD									
Yes	29.2 ± 3.7	27.9 ± 3.9	26.8 ± 3.9	89.6 ± 9.2	88.7 ± 9.2	89.9 ± 9.3	91.8 ± 9.0	93.7 ± 7.9	92.6 ± 8.6
No	23.3 ± 3.2	23.6 ± 4.2	23.9 ± 3.4	81.3 ± 9.0	82.3 ± 9.0	82.3 ± 9.1	81.1 ± 9.0	82.5 ± 7.6	82.7 ± 8.1
p	0.10	0.10	0.10	0.10	0.10	0.10	0.10	0.10	0.10
Hypertension									
yes	23.6 ± 4.1	24.0 ± 3.9	24.4 ± 3.9	87.7 ± 9.2	89.7 ± 9.2	89.9 ± 9.0	91.1 ± 9.0	93.5 ± 7.7	92.4 ± 8.2
No	27.9 ± 4.3	28.5 ± 3.9	28.9 ± 3.4	83.6 ± 9.0	83.9 ± 9.0	83.2 ± 9.1	81.5 ± 10.3	82.5 ± 7.5	83.1 ± 7.4
p	0.25	0.25	0.15	0.15	0.15	0.15	0.15	0.10	0.15
Diabetes Mellitus									
Yes	29.5 ± 3.5	32.1 ± 4.0	32.1 ± 3.9	94.9 ± 8.2	96.8 ± 8.8	94.6 ± 8.0	96.3 ± 8.5	95.4 ± 8.10	96.9 ± 8.9
No	21.8 ± 3.0	22.3 ± 3.7	21.9 ± 3.1	79.6 ± 7.5	80.1 ± 7.5	80.1 ± 8.0	80.1 ± 7.6	79.9 ± 7.7	80.1 ± 7.8
p	0.01	0.01	0.01	0.01	0.01	0.01	0.01	0.01	0.01

*X, mean; SD, standard deviation. Values expressed in pg/ml [n = 15,397 (2017), 12,144 (2018), and 11,762 (2019)]. IL-6, interleukin-6; MCP-1, TNF-α, tumor necrosis factor-α; MCP-1, monocyte chemoattractant protein-1. CVD indicates cardiovascular disease; CHD, coronary heart disease; BP, blood pressure; LDL, low-density lipoprotein; and HDL, high-density lipoprotein. #Dyslipidemia was defined as total cholesterol 240 mg/dl, and/or triglyceride ≥160 mg/dl, and/or LDL cholesterol 160 mg/dl, and/or HDL cholesterol 40 mg/dl, and/or use of lipid-lowering medications. ^Smoking was defined as current daily smoking or quit less than 5 years; Non-smoking is defined as never smoking cigarettes daily or quit smoking more than 5 years. †Alcohol drinking was defined as consumption of 30 g of alcohol per week for 1 year. § Overweight was defined as a body mass index (kg/m^2) value of 24 or more; Obesity was defined as a body mass index (kg/m^2) value of 28 and above. ¶High circumference is defined as a waist circumference over 85 cm for men and over 80 cm for women. ~ Defined as an exercise of moderate or vigorous activity at least for 30 min per day with 3 days per week.

recognized in cross-sectional surveys in Venezuela (35), Iran (36), India (37), South Africa (38), and Europe (39). Furthermore, the prevalence of dyslipidemia among middle-aged men (40 years and above) and women (30 years and above) is higher than what was previously reported in the general Chinese population, with 22.2% in men and 15.9% in women (20). Compared to some main metropolises, such as Beijing and Shanghai, urban adults residing in east coast China have a relatively equal prevalence of dyslipidemia (22). A comparably higher prevalence among middle-aged adults is different from that in the developed world (40–43) where a higher dyslipidemia occurred commonly among elders (44). In fact, our study showed a higher prevalence of dyslipidemia among urban adults with a history of CVD, CHD, or hypertension than those without it. Many factors may contribute to the trend including rapid demographic, social, and economic changes.

TABLE 6 The levels of serum oxidative status according to demographic and socioeconomic variables and familial history among adults in East Coast, Fujian, China in 2017 and 2-year follow-up.

Serum oxidate status*

		TBARS (μM)			TAC (mmol DPPH/L)		
		1st year (2017)	Follow-up I (2018)	Follow-up II (2019)	1st year (2017)	Follow-up I (2018)	Follow-up II (2019)
Sex	**Group (years)**	**X ± SD**	**X ± SD**	**X ± SD**	**X ± SD**	**X ± SD**	**X ± SD**
Male							
	18–29	3.99 ± 0.34	3.76 ± 0.33	3.95 ± 0.41	0.32 ± 0.05	0.33 ± 0.05	0.33 ± 0.03
	30–39	3.93 ± 0.34	3.98 ± 0.35	3.96 ± 0.40	0.32 ± 0.06	0.30 ± 0.6	0.32 ± 0.05
	40–49	4.02 ± 0.43	4.10 ± 0.41	4.09 ± 0.52	0.36 ± 0.05	0.37 ± 0.6	0.36 ± 0.06
	50–59	4.12 ± 0.58	4.19 ± 0.44	4.14 ± 0.55	0.39 ± 0.05	0.39 ± 0.06	0.40 ± 0.07
	60–69	4.19 ± 0.60	4.22 ± 0.55	4.29 ± 0.56	0.37 ± 0.05	0.38 ± 0.04	0.38 ± 0.06
	≥70	4.38 ± 0.60	4.48 ± 0.62	4.49 ± 0.56	0.33 ± 0.04	0.34 ± 0.05	0.33 ± 0.05
Total							
Mean		4.11 ± 0.44	4.12 ± 0.48	4.15 ± 0.47	0.35 ± 0.04	0.35 ± 0.04	0.35 ± 0.04
P values for linear trend		<0.01	<0.01	<0.01	<0.01	<0.01	<0.01
Female							
	18–29	3.76 ± 0.40	3.72 ± 0.37	3.79 ± 0.35	0.33 ± 0.03	0.33 ± 0.04	0.34 ± 0.03
	30–39	3.91 ± 0.42	3.99 ± 0.41	3.94 ± 0.38	0.35 ± 0.6	0.33 ± 0.04	0.32 ± 0.04
	40–49	4.04 ± 0.43	4.01 ± 0.42	4.09 ± 0.51	0.38 ± 0.07	0.39 ± 0.06	0.37 ± 0.04
	50–59	4.10 ± 0.43	4.13 ± 0.45	4.12 ± 0.47	0.40 ± 0.06	0.40 ± 0.06	0.39 ± 0.08
	60–69	4.14 ± 0.45	4.18 ± 0.41	4.22 ± 0.48	0.38 ± 0.06	0.36 ± 0.05	0.37 ± 0.04
	≥70	4.39 ± 0.46	4.49 ± 0.50	4.44 ± 0.48	0.34 ± 0.04	0.31 ± 0.05	0.32 ± 0.03
Total							
Mean		4.06 ± 0.48	4.09 ± 0.43	4.10 ± 0.47	0.36 ± 0.05	0.35 ± 0.06	0.35 ± 0.06
p-values for linear trend		<0.01	<0.01	<0.005	<0.01	<0.01	<0.01
Dyslipidemia in family							
	Yes	4.78 ± 0.71	4.79 ± 0.69	4.81 ± 0.71	0.31 ± 0.05	0.31 ± 0.06	0.29 ± 0.05
	No	3.39 ± 0.60	3.52 ± 0.65	3.63 ± 0.66	0.40 ± 0.05	0.42 ± 0.06	0.39 ± 0.06
	p	0.03	0.06	0.07	0.06	0.06	0.05
Education level							
	Low education	4.41 ± 0.62	4.28 ± 0.66	4.35 ± 0.62	0.33 ± 0.06	0.30 ± 0.06	0.31 ± 0.06
	College/higher education	3.76 ± 0.69	3.93 ± 0.66	3.90 ± 0.63	0.38 ± 0.05	0.40 ± 0.06	0.39 ± 0.06
	p	0.10	0.20	0.25	0.25	0.06	0.25
History of smoking ^							
	Yes	4.78 ± 0.68	4.81 ± 0.69	4.82 ± 0.69	0.30 ± 0.06	0.28 ± 0.06	0.28 ± 0.06
	No	3.39 ± 0.69	3.40 ± 0.64	3.42 ± 0.70	0.42 ± 0.06	0.42 ± 0.06	0.41 ± 0.06
	p	0.01	0.01	0.04	0.05	0.04	0.04
Alcohol drinking †							
	Yes	4.76 ± 0.69	4.79 ± 0.65	4.80 ± 0.71	0.32 ± 0.06	0.29 ± 0.05	0.28 ± 0.05
	No	3.31 ± 0.68	3.42 ± 0.63	3.35 ± 0.70	0.39 ± 0.07	0.41 ± 0.06	0.42 ± 0.07
	p	0.04	0.02	0.04	0.10	0.04	0.01
Overweight §							
	Yes	4.61 ± 0.69	4.76 ± 0.71	4.79 ± 0.70	0.33 ± 0.06	0.29 ± 0.06	0.29 ± 0.05
	No	3.56 ± 0.63	3.45 ± 0.69	3.36 ± 0.65	0.38 ± 0.06	0.41 ± 0.06	0.41 ± 0.07
	p	0.08	0.04	0.05	0.20	0.07	0.07

(Continued)

TABLE 6 Continued

Serum oxidate status*

		TBARS (μM)			TAC (mmol DPPH/L)		
		1st year (2017)	Follow-up I (2018)	Follow-up II (2019)	1st year (2017)	Follow-up I (2018)	Follow-up II (2019)
Sex	**Group (years)**	**X ± SD**	**X ± SD**	**X ± SD**	**X ± SD**	**X ± SD**	**X ± SD**
Obesity							
	Yes	4.69 ± 0.69	4.79 ± 0.70	4.81 ± 0.73	0.31 ± 0.05	0.29 ± 0.05	0.29 ± 0.06
	No	3.48 ± 0.66	3.42 ± 0.66	3.34 ± 0.66	0.40 ± 0.07	0.41 ± 0.06	0.42 ± 0.06
		0.06	0.04	0.03	0.09	0.04	0.04
Waist circumference ¶							
	High	4.51 ± 0.63	4.67 ± 0.70	4.57 ± 0.70	0.32 ± 0.05	0.32 ± 0.05	0.31 ± 0.06
	Normal	3.66 ± 0.70	3.54 ± 0.65	3.38 ± 0.60	0.39 ± 0.07	0.38 ± 0.06	0.39 ± 0.06
	p	0.09	0.07	0.05	0.15	0.15	0.10
Lifestyle							
	Regular physical activity ~	4.54 ± 0.70	4.58 ± 0.70	4.49 ± 0.71	0.33 ± 0.05	0.38 ± 0.05	0.39 ± 0.06
	Sedentary Leisure	3.63 ± 0.62	3.63 ± 0.69	3.66 ± 0.60	0.38 ± 0.09	0.32 ± 0.06	0.31 ± 0.06
	p	0.10	0.15	0.15	0.20	0.25	0.15
History of CHD							
	Yes	4.62 ± 0.69	4.55 ± 0.69	4.54 ± 0.69	0.32 ± 0.05	0.32 ± 0.05	0.31 ± 0.05
	No	3.55 ± 0.67	3.66 ± 0.69	3.61 ± 0.61	0.39 ± 0.07	0.38 ± 0.06	0.39 ± 0.06
	p	0.20	0.20	0.10	0.10	0.10	0.05
History of CVD							
	Yes	4.63 ± 0.65	4.54 ± 0.69	4.53 ± 0.68	0.32 ± 0.04	0.32 ± 0.05	0.32 ± 0.05
	No	3.54 ± 0.68	3.67 ± 0.64	3.62 ± 0.60	0.39 ± 0.07	0.38 ± 0.06	0.39 ± 0.06
	p	0.20	0.20	0.15	0.10	0.10	0.07
Hypertension							
	Yes	4.73 ± 0.68	4.61 ± 0.68	4.49 ± 0.63	0.33 ± 0.05	0.32 ± 0.05	0.32 ± 0.05
	No	3.44 ± 0.66	3.60 ± 0.69	3.66 ± 0.60	0.38 ± 0.06	0.38 ± 0.06	0.39 ± 0.07
	p	0.09	0.12	0.10	0.15	0.10	0.09
Diabetes Mellitus							
	Yes	4.75 ± 0.69	4.79 ± 0.68	4.76 ± 0.68	0.30 ± 0.05	0.29 ± 0.04	0.29 ± 0.06
	No	3.42 ± 0.63	3.42 ± 0.69	3.39 ± 0.62	0.41 ± 0.07	0.41 ± 0.06	0.42 ± 0.06
	p	0.04	0.04	0.03	0.07	0.04	0.03

*X, mean; SD, standard deviation. Values expressed in pg/ml [n = 15,397 (2017), 12,144 (2018), and 11,762 (2019)]. IL-6, interleukin-6; MCP-1, monocyte chemoattractant protein-1; TNF-α, tumor necrosis factor-α. CVD indicates cardiovascular disease; CHD, coronary heart disease; BP, blood pressure; LDL, low-density lipoprotein; and HDL, high-density lipoprotein. # Dyslipidemia was defined as total cholesterol 240 mg/dl, and/or triglyceride ≥160 mg/dl, and/or LDL cholesterol 160 mg/dl, and/or HDL cholesterol 40 mg/dl, and/or use of lipid-lowering medications. ^Smoking was defined as current daily smoking or quit less than 5 years; Non-smoking is defined as never smoking cigarettes daily or quit smoking more than 5 years. † Alcohol drinking was defined as consumption of 30 g of alcohol per week for 1 year. § Overweight was defined as a body mass index (kg/m^2) value of 24 or more; Obesity was defined as a body mass index (kg/m^2) value of 28 and above. ¶High circumference is defined as a waist circumference over 85 cm for men and over 80 cm for women. ~ Defined as an exercise of moderate or vigorous activity at least for 30 min per day with 3 days per week.

Thus, our study suggested an important necessity of preventive interventions particularly among middle-aged adults to reduce the burden of resultant cardiovascular diseases and coronary heart diseases in east coast China.

The study showed that the five classified types of dyslipidemia had increased circulating levels of IL-6, TNF-α, and MCP-1 compared with a normal lipid group in male adults. The significance is not explained by sub-aged groups although the aging tread is partially independent of major confounders (45, 46). There were no significantly different levels of cytokines found during the three consecutive years. This evidence indicates that proinflammatory cytokine serum concentration increases with lipid abnormalities. The result that increased proinflammatory cytokines are associated with obesity is consistent with other reports (47), suggesting that body fat accumulation may induce inflammatory response through

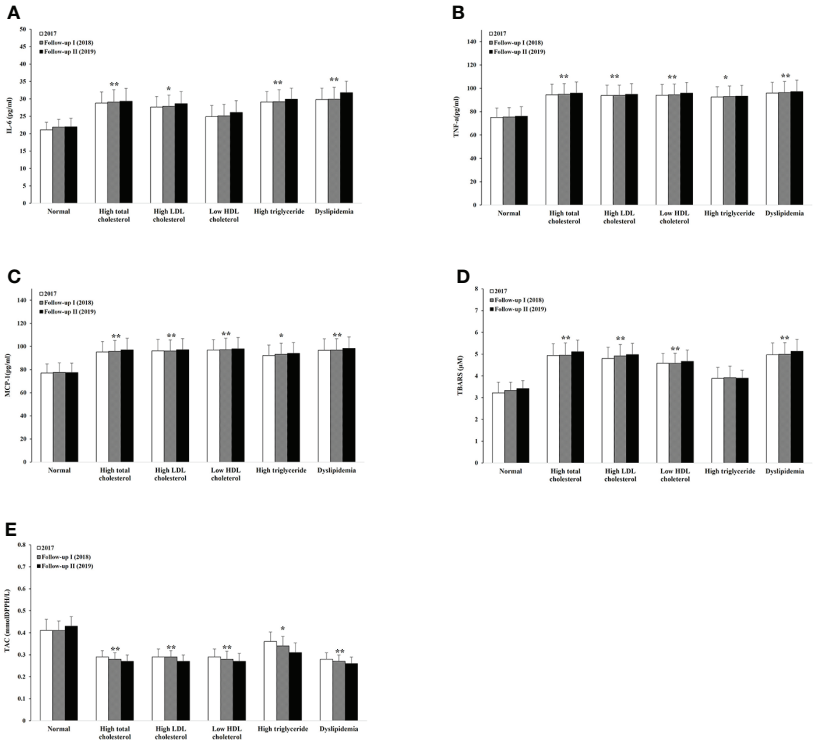

FIGURE 3
Serum levels of proinflammatory cytokines, oxidative stress, and antioxidant capacity within different lipid abnormalities among male adults. IL-6 **(A)**, TNF-β **(B)**, MCP-1 **(C)**, TBARS **(D)**, and TAC **(E)**. Logistic regression analysis indicated: *$p < 0.05$, **$p < 0.01$ overall difference vs. the level of lipid normal group.

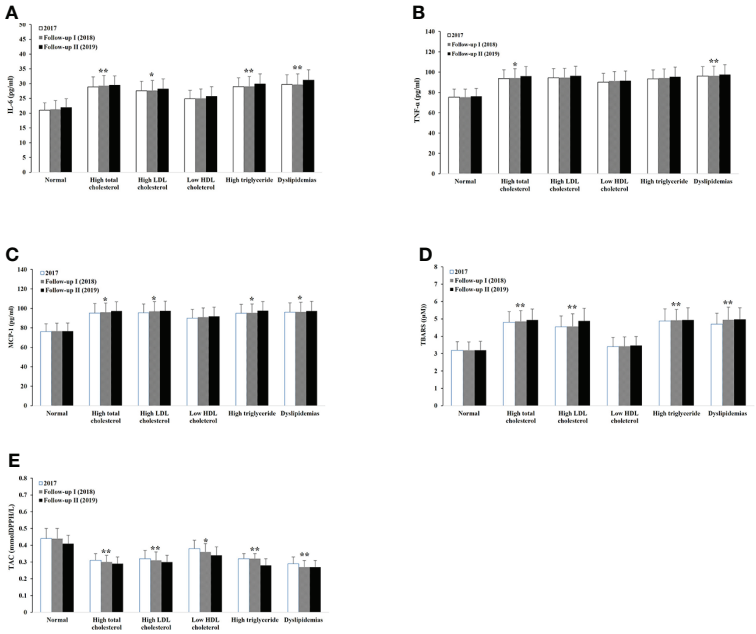

FIGURE 4
Serum levels of proinflammatory cytokines, oxidative stress, and antioxidant capacity within different lipid abnormalities among female adults. IL-6 **(A)**, TNF-β **(B)**, MCP-1 **(C)**, TBARS **(D)**, and TAC **(E)**. Logistic regression analysis indicated: *$p < 0.05$, **$p < 0.01$, overall difference vs. the level of lipid normal group.

TABLE 7 Correlation of the serum proinflammatory cytokines, oxidative status, and antioxidant capacity with relevant parameters among adults in East Coast, Fujian, China.

Correlated parameter*	Proinflammatory cytokine						Oxidative stress		TAC	
	IL-6		TNF-a		MCP-1		TBARS			
	R	*p*-value	*R*	*p*-value	*R*	p-value	*R*	*p*-value	*R*	*p*-value
Demographic/socioeconomic variables										
Age	0.380	<0.01	0.455	<0.005	0.453	<0.005	0.376	<0.01	-0.376	<0.01
Sex	0.150	0.12	0.118	0.16	0.144	0.12	0.153	0.12	0.131	0.15
Lifestyle of sedentary leisure	0.101	0.180	0.124	0.150	0.122	0.150	0.144	0.130	0.095	0.200
Waist circumference	0.163	0.090	0.168	0.090	0.166	0.090	0.196	0.060	-0.151	0.120
Obesity	0.462	<0.005	0.453	<0.005	0.464	<0.005	0.240	0.040	-0.227	0.050
CVD	0.171	0.100	0.172	0.100	0.170	0.100	0.118	0.190	-0.179	0.080
CHD	0.137	0.130	0.133	0.130	0.122	0.150	0.109	0.170	-0.170	0.100
Hypertension	0.100	0.180	0.126	0.150	0.150	0.120	0.172	0.100	-0.150	0.120
Diabetes mellitus	0.376	<0.01	0.373	<0.01	0.374	<0.01	0.277	<0.04	-0.280	<0.04
Dyslipidemia in family	0.167	0.09	0.186	0.07	0.167	0.09	0.201	0.06	0.196	0.06
Lipid-related variables										
Total Cholesterol	0.577	<0.001	0.558	<0.001	0.481	<0.001	0.603	<0.001	-0.548	<0.001
LDL-C	0.373	<0.01	0.395	<0.01	0.451	<0.005	0.459	<0.005	-0.520	<0.001
HDL-C	0.188	0.090	0.189	0.060	0.225	0.050	0.242	0.060	-0.451	<0.005
Triglyceride (TG)	0.644	<0.001	0.355	<0.03	0.657	<0.001	0.560	<0.001	-0.444	<0.005
Non-HDL-C	0.540	<0.005	0.541	<0.005	0.523	<0.005	0.564	<0.001	-0.471	<0.005
TG/HDL	0.379	<0.01	0.265	<0.05	0.395	<0.01	0.403	<0.01	0.268	<0.05
Dyslipidemia	0.584	<0.001	0.579	<0.001	0.587	<0.001	0.565	<0.001	-0.475	<0.002

*Presented by Pearson correlation coefficient and p-value. IL-6, interleukin-6; MCP-1, monocyte chemoattractant protein-1; TNF-α, tumor necrosis factor-α. TBARS, thiobarbituric acid-reactant substances; TAC, total antioxidant capacity.

excessive intake of carbohydrates. We also stated that history of diabetes positively correlated with cytokine levels. A possible mechanism is that insulin resistance or elevated glucose is developed based on the increase in the cytokines; another possibility is that acute phase proteins such as CRP and alpha-a-acid glycoprotein induced by inflammatory response may lead to abnormal glucose metabolism in adipocytes. The evidence by some reports showed that proprotein convertase subtilisin/kexin Type 9 (PCSK9) level is positively associated with LDL-C levels in members with FH (48, 49). It possibly plays a role in inflammation balance at the atherosclerotic vascular wall by inducing the expression of inflammatory cytokines, adhesion molecules, and chemoattractants (50). One should consider measuring PCSK9 levels and vascular inflammation among the Chinese population.

Our results showed an increase in TBARS and a decrease in TAC level in most subtypes of dyslipidemia as compared to non-dyslipidemia groups, suggesting increased lipid peroxidation and decreased activity of enzymatic antioxidants in dyslipidemia among adults. Free radical production during the peroxidation of cholesterol and fatty acid is regulated by a large number of antioxidant factors. Our study shows that dyslipidemia in urban adults might be associated with a disturbance of the oxidative stress/antioxidant balance, which can be due to enhanced accumulations of free radicals and excessive antioxidant consumption. This finding supported the elevated levels of lipid hydroperoxide in the serum and is parallel to the generation of oxidative and antioxidant enzyme inactivation such as SOD and G-Px (51, 52). We also explored the correlation between diabetes and oxidative stress, indicating that hyperglycemia in diabetes contributes to oxidative stress and thus agreeing with previous studies (53, 54).

Many factors contribute to the complex changes of proinflammatory cytokines and oxidative stress among the dyslipidemias. Family history, smoking, and alcohol drinking, as well as medication compounds, can initiate the inflammatory response and oxidative stress by activating a variety of humoral and cellular mediators. In particular, excessive amounts of proinflammatory cytokines are stimulated in the early phase of inflammation and enhanced accumulations of free radicals, leading to an uncontrolled oxidative stress in the pathogenesis of lipid abnormalities.

Thus, our study suggests that proinflammatory cytokines and oxidative stress are predictive of lipid abnormalities. It is conceivable that prevention of elevated levels of cytokines and oxidative stress may delay the development of dyslipidemias, resulting in a low risk of CVD, CHD, and diabetes mortalities (55). The current study showed no sex difference in the level of

proinflammatory cytokines and oxidative stress in east coast China. This fact indicates that the influence of estrogen on serum cytokines and TBARS, as well as TAC, seems to be not far-reaching.

The finding that an increase in the prevalence of dyslipidemias was associated with circumference and sedentary lifestyle may result from a considerable shift from traditional diets to high-fat diets especially those with a higher ratio of saturated to unsaturated fats in the adult population (56). The result suggests that a rapid increase in overweight/obesity likely interacts with dyslipidemia-related complications especially CHD/CVD (57). The prevalence of insufficiently physically active adults may be related to workplace conditions, the daily transport, and urban environment. The resulting positive effect on individuals' physical inactivity is recognized as a public problem caused by industrialization, urbanization, and mechanization, as well as the high income among them, which is agreeable with other reports (58). Thus, the effective prevention and control of a high lipid profile involves a healthy lifestyle and diet (44). In terms of the prevention of the rapid increase in obesity, the WHO recommends 150 min of moderate to vigorous intensity per week in addition to usual activities. It is interesting that our study showed no significant association between serum cytokines, TBARS, and TAC, and either regular physical activity or sedentary lifestyle. A previous study indicated regular physical activity counteracts mitochondrial dysfunction and ROS generation, which present oxidative stress and inflammation in aging (59). However, some studies showed that regular exercise can induce oxidative stress and inflammation (60). The alleviative effect of regular activity on proinflammatory cytokines and oxidative stress may vary depending on the type, intensity, frequency, and duration of exercise as well as on the individual's characteristics.

The present finding suggests an increasing burden of dyslipidemia in east coast China compared to the general Chinese population. Considering the data observed in this investigation, we suggest that proinflammation induces peroxidation of unsaturated fatty acid and oxidative modification in cholesterol due to decreased activity of enzymatic antioxidants.

Limitations

First, although our results suggested the link between dyslipidemia and cytokines and oxidative stress, there may have been concerns as to the integrity of the current study results due to the limited ability to collect upstream social determinants of health including the long and complex causal pathways in social disadvantages, risk exposure, and health inequities. Our investigation has limited value in assessing long-term relevant risk factors such as genotype, diet intake, and energy expenditure in physical activity associated with certain changes in proinflammation indicators and oxidative stress since it was quite difficult to determine periods in exposure to risk factors of an individual's life history on the regulation of genes controlling lipid metabolism and immune functioning. An understanding of the critical or sensitive determinants would be greatly appreciated to improve clinically meaningful results.

Second, due to the relatively modest number of sample size considering the significant population of east coast China, the relationship between dyslipidemia and proinflammation/oxidative stress generated in the study may be outright oversignified. Third, some of the data about relevant demographic and socioeconomic variables were collected and analyzed based on self-report measures; therefore, the data may be subject to bias.

Fourth, we did not have complete knowledge about potential predictors or certain definitive indicators involved in lipoprotein uptake, cholesterol synthesis, and recruitment, as well oxidative modification cholesterol such as the thickness of the inner and middle layers of the arteries, resulting in the limitations of exploring the high standard classification of dyslipidemia. Fifth, the current study did not evaluate biochemical parameters such as glutathione peroxidase, superoxide dismutase, catalase activity, and reactive oxygen species (ROS) particularly related to inflammation, oxidative stress, and antioxidants status. Recent reports indicated that high sensitivity C-reactive protein (hsCRP) concentration can reflect active systemic inflammation and independently associated with the severity of atherosclerosis (61–63). Our future study will address the role of hsCRP as an independent predictor of the risk of premature cardiovascular events within specific settings of investigation.

Finally, our study did not well analyze those who received lipid-lowering therapies (LLTs) especially non-statin lipid-lowering drugs, although only less than 6% had LLT as secondary prevention of atherosclerosis in Chinese primary care. However, it was suggested that most LLTs may have anti-inflammatory or immunomodulatory properties, either independent or not of a decrease in LDL-C (64–66).

Therefore, the noise-to-signal ratio for our current surveillance is possibly moderate, potentially leading to a biased estimate of the associations between dyslipidemia and proinflammation/oxidative stress; however, our team would like to effectively identify and accurately measure the key confounding factors in a future study but not eliminate them. Accordingly, a fulfillment of randomization with a larger sample size in distributing both known and more importantly unknown risk factors may mitigate the potential for high bias and enable the level of certainty needed to influence a clinical outcome and health policy decision.

Overall, the present study is noteworthy and has a contribution in current literature concerning the roles of proinflammatory and oxidative stress in dyslipidemia and its contribution to the various subtypes among adults. This finding

is consistent with a very important public health implication: without an effective approach in prevention and control of inflammation and oxidative stress, the greater incidence of dyslipidemia can occur, and potentially, its complications such as cardiovascular disease and atherosclerosis may develop in the near future.

Conclusion

A correlation between the prevalence of dyslipidemia and the modification of inflammation status was statistically significant. The levels of proinflammatory cytokines, oxidative stress, and antioxidant capacity in serum may reflect the contextual severity of the lipid abnormalities. The prevention and treatment of dyslipidemia and abnormal proinflammation and oxidative stress are highly recommended to be a mandatory objective to pursue in east coast China to reduce the burden of cardiovascular morbidity and mortality. Therefore, these promising results in the current study further warrant a thorough medical screening in enhanced anti-inflammatory and reduced oxidative stress to better diagnose and comprehensively treat dyslipidemia at an early stage.

Data availability statement

The original contributions presented in the study are included in the article/Supplementary Material. Further inquiries can be directed to the corresponding author.

Ethics statement

The studies involving human participants were reviewed and approved by Ethics committee of The First Hospital of Quanzhou affiliated to Fujian Medical University. The patients/participants provided their written informed consent to participate in this study. Written informed consent was obtained from the individual(s) for the publication of any potentially identifiable images or data included in this article.

Author contributions

NH and SX conceived of the presented pilot study direction. NH, YL and ZY developed the project and performed the data collections. NH, CY, YH and QD verified the analytical methods. SX supervised the findings of this work. All authors discussed the results and contributed to the final manuscript.

Acknowledgments

We thank all the participants of the study in the cities. Our thanks also go to Dr. Lijun Tang and Mr. Brett Callahan for their valuable assistance in writing review.

Conflict of interest

The authors declare that the research was conducted in the absence of any commercial or financial relationships that could be construed as a potential conflict of interest.

Publisher's note

All claims expressed in this article are solely those of the authors and do not necessarily represent those of their affiliated organizations, or those of the publisher, the editors and the reviewers. Any product that may be evaluated in this article, or claim that may be made by its manufacturer, is not guaranteed or endorsed by the publisher.

References

1. Marcucci R, Alessandrello Liotta A, Cellai AP, Rogolino A, Berloco P, et al. Cardiovascular and thrombophilic risk factors for idiopathic sudden sensorineural hearing loss. *J Thromb Haemost* (2005) 3(5):929–34. doi: 10.1111/j.1538-7836.2005.01310.x

2. Eisen A, Tenenbaum A, Koren-Morag N, Tanne D, Shemesh J, Imazio M, et al. Calcification of the thoracic aorta as detected by spiral computed tomography among stable angina pectoris patients: Association with cardiovascular events and death. *Circulation* (2008) 118(13):1328–34. doi: 10.1161/CIRCULATIONAHA.107.712141

3. Kumar H. Approaches for deciphering the molecular basis of disease and its translational benefits. *Int Rev Immunol* (2019) 38(6):247–8. doi: 10.1080/08830185.2019.1689654

4. Popko K, Gorska E, Stelmaszczyk-Emmel A, Plywaczewski R, Stoklosa A, Gorecka D, et al. Proinflammatory cytokines IL-6 and TNF-α and the development of inflammation in obese subjects. *Eur J Med Res* (2019) 15:120. doi: 10.1186/2047-783X-15-S2-120

5. Scicali R, Di Pino A, Urbano F, Ferrara V, Marchisello S, Di Mauro S, et al. Analysis of S100A12 plasma levels in hyperlipidemic subjects with or without familial hypercholesterolemia. *Acta Diabetol* (2019) 56:899–906. doi: 10.1007/s00592-019-01338-1

6. Yang Z, Yan WX, Cai H, Tedla N, Armishaw C, Di Girolamo N, et al. S100A12 provokes mast cell activation: a potential amplification pathway in asthma and innate immunity. *J Allergy Clin Immunol* (2007) 119(1):106–14. doi: 10.1016/j.jaci.2006.08.021

7. Kim J-K, Park S, Lee MJ, Song YR, Han SH, Kim SG, et al. Plasma levels of soluble receptor for advanced glycation end products (sRAGE) and proinflammatory ligand for RAGE (EN-RAGE) are associated with carotid atherosclerosis in patients with peritoneal dialysis. *Atherosclerosis* (2012) 220(1):208–14. doi: 10.1016/j.atherosclerosis.2011.07.115

8. Bernelot Moens SJ, Verweij SL, Schnitzler JG, Stiekema LC, Bos M, Langsted A, et al. Remnant cholesterol elicits arterial wall inflammation and a multilevel

cellular immune response in humans. *Arterioscler thromb Vasc Biol* (2017) 37:5, 969–975. doi: 10.1161/ATVBAHA.116.308834

9. Nadeem A, Masood A, Masood N, Gilani RA, Shah ZA. Immobilization stress causes extra-cellular oxidant–antioxidant imbalance in rats: Restoration by l-NAME and vitamin e. *Eur Neuropsychopharmacol* (2006) 16(4):260–26. doi: 10.1016/j.euroneuro.2005.08.001

10. Canaud B, Cristol JP, Morena M, Leray-Moragues H, Bosc JY, Vaussenat F. Imbalance of oxidants and antioxidants in haemodialysis patients. *Blood purif* (1999) 17(2-3):99–106. doi: 10.1159/000014381

11. Jurgoński A, Opyd PM, Fotschki B. Effects of native or partially defatted hemp seeds on hindgut function, antioxidant status and lipid metabolism in diet-induced obese rats. *J Funct Foods* (2020) 72:104071. doi: 10.1016/j.jff.2020.104071

12. Petrovic S, Arsic A, Ristic-Medic D, Cvetkovic Z, Vucic V. Lipid peroxidation and antioxidant supplementation in neurodegenerative diseases: A review of human studies. *Antioxidants* (2020) 9(11):1128. doi: 10.3390/antiox9111128

13. Goldstein DS, McEwen B. Allostasis, homeostasis, and the nature of stress. *Stress* (2002) 5(1):55–8. doi: 10.1080/102538902900012345

14. Garcez MR, Pereira JL, Fontanelli MDM, Marchioni DML, Fisberg RM. Prevalence of dyslipidemia according to the nutritional status in a representative sample of são paulo. *Arquivos brasileiros cardiol* (2014) 103:476–84. doi: 10.5935/abc.20140156

15. Tóth PP, Potter D, Ming EE. Prevalence of lipid abnormalities in the united states: the national health and nutrition examination survey 2003–2006. *J Clin lipidol* (2012) 6(4):325–30. doi: 10.1016/j.jacl.2012.05.002

16. Narindrarangkura P, Bosl W, Rangsin R, Hatthachote P. Prevalence of dyslipidemia associated with complications in diabetic patients: a nationwide study in Thailand. *Lipids Health dis* (2019) 18(1):1–8. doi: 10.1186/s12944-019-1034-3

17. Bayram F, Kocer D, Gundogan K, Kaya A, Demir O, Coskun R. Gedik, V.Prevalence of dyslipidemia and associated risk factors in Turkish adults. *J Clin lipidol* (2014) 8(2):206–16. doi: 10.1016/j.jacl.2013.12.011

18. Joshi SR, Anjana RM, Deepa M, Pradeepa R, Bhansali A, Dhandania VK, et al. Prevalence of dyslipidemia in urban and rural India: the ICMR–INDIAB study. *PloS One* (2014) 9(5):e96808. doi: 10.1371/journal.pone.0096808

19. Akiyama M, Mawatari T, Nakashima Y, Miyahara H, Yamada H, Okazaki K, et al. Prevalence of dyslipidemia in Japanese patients with rheumatoid arthritis and effects of atorvastatin treatment. *Clin Rheumatol* (2015) 34:1867–75. doi: 10.1007/s10067-015-3049-0

20. Zhao WH, Zhang J, Zhai Y, You Y, Man QQ, Wang CR, et al. Blood lipid profile and prevalence of dyslipidemia in Chinese adults. *Biomed Environ Sci* (2007) 20(4):329–35. doi: 10.1186/s12963-014-0028-7

21. Gong P, Liang S, Carlton EJ, Jiang Q, Wu J, Wang L, et al. Urbanisation and health in China. *Lancet* (2012) 379(9818):843–52. doi: 10.1016/S0140-6736(11)61878-3

22. Stevens J, Truesdale KP, Katz EG, Cai J. Impact of body mass index on incident hypertension and diabetes in Chinese asians, American whites, and American blacks. *Am J Epidemiol* (2008) 167(11):1365–74. doi: 10.1093/aje/kwn060

23. He J, Gu D, Reynolds K, Wu X, Muntner P, Zhao J, et al. Serum total and lipoprotein cholesterol levels and awareness, treatment, and control of hypercholesterolemia in China. *Circulation* (2004) 110(4):405–11. doi: 10.1161/01.CIR.0000136583.52681.0D

24. Li JH, Wang LM, Li YC, Bi YF, Jiang Y, Mi SQ, et al. Epidemiologic characteristics of dyslipidemia in Chinese adults 2010. *Zhonghua Yu Fang Yi Xue Za Zhi* (2012) 46(5):414–8.

25. Li JH, Mi SQ, Li YC, Zhang M, Bi YF, Jiang Y, et al. The levels and distribution of the serum lipids in Chinese adults, 2010. *Zhonghua Yu Fang Yi Xue Za Zhi* (2012) 46(7):607–12.

26. Yang W, Xiao J, Yang Z, Ji L, Jia W, Weng J, et al. Serum lipids and lipoproteins in Chinese men and women. *Circulation* (2012) 125(18):2212–21. doi: 10.1161/CIRCULATIONAHA.111.065904

27. Kish L. Studies of interviewer variance for attitudinal variables. *J Am Stat Assoc* (1962) 57(297):92–115. doi: 10.1080/01621459.1962.10482153

28. Shen M, Hu M, Liu S, Chang Y, Sun Z. Assessment of the Chinese resident health literacy scale in a population-based sample in south China. *BMC Public Health* (2015) 15:637. doi: 10.1186/s12889-015-1958-0

29. Li L, Li YH, Nie XQ, Huang XG, Shi MF, et al. Influence factors of health literacy monitoring of Chinese residents on 2012. *Chin J Health Educ* (2015) 2(31):104–7.

30. Mei X, Zhong Q, Chen G, Huang Y, Li J. Exploring health literacy in wuhan, China: a cross-sectional analysis. *BMC Public Health* (2020) 20:1417. doi: 10.1186/s12889-020-09520-9

31. *China Census bureau* . Available at: http://www.gov.cn/guoqing/2013-04/11/content_5046157.htm.

32. Kamel E-N, Shehata M. Effect of toluene exposure on the antioxidant status and apoptotic pathway in organs of the rat. *Br J Biomed Sci* (2008) 65(2):75–9. doi: 10.1080/09674845.2008.11732801

33. Folsom AR, Li Y, Rao X, Cen R, Zhang K, Liu X, et al. Body mass, fat distribution and cardiovascular risk factors in a lean population of south China. *J Clin Epidemiol* (1994) 47(2):173–81. doi: 10.1016/0895-4356(94)90022-1

34. Gu D, Gupta A, Muntner P, Hu S, Duan X, Chen J, et al. Prevalence of cardiovascular disease risk factor clustering among the adult population of China: results from the international collaborative study of cardiovascular disease in Asia (InterAsia). *Circulation* (2005) 112(5):658–65. doi: 10.1161/CIRCULATIONAHA.104.515072

35. Florez H, Silva E, Fernández V, Ryder E, Sulbarán T, Campos G, et al. Prevalence and risk factors associated with the metabolic syndrome and dyslipidemia in white, black, Amerindian and mixed hispanics in zulia state, Venezuela. *Diabetes Res Clin Pract* (2005) 69(1):63–77. doi: 10.1016/j.diabres.2004.11.018

36. Esteghamati A, Meysamie A, Khalilzadeh O, Rashidi A, Haghazali M, Asgari F, et al. Third national surveillance of risk factors of non-communicable diseases (SuRFNCD-2007) in Iran: methods and results on prevalence of diabetes, hypertension, obesity, central obesity, and dyslipidemia. *BMC Public Health* (2009) 29(9):167. doi: 10.1186/1471-2458-9-167

37. Reddy KS, Prabhakaran D, Jeemon P, Thankappan KR, Joshi P, Chaturvedi V, et al. Educational status and cardiovascular risk profile in indians. *Proc Natl Acad Sci U S A* (2007) 104(41):16263–8. doi: 10.1073/pnas.0700933104

38. Raal F, Schamroth C, Blom D, Marx J, Rajput M, Haus M, et al. CEPHEUS SA: a south African survey on the undertreatment of hypercholesterolaemia. *Cardiovasc J Afr* (2011) 22:234–40. doi: 10.5830/CVJA-2011-044

39. Hermans MP, Castro Cabezas M, Strandberg T, Ferrières J, Feely J, Elisaf M, et al. Centralized PanEuropean survey on the under-treatment of hypercholesterolaemia (CEPHEUS): overall findings from eight countries. *Curr Med Res Opin* (2010) 26:445–54. doi: 10.1185/03007990903500565

40. Steinhagen-Thiessen E, Bramlage P, Lösch C, Hauner H, Schunkert H, Vogt A, et al. Dyslipidemia in primary care–prevalence, recognition, treatment and control: data from the German metabolic and cardiovascular risk project (GEMCAS). *Cardiovasc Diabetol* (2008) 10(15):7–31. doi: 10.1186/1475-2840-7-31

41. Petrella RJ, Merikle E, Jones J. Prevalence and treatment of dyslipidemia in Canadian primary care: a retrospective cohort analysis. *Clin Ther* (2007) 29(4):742–50. doi: 10.1016/j.clinthera.2007.04.009

42. Goff DCJr, Bertoni AG, Kramer H, Bonds D, Blumenthal RS, Tsai MY, et al. Dyslipidemia prevalence, treatment, and control in the multi-ethnic study of atherosclerosis (MESA): gender, ethnicity, and coronary artery calcium. *Circulation* (2006) 113(5):647–56. doi: 10.1161/CIRCULATIONAHA.105.552737

43. Zweifler RM, McClure LA, Howard VJ, Cushman M, Hovater MK, Safford MM, et al. Racial and geographic differences in prevalence, awareness, treatment and control of dyslipidemia: the reasons for geographic and racial differences in stroke (REGARDS) study. *Neuroepidemiology* (2011) 37(1):39–44. doi: 10.1159/000328258

44. McDonald M, Hertz RP, Unger AN, Lustik MB. Prevalence, awareness, and management of hypertension, dyslipidemia, and diabetes among united states adults aged 65 and older. *J Gerontol A Biol Sci Med Sci* (2009) 64(2):256–63. doi: 10.1093/gerona/gln016

45. Maggio M, Guralnik JM, Longo DL, Ferrucci L. Interleukin-6 in aging and chronic disease: A magnificent pathway. *J Gerontol A Biol Sci Med Sci* (2006) 61(6):575–84. doi: 10.1093/gerona/61.6.575

46. Beharka A, Meydani M, Wu D, Leka LS, Meydani A, Meydani SN. Interleukin-6 production does not increase with age. *J Gerontol A Biol Sci Med Sci* (2001) 56(2):B81–8. doi: 10.1093/gerona/56.2.B81

47. Popko K, Gorska E, Stelmaszczyk-Emmel A, Plywaczewski R, Stoklosa A, Gorecka D, et al. Proinflammatory cytokines il-6 and TNF-α and the development of inflammation in obese subjects. *Eur J Med Res* (2010) 15(Suppl 2):120–2. doi: 10.1186/2047-783X-15-S2-120

48. Huijgen R, Fouchier SW, Denoun M, Hutten BA, Vissers MN, Lambert G, et al. Plasma levels of PCSK9 and phenotypic variability in familial hypercholesterolemia. *J Lipid Res* (2012) 53(5):979–83. doi: 10.1194/jlr.P023994

49. Toscano A, Cinquegrani M, Scuruchi M, Di Pino A, Piro S, Ferrara V, et al. PCSK9 plasma levels are associated with mechanical vascular impairment in familial hypercholesterolemia subjects without a history of atherosclerotic cardiovascular disease: Results of six-month add-on PCSK9 inhibitor therapy. *Biomolecules* (2022) 12(4):562. doi: 10.3390/biom12040562

50. Momtazi-Borojeni AA, Sabouri-Rad S, Gotto AM, Pirro M, Banach M, Awan Z, et al. PCSK9 and inflammation: a review of experimental and clinical evidence. *Eur Heart J - Cardiovasc Pharmacother* (2019) 5(4):237–45. doi: 10.1093/ehjcvp/pvz022

51. Örem A, Yandi YE, Vanizor B, Çimşit G, Uydu HA, Malkoç M. The evaluation of autoantibodies against oxidatively modified low-density lipoprotein

(LDL), susceptibility of LDL to oxidation, serum lipids and lipid hydroperoxide levels, total antioxidant status, antioxidant enzyme activities, and endothelial dysfunction in patients with behcet's disease. *Clin Biochem* (2002) 35(3):217–24. doi: 10.1016/S0009-9120(02)00290-4

52. Imai H. Biological significance of lipid hydroperoxide and its reducing enzyme, phospholipid hydroperoxide glutathione peroxidase, in mammalian cells. *Yakugaku zasshi* (2004) 124(12):937–57. doi: 10.1248/yakushi.124.937

53. Bonnefont-Rousselot D, Bastard JP, Jaudon MC, Delattre J. Consequences of the diabetic status on the oxidant/antioxidant balance. *Diabetes Metab* (2000) 26:162–76.

54. Bonnefont-Rousselot D. The role of antioxidant micronutrients in the prevention of diabetic complications. *Treat Endocrinol* (2004) 3:41–52. doi: 10.2165/00024677-200403010-00005

55. Tao SC, Huang ZD, Wu XG, Zhou BF, Xiao ZK, Hao JS, et al. CHD and its risk factors in the people's republic of China. *Int J Epidemiol* (1989) 18(3 Suppl 1): S159–63. doi: 10.1093/ije/18.3_Supplement_1.S159

56. Lee HY, Woo J, Chen ZY, Leung SF, Peng XH. Serum fatty acid, lipid profile and dietary intake of Hong Kong Chinese omnivores and vegetarians. *Eur J Clin Nutr* (2000) 54(10):768–73. doi: 10.1038/sj.ejcn.1601089

57. Alberti KG, Eckel RH, Grundy SM, Zimmet PZ, Cleeman JI, Donato KA, et al. Harmonizing the metabolic syndrome: A joint interim statement of the international diabetes federation task force on epidemiology and prevention; national heart, lung, and blood institute; American heart association; world heart federation; international atherosclerosis society; and international association for the study of obesity. *Circulation* (2009) 120(16):1640–5. doi: 10.1161/CIRCULATIONAHA.109.192644

58. Kruk J. Health and economic costs of physical inactivity. *Asian Pac J Cancer Prev* (2014) 15(18):7499–503. doi: 10.7314/APJCP.2014.15.18.7499

59. Simioni C, Zauli G, Martelli AM, Vitale M, Sacchetti G, Gonelli A, et al. Oxidative stress: role of physical exercise and antioxidant nutraceuticals in adulthood and aging. *Oncotarget* (2018) 9(24):17181–98. doi: 10.18632/oncotarget.24729

60. Sallam N, Laher I. Exercise modulates oxidative stress and inflammation in aging and cardiovascular diseases. *Oxid Med Cell Longevity* (2016), 7239639. doi: 10.1155/2016/7239639

61. Swastini DA, Wiryanthini IAD, Ariastuti NLP, Muliantara A. Atherosclerosis prediction with high sensitivity c-reactive protein (hs-CRP) and related risk factor in patient with dyslipidemia. *Open Access Maced J Med Sci* (2019) 7(22):3887–90. doi: 10.3889/oamjms.2019.526

62. Ridker PM, Hennekens CH, Buring JE, Rifai N. C-reactive protein and other markers of inflammation in the prediction of cardiovascular disease in women. *New Engl J Med* (2000) 342(12):836–43. doi: 10.1056/NEJM200003233421202

63. Pearson TA, Mensah GA, Alexander RW, Anderson JL, Cannon ROIII, Criqui M, et al. Markers of inflammation and cardiovascular disease:application to clinical and public health practice:a statement for healthcare professionals from the centers for disease control and prevention and the American heart association. *Circulation* (2003) 107(3):499–511. doi: 10.1161/01.CIR.0000052939.59093.45

64. Cannon CP, de Lemos JA, Rosenson RS, Ballantyne CM, Liu Y, Gao Q, et al. Use of lipid-lowering therapies over 2 years in GOULD, a registry of patients with atherosclerotic cardiovascular disease in the US. *JAMA Cardiol* (2021) 6(9):1060–8. doi: 10.1001/jamacardio.2021.1810

65. Tuñón J, Badimón L, Bochaton-Piallat ML, Cariou B, Daemen MJ, Egido J, et al. Identifying the anti-inflammatory response to lipid lowering therapy: a position paper from the working group on atherosclerosis and vascular biology of the European society of cardiology. *Cardiovasc Res* (2019) 115(1):10–9. DOI: 10.1093/cvr/cvy293

66. Taqueti VR, Ridker PM. Lipid-lowering and anti-inflammatory benefits of statin therapy: More than meets the plaque. *Circ Cardiovasc Imaging* (2017) 10(7): e006676. doi: 10.1161/CIRCIMAGING.117.006676

frontiers | Frontiers in Immunology

TYPE Review
PUBLISHED 19 August 2022
DOI 10.3389/fimmu.2022.934444

OPEN ACCESS

EDITED BY
Pedro Elias Marques,
KU Leuven, Belgium

REVIEWED BY
Siva Sankara Vara Prasad Sakamuri,
Tulane University, United States
Matheus Mattos,
KU Leuven, Belgium

*CORRESPONDENCE
Zhichao Fan
zfan@uchc.edu

SPECIALTY SECTION
This article was submitted to Inflammation, a section of the journal Frontiers in Immunology

RECEIVED 02 May 2022
ACCEPTED 19 July 2022
PUBLISHED 19 August 2022

CITATION
Cao Z, Zhao M, Sun H, Hu L, Chen Y and Fan Z (2022) Roles of mitochondria in neutrophils. *Front. Immunol.* 13:934444. doi: 10.3389/fimmu.2022.934444

Roles of mitochondria in neutrophils

Ziming Cao[1], Meng Zhao[2,3], Hao Sun[4], Liang Hu[5], Yunfeng Chen[6] and Zhichao Fan[1]*

[1]Department of Immunology, School of Medicine, UConn Health, Farmington, CT, United States, [2]Arthritis and Clinical Immunology Program, Oklahoma Medical Research Foundation, Oklahoma City, OK, United States, [3]Department of Microbiology and Immunology, University of Oklahoma Health Science Center, Oklahoma City, OK, United States, [4]Department of Medicine, University of California San Diego, La Jolla, CA, United States, [5]Academy of Integrative Medicine, Shanghai University of Traditional Chinese Medicine, Shanghai, China, [6]Department of Biochemistry and Molecular Biology and Department of Pathology, University of Texas Medical Branch, Galveston, TX, United States

Neutrophils are the most abundant leukocyte in human blood. They are critical for fighting infections and are involved in inflammatory diseases. Mitochondria are indispensable for eukaryotic cells, as they control the biochemical processes of respiration and energy production. Mitochondria in neutrophils have been underestimated since glycolysis is a major metabolic pathway for fuel production in neutrophils. However, several studies have shown that mitochondria are greatly involved in multiple neutrophil functions as well as neutrophil-related diseases. In this review, we focus on how mitochondrial components, metabolism, and related genes regulate neutrophil functions and relevant diseases.

KEYWORDS

neutrophils, mitochondria, respiratory burst, NETosis, migration, adhesion

Introduction

Neutrophils play a central role in the innate immune system. They are the most abundant circulating white blood cells in human blood. They are recruited to infection sites or damaged tissue by a recruitment cascade that involves rolling, arrest, spreading, intravascular crawling, transendothelial migration, and in-tissue migration/chemotaxis (1–4). Neutrophils have various methods to kill invading microorganisms, including phagocytosis (5–7), neutrophil extracellular traps (NETs; and process of NETosis) (6, 8, 9), degranulation (6, 10), and respiratory burst (11, 12).

Mitochondria are one of the most important organelles in eukaryotic cells. They are the powerhouses of eukaryotic cells since this is where adenosine triphosphate (ATP) is produced efficiently by oxidative phosphorylation (OXPHOS). Mitochondria are also central signaling hubs that regulate cell death (13). Until 2003, mitochondria had been underestimated for their role in neutrophils. Utilizing multiple specific dyes, Fossati et al.

identified mitochondria in neutrophils as complex networks extending through the cytoplasm (14), which kickstarted intensive research on neutrophil mitochondria. Mitochondria are now known to have several important functions in neutrophils, such as NET formation, adhesion/migration, respiration burst, development/differentiation, and death, which will be discussed in this review (Figure 1). We will also discuss diseases related to dysfunctions of neutrophil mitochondria.

Respiratory burst

Neutrophil respiratory burst, which involves the production of reactive oxygen species (ROS), plays an important role in controlling infections and the progression of inflammatory diseases. Here, the term ROS refers to reactive non-radical derivatives of molecular oxygen, such as H_2O_2, and reactive free radical species, such as O_2^-.

N-Formyl peptides (e.g., N-formyl-L-methionyl-L-leucyl-phenylalanine; fMLP) can stimulate neutrophil oxidative burst and produce ROS *via* formyl peptide receptors (FPRs) (15). Oligomycin and cyanide m-chlorophenylhydrazone (CCCP) that inhibit mitochondrial OXPHOS can reduce fMLP-induced neutrophil ROS production (15). Dihydrorhodamine (DHR) 123 was used to measure ROS production in this study. However, since mitochondrial OXPHOS also produces ROS (mitochondrial ROS, mROS), whether DHR123-indicated ROS are from mitochondrial OXPHOS or oxidative burst is unclear (15).

Another study showed that scavenging of mROS with mitochondria-targeted antioxidant SkQ1 could decrease neutrophil intracellular ROS upon cytochalasin D/fMLP stimulation in a dose-dependent manner (16). Then they investigated whether mROS directly contributes to the intracellular ROS or regulates intracellular ROS through an indirect mechanism. Intracellular ROS was labeled by the redox-sensitive dye 2′,7′-dichlorofluorescein-diacetate (DCFH-DA), which can be cleaved by intracellular esterases to form dichlorofluorescein and become fluorescent upon oxidation. Using membrane-impermeable catalase to scavenge extracellular ROS, they demonstrated that fMLP predominantly induced extracellular ROS formation, and the DCFH-DA-labeled intracellular ROS was coming from the penetration of extracellular ROS but not mROS. They also used MitoSOX to specifically label mROS, which were shown not to significantly contribute to fMLP-induced intracellular ROS accumulation. Thus, these results indicated that mROS does not directly contribute to intracellular ROS but is implicated in the NADPH oxidase (NOX)-dependent generation of extracellular ROS or transportation of extracellular ROS to the cytoplasm (16). Other mechanisms of how mROS regulate oxidative burst need further investigation. This study also found that SkQ1 can inhibit cytochalasin D/fMLP-induced degranulation based on decreased surface expression of azurophilic granule marker CD63 and specific granule marker CD66b, suggesting that mROS may influence granule exocytosis (16).

A recent study found that inhibition of complex III (cytochrome c reductase) with antimycin A can significantly reduce neutrophil superoxide O_2^- production (17). MitoTEMPO can accumulate in mitochondria and reduce superoxide. Pre-incubation of neutrophils with MitoTEMPO can significantly attenuate neutrophils' ability to kill *Staphylococcus aureus*. This effect is not enhanced by co-incubation with MitoTEMPO and antimycin A, suggesting that electron transport complex III is critical for mROS production and required for the bactericidal function of neutrophils (17). Rice et al. found that mitochondria contribute to prolonged H_2O_2 production. Moreover, if neutrophils have limited glucose, mitochondria can utilize fatty acid metabolism to maintain NADPH levels to support NOX-dependent respiratory burst instead of producing mROS (18).

NET formation

NETs were discovered while studying the unique antibacterial mechanisms of neutrophils. When neutrophils were stimulated with interleukin-8 (IL-8), phorbol 12-myristate 13-acetate (PMA), or lipopolysaccharide (LPS), Brinkmann et al. found that extracellular filamentous structures containing DNA and histones can ensnare bacteria, such as *Staphylococcus aureus*, *Salmonella typhimurium*, or *Shigella flexneri* (8). The process of formation of NETs is called NETosis, which is a unique form of cell death in neutrophils (19). NETosis is essential for the host to fight against microorganisms. However, it also contributes to many pathological processes, including cancer, thrombosis, and autoimmune diseases (20, 21).

Multiple stimuli can initiate NET formation, including nicotine (22), LPS, granulocyte-macrophage colony-stimulating factor (GM-CSF), PMA, ionomycin, and alum. However, each initiates NET formation using a different mechanism, which can be categorized into two types based on the dependence of NOX: NOX-dependent and NOX-independent (Figure 2).

PMA has been used as a stable NETosis inducer to study the mechanisms of NOX-dependent NETosis. The indispensable role of NOX was shown by using the NOX2 inhibitor DPI to significantly reduce PMA-induced NETosis, and that neutrophils from chronic granulomatous disease (CGD) patients—that have mutations in one of the genes encoding the components of the Nox2 NADPH oxidase complex—lose their ability for NETosis (19). PMA activates protein kinase C (PKC), which subsequently activates NOX2 through c-Raf/

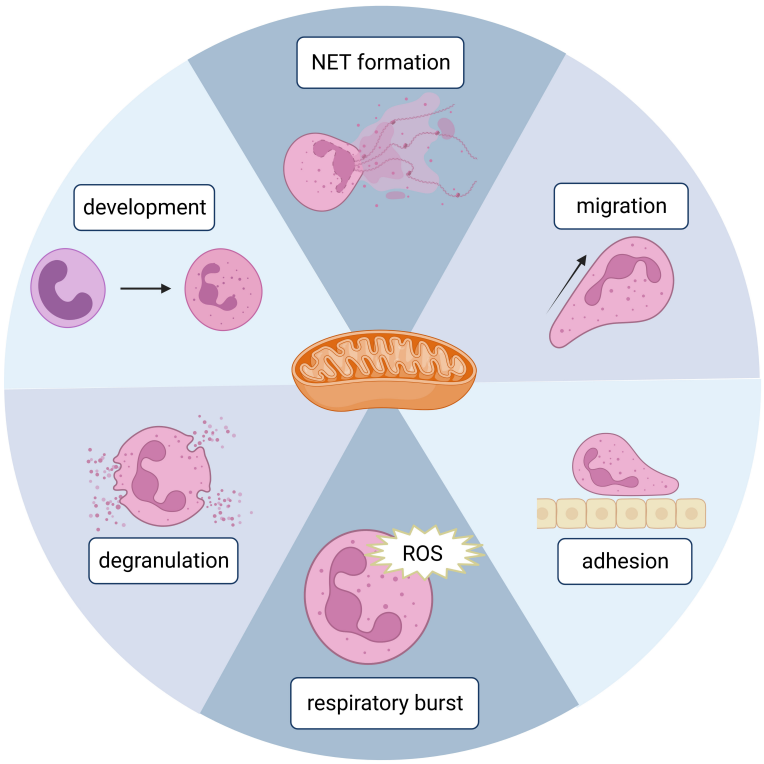

FIGURE 1
A schematic figure showing the involvement of mitochondria in different neutrophil functions. Created in BioRender.com.

MEK/Erk to produce cytosolic ROS (23). The release of neutrophil elastase (NE) and myeloperoxidase (MPO) follows the production of ROS, causing specific histone degradation and chromatin decondensation. However, signaling components between ROS and translocation of NE from azurophilic granules and to the nucleus are not clear (24). During this process, although PMA can induce the production of mROS, PMA-induced mROS cannot drive NETosis (25). Why ROS from different sources have distinct effects on NETosis is not clear.

PMA-induced NOX-dependent NETosis needs glucose. Human neutrophils cultured in glucose-free media are unable to form NETs. Further, glycolysis inhibitor 2-deoxyglucose, but not OXPHOS inhibitor oligomycin, abolishes neutrophil's ability to undergo PMA-induced NETosis (26). GM-CSF plus complement factor 5a (C5a)/LPS-dependent NET formation is also NOX-dependent, which is demonstrated by using NOX inhibitor DPI and neutrophils from CGD patients (27). However, it has also been shown that electron transport complex I localized on the inner membrane of mitochondria (IMM) is critical for GM-CSF plus C5a/LPS-dependent NET formation (28). This is because complex I produces nicotinamide adenine dinucleotide (NAD+), which participates in glycolysis to generate ATP. Blocking complex I with rotenone or piericidin A but not complex III or complex V leads to the inability of mouse and human neutrophils to release DNA upon stimulation with GM-CSF plus C5a (28). Optic atrophy 1 mitochondrial dynamin-like GTPase (OPA1) is one of the "mitochondria-shaping" proteins, bound to the outer space of the inner mitochondrial membrane. Patients with mutated OPA1 can develop autosomal dominant optic atrophy (ADOA). The neutrophils from some ADOA patients or OPA1-deficient mice cannot release DNA following GM-CSF plus C5a stimulation. Amini et al. further found that deficiency of OPA1 leads to the reduced activity of complex I, therefore reducing ATP production by limiting NAD+ availability in glycolysis, resulting in the inability to release DNA to extracellular space and failure of the mitochondrial network formation (28).

Calcium ionophore ionomycin and A23187 can drive NETosis *via* a NOX-independent pathway. mROS, but not NOX2-dependent ROS, is required for NOX-independent NETosis in dHL60 cells and human neutrophils (29). Mitochondrial uncouplers, such as 2,4-dinitrophenol (DNP) and carbonylcyanide-p-trifluoromethoxyphenylhydrazone (FCCP), dissipate the proton gradient and inhibit

mitochondrial ATP synthesis. DNP and FCCP inhibit NOX-independent NETosis in a dose-dependent manner (29). Takishita et al. used dideoxycytidine to generate mitochondria-deficient ρ^0 cells from HL60 cells. They also found that ρ^0 cells release less DNA compared to neutrophil-like HL60 cells after stimulating with A23187, but not PMA, suggesting that mitochondria are crucial for NOX-independent NETosis (30). MitoTEMPO can attenuate A23187-induced NET formation, suggesting that mROS is the key part of the NOX-independent pathway (30, 31).

Reithofer et al. proposed a mechanism of alum-induced NETosis regarding mitochondrial membrane potential as the major driving force (32). They first found that positively charged alum has a similar effect with calcium ionophore ionomycin on activating NETosis. However, alum-induced NETosis does not require extracellular Ca^{2+} like ionophores. Instead, the rupture of lysosomes followed by the release of lysosome-stored Ca^{2+} leads to an increased production of mROS. The authors further investigated the role of the respiration chain in mROS production and NETosis. They found that rotenone, the inhibitor of complex I, does not affect alum-induced NETosis, whereas antimycin, an inhibitor of complex III, decreased alum-induced NETosis to a similar extent as DNP. The inhibition of complex V inhibits retrograde proton transport, increases mitochondrial membrane potential, and enhances alum-induced NETosis. This suggests that alum/ionophore-induced NETosis uses a different pathway from C5a/LPS-induced NETosis, which is dependent on complex I-controlled, glycolytic ATP production (32).

Ca^{2+} signals were found important for NOX-independent NETosis. Mitochondria will sense Ca^{2+} either from extracellular space or intracellular components like ER or lysosome and produce ROS in response to that. The uptake of Ca^{2+} by the mitochondrial calcium uniporter (MCU) is regulated by mitochondrial calcium uptake 1 (MICU1), which acts as a gatekeeper for Ca^{2+} flux through the MCU. In the MICU1 conditional KO model, MCU-mediated ion flux coincides with increased production of mitochondrial O_2^- in response to *S. aureus*, thereby causing MICU1 knockout neutrophils to undergo accelerated and more robust suicidal NETosis and decreased azurophilic granule degranulation (33). Both pharmacological and genetic evidence showed that peptidylarginine deiminase 4 (PAD4) is critical for chromatin decondensation and NETosis (34, 35). Activation of PAD4 requires both ROS and Ca^{2+} signaling (21).

Although NETs are mainly composed of chromosomal DNA, mitochondrial DNA (mtDNA) can be released to extracellular space stimulated by GM-CSF C5a (27) or ribonucleoprotein immune complexes (36), suggesting a direct involvement of mitochondria in NET formation.

Current methods used to dissect the NETosis pathway are mainly pharmacological inhibition due to the short life of neutrophils. Here, we summarize studies showing cellular components participating in the pathway in Table 1.

Migration and adhesion

As the first-line defenders, neutrophils are critical for the innate immune system. The premise of nearly all functions of neutrophils is their ability to navigate and migrate to the infection or wound site. Mitochondria are one of the most important organelles in eukaryotic cells and work as a central hub for signal transduction and metabolism in the locomotion of most cells. Although mature neutrophils mainly rely on glycolysis for ATP (38), mitochondria still play an essential role in neutrophil locomotion (Figure 3). Inhibition of mitochondria by CCCP significantly reduced the migration speed of neutrophils and abolished chemotaxis (39). During chemotaxis, neutrophils release ATP from the leading edge of their cell surface to amplify chemotactic signals and direct cell orientation by feedback through P2Y2 nucleotide receptors and purinergic signaling (40). Mitochondria translocate to the front of the neutrophil, producing ATP to fuel the purinergic signaling (39). Meanwhile, P2Y2 receptors promote mTOR signaling and augment mitochondrial activity near the front of the cell (39). However, excessive mitochondrial ATP production induced by LPS impairs neutrophil chemotaxis (41). Unlike fMLP gradient-induced neutrophil ATP release from the leading edge of the cell surface, LPS uniformly disorganized intracellular trafficking of mitochondria, resulting in global ATP release that disrupted purinergic signaling, cell polarization, and chemotaxis. LPS-primed neutrophils cannot translocate mitochondria toward the leading edge in response to the fMLP gradient, but they can move their mitochondria uniformly toward the cell periphery. Neutrophil chemotaxis is impaired due to the lack of polarity. Removal of excessive extracellular ATP by adding apyrase can restore the chemotaxis of LPS-primed neutrophils (41). This study may partially explain the decreased chemotactic activity in neutrophils from septic patients compared to healthy controls (42). Zhou et al. first provided *in vivo* evidence that mitochondria regulate neutrophil motility in a zebrafish model (43). The gene encoding mtDNA polymerase, *polg*, was knocked out in a neutrophil-specific transgenic line and reduced the migration speed of neutrophils (43).

Intracellular NOX2-dependent ROS regulates neutrophil migration by modulating actin dynamics *via* inducing actin glutathionylation (44). Rotenone and metformin, the mitochondria complex I inhibitors, impair the electron transport chain, increase intracellular superoxide and hydrogen peroxide, and significantly reduce neutrophil recruitment in an acute LPS-induced lung inflammation mouse model (43, 45). Both mitochondria complex I inhibitor rotenone and complex III inhibitor antimycin significantly

TABLE 1 NETosis regulators.

Cell type	Stimuli	Component	Inhibitor	References
Mouse peripheral neutrophil	Ionomycin (NOX-independent)	PAD4	GSK488	(34)
Human peripheral neutrophil	*S. aureus*	PAD4	GSK488	(34)
Mouse peripheral neutrophil	LPS, H_2O_2, PMA	PAD4	knockout	(35)
Human peripheral neutrophil	PMA	NOX2	DPI	(29)
	A23187 (NOX-independent)	mROS	DNP	(29)
		mitochondria	FCCP	(29)
dHL 60	PMA	ERK	FR180204	(29)
		Akt	XI	(29)
	A23187 (NOX-independent)	Akt	XI	(29)
		mROS	DNP, FCCP	(29)
		SK3 channel	siRNA	(29)
Human peripheral neutrophil	A23187, ionomycin (NOX-independent)	mROS	MitoTEMPO	(31)
Human peripheral neutrophil	Nicotine (NOX-independent)	Akt	XI	(22)
		PAD4	CI-amidine	(22)
Mouse peripheral neutrophil	PMA	NOX2	Gp91phox knockout	(22)
Human peripheral neutrophil		c-Raf	GW5074	(23)
		MEK	U0216	(23)
		ERK2	Peptide inhibitor	(23)
		PKC	Staurosporine	(23)
Human peripheral neutrophil	Ionomycin (NOX-independent)	Extracellular Ca^{2+}	Ca^{2+}-free PBS	(32)
	Alum (NOX-independent)	Intracellular/lysosomal Ca2+	BAPTA-AM	(32)
		Lysosomal Ca^{2+}	Bafilomycin	(32)
		mROS	DNP	(32)
		PAD4	GSK484	(32)
		Mitochondrial complex III	Antimycin	(32)
Human peripheral neutrophils	IL-18 (NOX-independent)	mROS	MitoTEMPO	(37)
		Ca2+	BAPTA-AM	(37)

reduced neutrophil motility in zebrafish (43). Gene knockouts of *ndufs2* and *uqcrc1*, which are core components in complex I and III, respectively (46, 47), also resulted in a neutrophil motility reduction (43). Mitochondrial superoxide dismutase 1 and 2 (Sod1 and Sod2) mediate ROS reduction. The loss of Sod1 or 2 significantly reduces the speed of neutrophil migration, which can be rescued by N-acetylcysteine and/or MitoTEMPO. This implies that an excessive amount of intracellular ROS can inhibit neutrophil migration (43). However, this is in contrast to a certain condition where increased intracellular ROS may associate with increased neutrophil migration. Hv1/VSOP is a voltage-gated proton channel that mediates the extrusion of protons and supports intracellular ROS production (48). As expected, Hvcn1-deficient neutrophils produce more intracellular ROS. However, they exhibit stronger chemotaxis toward a low (0.25–1 μM) but not higher (10–50 μM) concentration of fMLP compared with wild-type (WT) neutrophils. Hvcn1-deficient neutrophils have a similar fMLP receptor expression and similar intracellular Ca^{2+} flux after fMLP stimulation compared to WT neutrophils. However, increased ERK activation was observed in Hvcn1-deficient neutrophils. The migration increase and ERK activation of Hvcn1-deficient neutrophils are NOX-dependent, supported by NADPH oxidase inhibitor DPI (49). Interestingly, they did not observe a change in migration of WT neutrophils treated with DPI, suggesting that the above migration changes in mitochondrial defect neutrophils might not be ROS-dependent. However, DPI has off-target effects where it inhibits cell redox metabolism and induces oxidative stress (50).

Recent work has highlighted the role of mitochondrial calcium homeostasis in regulating cell migration (51). Mitochondrial calcium uniporter (MCU), located on IMM, is responsible for mitochondrial calcium uptake. MCU knockdown impaired the migration of Hs578t cells, similar to the outcome of treatment with Ru360, a potent MCU inhibitor. This finding suggests that mitochondrial Ca^{2+} intake regulates cell migration. However, the study of MCU in neutrophils is limited by pharmacological treatment. Two independent groups have shown that MCU regulates neutrophil migration. Activation of MCU by treatment of spermine can promote primary human neutrophil chemotaxis; inhibition of MCU by Ru360 impairs the chemotaxis of human neutrophils (52) and

DMSO-differentiated HL60 (dHL60) cells (43). Dynamin-related protein (Drp1) regulates mitochondrial fission, maintaining mitochondria morphology. In some circumstances, phosphorylation of Drp1 serine 616 (S616) enhances Drp1 activity causing more mitochondria fragmentation (53). In fMLP-stimulated neutrophils, inhibition of MCU can downregulate the phosphorylation of Drp1 S616 and impair neutrophil chemotaxis. Selective suppression of Drp1 by mdivi-1 inhibits neutrophil polarization and chemotaxis but not MCU expression and Ca^{2+} uptake, suggesting that MCU regulates neutrophil chemotaxis partially *via* Drp1 (52). More genetic evidence is needed to connect Drp1 and neutrophil polarization and chemotaxis.

Intracellular Ca^{2+} is mainly stored in the endoplasmic reticulum (ER), and the juxtaposition of ER and mitochondria is essential due to the low affinity of MCU for Ca^{2+} (51). Mitofusin2 (MFN2) stabilizes the contact between ER and mitochondria. MFN2 is involved in neutrophil migration and adhesion. Mazaki et al. found that interfering with MFN2 expression using short-hairpin RNA (shRNA) can significantly suppress the chemotaxis of neutrophil-like dHL60 cells (54). The Deng group found that MFN2-knockdown dHL60 cells have slower chemotaxis and failed to firmly adhere to endothelial cells (55), which is consistent with an *in vitro* study by Mazaki et al. They also extend their finding to an *in vivo* zebrafish model, showing that MFN2-knockout neutrophils failed to recruit to the zebrafish tail wound, and a thioglycollate-induced mouse peritonitis model that showed fewer neutrophils was recruited to the peritoneal cavity in neutrophil-specific MFN-2 knockout mice (55). Also, transfecting an artificial ER-mitochondria tether (56), mimicking MFN2, can rescue the chemotaxis defect in MFN2 knockdown dHL60 cells (55).

In collaboration with Deng's group, our group investigated the mechanism of the adhesion defect in MFN2 knockdown dHL60 cells (57). Using microfluidic devices, we identified that MFN2 knockdown dHL60 cells have defects on β2 integrin-dependent slow rolling and arrest but not P-selectin glycoprotein ligand-1 (PSGL-1)-dependent rolling. MFN2 knockdown dHL60 cells have reduced formyl peptide receptor (FPR) expression and FPR-dependent (fMLP stimulation) and independent (PMA stimulation) β2 integrin activation defects. MFN2 knockdown dHL60 cells also show defects in actin polymerization after fMLP or PMA stimulation and Mn^{2+}-induced cell spreading on ICAM-1. We demonstrated that MFN2 knockdown HL60 cells are deficient in differentiating to neutrophil-like dHL60 cells by assessing the nuclear morphology and maturation markers CD35 and CD87. Using the CD87 maturation marker, we found that in a mature CD87high population, MFN2 knockdown HL60 cells still show defects in cell slow rolling, adhesion, and β2 integrin activation, indicating that besides effects on differentiation, MFN2 is directly involved in regulating β2 integrin activation. Please note that in these mature populations, MFN2 only affects integrin extension (which is reported by the KIM127 antibody), but not headpiece opening (which is reported by the mAb24 antibody), under PMA stimulation. This suggests that MFN2 might be important for the conformational changes of bent-open to extended-open β2 integrins, which is an alternative allosteric pathway of β2 integrins we observed before (58–61), in addition to the conical switchblade model (62).

A migrasome is an extracellular organelle in migrating cells newly discovered by Yu's group (63). During neutrophil migration, intracellular components can be released to extracellular space to form migrasomes, which is called mitocytosis. TSPAN9, a member of the tetraspanin family, is a key regulator of migrasome formation. In $TSPAN9^{-/-}$ mice, neutrophils produced fewer migrasomes than those in WT. The number of $TSPAN9^{-/-}$ neutrophils that can maintain mitochondria membrane potential (MMP) is reduced compared with WT, suggesting a defect in mitochondrial quality control. To directly link mitocytosis and mitochondrial quality control and exclude the other effects caused by TSPAN9 knockout, Jiao et al. compared MMP of both bone marrow and spleen neutrophils between TSPAN9-/- and WT. Since spleen neutrophils migrated a long distance while bone marrow neutrophils did not, there was less difference in MMP of bone marrow neutrophils than of spleen neutrophils, suggesting that migrasomes are mainly responsible for mitochondrial quality control (63).

Development and differentiation

During the differentiation of neutrophils, metabolism reprogramming that limits glycolytic activity while engaging mitochondrial respiration is required. Riffelmacher et al. defined five stages of neutrophil development: myeloblasts (MBs), myelocytes (MCs), metamyelocytes (MMs), band cells (BCs), and neutrophils (PMNs) (64). Taking advantage of *Map1lc3b*-GFP transgenic mice, they found stable autophagic flux in MBs and MCs and reduced flux in MMs and BCs, which is consistent with *Tfeb* and Atg7 expression changes. Their further use of $Atg7^{fl/fl}$-*Vav-Cre* mice revealed that knockout of Atg7 causes defects in neutrophil differentiation. Similar results were seen in $Atg5^{fl/fl}$-*Mx1-Cre* mice, indicating that this phenomenon is not Atg7-specific. Immature neutrophils only prevalent in Atg5 -/- $CD45.2^{+}$ but not WT $CD45.1^{+}$ cells in bone marrow chimeric mice prove that differentiation is independent of autophagy during development. Metabolic analysis showed metabolic reprogramming during G-CSF-induced neutrophil differentiation. The increased extracellular acidification rate (ECAR) and decreased oxygen consumption rate (OCR) of $Atg7^{-/-}$ myeloblasts suggest that metabolic reprogramming limits glycolysis and engages mitochondrial respiration. Depletion of free fatty acids (FFAs) was found in $Atg7^{-/-}$ but

not $Atg7^{+/+}$ myeloblasts. $Atg7^{-/-}$ neutrophil lipid droplet accumulation and colocalization of autophagosomes with lipid droplets suggest that degradation of lipid droplets is mediated by autophagy. Overall, this study showed that autophagy-mediated lipolysis provides free fatty acids to support the fatty acid β-oxidation (FAO) and OXPHOS pathway to produce ATP, which is essential for neutrophil differentiation (64).

Tanimura et al. found that both ER stress and unfolded-protein reactions (UPRs) are involved in neutrophil differentiation (65). During HL60 differentiation into neutrophils induced by ATRA, the ER-stress marker BiP expression is reduced. Treatment of 4-phenylbutyric acid (4-PBA), a chemical chaperone that can reduce ER stress, on HL60 cells can increase CD11b expression and induce morphological change. Detection of cleaved activating transcription factor (ATF) 6 and ATF4 suggests the activation of UPR in non-treated HL60 cells. Co-treatment of ATRA and UPR inhibitors on HL60 cells hindered its differentiation into neutrophils functionally and morphologically. Since both processes require ATP, they further investigated the role of mitochondrial ATP supply by using oligomycin. They found that disrupted neutrophil differentiation as a result of oligomycin treatment inhibited XBP-1 activation (65).

MFN2 conditional knockout/down mice were used to examine the role of MFN2 in neutrophil development. Luchsinger and colleagues found that in a competitive repopulation assay, $Mfn2^{fl/fl}$-*Vav-Cre* and $Mfn2^{fl/fl}$ $CD11b^{+}Gr1^{+}$ myeloid cells show similar numbers in the bone marrow (66). However, they did not further study different myeloid cell populations. Zhou et al. also found that there is no significant difference in neutrophil frequencies between $Mfn2^{fl/fl}$-*S100A8-Cre+* and *Cre-* lines. Of note, both the MFN2 transcript and protein were reduced by 50% in neutrophils of these mice (55, 57). The incomplete deletion of MFN2 suggests that the *S100A8*-Cre line may be too late for neutrophil differentiation studies. Our group used dHL60 cells to show that the MFN2 knockdown causes a neutrophil differentiation defect based on several maturation markers, including CD35, 87, 18, and nucleus segmentation (57).

Others

Human neutrophils produced more mROS in hypoxia *ex vivo* (67). The addition of MitoTEMPO accelerates neutrophil apoptosis, suggesting that mitochondrial O_2^- is needed for neutrophil survival. Neutrophils in hypoxia also display higher mitochondrial membrane potential compared to those in normoxia. Glycerol-3-phosphate dehydrogenase 2 (GPD2) is the mitochondrial component of glycerol 3-phosphate shuttle and produces mROS. To test whether GPD2 is involved in the hypoxia-induced mROS in neutrophils, Wilson et al. used iGP-1 to inhibit GPD2 and found that this inhibition led to decreased HIF-1a expression and mROS, suggesting that neutrophils use GPD2 to produce mROS and stabilize HIF-1a. Importantly, inhibition of GPD2 activity with the pro-apoptotic iGP-1 abrogates neutrophil phagocytosis of heat-killed *S. aureus* and degranulation, indicating that GPD2 activity is essential for neutrophil survival and key effector functions (67).

Neutrophil mitochondria-associated diseases

Neutrophil dysfunctions in mitochondria have been linked to many diseases (Table 2). Systemic lupus erythematosus (SLE) is an autoimmune disease, and low-density granulocytes, a pro-inflammatory subset of neutrophils, from SLE patients spontaneously form more NETs. Ribonucleoprotein immune complexes (RNP-IC) are prevalent in lupus patients and can induce NETosis through an mROS-dependent manner and release oxidized mtDNA. Both *in vitro* and *ex vivo* experiments showed that oxidized mtDNA is highly inflammatory (36).

TABLE 2 Neutrophil mitochondria-associated diseases.

Diseases	Neutrophil phenotype/neutrophil deficiency	References
Systemic lupus erythematosus (SLE)	SLE low-density granulocytes spontaneously release NETs enriched in oxidized mtDNA, leading to enhanced pro-inflammatory and interferogenic potential.	(36)
ADOA	The neutrophils from ADOA patients carrying OPA1 mutations cannot release DNA following GM-CSF/C5a stimulation	(28)
Atherosclerosis	Aged mice display high mitochondrial oxidative stress and enhanced atherosclerosis development.	(68)
Rheumatoid arthritis (RA)	Synovial fluid neutrophils from rheumatoid patients display a gene expression signature of oxidative stress that leads to mtDNA release.	(69)
Adult-onset still's disease (AOSD)	IL-18 induced mtDNA release from neutrophils, resulting in increased levels of NETs enriched in oxidized mtDNA in plasma from AOSD patients.	(37)
Breast cancer lung metastasis	Tumor-associated aged neutrophils release mitochondria-dependent NETs capturing tumor cells and promoting tumor cell retention in the lung.	(70)
Cancer immunosuppression	Tumor-elicited neutrophils maintain mitochondrial metabolism in glucose-limited TME to generate ROS and suppress T cells.	(18)

Atherosclerosis is a chronic inflammatory disorder where the roles of neutrophils in pathology are well recognized (71). NETs have been observed in atherosclerosis environments in mice and humans (72). Wang et al. used lethally irradiated low-density lipoprotein receptor-deficient mice ($Ldlr^{-/-}$) with transplanted bone marrow from WT mice and transgenic mice containing mitochondrial catalase (mCAT), which can reduce mitochondrial oxidative stress (mitoOS) to examine the neutrophil-specific mitoOS in atherosclerosis in aged settings. As a result, aged mCAT→$Ldlr^{-/-}$ chimeric mice had significantly less aortic root atherosclerotic lesions, fewer lesional neutrophils, and decreased NETs, compared with aged controls, suggesting the pathological role of mitoOS in atherosclerosis (68).

Rheumatoid arthritis (RA) is another chronic inflammatory disease, where osteoclasts play a vital role in the development and progression of bone loss. The receptor activator of nuclear factor kappa B ligand (RANKL) is an important factor that drives bone destruction by activating osteoclasts (73). Neutrophils highly express RANKL and activate osteoclastic bone resorption (74). Contis et al. performed a quantitative proteomic analysis of purified neutrophils isolated from synovial fluid (SF) and blood from RA patients. They found that only SF neutrophils from RA patients displayed oxidative stress gene expression signatures. They further found that SF from RA patients had a higher number of mtDNA copies than osteoarthritis patients. Moreover, the mtDNA copy number was higher in SF from RA patients with a higher disease activity score of 28, indicating that mtDNA is associated with disease severity. They also found that mtDNA can induce RANKL expression in neutrophils from healthy donors *in vitro*. Their findings suggest that neutrophils could release mtDNA in SF, which increases neutrophil RANKL expression and induce osteoclastic bone loss, forming an autocrine loop model contributing to RA progression (69).

Adult-onset Still's disease (AOSD) is a rare type of inflammatory arthritis that features fever, rash, and joint pain. Elevated levels of NETosis are found in AOSD patients (75). Liao et al. found that MitoTEMPO but not DPI can significantly inhibit AOSD patient-serum-induced NET formation, suggesting that elevated NETs in AOSD patients are mROS-dependent. They further investigated the role of IL-18 in the NETs of AOSD and found that MitoTEMPO and calcium chelator BAPTM-AM can suppress IL-18-induced NET formation. They conclude that IL-18 can induce calcium influx into neutrophils leading to mROS production and NETosis (37).

A unique subset of neutrophils regulates the lung metastasis of breast cancer in a mitochondria-dependent way (70). Tumor-associated aged neutrophils, defined by $CXCR4^{+}CD62L^{low}$, increased in the peripheral blood and lung metastasis in the 4T1 breast tumor model and mouse mammary tumor virus-polyoma middle tumor-antigen (MMTV-PyMT) model. Further, the blood of breast cancer patients had a higher proportion of aged neutrophils compared with patients with breast fibroadenoma. Transcriptomic analysis showed that transcription factor *SIRT1* is upregulated in aged neutrophils. SIRT1 can induce NETosis, which is different compared with

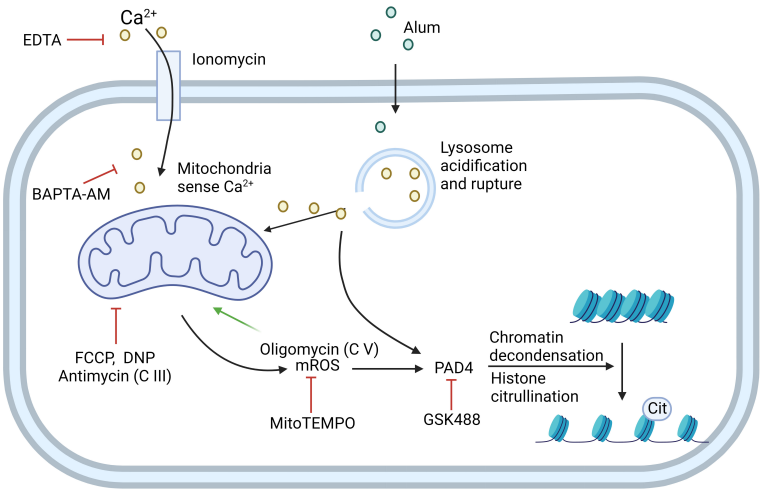

FIGURE 2
NOX-independent NETosis can be induced by ionomycin or alum. Ionomycin works as a Ca^{2+} ionophore to transfer extracellular calcium (Ca^{2+}) into cells. Alum causes lysosome acidification and rupture, which then leads to Ca^{2+} release. Mitochondria sense the elevation of Ca^{2+} in the cytoplasm and generate mitochondrial ROS (mROS). Cytoplasmic Ca^{2+} and mROS are both required to activate PAD4, which further induces histone citrullination and chromatin decondensation. EDTA and BAPTA-AM can chelate extracellular and cytoplasmic Ca^{2+}, respectively, to inhibit this process. Mitochondrial inhibitor FCCP, DNP, and mitochondria complex III inhibitor antimycin can inhibit this process. mROS-specific scavenger MitoTEMPO also inhibits the pathway. Mitochondria complex V inhibitor oligomycin inhibits the retrograde proton transport, therefore leading to the increased MMP which drives enhanced NETosis. GSK488 is an inhibitor of PAD4. C III: complex III; C V: complex V. Created in BioRender.com.

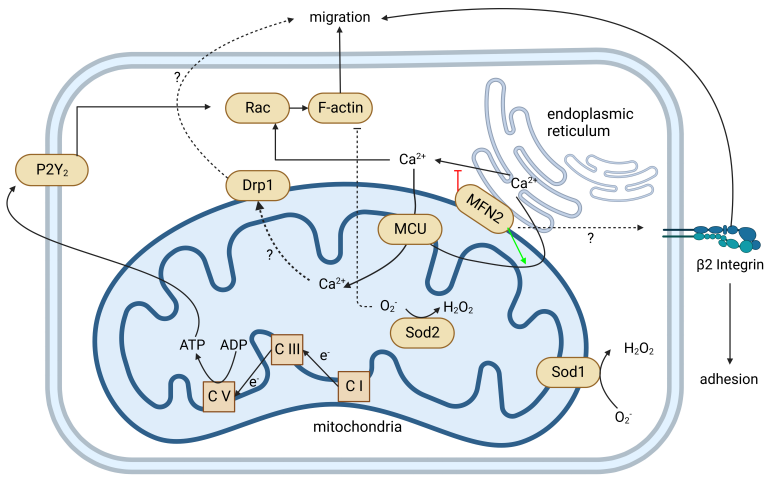

FIGURE 3
Mitochondria regulate neutrophil chemotaxis. Neutrophil mitochondria produce ATP to fuel neutrophil autocrine purinergic signaling, which is required for neutrophil chemotaxis. The production of ATP by mitochondria is through OXPHOS, coupled with an electron transport chain from complex I (C I) to complex V (C V). This is demonstrated by complexes I, III (C III), and V-specific inhibitors and/or gene knockouts. The P2Y2 receptor can recognize ATP, activate Rac, induce actin polymerization, and guide neutrophil migration. MFN2 can regulate *β2* integrin activation through an unknown mechanism that affects both neutrophil adhesion and migration. MFN2 also tethers the endoplasmic reticulum (ER) with mitochondria and promotes ER Ca^{2+} transfer into mitochondria. Loss of MFN2 may lead to more ER Ca^{2+} released into the cytoplasm. Elevated cytoplasmic Ca^{2+} hyperactivates Rac and impairs the directionality of neutrophil migration. MCU mediates cytoplasmic and ER Ca^{2+} transferring into mitochondria and regulates downstream Drp1 through an unclear mechanism. Both MCU and Drp1 are involved in neutrophil migration. Sod1 and Sod2 mediate the reduction of O_2^- to H_2O_2. Loss of Sod1 or Sod2 impairs the chemotaxis of neutrophils. Created in BioRender.com.

PMA induction in the following ways: 1) SIRT1-induced NETosis is independent of NOX and PAD4 signaling; 2) mitochondrial DNA dominates the components of SIRT1-induced neutrophil extracellular traps; and 3) SIRT1 agonist SRT1720 can activate the mitochondrial permeability transition pore. Immunofluorescence and scanning electron microscope images show that tumor-associated aged neutrophils can capture tumor cells and promote tumor cell retention in the lung through NETs. Moreover, the *SIRT1* knockdown can significantly reduce lung metastasis (70).

In cancer, neutrophils may promote tumor progression by suppressing T-cell (76–78) and NK-cell (79) activity. However, the tumor microenvironment (TME) is usually glucose-limited. As mentioned above, neutrophils mainly use glycolysis to produce energy; therefore, the glucose-limited TME may inhibit glycolysis-dependent neutrophil functions. Using 4T1 breast cancer tumor-bearing mice, Rice et al. showed that 4T1 tumors elicit the expansion of c-Kit+ neutrophils, which may indicate immaturity (18). These c-Kit+ neutrophils have increased mitochondrial metabolism that shows higher ATP synthase-dependent and maximal OCR, greater MMP, and higher expression of complexes I and IV. Moreover, these c-Kit+ neutrophils use mitochondrial fatty acid oxidation to support stronger NADPH oxidase-dependent ROS production while limiting glucose compared to neutrophils from naïve mice. The authors further hypothesize that tumor-produced stem cell factor (SCF), a c-Kit ligand, maintains mitochondrial metabolism *via* the c-Kit–SCF axis. Indeed, after using c-Kit antibody blockade or SCF-null tumors, neutrophil number and mitochondrial activity are decreased. They conclude that tumor-elicited c-Kit signaling is responsible for the increased neutrophil number and neutrophil oxidative adaptation. In the coculture assay, tumor-elicited neutrophils stimulated with PMA can induce significantly more T-cell death and suppress T-cell proliferation and interferon-γ (IFN-γ) production compared to neutrophils from naïve mice. Further, suppressing neutrophil glycolysis by 2-deoxy-D-glucose pretreatment did not abolish the T-cell killing ability of tumor-elicited neutrophils. Consistent with their mouse data, they found that neutrophils from peripheral blood of ovarian cancer patients have higher ATP synthase-dependent OCR.

Discussion

Neutrophil mitochondria participate in many neutrophil functions, such as respiratory burst, NET formation, migration, adhesion, differentiation/development, and degranulation. Dysfunction of neutrophil mitochondria is associated with many human diseases, such as cancer, lupus, and rheumatoid arthritis. In-depth investigations of mitochondria help people realize the heterogeneous and complicated nature of the neutrophil population, providing new insights into neutrophil biology and uncovering new targets to treat diseases.

Current research studying mitochondria and their components rely heavily on pharmacological inhibitors. Thus, the off-target effects of these inhibitors may lead to misleading interpretations. Gene editing of mitochondria-specific genes (33, 43, 55, 57) provides more precise interpretations of the function of different mitochondrial components in regulating neutrophil functions. However, the global knockout of most mitochondrial genes will cause severe developmental defects. Thus, several investigations were performed in the neutrophil-like HL60 cell line. Whether these findings are consistent in primary neutrophils remains to be further investigated. The conditional knockout using the Cre-loxP system provides a tool to study mitochondrial components in mouse neutrophils. Some cres, such as MRP8-cre (S100a8-cre) (80, p.; 55, 81) and Ly6G-cre (82, 83), are specific for neutrophils. The LysM-cre (80, 84, 85) targets both neutrophils and monocytes/macrophages. Since neutrophils are short-lived cells, even the genes of mitochondrial components are knocked out, and some cres are not efficient in eliminating protein expression of mitochondrial components. For example, in our study using $MFN2^{flox/flox}MRP8^{cre}$ mice (57), we found that MFN2 protein expression is only decreased by 50-60% in peripheral blood neutrophils. A cre expressing in an earlier stage of hematopoietic differentiation, such as Vav1-cre (80, 86), might increase the knockout efficiency but will lose the specificity to neutrophils.

An alternative to studying the roles of mitochondrial components in neutrophils is to use HoxB8-expressing neutrophil progenitors (87). HoxB8 expression blocks the terminal differentiation of progenitors into monocytes or granulocytes (88, 89). Gene editing can be done in HoxB8 neutrophil progenitors. HoxB8 neutrophil progenitors can differentiate into neutrophils *in vitro* (90–94) and *in vivo* (95, 96). These will provide a powerful tool to study the involvement of mitochondrial components in mouse neutrophils.

There are strategies to perform gene editing in human neutrophils and study the roles of mitochondrial components. One is using a highly effective di-peptide caspase inhibitor, Q-VD.OPh, to inhibit apoptosis in long-time *in vitro* culture of human neutrophils (97). However, whether it is possible to perform gene editing of human neutrophils in this system and whether this culture will affect some neutrophil functions is not clear. A better strategy is to use human-induced pluripotent stem cells (iPSCs), perform gene editing on them, and differentiate them into neutrophils (98–101). This may be the best strategy to study the roles of mitochondrial components in human neutrophils.

Besides nuclear genome-encoded genes of mitochondrial components, mitochondrial DNA also encodes genes that are associated with many diseases, such as Leigh syndrome (102–104), NARP (neuron, ataxia, and retinitis pigmentosa) syndrome (105), and Leber hereditary optic neuropathy (106, 107). Thus, mitochondrial gene editing is critical for studying the roles of mitochondria in human neutrophils. Several techniques to edit mitochondrial genes were highlighted in previous reviews (108, 109). One of the techniques used a modulated Cas9-CRISPR gene-editing technique by appending a gene targeting guide RNA to an RNA transport-derived stem loop element (RP-loop) and expressing the Cas9 enzyme with a preceding mitochondrial localization sequence (110). Another technique is using an interbacterial toxin, DddA, which catalyzes cytidine deamination within double-stranded DNA. Fusions of the split-DddA halves, transcription activator-like effector array proteins, and a uracil glycosylase inhibitor resulted in RNA-free DddA-derived cytosine base editors (DdCBEs) that catalyze C·G-to-T·A conversions in human mtDNA with high targeting specificity and product purity (111). Later, another technique using transcription-activator-like effector (TALE)-linked deaminases (TALEDs) can catalyze A·T-to-G·C conversions in human mtDNA (112). These mitochondrial gene-editing techniques will bring new insights into studying the roles of mitochondria in neutrophil functions.

Author contributions

ZC drafted the manuscript; ZC prepared the figure and tables; HS, LH, YC, MZ, and ZF edited and revised the manuscript; ZF approved the final version of the manuscript. All authors contributed to the article and approved the submitted version.

Funding

This research was supported by funding from the National Institutes of Health, USA (NIH, R01HL145454), and a startup fund from UConn Health.

Acknowledgments

We acknowledge Dr. Christopher “Kit” Bonin and Dr. Geneva Hargis from UConn Health School of Medicine for their help scientific writing and editing of this manuscript.

Conflict of interest

The authors declare that the research was conducted in the absence of any commercial or financial relationships that could be construed as a potential conflict of interest.

Publisher’s note

All claims expressed in this article are solely those of the authors and do not necessarily represent those of their affiliated

References

1. Kolaczkowska E, Kubes P. Neutrophil recruitment and function in health and inflammation. *Nat Rev Immunol* (2013) 13(3):159–75.

2. Ley K, Laudanna C, Cybulsky MI, Nourshargh S. Getting to the site of inflammation: The leukocyte adhesion cascade updated. *Nat Rev Immunol* (2007) 7 (9):678–89.

3. Ley K, Hoffman HM, Kubes P, Cassatella MA, Zychlinsky A, Hedrick CC, et al. Neutrophils: New insights and open questions. *Sci Immunol* (2018) 3(30): eaat4579.

4. Morikis VA, Simon SI. Neutrophil mechanosignaling promotes integrin engagement with endothelial cells and motility within inflamed vessels. *Front Immunol* (2018) 2774.

5. Boero E, Brinkman I, Juliet T, van Yperen E, van Strijp JAG, Rooijakkers SHM, et al. Use of flow cytometry to evaluate phagocytosis of staphylococcus aureus by human neutrophils. *Front Immunol* (2021) 12:635825. doi: 10.3389/fimmu.2021.635825

6. Gierlikowska B, Stachura A, Gierlikowski W, Demkow U. Phagocytosis, degranulation and extracellular traps release by neutrophils–the current knowledge, pharmacological modulation and future prospects. *Front Pharmacol* (2021) 12:666732. doi: 10.3389/fphar.2021.666732

7. Payne JA, Tailhades J, Ellett F, Kostoulias X, Fulcher AJ, Fu T, et al. Antibiotic-chemoattractants enhance neutrophil clearance of staphylococcus aureus. *Nat Commun* (2021) 12(1):1–15.

8. Brinkmann V, Reichard U, Goosmann C, Fauler B, Uhlemann Y, Weiss DS, et al. Neutrophil extracellular traps kill bacteria. *Science* (2004) 303(5663):1532–5.

9. Monteith AJ, Miller JM, Maxwell CN, Chazin WJ, Skaar EP. Neutrophil extracellular traps enhance macrophage killing of bacterial pathogens. *Sci Adv* (2021) 7(37):eabj2101.

10. Eichelberger KR, Goldman WE. Manipulating neutrophil degranulation as a bacterial virulence strategy. *PLoS Pathog* (2020) 16(12):e1009054. doi: 10.1371/journal.ppat.1009054

11. Beavers WN, Skaar EP. Neutrophil-generated oxidative stress and protein damage in staphylococcus aureus. *Pathog Dis* (2016) 74(6):ftw060. doi: 10.1093/femspd/ftw060

12. Nauseef WM. How human neutrophils kill and degrade microbes: An integrated view. *Immunol Rev* (2007) 219(1):88–102.

13. Bock FJ, Tait SW. Mitochondria as multifaceted regulators of cell death. *Nat Rev Mol Cell Biol* (2020) 21(2):85–100.

14. Fossati G, Moulding DA, Spiller DG, Moots RJ, White MR, Edwards SW. The mitochondrial network of human neutrophils: Role in chemotaxis, phagocytosis, respiratory burst activation, and commitment to apoptosis. *J Immunol* (2003) 170(4):1964–72.

15. Bao Y, Ledderose C, Seier T, Graf AF, Brix B, Chong E, et al. Mitochondria regulate neutrophil activation by generating ATP for autocrine purinergic signaling. *J Biol Chem* (2014) 289(39):26794–803.

16. Vorobjeva N, Prikhodko A, Galkin I, Pletjushkina O, Zinovkin R, Sud'ina G, et al. Mitochondrial reactive oxygen species are involved in chemoattractant-induced oxidative burst and degranulation of human neutrophils *in vitro*. *Eur J Cell Biol* (2017) 96(3):254–65.

17. Dunham-Snary KJ, Surewaard BG, Mewburn JD, Bentley RE, Martin AY, Jones O, et al. Mitochondria in human neutrophils mediate killing of staphylococcus aureus. *Redox Biol* (2022) 49:102225.

18. Rice CM, Davies LC, Subleski JJ, Maio N, Gonzalez-Cotto M, Andrews C, et al. Tumour-elicited neutrophils engage mitochondrial metabolism to circumvent nutrient limitations and maintain immune suppression. *Nat Commun* (2018) 9 (1):1–13.

19. Fuchs TA, Abed U, Goosmann C, Hurwitz R, Schulze I, Wahn V, et al. Novel cell death program leads to neutrophil extracellular traps. *J Cell Biol* (2007) 176(2):231–41.

20. Castanheira FV, Kubes P. Neutrophils and NETs in modulating acute and chronic inflammation. *Blood J Am Soc Hematol* (2019) 133(20):2178–85.

21. Papayannopoulos V. Neutrophil extracellular traps in immunity and disease. *Nat Rev Immunol* (2018) 18(2):134–47.

22. Hosseinzadeh A, Thompson PR, Segal BH, Urban CF. Nicotine induces neutrophil extracellular traps. *J Leukoc Biol* (2016) 100(5):1105–12.

23. Hakkim A, Fuchs TA, Martinez NE, Hess S, Prinz H, Zychlinsky A, et al. Activation of the raf-MEK-ERK pathway is required for neutrophil extracellular trap formation. *Nat Chem Biol* (2011) 7(2):75–7.

24. Papayannopoulos V, Metzler KD, Hakkim A, Zychlinsky A. Neutrophil elastase and myeloperoxidase regulate the formation of neutrophil extracellular traps. *J Cell Biol* (2010) 191(3):677–91.

25. Azevedo EP, Rochael NC, Guimarães-Costa AB, de Souza-Vieira TS, Ganilho J, Saraiva EM, et al. A metabolic shift toward pentose phosphate pathway is necessary for amyloid fibril-and phorbol 12-myristate 13-acetate-induced neutrophil extracellular trap (NET) formation. *J Biol Chem* (2015) 290 (36):22174–83.

26. Rodríguez-Espinosa O, Rojas-Espinosa O, Moreno-Altamirano MMB, López-Villegas EO, Sánchez-García FJ. Metabolic requirements for neutrophil extracellular traps formation. *Immunology* (2015) 145(2):213–24.

27. Yousefi S, Mihalache C, Kozlowski E, Schmid I, Simon H-U. Viable neutrophils release mitochondrial DNA to form neutrophil extracellular traps. *Cell Death Differ* (2009) 16(11):1438–44.

28. Amini P, Stojkov D, Felser A, Jackson CB, Courage C, Schaller A, et al. Neutrophil extracellular trap formation requires OPA1-dependent glycolytic ATP production. *Nat Commun* (2018) 9(1):1–16.

29. Douda DN, Khan MA, Grasemann H, Palaniyar N. SK3 channel and mitochondrial ROS mediate NADPH oxidase-independent NETosis induced by calcium influx. *Proc Natl Acad Sci* (2015) 112(9):2817–22.

30. Takishita Y, Yasuda H, Shimizu M, Matsuo A, Morita A, Tsutsumi T, et al. Formation of neutrophil extracellular traps in mitochondrial DNA-deficient cells. *J Clin Biochem Nutr* (2019) 66(1):15–23.

31. Naffah de Souza C, Breda LCD, Khan MA, Almeida SR, Câmara NOS, Sweezey N, et al. Alkaline pH promotes NADPH oxidase-independent neutrophil extracellular trap formation: A matter of mitochondrial reactive oxygen species generation and citrullination and cleavage of histone. *Front Immunol* (2018) 8:1849. doi: 10.3389/fimmu.2017.01849

32. Reithofer M, Karacs J, Strobl J, Kitzmüller C, Polak D, Seif K, et al. Alum triggers infiltration of human neutrophils ex vivo and causes lysosomal destabilization and mitochondrial membrane potential-dependent NET-formation. *FASEB J* (2020) 34(10):14024–41.

33. Monteith AJ, Miller JM, Beavers WN, Maloney KN, Seifert EL, Hajnoczky G, et al. Mitochondrial calcium uniporter affects neutrophil bactericidal activity during staphylococcus aureus infection. *Infect Immun* (2021) 90(2):e0055121.

34. Lewis HD, Liddle J, Coote JE, Atkinson SJ, Barker MD, Bax BD, et al. Inhibition of PAD4 activity is sufficient to disrupt mouse and human NET formation. *Nat Chem Biol* (2015) 11(3):189–91.

35. Li P, Li M, Lindberg MR, Kennett MJ, Xiong N, Wang Y. PAD4 is essential for antibacterial innate immunity mediated by neutrophil extracellular traps. *J Exp Med* (2010) 207(9):1853–62. doi: 10.1084/jem.20100239

36. Lood C, Blanco LP, Purmalek MM, Carmona-Rivera C, De Ravin SS, Smith CK, et al. Neutrophil extracellular traps enriched in oxidized mitochondrial DNA are interferogenic and contribute to lupus-like disease. *Nat Med* (2016) 22(2):146–53.

37. Liao T-L, Chen Y-M, Tang K-T, Chen P-K, Liu H-J, Chen D-Y. MicroRNA-223 inhibits neutrophil extracellular traps formation through regulating calcium influx and small extracellular vesicles transmission. *Sci Rep* (2021) 11(1):1–17.

38. Maianski N, Geissler J, Srinivasula S, Alnemri E, Roos D, Kuijpers T. Functional characterization of mitochondria in neutrophils: A role restricted to apoptosis. *Cell Death Differ* (2004) 11(2):143–53.

39. Bao Y, Ledderose C, Graf AF, Brix B, Birsak T, Lee A, et al. MTOR and differential activation of mitochondria orchestrate neutrophil chemotaxis. *J Cell Biol* (2015) 210(7):1153–64.

40. Chen Y, Corriden R, Inoue Y, Yip L, Hashiguchi N, Zinkernagel A, et al. ATP release guides neutrophil chemotaxis *via* P2Y2 and A3 receptors. *Science* (2006) 314(5806):1792–5.

41. Kondo Y, Ledderose C, Slubowski CJ, Fakhari M, Sumi Y, Sueyoshi K, et al. Frontline science: Escherichia coli use LPS as decoy to impair neutrophil

chemotaxis and defeat antimicrobial host defense. *J Leukoc Biol* (2019) 106 (6):1211–9. doi: 10.1002/JLB.4HI0319-109R

42. Tavares-Murta BM, Zaparoli M, Ferreira RB, Silva-Vergara ML, Oliveira CH, Murta EFC, et al. Failure of neutrophil chemotactic function in septic patients*. *Crit Care Med* (2002) 30(5):1056–61.

43. Zhou W, Cao L, Jeffries J, Zhu X, Staiger CJ, Deng Q. Neutrophil-specific knockout demonstrates a role for mitochondria in regulating neutrophil motility in zebrafish. *Dis Models Mech* (2018) 11(3):dmm033027.

44. Sakai J, Li J, Subramanian KK, Mondal S, Bajrami B, Hattori H, et al. Reactive oxygen species-induced actin glutathionylation controls actin dynamics in neutrophils. *Immunity* (2012) 37(6):1037–49.

45. Zmijewski JW, Lorne E, Zhao X, Tsuruta Y, Sha Y, Liu G, et al. Mitochondrial respiratory complex I regulates neutrophil activation and severity of lung injury. *Am J Respir Crit Care Med* (2008) 178(2):168–79.

46. Mimaki M, Wang X, McKenzie M, Thorburn DR, Ryan MT. Understanding mitochondrial complex I assembly in health and disease. *Biochim Biophys Acta* (2012) 1817:851–62. doi: 10.1016/j.bbabio.2011.08.010

47. Smith PM, Fox JL, Winge DR. Biogenesis of the cytochrome bc(1) complex and role of assembly factors. *Biochim Biophys Acta* (2012) 1817:276–86. doi: 10.1016/j.bbabio.2011.11.009

48. El Chemaly A, Okochi Y, Sasaki M, Arnaudeau S, Okamura Y, Demaurex N. VSOP/Hv1 proton channels sustain calcium entry, neutrophil migration, and superoxide production by limiting cell depolarization and acidification. *J Exp Med* (2010) 207(1):129–39.

49. Okochi Y, Umemoto E, Okamura Y. Hv1/VSOP regulates neutrophil directional migration and ERK activity by tuning ROS production. *J Leukoc Biol* (2020) 107(5):819–31.

50. Riganti C, Gazzano E, Polimeni M, Costamagna C, Bosia A, Ghigo D. Diphenyleneiodonium inhibits the cell redox metabolism and induces oxidative stress. *J Biol Chem* (2004) 279(46):47726–31.

51. Paupe V, Prudent J. New insights into the role of mitochondrial calcium homeostasis in cell migration. *Biochem Biophys Res Commun* (2018) 500 (1):75–86.

52. Zheng X, Chen M, Meng X, Chu X, Cai C, Zou F. Phosphorylation of dynamin-related protein 1 at Ser616 regulates mitochondrial fission and is involved in mitochondrial calcium uniporter-mediated neutrophil polarization and chemotaxis. *Mol Immunol* (2017) 87:23–32.

53. Cho B, Choi SY, Cho HM, Kim HJ, Sun W. Physiological and pathological significance of dynamin-related protein 1 (drp1)-dependent mitochondrial fission in the nervous system. *Exp Neurobiol* (2013) 22(3):149.

54. Mazaki Y, Takada S, Nio-Kobayashi J, Maekawa S, Higashi T, Onodera Y, et al. Mitofusin 2 is involved in chemotaxis of neutrophil-like differentiated HL-60 cells. *Biochem Biophys Res Commun* (2019) 513(3):708–13.

55. Zhou W, Hsu AY, Wang Y, Syahirah R, Wang T, Jeffries J, et al. Mitofusin 2 regulates neutrophil adhesive migration and the actin cytoskeleton. *J Cell Sci* (2020) 133(17):jcs248880.

56. Kornmann B, Currie E, Collins SR, Schuldiner M, Nunnari J, Weissman JS, et al. An ER-mitochondria tethering complex revealed by a synthetic biology screen. *Science* (2009) 325(5939):477–81.

57. Liu W, Hsu AY, Wang Y, Lin T, Sun H, Pachter JS, et al. Mitofusin-2 regulates leukocyte adhesion and β2 integrin activation. *J Leukoc Biol* (2021) 111 (4):771–91.

58. Fan Z, McArdle S, Marki A, Mikulski Z, Gutierrez E, Engelhardt B, et al. Neutrophil recruitment limited by high-affinity bent β2 integrin binding ligand in cis. *Nat Commun* (2016) 7(1):1–14.

59. Fan Z, Kiosses WB, Sun H, Orecchioni M, Ghosheh Y, Zajonc DM, et al. High-affinity bent β2-integrin molecules in arresting neutrophils face each other through binding to ICAMs in cis. *Cell Rep* (2019) 26(1):119–30.

60. Sun H, Hu L, Fan Z. β2 integrin activation and signal transduction in leukocyte recruitment. *Am J Physiol-Cell. Physiol* (2021) 321(2):C308–16.

61. Sun H, Zhi K, Hu L, Fan Z. The activation and regulation of β2 integrins in phagocytes. *Front Immunol* (2021) 12:978.

62. Luo B-H, Carman CV, Springer TA. Structural basis of integrin regulation and signaling. *Annu Rev Immunol* (2007) 25:619–47.

63. Jiao H, Jiang D, Hu X, Du W, Ji L, Yang Y, et al. Mitocytosis, a migrasome-mediated mitochondrial quality-control process. *Cell* (2021) 184(11):2896–910.

64. Riffelmacher T, Clarke A, Richter FC, Stranks A, Pandey S, Danielli S, et al. Autophagy-dependent generation of free fatty acids is critical for normal neutrophil differentiation. *Immunity* (2017) 47(3):466–80.

65. Tanimura A, Miyoshi K, Horiguchi T, Hagita H, Fujisawa K, Noma T. Mitochondrial activity and unfolded protein response are required for neutrophil differentiation. *Cell Physiol Biochem* (2018) 47(5):1936–50.

66. Luchsinger LL, de Almeida MJ, Corrigan DJ, Mumau M, Snoeck H-W. Mitofusin 2 maintains haematopoietic stem cells with extensive lymphoid potential. *Nature* (2016) 529(7587):528–31.

67. Willson JA, Arienti S, Sadiku P, Reyes L, Coelho P, Morrison T, et al. Neutrophil HIF-1α stabilization is augmented by mitochondrial ROS produced *via* the glycerol 3-phosphate shuttle. *Blood J Am Soc Hematol* (2022) 139(2):281–6.

68. Wang Y, Wang W, Wang N, Tall AR, Tabas I. Mitochondrial oxidative stress promotes atherosclerosis and neutrophil extracellular traps in aged mice. *Arteriosclerosis. Thromb. Vasc Biol* (2017) 37(8):e99–e107.

69. Contis A, Mitrovic S, Lavie J, Douchet I, Lazaro E, Truchetet M-E, et al. Neutrophil-derived mitochondrial DNA promotes receptor activator of nuclear factor κB and its ligand signalling in rheumatoid arthritis. *Rheumatology* (2017) 56 (7):1200–5.

70. Yang C, Wang Z, Li L, Zhang Z, Jin X, Wu P, et al. Aged neutrophils form mitochondria-dependent vital NETs to promote breast cancer lung metastasis. *J Immunotherapy. Cancer* (2021) 9(10):e002875.

71. Soehnlein O. Multiple roles for neutrophils in atherosclerosis. *Circ Res* (2012) 110(6):875–88.

72. Megens RT, Vijayan S, Lievens D, Doering Y, van Zandvoort MA, Grommes J, et al. Presence of luminal neutrophil extracellular traps in atherosclerosis. *Thromb Haemostasis* (2012) 107(03):597–8.

73. Yeo L, Toellner K-M, Salmon M, Filer A, Buckley CD, Raza K, et al. Cytokine mRNA profiling identifies b cells as a major source of RANKL in rheumatoid arthritis. *Ann Rheumatic. Dis* (2011) 70(11):2022–8.

74. Chakravarti A, Raquil M-A, Tessier P, Poubelle PE. Surface RANKL of toll-like receptor 4–stimulated human neutrophils activates osteoclastic bone resorption. *Blood J Am Soc Hematol* (2009) 114(8):1633–44.

75. Hu Q, , Shi H, , Zeng T, , Liu H, , Su Y, , Cheng X, , et al. . Increased neutrophil extracellular traps activate NLRP3 and inflammatory macrophages in adult-onset Still's disease. *Arthritis Res Ther* (2019) 21(1):276–86. doi: 10.1186/s13075-018-1800-z

76. Kalyan S, Kabelitz D. When neutrophils meet T cells: Beginnings of a tumultuous relationship with underappreciated potential. *Eur J Immunol* (2014) 44 (3):627–33.

77. Leliefeld PH, Koenderman L, Pillay J. How neutrophils shape adaptive immune responses. *Front Immunol* (2015) 6:471.

78. Pillay J, Tak T, Kamp VM, Koenderman L. Immune suppression by neutrophils and granulocytic myeloid-derived suppressor cells: Similarities and differences. *Cell Mol Life Sci* (2013) 70(20):3813–27.

79. Spiegel A, Brooks MW, Houshyar S, Reinhardt F, Ardolino M, Fessler E, et al. Neutrophils suppress intraluminal NK cell–mediated tumor cell clearance and enhance extravasation of disseminated carcinoma CellsNeutrophil-mediated tumor cell survival and extravasation. *Cancer Discovery* (2016) 6(6):630–49.

80. Abram CL, Roberge GL, Hu Y, Lowell CA. Comparative analysis of the efficiency and specificity of myeloid-cre deleting strains using ROSA-EYFP reporter mice. *J Immunol Methods* (2014) 408:89–100.

81. Passegué E, Wagner EF, Weissman IL. JunB deficiency leads to a myeloproliferative disorder arising from hematopoietic stem cells. *Cell* (2004) 119(3):431–43.

82. Ancey P-B, Contat C, Boivin G, Sabatino S, Pascual J, Zangger N, et al. GLUT1 expression in tumor-associated neutrophils promotes lung cancer growth and resistance to radiotherapy. *Cancer Res* (2021) 81(9):2345–57.

83. Hasenberg A, Hasenberg M, Männ L, Neumann F, Borkenstein L, Stecher M, et al. Catchup: A mouse model for imaging-based tracking and modulation of neutrophil granulocytes. *Nat Methods* (2015) 12(5):445–52.

84. Clausen B, Burkhardt C, Reith W, Renkawitz R, Förster I. Conditional gene targeting in macrophages and granulocytes using LysMcre mice. *Transgenic Res* (1999) 8(4):265–77.

85. Shi J, Hua L, Harmer D, Li P, Ren G. Cre driver mice targeting macrophages. In: *Methods Mol Biol*. Springer (2018). 1784:263–75.

86. de Boer J, Williams A, Skavdis G, Harker N, Coles M, Tolaini M, et al. Transgenic mice with hematopoietic and lymphoid specific expression of cre. *Eur J Immunol* (2003) 33(2):314–25.

87. Wang GG, Calvo KR, Pasillas MP, Sykes DB, Häcker H, Kamps MP. Quantitative production of macrophages or neutrophils ex vivo using conditional Hoxb8. *Nat Methods* (2006) 3(4):287–93.

88. Knoepfler PS, Sykes DB, Pasillas M, Kamps MP. HoxB8 requires its pbx-interaction motif to block differentiation of primary myeloid progenitors and of most cell line models of myeloid differentiation. *Oncogene* (2001) 20(39):5440–8.

89. Krishnaraju K, Hoffman B, Liebermann DA. Lineage-specific regulation of hematopoiesis by HOX-B8 (HOX-2.4): Inhibition of granulocytic differentiation and potentiation of monocytic differentiation. *Blood J Am Soc Hematol* (1997) 90 (5):1840–9.

90. Chu JY, McCormick B, Mazelyte G, Michael M, Vermeren S. HoxB8 neutrophils replicate fcγ receptor and integrin-induced neutrophil signaling and functions. *J Leukoc. Biol* (2019) 105(1):93–100.

91. McDonald JU, Cortini A, Rosas M, Fossati-Jimack L, Ling GS, Lewis KJ, et al. *In vivo* functional analysis and genetic modification of *in vitro*-derived mouse neutrophils. *FASEB J* (2011) 25(6):1972–82.

92. Saul S, Castelbou C, Fickentscher C, Demaurex N. Signaling and functional competency of neutrophils derived from bone-marrow cells expressing the ER-HOXB8 oncoprotein. *J Leukoc Biol* (2019) 106(5):1101–15.

93. Weiss E, Hanzelmann D, Fehlhaber B, Klos A, von Loewenich FD, Liese J, et al. Formyl-peptide receptor 2 governs leukocyte influx in local staphylococcus aureus infections. *FASEB J* (2018) 32(1):26–36.

94. Zehrer A, Pick R, Salvermoser M, Boda A, Miller M, Stark K, et al. A fundamental role of Myh9 for neutrophil migration in innate immunity. *J Immunol* (2018) 201(6):1748–64.

95. Cohen JT, Danise M, Hinman KD, Neumann BM, Johnson R, Wilson ZS, et al. Engraftment, fate, and function of HoxB8-conditional neutrophil progenitors in the unconditioned murine host. *Front Cell Dev Biol* (2022) 41.

96. Orosz A, Walzog B, Mócsai A. *In vivo* functions of mouse neutrophils derived from hoxb8-transduced conditionally immortalized myeloid progenitors. *J Immunol* (2021) 206(2):432–45.

97. Wardle DJ, Burgon J, Sabroe I, Bingle CD, Whyte MK, Renshaw SA. Effective caspase inhibition blocks neutrophil apoptosis and reveals mcl-1 as both a regulator and a target of neutrophil caspase activation. *PLoS One* (2011) 6(1):e15768.

98. Brok-Volchanskaya VS, Bennin DA, Suknuntha K, Klemm LC, Huttenlocher A, Slukvin I. Effective and rapid generation of functional neutrophils from induced pluripotent stem cells using ETV2-modified mRNA. *Stem Cell Rep* (2019) 13(6):1099–110.

99. Majumder A, Suknuntha K, Bennin D, Klemm L, Brok-Volchanskaya VS, Huttenlocher A, et al. Generation of human neutrophils from induced pluripotent stem cells in chemically defined conditions using ETV2 modified mRNA. *STAR. Protoc* (2020) 1(2):100075.

100. Trump LR, Nayak RC, Singh AK, Emberesh S, Wellendorf AM, Lutzko CM, et al. Neutrophils derived from genetically modified human induced pluripotent stem cells circulate and phagocytose bacteria *in vivo*. *Stem Cells Trans Med* (2019) 8(6):557–67.

101. Tsui M, Min W, Ng S, Dobbs K, Notarangelo LD, Dror Y, et al. The use of induced pluripotent stem cells to study the effects of adenosine deaminase deficiency on human neutrophil development. *Front Immunol* (2021) 12.

102. Pelnena D, Burnyte B, Jankevics E, Lace B, Dagyte E, Grigalioniene K, et al. Complete mtDNA sequencing reveals mutations m. 9185T> c and m. 13513G> a in three patients with Leigh syndrome. *Mitochondrial. DNA Part A* (2018) 29(7):1115–20.

103. Sofou K, de Coo IF, Ostergaard E, Isohanni P, Naess K, De Meirleir L, et al. Phenotype-genotype correlations in Leigh syndrome: New insights from a multicentre study of 96 patients. *J Med Genet* (2018) 55(1):21–7.

104. Wei Y, Cui L, Peng B. Mitochondrial DNA mutations in late-onset Leigh syndrome. *J Neurol* (2018) 265(10):2388–95.

105. Mordel P, Schaeffer S, Dupas Q, Laville M-A, Gérard M, Chapon F, et al. A 2 bp deletion in the mitochondrial ATP 6 gene responsible for the NARP (neuropathy, ataxia, and retinitis pigmentosa) syndrome. *Biochem Biophys Res Commun* (2017) 494(1–2):133–7.

106. Carelli V, Carbonelli M, Irenaeus F, Kawasaki A, Klopstock T, Lagrèze WA, et al. International consensus statement on the clinical and therapeutic management of leber hereditary optic neuropathy. *J Neuro-Ophthalmology* (2017) 37(4):371–81.

107. Wallace DC, Singh G, Lott MT, Hodge JA, Schurr TG, Lezza AM, et al. Mitochondrial DNA mutation associated with leber's hereditary optic neuropathy. *Science* (1988) 242(4884):1427–30.

108. Yang X, Jiang J, Li Z, Liang J, Xiang Y. Strategies for mitochondrial gene editing. *Comput Struct Biotechnol J* (2021) 19:3319–29.

109. Yin T, Luo J, Huang D, Li H. Current progress of mitochondrial genome editing by CRISPR. *Front Physiol* (2022) 884.

110. Hussain S-RA, Yalvac ME, Khoo B, Eckardt S, McLaughlin KJ. Adapting CRISPR/Cas9 system for targeting mitochondrial genome. *Front Genet* (2021) 12:627050.

111. Mok BY, de Moraes MH, Zeng J, Bosch DE, Kotrys AV, Raguram A, et al. A bacterial cytidine deaminase toxin enables CRISPR-free mitochondrial base editing. *Nature* (2020) 583(7817):631–7.

112. Cho S-I, Lee S, Mok YG, Lim K, Lee J, Lee JM, et al. Targeted a-to-G base editing in human mitochondrial DNA with programmable deaminases. *Cell* (2022) 185(10):1764–76.

frontiers | Frontiers in Immunology

TYPE Original Research
PUBLISHED 14 November 2022
DOI 10.3389/fimmu.2022.1007080

OPEN ACCESS

EDITED BY
Andrea Baragetti,
University of Milan, Italy

REVIEWED BY
Yanmin Wan,
Fudan University, China
Sreelekshmy Mohandas,
Indian Council of Medical Research (ICMR), India

*CORRESPONDENCE
Maria Cecilia C. Canesso
mcamposcan@rockefeller.edu

†These authors have contributed equally to this work

SPECIALTY SECTION
This article was submitted to Inflammation, a section of the journal Frontiers in Immunology

RECEIVED 29 July 2022
ACCEPTED 24 October 2022
PUBLISHED 14 November 2022

CITATION
Nakandakari-Higa S, Parsa R, Reis BS, de Carvalho RVH, Mesin L, Hoffmann H-H, Bortolatto J, Muramatsu H, Lin PJC, Bilate AM, Rice CM, Pardi N, Mucida D, Victora GD and Canesso MCC (2022) A minimally-edited mouse model for infection with multiple SARS-CoV-2 strains. *Front. Immunol.* 13:1007080. doi: 10.3389/fimmu.2022.1007080

A minimally-edited mouse model for infection with multiple SARS-CoV-2 strains

Sandra Nakandakari-Higa[1], Roham Parsa[2†], Bernardo S. Reis[2†], Renan V. H. de Carvalho[1], Luka Mesin[1], Hans-Heinrich Hoffmann[3], Juliana Bortolatto[1,2], Hiromi Muramatsu[4], Paulo. J. C. Lin[5], Angelina M. Bilate[2], Charles M. Rice[3], Norbert Pardi[4], Daniel Mucida[2,6], Gabriel D. Victora[1] and Maria Cecilia C. Canesso[1,2*]

[1]Laboratory of Lymphocyte Dynamics, The Rockefeller University, New York, NY, United States, [2]Laboratory of Mucosal Immunology, The Rockefeller University, New York, NY, United States, [3]Laboratory of Virology and Infectious Disease, The Rockefeller University, New York, NY, United States, [4]Department of Microbiology, Perelman School of Medicine, University of Pennsylvania, Philadelphia, PA, United States, [5]Acuitas Therapeutics, Vancouver, BC, Canada, [6]Howard Hughes Medical Institute, The Rockefeller University, New York, NY, United States

Efficient mouse models to study SARS-CoV-2 infection are critical for the development and assessment of vaccines and therapeutic approaches to mitigate the current pandemic and prevent reemergence of COVID-19. While the first generation of mouse models allowed SARS-CoV-2 infection and pathogenesis, they relied on ectopic expression and non-physiological levels of human angiotensin-converting enzyme 2 (hACE2). Here we generated a mouse model carrying the minimal set of modifications necessary for productive infection with multiple strains of SARS-CoV-2. Substitution of only three amino acids in the otherwise native mouse *Ace2* locus (*Ace2*^{TripleMutant} or *Ace2*™), was sufficient to render mice susceptible to both SARS-CoV-2 strains USA-WA1/2020 and B.1.1.529 (Omicron). Infected *Ace2*™ mice exhibited weight loss and lung damage and inflammation, similar to COVID-19 patients. Previous exposure to USA-WA1/2020 or mRNA vaccination generated memory B cells that participated in plasmablast responses during breakthrough B.1.1.529 infection. Thus, the *Ace2*™ mouse replicates human disease after SARS-CoV-2 infection and provides a tool to study immune responses to sequential infections in mice.

KEYWORDS

SARS-CoV-2, mouse ACE2, lung inflammation, mRNA vaccine, memory B cells

Introduction

The coronavirus disease 2019 (COVID-19) pandemic, caused by severe acute respiratory syndrome coronavirus 2 (SARS-CoV-2), is an ongoing global health crisis. Rapid development of vaccines against SARS-CoV-2 has been critical to minimizing morbidity and mortality. However, SARS-CoV-2 has shown rapid antigenic drift, which gradually erodes the ability of established antibody responses to control infection. Individuals previously vaccinated or infected with SARS-CoV-2 therefore remain susceptible to emerging viral variants (1–4).

Small animal model systems are key tools in the effort to understand the mechanisms of COVID-19 disease and evaluate therapies and vaccines targeting SARS-CoV-2. However, standard laboratory mice do not support infection with the original USA-WA1/2020 SARS-CoV-2 strain—used in currently available vaccines—due to inefficient interactions between the receptor-binding domain (RBD) of Spike (S) protein and mouse angiotensin-converting enzyme 2 (mACE2) (5, 6). One way to circumvent this limitation has been to develop mouse-adapted strains of SARS-CoV-2 by *in vivo* passaging or reverse genetics (7–10). Conversely, several mouse models that express the full-length human ACE2 (hACE2) protein have been developed, including Ad5-hACE2 (11) or AAV-hACE2 transduced models (12), hACE2 transgenic mice and hACE2 knock-in mice (13–18). A caveat of these mouse models is that the full-length human ACE2 is expressed nonphysiologically and ectopically, altering the tissue or cellular tropism of the virus.

In this study, we sought to establish a mouse model carrying the minimal set of modifications necessary to support infection with multiple strains of SARS-CoV-2. We show that only three amino acid substitutions in the otherwise native mouse *Ace2* locus (*Ace2*$^{\text{TripleMutant}}$ or *Ace2*$^{\text{TM}}$) are sufficient to allow infection of mice with both SARS-CoV-2 USA-WA1/2020 (WA-1) strain and the variant B.1.1.529 (Omicron). *Ace2*$^{\text{TM}}$ mice can support SARS-CoV-2 WA and Omicron replication in the lungs after intranasal infection, which is accompanied by weight loss and lung damage. Prior exposure to WA-1 infection or vaccination with nucleoside-modified mRNA-lipid nanoparticles (mRNA-LNPs) encoding SARS-CoV-2 spike protein generated memory B cells that participated in plasmablast (PB) responses following Omicron challenge. Our study shows that *Ace2*$^{\text{TM}}$ mice are susceptible to all tested variants of SARS-CoV-2, reproducing human pathology after infection and providing a tool to study immune responses to sequential infections in mice.

Materials and methods

In vitro experiments

Human and mouse ACE2 proteins were expressed in HEK293T cells (purchased from ATCC) after transfection with calcium phosphate. Forty hours after transfection, cells were detached using a non-enzymatic cell dissociation reagent (Thermo Fisher Scientific), washed, and resuspended at 5 x 10^6 cells per ml in PBE 1x (PBS supplemented with 0.5% BSA + 1 mM EDTA). For each binding reaction, 100 µl of cells were incubated with either recombinant his-tag SARS-COV2 Spike RBD_{WA} or $RBD_{Omicron}$ (Sino Biological) at 3µg/ml, 1µg/ml, 0.3 µg/ml or no protein at 4°C for 30 minutes. Cells were washed two times with PBE 1x and the bound protein was detected with a His-tag mAb APC-conjugated (Cell Signaling Cat. No. 14931S) by flow cytometry. Experiments were performed twice with three wells per condition each time.

Cell lines

VeroE6 cells (*Chlorocebus sabaeus*; sex: female, kidney epithelial) obtained from ATCC (CRL-1586$^{\text{TM}}$) and from Ralph Baric (University of North Carolina at Chapel Hill), and Caco-2 cells (*Homo sapiens*; sex: male, colon epithelial) obtained from the ATCC (HTB-37$^{\text{TM}}$) were cultured in Dulbecco's Modified Eagle Medium (DMEM) supplemented with 1% nonessential amino acids (NEAA) and 10% fetal bovine serum (FBS) at 37°C and 5% CO_2. All cell lines tested negative for contamination with mycoplasma.

Virus and virus titration

SARS-CoV-2 strains USA-WA1/2020 (WA-1) and the variant B.1.1.529 sublineage BA.1 (Omicron) were obtained from BEI Resources (catalog no. NR-52281 and NR-56461, respectively). WA virus was amplified in Caco-2 cells, which were infected at a multiplicity of infection (MOI) of 0.05 plaque forming units (PFU)/cell and incubated for 5 days at 37°C. The Omicron variant was amplified in VeroE6 cells obtained from ATCC that were engineered to stably express TMPRSS2 ($VeroE6_{TMPRSS2}$). $VeroE6_{TMPRSS2}$ cells were infected at a MOI = 0.05 PFU/cell and incubated for 4 days at 33°C. Virus-containing supernatants were subsequently harvested, clarified by centrifugation (3,000 g × 10 min), filtered using a disposable vacuum filter system with a 0.22 µm membrane, and stored at -80°C. Virus stock titers were measured by standard plaque assay on VeroE6 cells obtained from Ralph Baric (referred to as $VeroE6_{UNC}$). Briefly, 500 µL of serial 10-fold virus dilutions in Opti-MEM were used to infect 4x10^5 cells seeded the day prior into wells of a 6-well plate. After 1.5 h adsorption, the virus inoculum was removed, and cells were overlayed with DMEM containing 10% FBS with 1.2% microcrystalline cellulose (Avicel). Cells were incubated for 4 days at 33°C, followed by fixation with 7% formaldehyde and crystal violet staining for plaque enumeration. All SARS-CoV-2 experiments were performed in a biosafety level 3 laboratory (BSL3).

Experimental mice

All mice used in this study were maintained under specific pathogen-free conditions at the Rockefeller University Comparative for Biosciences Center. All experimental procedures involving SARS-CoV-2 infection were conducted BSL3 and approved by the Rockefeller University's Institutional Animal Care and Use Committee (IACUC protocol number 19033H). Wild-type C57BL/6J and Ai14 (*Rosa26*$^{\text{Lox-Stop-Lox-tdTomato}}$) mice were obtained from the Jackson Laboratory. *S1pr2*^{CreERT2} BAC-transgenic mice (19) were generated and kindly provided by T. Kurosaki and T. Okada (Osaka University and RIKEN-Yokohama). *Ace2*^{TM} mice were generated following two rounds of the EASI-CRISPR protocol to first insert mutation H353K and later S82M/F83Y (20). Briefly, fertilized C57BL/6J zygotes at the one-cell stage were cytoplasmically injected with Cas9 protein, sgRNA targeting *Ace2* exon 9 or exon 3 and the corresponding repair ssDNA template for mutation H353K and S82M/F83Y, respectively. The resulting mice were genotyped using primers Exon9_F (tgcagaaaggatatttcaagaggcag) and Exon9_R (atgttctcccttggacttccagtc) followed by AvaI (NEB) digestion; and primers Exon3_F (aggactaagccatgcaggaagtag), Exon3_R (tcagtgctgaccatggtgtagcag) followed by digestion with TatI (Thermo Fisher Scientific). Single-targeted *Ace2*^{H353K} and *Ace2*$^{S82M/F83Y}$ mice were generated as byproducts of the double-targeting process. For fate-mapping experiments, *Ace2*$^{TM/TM}$ females were crossed with *R26*$^{Tom/Tom}$ homozygous *S1pr2*^{CreERT2} transgenic males. Male and female littermates 8-14 weeks old were used for all experiments and mice were randomly distributed to cages. Because of the high chance of contamination, it was not possible to house mice infected with different variants or non-infected mice together. A minimum of biological triplicates was used throughout the study. For weight loss measurements a total of 5 to 16 mice per group were analyzed; for qPCR and histological score measurements a total of 3 to 6 mice per group were analyzed; for longitudinal analysis of lung immune response to B.1.1.529 sublineage BA.1, a total of 3 mice per group were analyzed; for fate-mapping experiments a total of 4 to 5 mice per group were analyzed. Blinding was not possible in this study as the experimenters treating the mice were the same as those that analyzed the data. The treatment groups had to be clearly identified throughout the study to prevent cross contamination.

Infection models, vaccination and fate-mapping

8–14-week-old mice were anesthetized with ketamine/xylazine diluted in sterile PBS 1x (Gibco, Inc.) and infected intranasally with $2.34x10^5$ PFU in 30 µl of SARS-CoV-2 strain USA-WA1/2020 (WA-1) (P3) or $3.3x10^5$ PFU in 30 ul of variant B.1.1.529 sublineage BA.1 (P2). Membrane-bound full-length Spike (S) protein mRNA-LNPs with a proline substitution in the S2 subunit (K986P and V987P) to stabilize the prefusion conformation were designed using the full S protein sequence of SARS-CoV-2 Wuhan-Hu-1 strain (GenBank MN908947.3) as previously described (21). mRNA was produced and encapsulated in LNPs as previously reported (22). Mice were immunized in the gastrocnemius muscle with 30 µg mRNA-LNP. Fate-mapping of germinal centers (GCs) in S1pr2-Tomato mice was carried out by intragastric administration of two doses of 2.5 mg of tamoxifen citrate (Sigma Aldrich) diluted in corn oil at day 7 and day 14 post-infection or vaccination (10mg/ml). Weight loss was assessed until day 6 post infection and results show a pool of three independent experiments (n = 4, 3, 8 per experiment for *Ace2*^{TM}+WA-1 group; n = 3, 3, 5 per experiment for *Ace2*^{TM}+Omicron group; n = 3, 3, 3 per experiment for WT +Omicron group, n = 3, 2 per experiment for WT+WA-1 group). For lungs of WT and *Ace2*^{TM} mice were dissected 3 days post infection and equally distributed for qPCR and histology analysis. Results show a representative of two independent experiments (n = 3, 3 per experiment for *Ace2*^{TM}+WA-1 group; n = 3, 3 per experiment for *Ace2*^{TM}+Omicron group; n = 3, 3 per experiment for WT +Omicron group, n = 3, 3 for WT+WA-1 group. Lungs and mediastinal lymph nodes of *Ace2*^{TM} mice were dissected at different time points post Omicron infection, as indicated in the figure, and digested for flow cytometry analysis (n = 3 mice per group for each time point). *Ace2*^{TM} S1pr2-Tomato mice were infected with WA-1 or vaccinated with S-encoding mRNA-LNPs, followed by tamoxifen treatment 7 and 14 days later. Infected and vaccinated animals were then subjected to breakthrough infection with Omicron virus 4 weeks after the primary exposure. Serum was collected before infection or vaccination (week 0) and at weeks 1, 2 and 4 post primary infection or vaccination and 10 days after Omicron infection. Mediastinal lymph nodes were collected for flow cytometry analysis 10 days post Omicron infection. Results show a pool of two independent experiments (n = 3, 1 per experiment for WA-1 group; n = 3, 1 per experiment for WA-1+Omicron group; and n = 3, 2 per experiment for mRNA+Omicron).

Tissue preparations

Disposable micropestles (Axygen) were used to mechanically disassociate LNs into cell suspensions. For lung preparation, to identify blood contamination during flow cytometer analysis mice were first intravenously injected with 3 µg of anti-mouse CD45-FITC (Fisher Scientific Cat. No. 553080) 3 minutes before euthanasia by exposure to high dose isoflurane. All lung lobes were dissected and distributed for qPCR, flow cytometer and histology analysis, roughly 1/3 of the lobes for each assay. For qPCR, the lung lobes were homogenized

in 3 ml of Trizol (Invitrogen) using a gentleMACS Dissociator (Miltenyi Biotec). Total RNA was extracted with phenol-chloroform followed by RNeasy Mini kit (Qiagen). Viral RNA titers were calculated by RT-qPCR targeting the S gene of SARS-CoV-2 with primers SARS-CoV-F (tcctggtgattcttcttcaggt) and SARS-CoV-R (tctgagagagggtcaagtgc) (15) using SYBR Green Real-Time PCR master mix (Thermo Fisher Scientific). For histology, the lung lobes were fixed in 4% paraformaldehyde for further paraffin tissue preparation. For flow cytometry, the lung lobes were first cut into smaller pieces and then digested in RPMI solution containing 1.5 mg/ml Collagenase A (Sigma-Aldrich) and 1 mg/ml Dnase I (Roche) for 45 min at 37°C and 80 rpm shaking. Next, the digested tissue was transferred through a 70 µm nylon mesh and immune cells were isolated by gradient centrifugation (underlayer 40% and top layer 80% containing cells) using Percoll. Mediastinal LNs (mLNs) were harvested and mechanically dissociated into cell suspensions using disposable micropestles (Axigen).

Flow cytometry

Cells from each tissue were resuspended in PBE 1x (PBS supplemented with 0.5% BSA + 1 mM EDTA) and incubated for 30 min on ice with fluorescently labeled antibodies: CD45-AF700 (BioLegend Cat. No. 103127), CD4-BUV495 (BD Biosciences Cat. No. 565974), CD8α-BUV805 (BD Biosciences Cat. No. 612898), TCRβ-BUV395 (BD Biosciences Cat. No. 742485), NK1.1-BV785 (BioLegend Cat. No. 108749), CD11b-BV711 (BioLegend Cat. No. 101241), CD11c-BUV496 (BD Biosciences Cat. No. 750483), I-A/I-E-BUV395 (BD Biosciences Cat. No. 743876), Ly6G-BV605 (BioLegend Cat. No. 127639), F4/80-BV785 (BioLegend Cat. No. 123141), IFN-δ-PerCP-Cy5.5 (BD Biosciences Cat. No. 560660), TNF-α-PE-Cy7 (BioLegend Cat. No. 506323), IL-17α-BV421 (BioLegend Cat. No. 506925), B220-BV785 (BioLegend Cat. No. 103245), FAS-PE-Cy7 (BioLegend Cat. No. 152617), CD38- PerCP-Cy5.5 (BioLegend Cat. No. 102721) and CD138-BV650 (BioLegend Cat. No. 142517). WA-1 RBD and Omicron RBD biotinylated were purchased from Sino Biological and conjugated with streptavidin. LIVE/DEAD Fixable Aqua Dead Cell Stain Kit, L-34965, was purchased from Life Technologies. Cells were filtered and washed with PBE 1x again before analysis on BD FACS Symphony cytometer. Analyses were performed using FlowJo v. 10 software.

ELISA

RBD_{WA-1} and $RBD_{Omicron}$-specific antibodies were measured by ELISA using 1µg/ml of recombinant his-tag SARS-COV2 Spike RBD_{WA-1} or $RBD_{Omicron}$ (Sino Biological), respectively. Serum was assayed in 3-fold dilutions starting at 1/100 and total IgG antibodies were detected using goat anti-mouse IgG conjugated to horseradish peroxidase and developed with tetrametghylbenzidine (Sigma). OD450 was measured with an accuSkan FC microplate photometer (Fisher Scientific) and antibody titers were calculated by logarithmic interpolation of the dilutions with readings immediately above and immediately below an OD450 of 0.1.

Histological score

15 µm-thick sections were stained with hematoxylin and eosin (H&E) and imaged using a brightfield microscope (Keyence, BZ X-810). Histological scoring was done according to a previous publication (7). Briefly, images were scored from 0-12 based on the presence of interstitial congestion, epithelial damage, inflammatory infiltrate, peribronchiolar lymphatic inflammation, hemorrhage, and intrabronchial macrophages. Tissue pathology scores were performed blinded and samples were scored for each feature as 0 (absence), 1 (low prevalence) or 2 (high prevalence).

Statistical analyses

Statistical tests used to compare conditions are indicated in the figure legends. Statistical analysis was carried out using GrahPad Prism v.9. Flow cytometry analysis was carried out using FlowJo v.10 software. Graphs were plotted using Prism v.9 and edited for appearance using Adobe Illustrator CS. Comparisons between two treatment conditions were analyzed using two-tailed Student's t-test. Multivariate data were analyzed by applying one-way ANOVA and Tukey's multiple comparison *post hoc* test. Mixed-effects analysis followed by Tukey's multiple comparison test was used for weight loss experiments. Statistical details of experiments are provided in the results, figures, and corresponding figure legends. A *P*-value of less than 0.05 was considered significant.

Results

Development of a mouse model that supports infection with different variants of SARS-CoV-2

Small animal models that recapitulate the progression of SARS-CoV-2 pathogenicity in humans are critical for advancing COVID-19 knowledge. However, SARS-CoV-2 does not use mACE2 as its receptor for cellular entry and infection (5). To first test whether we could increase mACE2 binding to SARS-CoV-2 by substituting a limited number of amino acids with their human counterparts, we introduced amino acid

substitutions previously reported to be important for binding to SARS-CoV-2 spike protein in two sites of the murine *Ace2* cDNA (Figure 1A). The first was a His to Lys substitution at position 353 (H353K), a residue at the core of the ACE2–RBD interaction which has been shown to allow replication of the original SARS coronavirus in mouse cells (24), and the second was a Phe to Tyr substitution at position 83 (F83Y), which makes multiple direct contacts with the SARS-CoV-2 RBD (25) (Figure 1B). Because of its proximity to F83 and of the nonconservative nature of the replacement, we also humanized neighboring position 82 by introducing a Ser to Met substitution (S82M). We transfected HEK293T cells with versions of mACE2 carrying S82M/F83Y, H353K, or all three mutations ^{TM} and tested their ability to bind to the WA-1 and Omicron RBDs. mACE2 binding to RBD_{WA-1} was partially rescued to hACE2 levels by either the H353K or the S82M/F83Y substitutions, whereas mACE2 TM restored binding to WA-1 RBD to comparable levels to that of hACE2 (Figure 1C). In line with other groups showing mouse susceptibility to Omicron infection (26), we observed substantial mACE2 binding to $RBD_{Omicron}$. Nevertheless, introduction of all three mutations doubled the binding of mACE2 to hACE2 levels (Figure 1D).

We next developed a genetically engineered mouse line by inserting these three mutations into the endogenous mouse *Ace2* locus. Using two rounds of CRISPR/Cas9 targeting, we edited *Ace2* exons 3 and 9 with 2 different sgRNAs and their corresponding repair templates (Figure 2A). To evaluate whether the *Ace2*^{TM} allele was sufficient to allow infection with SARS-CoV-2, wild-type C57BL/6 (WT) mice and *Ace2*^{TM} mice were infected intranasally with WA-1 or Omicron strains of SARS-CoV-2. *Ace2*^{TM} mice infected with WA-1 exhibited significant weight loss starting at 2 days post infection (dpi), whereas no weight loss was observed for WT mice infected with this strain (Figure 2B). In agreement with the *in vitro* data, *Ace2*^{H353K} single mutant mice and *Ace2*$^{S82M/F83Y}$ double mutant mice infected with WA-1 did not exhibit significant changes in body weight (Supplementary Figure 1). When infected with Omicron, *Ace2*^{TM} mice exhibited a transient decrease in body weight at 1 dpi that was only slightly more severe than that experienced by similarly infected WT mice (Figure 2B). To confirm that *Ace2*^{TM} mice were indeed infected with each strain, we harvested the lungs of WT and *Ace2*^{TM} mice at 3 dpi and performed PCR for viral RNA. *Ace2*^{TM} mice showed a >100,000-fold increase in WA-1 and a >1,000-fold increase in Omicron viral RNA signal over background levels seen in non-infected mice (Figure 2C). Of note, WT mice showed similar lung viral loads to *Ace2*^{TM} mice when infected with Omicron, but much lower viral RNA levels when infected with WA-1.

Histopathologic examination of lung sections harvested at 3 dpi showed that *Ace2*^{TM} mice infected with WA-1 displayed increased peribronchiolar lymphocytic inflammation, luminal macrophages, hemorrhage, and epithelial damage in the lung when compared to WT mice (Figure 2D and Supplementary Figure 2). Both WT and *Ace2*^{TM} mice infected with Omicron displayed mild diffuse peribronchial infiltrates and hemorrhage (Figure 2D), consistent with the lower titers of viral RNA and weight loss caused by Omicron infection. Together, these data show that *Ace2*^{TM} mice support infection and develop disease with both WA-1 and Omicron strains of SARS-CoV-2.

The immune response to Omicron B.1.1.529 infection

To evaluate the composition of the immune cell response in *Ace2*^{TM} mice infected with Omicron, we performed flow cytometric analysis on lung homogenates at days 3, 10 and 21 after intranasal virus inoculation (Figure 3A). We observed an infiltration of innate immune cells in the lung of *Ace2*^{TM} mice, characterized mainly by $Ly6G^+$ neutrophils, $F4/80^+$ macrophages, $MHCII^+CD11c^+$ dendritic cells and $NK1.1^+$ natural killer cells at 3 dpi (Figure 3B). The frequencies of these cells decreased by 10 dpi, with the exception of macrophages, which were still present in the lungs at this timepoint. By 10 dpi, we also observed an accumulation of $CD4^+$ and $CD8^+$ T cells in the lungs, which was maintained until 21 dpi (Figure 3C). Progression and severity of COVID-19 disease is associated with changes in cytokine profile (27, 28). Accordingly, we observed an increase in TNF-α and IL-17 production by $CD4^+$ T cells 10 dpi, whereas IFN-γ production by these populations began later, at around 21 dpi (Figure 3D). Production of TNF-α and IFN-γ by $CD8^+$ T cells followed a similar temporal trend (Figure 3E).

Antibodies specific for the SARS-CoV-2 spike (S) protein, and especially those binding the RBD, are important for controlling and preventing reinfection. Antibody producing cells are formed in germinal centers (GCs), specialized microstructures in secondary lymphoid tissues that harbor B cell proliferation and antibody affinity maturation (29). To assess the formation of GCs upon Omicron infection in *Ace2*^{TM} mice, we isolated mediastinal lymph nodes (mLN) from infected animals at day 10 and 21 post-infection. *Ace2*^{TM} mice infected with Omicron displayed large GCs ($CD38^{low/-}$ Fas^{hi} B cells) at 10 dpi, which accounted for an average of 8.7% of all B cells in the mLN. GC size was maintained at least through 21 dpi (Figure 3F). These data show that, despite mild histopathological damage, robust innate and adaptive immune responses are elicited in the lungs of *Ace2*^{TM} mice infected with Omicron.

Memory B cell dynamics in breakthrough Omicron infection

Rapid mutations in SARS-CoV-2 have resulted in increased susceptibility to new variants of the virus, especially of the

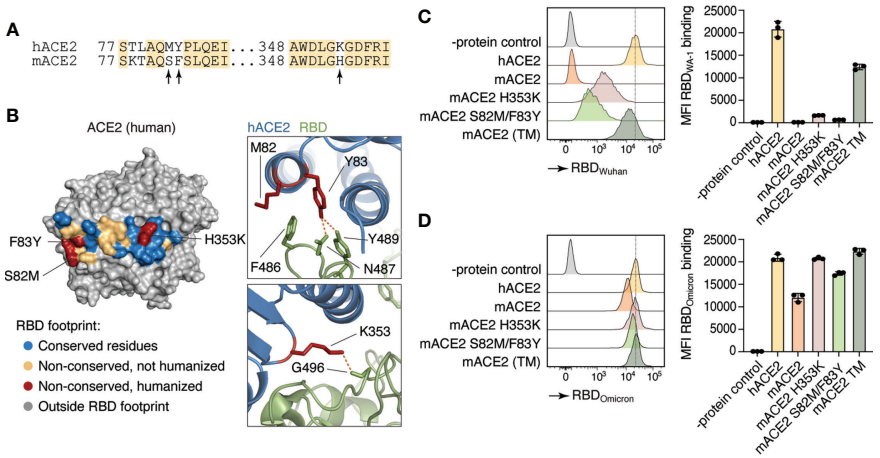

FIGURE 1
Differences in human and mouse ACE2 protein structure and SARS-CoV-2 Spike binding capacity. **(A)** Amino acid sequence of human ACE2 (hACE2) and mouse ACE2 (mACE2). Arrows indicate amino acid residues involved in SARS-CoV-2 Spike binding site. **(B)** Crystal structure of human ACE2 (23). Colored residues denote the SARS-CoV-2 S binding interface (inter-chain distance <5.0 Å). Residues conserved between human and mice are shown in blue. Non-conserved residues are shown in yellow and red, the latter indicating the three positions humanized in *Ace2*^{TM}. **(C, D)** Human (hACE2), mouse (mACE2) or mutant mouse ACE2 (H353K, S82M/F83Y, or TM) proteins were expressed in HEK293T cells and incubated with APC-labeled recombinant WA-1 **(C)** or Omicron **(D)** RBDs. Binding capacity was measured by flow cytometry. Histogram and MFI quantification are depicted. Dotted line shows hACE2-RDB binding MFI as a reference. HEK293T cells expressing an irrelevant protein were used as controls.

Omicron lineage, in individuals previously vaccinated or infected with other variants of SARS-CoV-2. Using the *Ace2*^{TM} model, we sought to determine how memory B cells elicited by WA-1 infection or mRNA vaccination respond to breakthrough infection with Omicron. To label memory cells generated by primary exposure, we crossed *Ace2*^{TM} mice with mice carrying the S1pr2-CreERT2 BAC-transgenic driver and the *Rosa26*$^{Lox\text{-}Stop\text{-}Lox\text{-}tdTomato}$ reporter (S1pr2-Tomato), a combination that allows highly efficient fate-mapping of GC B cells and their progeny by tamoxifen administration (19). To test our ability to fate-map GC B cells responding to WA-1 infection, we infected *Ace2*^{TM} S1pr2-Tomato mice with WA-1 and administered tamoxifen at 7 and 14 dpi (Figure 4A). Five weeks post-infection, ~56.7% of all GC B cells (and 88.9% of RBD-binding cells) in mLNs expressed tdTomato, indicating that fate-mapping is able to enrich for GC B cells responding to the primary infection (Figures 4B–D).

To investigate the recruitment of memory B cells elicited by primary SARS-CoV-2 infection or vaccination by secondary Omicron challenge, we either infected or vaccinated *Ace2*^{TM} S1pr2-Tomato mice with WA-1 or S-encoding mRNA-LNPs, followed by tamoxifen treatment 7 and 14 dpi. Infected and vaccinated animals were then subjected to breakthrough infection with Omicron virus 4 weeks after the primary exposure (Figure 4E). GC size across all three groups (WA-1 only, WA-1+Omicron and mRNA+Omicron) remained similar, indicating that Omicron challenge did not induce a significant expansion of the GC compartment (Figure 4F). The WA-1+Omicron reinfection group had similar percentages (~58.3%) of fate-mapped cells to the WA-1-only infected group (~62.6%) in mLN GCs, suggesting efficient maintenance of fate-mapped cells in the GC following challenge and inefficient recruitment of new B cell clones into the ongoing GCs after Omicron breakthrough infection (Figure 4G). When breakthrough infection followed mRNA vaccination, recruitment of fate-mapped memory B cells generated in the vaccine-draining lymph node (inguinal LNs) into the mLN GCs was inefficient (~10.3% in the mRNA+Omicron group; Figure 4G). Fate-mapped cells were present in the plasmablast (PB) compartment at similar frequencies in all 3 groups (Figure 4H); however, the total number of fate-mapped PB cells upon breakthrough Omicron infection was increased in previously vaccinated or WA-1-infected mice compared to unexposed controls (Figure 4I). Together, these observations support a model in which, upon challenge, memory B cells are preferentially recruited to the antibody-secreting plasma cell compartment rather than reentering secondary GCs (30). This is further supported by the increase in $RBD_{WA\text{-}1}$-specific IgG serum antibody titers after Omicron infection in the vaccination and reinfection groups, compared to the WA-1-only group (Figure 4J). Interestingly, $RBD_{Omicron}$-specific serum antibodies were detected in the mRNA+Omicron group even prior to Omicron challenge, but in the WA-1-infected group only after exposure to the Omicron variant, and at lower levels (Figure 4K).

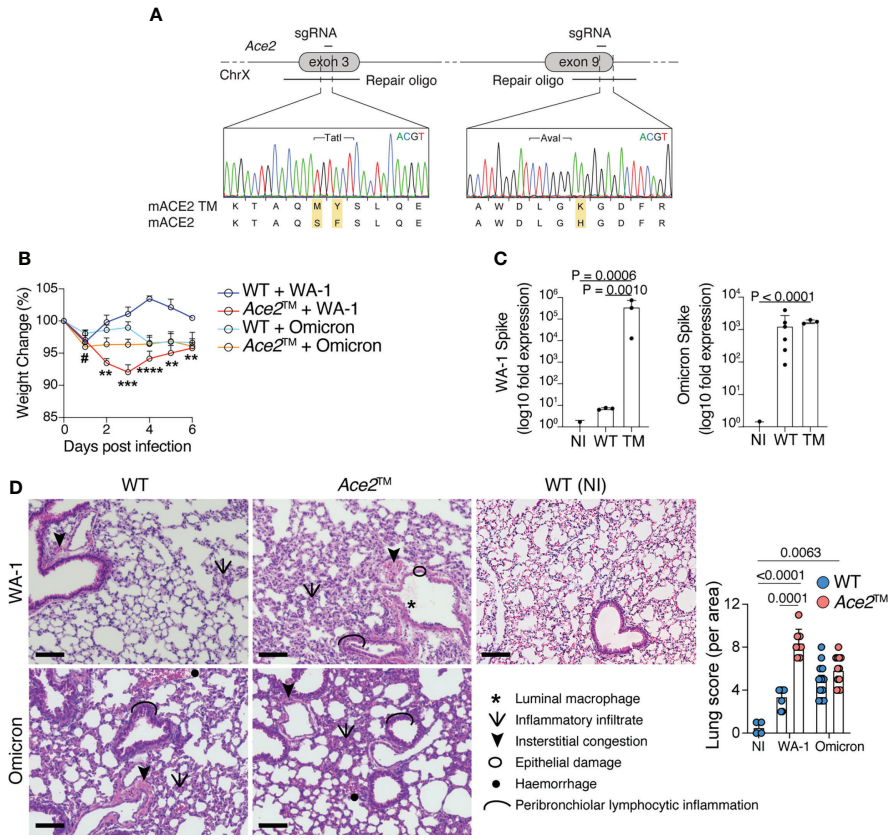

FIGURE 2
Ace2^{TM} mice are susceptible to different variants of SARS-CoV-2. **(A)** Design of the *Ace2*^{TM} allele, depicting the double S82M/F83Y replacement in exon 3 and the H353K replacement in exon 9 of mouse *Ace2*, with representative chromatograms obtained by Sanger sequencing of targeted mice. **(B–D)** 8-14-week-old wild-type (WT) and *Ace2*^{TM} mice were infected with WA-1 (2.34x10^5 PFU) or Omicron (3.3x10^5 PFU) strains. **(B)** Percent change in body weight in different experimental groups (n = 5 to 16 mice per group, pool of three independent experiments). **(C)** qRT-PCR of WA-1 *Spike* (left) and Omicron *Spike* (right) RNA loads in the lungs of mice at 3 dpi, shown as fold-change over background levels in non-infected (NI) control mice. Total RNA input was normalized prior to qRT-PCR analysis (n = 3 to 6 mice per group, representative of two independent experiments). **(D)** Pathological scores of lung specimens from NI control mice or WA-1 and Omicron infected *Ace2*^{TM} and WT mice. Tissue pathology was assessed based on the presence of the indicated features in distinct areas from each lung specimen (n = 3 mice per group). Data were analyzed by one-way ANOVA. Scale Bar = 100 µm. $^{\#}p \leq 0,05$ comparison between *Ace2*^{TM} and WT animals infected with B.1.1.529 1 dpi; $^{**}p \leq 0.01$, $^{***}p \leq 0.001$, $^{****}p \leq 0.0001$ comparison between *Ace2*^{TM} and WT animals infected with USA-WA1/2020. Data were analyzed by mixed-effects analysis followed by Tukey's multiple comparison test.

We conclude that WA-1 infection and S protein mRNA vaccination generate cross-reactive memory B cells that are reengaged by breakthrough Omicron infection, recapitulating findings in the human system (31).

Discussion

The COVID-19 pandemic has raised an urgent need for novel drugs and therapeutics aimed at preventing infection and severe disease. Achieving this requires animal models that recapitulate human COVID-19 disease progression and innate and adaptive immune responses. In this study, we developed one such model by humanizing three amino acid positions of the mouse *Ace2* gene (*Ace2*^{TM}). This model supports infection by at least two isolates of SARS-CoV-2, USA-WA1/2020 (WA-1) and variant B.1.1.529 (Omicron), as well as lung damage and inflammatory infiltrate, reproducing the effects of COVID-19 disease in humans. Higher morbidity and mortality rates have been consistently observed in humans exposed to the original SARS-CoV-2 strain when compared to the those exposed to Omicron variants, which cause milder respiratory infection (32). *Ace2*^{TM} mice recapitulate this feature, as mice infected with WA-1 exhibit greater weight loss and more severe lung inflammation

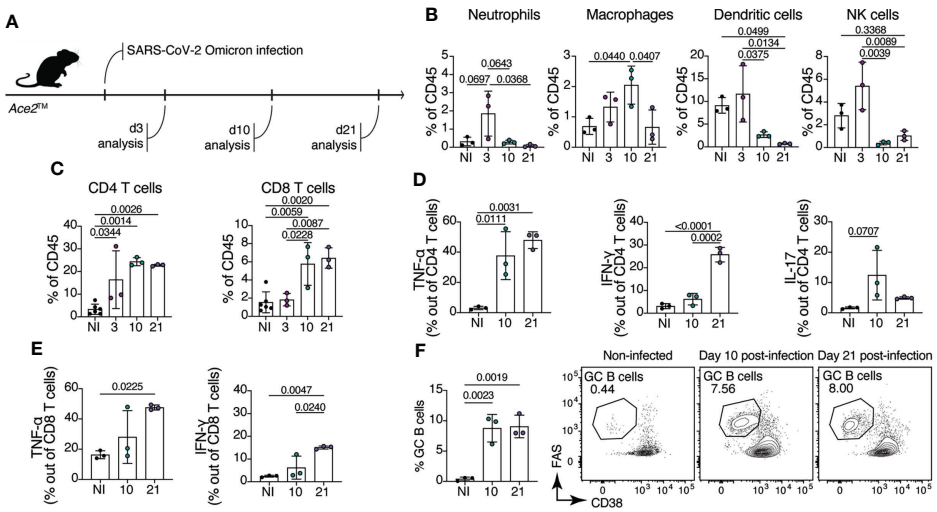

FIGURE 3
Immune response of *Ace2*^{TM} mice to B.1.1.529 infection. **(A-F)** 8-14-week-old *Ace2*^{TM} mice were infected with Omicron and lung cells were harvested for flow cytometry at 3, 10, and 21 dpi. **(A)** Schematic of the infection and analysis protocol. **(B)** Frequency of neutrophils (CD11b^{+}Ly6G^{+}), macrophages (CD11b^{+}F4/80^{+}), dendritic cells (MHCII^{+}CD11c^{+}) and NK cells (NK1.1^{+}) among total lung CD45^{+} cells from infected animals. **(C)** Frequency of CD4^{+} (TCRβ^{+}CD4^{+}) and CD8^{+} (TCRβ^{+}CD8a^{+}) T cells among total lung CD45^{+} cells. **(D, E)** Lung cells isolated at 10 and 21 dpi were stimulated with PMA and ionomycin for 4 hours prior cytokine staining. **(D)** Frequency of TNF-α^{+} (left), IFN-γ^{+} (center) and IL-17^{+} (right) CD4^{+} T cells. **(E)** Frequency of TNF-α^{+} (left), IFN-γ^{+} (right) CD8^{+} T cells. **(F)** Frequency of germinal center B cells (CD38$^{low/-}$Fas^{hi}) in the mediastinal lymph node (mLN) of infected animals at 10 and 21 dpi (n = 3 mice per group). Data were analyzed by one-way ANOVA.

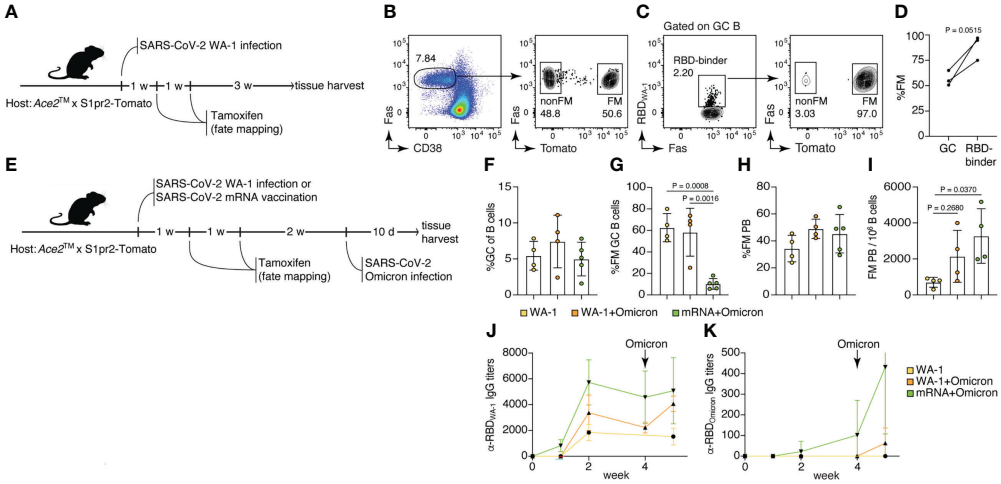

FIGURE 4
Memory B cells generated by USA-WA1/2020 infection or mRNA vaccination are preferentially recruited to the plasmablast compartment upon B.1.1.529 breakthrough infection. **(A–D)** 8-14-week-old *Ace2*^{TM} mice were infected with WA-1 SARS-Cov-2 strain, and GC B cells were fate-mapped (FM) by tamoxifen administration at 7 and 14 dpi. **(B)** Frequency of FM cells among total GC B cells. **(C, D)** Frequency of FM cells among WA-1 Spike RBD binders. **(E–K)** *Ace2*^{TM} mice were either infected with WA-1 or vaccinated with SARS-CoV-2 S protein-encoding mRNA-LNP, fate-mapped, then and challenged with Omicron variant 4 weeks later. **(F)** Frequency of GC B cells among total B cells; **(G)** frequency of FM cells among GC B cells; **(H)** frequency of FM cells among PB; and **(I)** frequency of FM PB per million B cells in the WA-only infected group (yellow), WA+Omicron reinfection group (orange), and mRNA+Omicron challenge group (green). **(J)** WA-1 RBD-specific and **(K)** Omicron RBD-specific serum IgG antibody titers among groups (n = 2, 3 mice per group, pool of two independent experiments). Data were analyzed by t-test or one-way ANOVA.

when compared to mice infected with Omicron. Even though the effects of Omicron infection are milder in *Ace2*^{TM} mice, infection still elicits a robust immune response characterized by neutrophil and macrophage infiltration in the lungs in early infection, followed by $CD4^+$ and $CD8^+$ T cells producing TNF-α and IFN-γ and formation of GCs in the mLN. We did not observe mortality related to either infection, again in line with the typical outcome of SARS-CoV-2 infection in healthy humans.

Although C57BL/6 WT mice cannot be infected by WA-1-type viruses (5, 6), Omicron variants, similarly to other variants of SARS-CoV-2 that emerged throughout the pandemic, acquired a mouse-adapting S substitution (N501Y) that allows viral infection to proceed through mouse ACE2 (26, 33–35). In accordance with other studies (26, 36), our data show that C57BL/6 WT mice are susceptible to Omicron infection at similar levels as the *Ace2*^{TM} mice, although virus titers are slightly higher in the latter. An advantage of the *Ace2*^{TM} model is that these mice are susceptible to both WA-1 and Omicron variant, allowing us to study omicron breakthrough reinfection after WA-1 infection or mRNA-vaccination, a common sequence of events in the human COVID-19 pandemic (37, 38).

As previously reported in other models, memory B cells generated at a distal site (in this study at inguinal LNs after vaccination) made up a small percentage of secondary GCs, which were composed primarily of B cells of naïve origin (30). The increased participation of memory cells in the PB compartment for both the WA-1+Omicron and mRNA+Omicron groups compared to WA-1-only infection indicates a robust antibody response to a new challenge even in the presence of an ongoing response. Taken together, our results support a model in which memory B cells preferentially become antibody-secreting cells after exposure to related antigens. Whether these memory-derived antibodies are protective against a new challenge and the extent of their contribution in the total antigen-specific serum antibody pool still needs to be elucidated.

A variety of mouse models have been previously developed to render mice susceptible to SARS-CoV-2 infection by expression of hACE2 *via* genomic transgenes or knock-in alleles (13–17) or viral vectors (11, 12). Although these studies have made significant contributions to our understanding of SARS-CoV-2 infection, some limitations related to the immunogenicity and expression kinetics of AdV and AAV should be considered, especially when studying the intensity and duration of the immune response and repeated infections over time. Another caveat with some of the transgenic mice expressing hACE2 is the high number of hACE2 transgene insertions as well as ectopic expression of the gene, which can change tissue and cellular tropism of the virus. One example is the SARS-CoV-2 infection in the brain of K18-hACE2 transgenic mouse and the high levels of mortality observed in this mouse model (39, 40). The three mutations we used here to develop the *Ace2*^{TM} mouse model represent the minimum alterations necessary to make mice fully susceptible to all tested variants of SARS-CoV-2 without affecting the organization of the mouse *Ace2* gene.

Data availability statement

The raw data supporting the conclusions of this article will be made available by the authors, without undue reservation.

Ethics statement

The animal study was reviewed and approved by Institutional Animal Care and Use Committee (IACUC).

Author contributions

SN-H and MCCC conducted the majority of the experiments performed in this study, with assistance from RP, BR and RVHC. H-HH assisted with SARS-CoV-2 viral production. NP designed the mRNA vaccine. HM and PJCL produced the mRNA vaccine. GDV designed the *Ace2*^{TM} allele and zygote targeting strategy. SN-H and MCCC conceptualized the work, designed all experiments and analyzed the data. SN-H, GDV and MCCC wrote the manuscript. All authors contributed to the article and approved the submitted version.

Funding

This work was funded by Rockefeller University COVID-19 response grants to GDV and DM. SN-H is supported by a Bulgari Women & Science Fellowship. The funder was not involved in the study design, collection, analysis, interpretation of data, the writing of this article or the decision to submit it for publication. RVHC is supported by a long-term postdoctoral fellowship from Human Frontier Science Program (HFSP- LT000892/2020-L), MCCC is a Pew Latin American Fellow. DM is a Howard Hughes Investigator. GDV is a Burroughs-Wellcome Investigator in the Pathogenesis of Infectious Disease, a Pew-Stewart Scholar, and a MacArthur Fellow. CMR and H-HH were supported in part by the G. Harold and Leila Y. Mathers Charitable Foundation, the Bawd Foundation, Fast Grants, a part of Emergent Ventures at the Mercatus Center, George Mason University, and NIAID P01AI165075. NP was supported by the National Institute of Allergy and Infectious Diseases (R01AI146101 and R01AI153064).

Acknowledgments

We thank the Rockefeller University staff for their invaluable support; T. Kurosaki (Osaka University) and T. Okada (RIKEN-Yokohama) for the S1pr2-CreERT2 strain.

Conflict of interest

NP is named on a patent describing the use of nucleoside-modified mRNA in lipid nanoparticles as a vaccine platform. He has disclosed those interests fully to the University of Pennsylvania and has an approved plan in place for managing any potential conflicts arising from the licensing of that patent. PJCL is an employee of Acuitas Therapeutics, a company involved in the development of mRNA-LNP therapeutics. GDV is a scientific advisor for Vaccine Company, Inc.

The remaining authors declare that the research was conducted in the absence of any commercial or financial relationships that could be construed as a potential conflict of interest.

Publisher's note

Supplementary material

The Supplementary Material for this article can be found online at: https://www.frontiersin.org/articles/10.3389/fimmu.2022.1007080/full#supplementary-material

References

1. Reynolds CJ, Pade C, Gibbons JM, Otter AD, Lin KM, Muñoz Sandoval D, et al. Immune boosting by B.1.1.529 (Omicron) depends on previous SARS-CoV-2 exposure. *Science* (2022) 377(6603):eabq1841. doi: 10.1126/science.abq1841.

2. Andrews N, Stowe J, Kirsebom F, Toffa S, Rickeard T, Gallagher E, et al. Covid-19 vaccine effectiveness against the omicron (B.1.1.529) variant. *N Engl J Med* (2022) 386(16):1532–46. doi: 10.1056/NEJMoa2119451

3. Planas D, Saunders N, Maes P, Guivel-Benhassine F, Planchais C, Buchrieser J, et al. Considerable escape of SARS-CoV-2 omicron to antibody neutralization. *Nature* (2022) 602(7898):671–5. doi: 10.1038/s41586-021-04389-z

4. Liu L, Iketani S, Guo Y, Chan JF, Wang M, Luo Y, et al. Striking antibody evasion manifested by the omicron variant of SARS-CoV-2. *Nature* (2022) 602 (7898):676–81. doi: 10.1038/s41586-021-04388-0

5. Hoffmann M, Kleine-Weber H, Schroeder S, Krüger N, Herrler T, Erichsen S, et al. SARS-CoV-2 cell entry depends on ACE2 and TMPRSS2 and is blocked by a clinically proven protease inhibitor. *Cell* (2020) 181(2):271–80.e8. doi: 10.1016/j.cell.2020.02.052

6. Letko M, Marzi A, Munster V. Functional assessment of cell entry and receptor usage for SARS-CoV-2 and other lineage b betacoronaviruses. *Nat Microbiol* (2020) 5(4):562–9. doi: 10.1038/s41564-020-0688-y

7. Dinnon KH, Leist SR, Schäfer A, Edwards CE, Martinez DR, Montgomery SA, et al. A mouse-adapted model of SARS-CoV-2 to test COVID-19 countermeasures. *Nature* (2020) 586(7830):560–6. doi: 10.1038/s41586-020-2708-8

8. Gu H, Chen Q, Yang G, He L, Fan H, Deng YQ, et al. Adaptation of SARS-CoV-2 in BALB/c mice for testing vaccine efficacy. *Science* (2020) 369(6511):1603–7. doi: 10.1126/science.abc4730

9. Leist SR, Dinnon KH, Schäfer A, Tse LV, Okuda K, Hou YJ, et al. A mouse-adapted SARS-CoV-2 induces acute lung injury and mortality in standard laboratory mice. *Cell* (2020) 183(4):1070–85.e12. doi: 10.1016/j.cell.2020.09.050

10. Sun S, Gu H, Cao L, Chen Q, Ye Q, Yang G, et al. Characterization and structural basis of a lethal mouse-adapted SARS-CoV-2. *Nat Commun* (2021) 12 (1):5654. doi: 10.1038/s41467-021-25903-x

11. Sun J, Zhuang Z, Zheng J, Li K, Wong RL, Liu D, et al. Generation of a broadly useful model for COVID-19 pathogenesis, vaccination, and treatment. *Cell* (2020) 182(3):734–43.e5. doi: 10.1016/j.cell.2020.06.010

12. Israelow B, Song E, Mao T, Lu P, Meir A, Liu F, et al. Mouse model of SARS-CoV-2 reveals inflammatory role of type I interferon signaling. *J Exp Med* (2020) e20201241. doi: 10.1084/jem.20201241

13. Bao L, Deng W, Huang B, Gao H, Liu J, Ren L, et al. The pathogenicity of SARS-CoV-2 in hACE2 transgenic mice. *Nature* (2020) 583(7818):830–3. doi: 10.1038/s41586-020-2312-y

14. Jiang RD, Liu MQ, Chen Y, Shan C, Zhou YW, Shen XR, et al. Pathogenesis of SARS-CoV-2 in transgenic mice expressing human angiotensin-converting enzyme 2. *Cell* (2020) 182(1):50–8.e8. doi: 10.1016/j.cell.2020.05.027

15. Sun SH, Chen Q, Gu HJ, Yang G, Wang YX, Huang XY, et al. A mouse model of SARS-CoV-2 infection and pathogenesis. *Cell Host Microbe* (2020) 28 (1):124–33.e4. doi: 10.1016/j.chom.2020.05.020

16. Winkler ES, Bailey AL, Kafai NM, Nair S, McCune BT, Yu J, et al. SARS-CoV-2 infection of human ACE2-transgenic mice causes severe lung inflammation and impaired function. *Nat Immunol* (2020) 21(11):1327–35. doi: 10.1038/s41590-020-0778-2

17. Zheng J, Wong LR, Li K, Verma AK, Ortiz ME, Wohlford-Lenane C, et al. COVID-19 treatments and pathogenesis including anosmia in K18-hACE2 mice. *Nature* (2021) 589(7843):603–7. doi: 10.1038/s41586-020-2943-z

18. Zhou B, Thao TTN, Hoffmann D, Taddeo A, Ebert N, Labroussaa F, et al. SARS-CoV-2 spike D614G change enhances replication and transmission. *Nature* (2021) 592(7852):122–7. doi: 10.1038/s41586-021-03361-1

19. Shinnakasu R, Inoue T, Kometani K, Moriyama S, Adachi Y, Nakayama M, et al. Regulated selection of germinal-center cells into the memory b cell compartment. *Nat Immunol* (2016) 17(7):861–9. doi: 10.1038/ni.3460

20. Miura H, Quadros RM, Gurumurthy CB, Ohtsuka M. Easi-CRISPR for creating knock-in and conditional knockout mouse models using long ssDNA donors. *Nat Protoc* (2018) 13(1):195–215. doi: 10.1038/nprot.2017.153

21. Laczkó D, Hogan MJ, Toulmin SA, Hicks P, Lederer K, Gaudette BT, et al. A single immunization with nucleoside-modified mRNA vaccines elicits strong cellular and humoral immune responses against SARS-CoV-2 in mice. *Immunity* (2020) 53(4):724–32.e7. doi: 10.1016/j.immuni.2020.07.019

22. Freyn AW, Ramos da Silva J, Rosado VC, Bliss CM, Pine M, Mui BL, et al. A multi-targeting, nucleoside-modified mRNA influenza virus vaccine provides broad protection in mice. *Mol Ther* (2020) 28(7):1569–84. doi: 10.1016/j.ymthe.2020.04.018

23. Lan J, Ge J, Yu J, Shan S, Zhou H, Fan S, et al. Structure of the SARS-CoV-2 spike receptor-binding domain bound to the ACE2 receptor. *Nature* (2020) 581 (7807):215–20. doi: 10.1038/s41586-020-2180-5

24. Li F, Li W, Farzan M, Harrison SC. Structure of SARS coronavirus spike receptor-binding domain complexed with receptor. *Science* (2005) 309 (5742):1864–8. doi: 10.1126/science.1116480

25. Ren W, Zhu Y, Wang Y, Shi H, Yu Y, Hu G, et al. Comparative analysis reveals the species-specific genetic determinants of ACE2 required for SARS-CoV-2 entry. *PloS Pathog* (2021) 17(3):e1009392. doi: 10.1371/journal.ppat.1009392

26. Halfmann PJ, Iida S, Iwatsuki-Horimoto K, Maemura T, Kiso M, Scheaffer SM, et al. SARS-CoV-2 omicron virus causes attenuated disease in mice and hamsters. *Nature* (2022) 603(7902):687–92. doi: 10.1038/s41586-022-04441-6

27. Chua RL, Lukassen S, Trump S, Hennig BP, Wendisch D, Pott F, et al. COVID-19 severity correlates with airway epithelium-immune cell interactions identified by single-cell analysis. *Nat Biotechnol* (2020) 38(8):970–9. doi: 10.1038/s41587-020-0602-4

28. Lucas C, Wong P, Klein J, Castro TBR, Silva J, Sundaram M, et al. Longitudinal analyses reveal immunological misfiring in severe COVID-19. *Nature* (2020) 584(7821):463–9. doi: 10.1038/s41586-020-2588-y

29. Victora GD, Nussenzweig MC. Germinal centers. *Annu Rev Immunol* (2022) 40:413–42. doi: 10.1146/annurev-immunol-120419-022408

30. Mesin L, Schiepers A, Ersching J, Barbulescu A, Cavazzoni CB, Angelini A, et al. Restricted clonality and limited germinal center reentry characterize memory b cell reactivation by boosting. *Cell* (2020) 180(1):92–106.e11. doi: 10.1016/j.cell.2019.11.032

31. Wang Z, Muecksch F, Cho A, Gaebler C, Hoffmann HH, Ramos V, et al. Analysis of memory b cells identifies conserved neutralizing epitopes on the n-terminal domain of variant SARS-Cov-2 spike proteins. *Immunity* (2022) 55 (6):998–1012.e8. doi: 10.1016/j.immuni.2022.04.003

32. Kupferschmidt K, Vogel G. How bad is omicron? some clues are emerging. *Science* (2021) 374(6573):1304–5. doi: 10.1126/science.acx9782

33. Chen RE, Winkler ES, Case JB, Aziati ID, Bricker TL, Joshi A, et al. *In vivo* monoclonal antibody efficacy against SARS-CoV-2 variant strains. *Nature* (2021) 596(7870):103–8. doi: 10.1038/s41586-021-03720-y

34. Kibler KV, Szczerba M, Lake D, Roeder AJ, Rahman M, Hogue BG, et al. Intranasal immunization with a vaccinia virus vaccine vector expressing pre-fusion stabilized SARS-CoV-2 spike fully protected mice against lethal challenge with the heavily mutated mouse-adapted SARS2-N501Y. *Vaccines* (2021) 10(8):1172. doi: 10.1101/2021.12.06.471483

35. Wei C, Shan KJ, Wang W, Zhang S, Huan Q, Qian W. Evidence for a mouse origin of the SARS-CoV-2 omicron variant. *J Genet Genomics* (2021) 48(12):1111–21. doi: 10.1016/j.jgg.2021.12.003

36. Tarrés-Freixas F, Trinité B, Pons-Grífols A, Romero-Durana M, Riveira-Muñoz E, Ávila-Nieto C, et al. Heterogeneous infectivity and pathogenesis of SARS-CoV-2 variants beta, delta and omicron in transgenic K18-hACE2 and wildtype mice. *Front Microbiol* (2022) 13:840757. doi: 10.3389/fmicb.2022.840757

37. Kuhlmann C, Mayer CK, Claassen M, Maponga T, Burgers WA, Keeton R, et al. Breakthrough infections with SARS-CoV-2 omicron despite mRNA vaccine booster dose. *Lancet* (2022) 399(10325):625–6. doi: 10.1016/S0140-6736(22)00090-3

38. Collie S, Champion J, Moultrie H, Bekker LG, Gray G. Effectiveness of BNT162b2 vaccine against omicron variant in south Africa. *N Engl J Med* (2022) 386(5):494–6. doi: 10.1056/NEJMc2119270

39. Oladunni FS, Park JG, Pino PA, Gonzalez O, Akhter A, Allué-Guardia A, et al. Lethality of SARS-CoV-2 infection in K18 human angiotensin-converting enzyme 2 transgenic mice. *Nat Commun* (2020) 11(1):6122. doi: 10.1038/s41467-020-19891-7

40. Winkler ES, Chen RE, Alam F, Yildiz S, Case JB, Uccellini MB, et al. SARS-CoV-2 causes lung infection without severe disease in human ACE2 knock-in mice. *J Virol* (2022) 96(1):e0151121. doi: 10.1128/JVI.01511-21

Frontiers in Immunology

Explores novel approaches and diagnoses to treat immune disorders.

The official journal of the International Union of Immunological Societies (IUIS) and the most cited in its field, leading the way for research across basic, translational and clinical immunology.

Discover the latest Research Topics

See more →

Frontiers

Avenue du Tribunal-Fédéral 34
1005 Lausanne, Switzerland
frontiersin.org

Contact us

+41 (0)21 510 17 00
frontiersin.org/about/contact